Acanthamoeba Mannose-Binding Protein: Structural and functional characterisation of a therapeutic target for *Acanthamoeba* keratitis

A thesis submitted to the

College of Medicine, Biological Sciences & Psychology,

University of Leicester

for the degree of

Doctor of Philosophy

Taiwo Abayomi Banjo

Department of Infection, Immunity and Inflammation

University of Leicester

December 2017

STATEMENT OF ORIGINALITY

I, Taiwo A. Banjo, confirm that the research work presented in this thesis for the degree of PhD entitled "*Acanthamoeba* mannose-binding protein: structural and functional characterisation of a therapeutic target for *Acanthamoeba* keratitis" was carried out by me in the Department of Infection, Immunity and Inflammation, University of Leicester, Leicester, United Kingdom.

I have referenced information from other sources appropriately.

None of this work has been submitted for another degree in this or any other University.

Acanthamoeba Mannose-Binding Protein: structural and functional characterisation of a therapeutic target for *Acanthamoeba* keratitis

Taiwo A. Banjo

Department of Infection, Immunity and Inflammation, University of Leicester
submitted for the degree of Doctor of Philosophy
2017

ABSTRACT

Acanthamoeba mannose-binding protein (AcMBP) is a virulence factor of the free-living amoeba, *Acanthamoeba castellanii*. It is crucial for the development of *Acanthamoeba* keratitis (AK), a corneal infection that often causes blindness. AK is associated with contact lens use and contaminated water sources. Therapeutic unresponsiveness is attributed to similarities in the biological processes that *Acanthamoeba* shares with humans and its ability to form drug-resistant cysts. I aimed to characterise AcMBP as a basis for developing future drugs against *Acanthamoeba.*

To start with, I carried out morphological studies on the two well-known life stages of *Acanthamoeba* and characterised a third stage: the protocysts. Mature cysts and protocysts could not interconvert directly, but always excysted to trophozoites. This is important because *Acanthamoeba* can potentially be trapped as protocysts, which are likely to be more susceptible to drugs. I also studied *Acanthamoeba* adhesion towards various surfaces and cytopathic activities towards cells (including human corneal epithelial cells). Whilst AcMBP was important for adhesion, it is not the only receptor involved.

To gain structure/function information, I expressed the extracellular portion of AcMBP and three truncated fragments. AcMBP is a Ca^{2+}-dependent lectin (~100 kDa) that binds to mannose. Ca^{2+} is essential for lectin activity and stability. The extracellular fragment is monomeric, indicating that trimerisation, shown previously, depends on the membrane-spanning and/or intracellular regions. Bioinformatics revealed that lectin activity is almost certainly located in a DUF 4114 domain (~10 kDa, DUF: domain of unknown function). N-terminal fragments, including the DUF4114 domain did not bind to mannose-Sepharose, suggesting that part of the cysteine-rich domain is also important. AcMBP bound to a variety of mammalian glycans so may have more than one lectin activity.

Although attempts to crystallise AcMBP were unsuccessful, future structural analysis will be useful for defining the domains and determining how it binds to mannose.

Keywords: *Acanthamoeba*, extracellular, Mannose-binding, protein, monomer, Calcium, drug targets.

Word count: 298 words.

DEDICATION

Unto the Most High God, the Ancient of Days who sits enthroned between the cherubim and exalted over all the nations. ….. for He is HOLY!

(Psalm 99:1)

Great are God's riches, wisdom, and knowledge!

(Romans 11:33)

His merciful kindness is great toward us; and the truth of the Lord endureth forever.

(Psalm 117:2)

ACKNOWLEDGEMENTS

mention. They have always listened to me, providing me with unlimited encouragement and support at every turn.

On a very personal note, I sincerely express my deepest gratitude to 'my love' --Monisola, and my children, Opemipo Oluwaromilola and Emmanuel for their unfailing sacrifices and perseverance especially during this journey. I am also grateful to Apostle Olanrewaju Aluko and Ibukun Aluko for their passionate and affectionate love to my family.

The memories of my kind, affectionate and prayerful role-model late parents, Pa Abraham F. Banjo (whose demise during the course of this research was a big loss to me) and my mum, Mrs Abosede Banjo are still fresh in my mind. The time past cannot dull the effective inspirational words of wisdom, fatherly care and the sweet motherly affection you have both given me.

Importantly, I am in complete gratitude and appreciation to the Federal Government of Nigeria for the grant in exploring this research. Finally, I hope that this research would not only succeed in conveying my concern for the contact lens-users infected with *Acanthamoeba* keratitis but the sense of relevance of this discovery would provide a step forward as AK therapeutics mainstay in the years to come towards improving the quality of your care and treatments.

"Quality is never an accident; it is always the result of high intention, sincere effort, intelligent direction and skillful execution; it represents the wise choice of many alternatives." William A. Foster.

TABLE OF CONTENTS

LIST OF TABLES

LIST OF FIGURES

Figures   **Pages**

LIST OF ABBREVIATIONS

AcMBP	*Acanthamoeba* Mannose-binding protein
AcDUF	*Acanthamoeba* –domain of unknown function
AcDUFCS	*Acanthamoeba* –domain of unknown function (Cysteine → Serine)
AK	*Acanthamoeba* keratitis
ATCC	American Type Culture Collection
BLAST	Basic local Alignment Search Tool
bp	Base pair
cDNA	Complementary deoxyribo-nucleic acid
CHO	Chinese hamster ovary
CPE	Cytopathic effect
CRD	Carbohydrate-recognition domain
° C	Degree Celsius
DHFCS	Dialysed heat-treated foetal calf serum
DHFR	Dihydrofolate reductase
DMSO	Dimethylsulfoxide
EDTA	Ethylene-diamine-tetra-acetic acid
ESMS	Electron spray mass spectroscopy
FBS	Foetal Bovine serum
g	Gram
HCEC	Human corneal epithelial cell
HEPES	4-(2-hydroxyethyl)-1-piperazineethanesulfonic acid
HPLC	High pressure liquid chromatography
IL	Interleukins
KDa	Kilo Dalton
KH$_2$PO$_4$	Potassium dihydrogen orthophosphate
ƛ	Lambda
L	Litre

LA	Luria Bertani agar
LB	Luria Bertani broth
M	Molar
m/z	Mass charge ratio
MCS	Multiple cloning site
MEM	Minimum essential medium
MTX	Methotrexate
μ	Micron
μg	Microgram
μl	Microlitre
mg	Milligram
mmol	Millimole
NCBI	National centre for biotechnology information
nH_2O	Nano-pure water
Ni NTA	Nickel nitriloacetic acid
NNA	Non-nutrient agar
OD	Optical density (e.g. OD_{600} = optical density at absorbance of 600 nm)
PAGE	Poly-acrylamide gel electrophoresis
PBS	Phosphate Buffered Saline
PCR	Polymerase chain reaction
PEG	Polyethylene glycol
PNACL	Protein Nucleic Acid Chemistry Laboratory
rpm	Revolutions per minute
RT	Room temperature
SDS	Sodium dodecyl sulfate
UV	Ultraviolet
v/v	volume / volume

1. General Introduction-*Acanthamoeba* in human infection and consequences

1.1 Background

The burden and persistence of parasitic protozoan infections have been characterised by debilitating and sometimes fatal health consequences. Most often, free-living amoebae (FLA) comprising of *Acanthamoeba spp., Naegleria fowleri, Balamuthia mandrillaris and Sappinia diploidea* (Khan, 2006b, Lorenzo-Morales et al., 2015) have been implicated. Of major concern is a foremost parasitic agent of human disease dated back to the late 1950s, the genus *Acanthamoeba*--an aerobic, single-cell, eukaryotic protist and amphizoic organism that exists as both FLA and parasitic pathogen.

The study of amoeba dates back to the discovery of the early microscope in the 1870s (Schuster and Visvesvara, 2004). They diverged from the earliest eukaryotes about an estimated 1×10^9 years ago, based on its sRNA analysis (Siddiqui and Khan, 2012a).

1.2 Classification of Free-living Amoebae

Remarkably, there are only four out of the many genera of FLA that are linked with human disease. These include *Naegleria fowleri, Sappinia diploidea, Balamuthia mandillaris and Acanthamoeba spp.* (Figure 1.1; Table 1.1). However, according to Dart (Dart et al., 2009), *Acanthamoeba castellanii* is the most commonly isolated of all FLA.

Naegleria spp. is a thermophilic, amoebo-flagellate, free-living protozoan responsible for primary amoebic meningo-encephalitis (PAM), a fatal human infection of the central nervous system (De Jonckheere, 2002). This protozoan parasite is universally dispersed in water and soil at temperatures ranging between 30°C and 45°C. Its characteristic life cycle includes three stages of infective trophozoites, a brief non-dividing flagellate stage and the cystic stage (Visvesvara et al., 2011).

Sappinia diploidea was described as a FLA isolated from lizard faecal droppings and soil. It causes granulomatous amoebic encephalitis (an inflammatory necrosis of the brain tissue following amoebic infiltrates that presents with focal paralysis, seizures, brainstem symptoms and other neurological problems) in immuno-compromised individuals (Gelman et al., 2001). It causes various infections of the central nervous system, lungs

and skin (Visvesvara et al., 2007a). *Balamuthia mandillaris* was recently isolated from the brain of a baboon that had died of suspected meningo-encephalitis (Khan and Siddiqui, 2009). In humans, *Balamuthia mandillaris* causes subacute or chronic granulomatous meningoencephalitis that may result in death within one week to few months of onset of neurological symptoms in both immunocompetent children and immunocompromised elderly individuals whose susceptibility to infection is due to decrease in activity of their immune system.
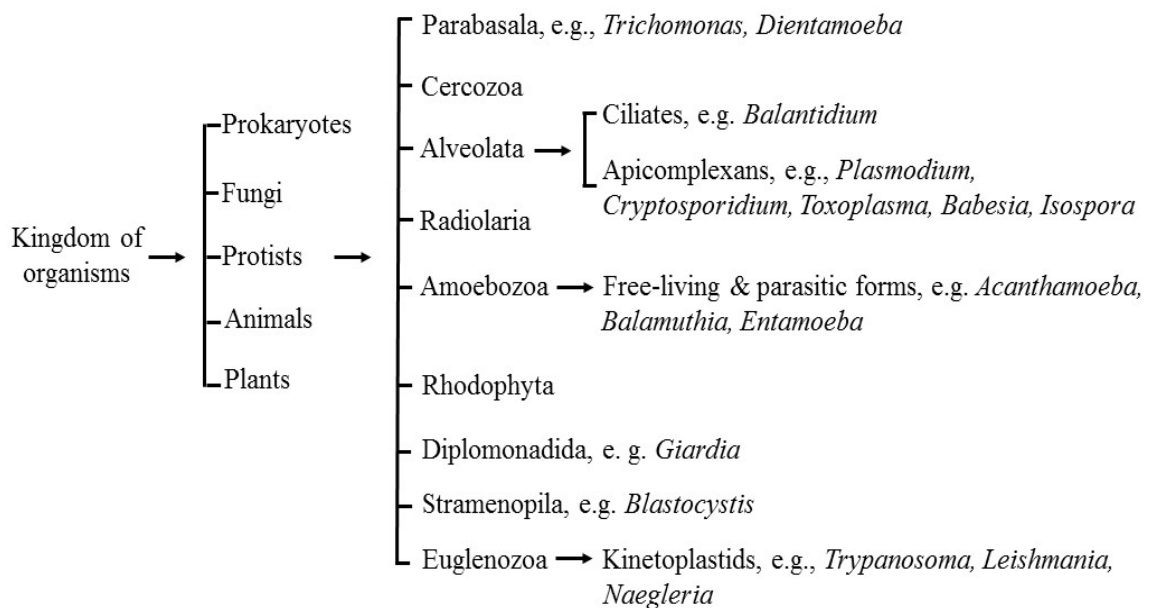
Figure 1-1: Classification of protists based on their ribosomal RNA sequence. All living organisms are divided into three domains based on the development of molecular methods of ribosomal RNA sequence: **(i) Archaea** containing prokaryotes that inhabits the extreme environments, **(ii) Bacteria** containing the prokaryotes that comprise an extensive large group of microorganisms, and **(iii) the Eukarya,** that includes all remaining nucleated uni- and multicellular organisms. The Protists were the first to evolve from eukaryotes about 1.5 billion years ago. Further illustration of the phylogenetic divergence of the FLA protists is shown (Modified from Khan, N.A. (2009)).

Balamuthia mandillaris and *Acanthamoeba spp.* are known as opportunistic pathogens. *Acanthamoeba spp.* have been found to cause keratitis of the human cornea resulting in inflammation that can ultimately lead to blindness. It is also responsible for granulomatous amoebic encephalitis (GAE), a disease of the central nervous system (Visvesvara et al., 2007a, Visvesvara et al., 1993, Ma et al., 1990a). These free-living

amoebae can become pathogenic to humans in their parasitic forms, according to the reports of Page (Page, 1967).

Table 1-1: Comparative features of four genera of pathogenic free-living amoebae

	Acanthamoeba spp. (systemic infections)	*Acanthamoeba* spp. (keratitis)	*Naegleria fowleri*	*Balamuthia mandrillaris*	*Sappinia diploidea*
Trophic amoeba	15–30 µm, with acanthopodia; vesicular nucleus; speed 0.3–0.4 µm/s		15–30 µm, with anterior, eruptive, ectoplasmic pseudopod; speed ~1.0 µm/s	12–60 µm, polymorphic; speed ~0.25 µm/s	45–85 µm, with thick pellicle, often with wrinkles; binucleate; sluggish movement
Flagellate stage	Not found		Transforms into flagellates; typically with two flagella	Not found	Not found
Cyst stage	2-layered wall with pores; 10–15 µm diameter; cysts form in brain and corneal tissues		2-Layered wall with pores; 7–15 µm diameter; cysts not formed in brain tissue	3-Layered wall, lacking pores; 10–30 µm diameter; cysts form in brain tissue	Thick-walled, 13–37 µm diameter; binucleate; pores (?); cysts not seen in tissue
Habitat	Soil, water, domestic and hospital environments		Soil; warm fresh waters, thermally polluted streams	Soil, possibly fresh water	Soil, fresh water; isolated from herbivore faeces
Diseases	Granulomatous amoebic encephalitis; cutaneous and sinus infections	Amoebic keratitis	Primary amoebic meningoencephalitis	Granulomatous amoebic encephalitis; cutaneous and sinus infections	Amoebic encephalitis; granuloma not seen; possibly sinus infections
Risk factors	Immuno-compromised status	Soft contact lens wear; wearing lenses while swimming	Activity in warm fresh waters; getting water into nostrils (diving)	Immunocompromised status; breaks in skin contaminated with soil	Insufficient information
Diagnosis	IFA staining; biopsy of lesions; neuroimaging	Corneal scrapings and culturing	CSF examination for trophic amoebae	IFA staining; biopsy of lesions; neuroimaging	Biopsy of lesions; neuroimaging

Incubation period	Weeks to months	Days	Days	Weeks to months, even years	No data, but probably similar to *Acanthamoeba*
Symptoms	Headache, fever, abnormal behaviour	Intense pain, lacrimation, photophobia	Headache, fever, abnormal behaviour	Headache, fever, abnormal behaviour	Headache, photophobia, vomiting, loss of consciousness
CSF	Elevated WBCs and protein; glucose level normal to low	Not relevant	Elevated WBCs and protein; glucose level normal to low	Elevated WBC's and protein; glucose level normal to low	Insufficient information
Antimicrobial therapy	Azole compounds, pentamidine, flucytosine	Chlorhexidine or PHMB, along with propamidine or hexamidine	Amphotericin B, rifampin, miconazole	Fluconazole, azithromycin, pentamidine, flucytosine	Azithromycin, pentamidine, itraconazole, flucytosine
Prognosis for recovery	Poor	Excellent	Poor	Poor	Insufficient information
Estimated numbers of cases	~200	>3000	~200	>100	1

Table 1.1 was modified and adapted from (Schuster and Visvesvara, 2004)

1.3 Types of *Acanthamoeba* spp.

In 2005, Booton and colleagues (Booton et al., 2005) reported 25 named species of the *Acanthamoeba* genus composition with several pathogenic *Acanthamoeba,* including *A. castellanii, A. culbertsoni, A. hatchetti, A. palestinensis, A. polyphaga, A. lugdunensis, A. keratitis, A. rhysodes, A. astronyxis*, and A. *byersi*. Non-pathogenic types include *A. comandoni, A. triangularis, A. tubiashi, A. divionensis, A. griffini,* A. *jacobsi, A. lenticulata, A. mauritaniensis, A. pustulosa, and A. terricola* (now known as *A. castellanii* Poussard). Curiously, there is little knowledge of the genetic differences between the pathogenic and non-pathogenic strains of *Acanthamoeba* spp. (Costas et al., 1983); (Yagita and Endo, 1990, Khan et al., 2001).

1.4 Biology of *Acanthamoeba* spp.

Acanthamoeba derived its name from the Greek word 'Acantha' meaning a spiky, thorny surface membrane projection. Castellanii discovered *Acanthamoeba* in 1930 from a contaminated cell culture of the fungus *Cryptococcus pararoseous* (Page, 1967). It was initially identified as *Hartmanella castellanii* of the genus *Hartmanella* as either an oval

shaped pseudopodia-amoebae (13.5-22.5 μm in diameter) or as a double-walled cyst of 9-12 μm in diameter. The following year, Volkonsky re-classified the amoebae into a new genus *Acanthamoeba* based on its morphology, locomotion and its ability to form cysts (Volkonsky, 1931).

Acanthamoeba is aerobic in nature and has been classified into classes I, II and III according to the rRNA sequences or based on the morphological features of the mature cysts (Khan, 2006b, Visvesvara et al., 2007a, P. Stratford and Griffiths, 1978). Recently, about 25 species of the *Acanthamoeba* genus exist but some of them are known as causative agents of AK. About 20 different genotypes (T1-T20) of this unicellular protist have been recognised (Corsaro et al., 2015, Magnet et al., 2014, Fuerst et al., 2015, Qvarnstrom et al., 2013a, Siddiqui and Khan, 2012a, Adamska, 2016) based on the gene encoding its 18S rDNA sequences. According to previous reports, Stothard and colleagues (Stothard et al., 1998a) were the first group to describe the complete phylogenetic/molecular genotyping of *Acanthamoeba* nuclear 18S rRNA gene sequence (Gast et al., 1996a, Adamska, 2016). Appendix I shows the *Acanthamoeba* strains classified according to the description of the genotypes (introns was removed for analytical purpose) and species (Magnet et al., 2014) while I highlight the morphological classes of selected pathological strains.

About 8 species, 5 genotypic classes of pathogenic *Acanthamoeba* have been implicated in *Acanthamoeba* keratitis (AK) among the immunocompetent individuals (Maycock and Jayaswal, 2016). AK is a very painful, slowly worsening, vision-threatening corneal infection caused by *Acanthamoeba* following exposure of the traumatised cornea (Tomlinson et al., 2000, Zimmerman et al., 2016) to *Acanthamoeba*-contaminated water sources. It is often associated with contact lens use. GAE, the other main disease condition associated with *Acanthamoeba* have been linked with the *Acanthamoeba* T4 genotype. The *Acanthamoeba* T4 genotype are thought to reflect increasing expression of mannose-binding protein as been reported in most *Acanthamoeba* strains known to cause AK in both contact lens wearers and non-lens wearers (Kilvington, 2004). In immuno-compromised individuals, *Acanthamoeba* can cause other diseases, including cutaneous lesions and sinusitis. Since the earliest reported cases of *Acanthamoeba* in human subjects: GAE (Jager and Stamm, 1972), AK in the United Kingdom (Nagington et al., 1974) and the United States of America (Jones, 1979, Visvesvara et al., 1975), several thousand cases have been described worldwide (Kilvington and White, 1994).

1.5 Life Cycle of *Acanthamoeba* spp.

Until recently, it was thought that there are only two distinct parts of *Acanthamoeba* life cycle namely the vegetative (feeding), actively motile trophozoites; and the double layered, ring-shaped, immotile, dormant mature-cysts (Schuster, 2002, Khan, 2006b, Siddiqui and Khan, 2012b) which are produced under adverse conditions (figure 1.2). Thus, *Acanthamoeba* possesses two distinct cellular differentiation processes of encystment and excystment forms (Hirukawa et al., 1998). Nevertheless, in the first year of my project, I characterised a third life-stage: the fragile protocysts, which are likely to be more susceptible to anti-parasitic drugs because they lack the double cell wall of mature cysts (Chapter 2)**.**
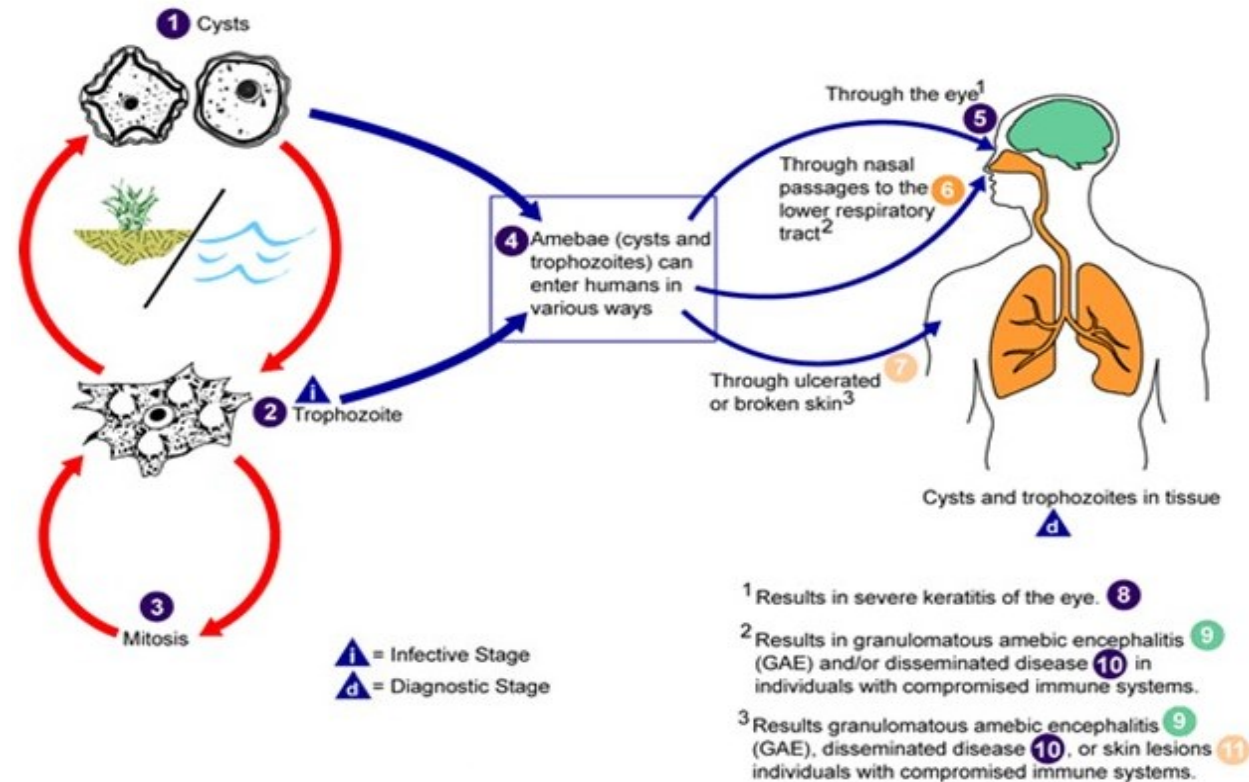
Figure 1-2: Life cycle of free-living *Acanthamoeba*. During unfavourable conditions, *Acanthamoeba* begin to encyst to form the (1) mature cyst but when normal growth conditions prevail, the amoeba exits as (2) trophozoites. (3) Reproduction is by asexual method. (4) *Acanthamoeba* infects human host either in the form of the trophozoites or the mature cyst by direct contact through (5-6) contaminated water supplies or indirectly through infected hydrogel contact lens on cornea. (7) Other sources of infection is through the lacerated skin, nasal passage or other body tissues to cause (8) *Acanthamoeba* keratitis (AK) or (9-11) Granulomatous Amoebic encephalitis (GAE) and skin lesions in the immune-compromised individuals (Adapted from CDC, 2016).

1.5.1 *Acanthamoeba* trophozoites

The uni-nucleated amoebic trophozoite is a flat, irregular shaped protozoan of diameter between 12-35 μm, with differences in size dependent on the isolate, species and genotype. They possess fine surface protoplasmic projections, termed acanthapodia, 20-50 μm in length (Visvesvara, 1991), slightly bigger than an average cell of ~1-30 μm in diameter. This morphological feature is present during the logarithmic growth phase of *Acanthamoeba* under either a naturally nourishing environment and/or in artificial nutrient medium. Under favourable environmental conditions characterised by abundant food supply (see Section 1.5.1.1. below), neutral pH, appropriate temperature (i.e. 30°C) and osmolality (50-80 mOsmol), *Acanthamoeba* exist in the trophozoites stage and reproduce asexually by binary fission (Khan, 2006a) every 8 to 24 hours. The acanthapodia or pseudopodia support its active feeding based on chemotactic response to signals of concentration gradients of food particles in its immediate environment.

However, in the laboratory, *Acanthamoeba* can be cultivated either in 2.5% non-nutrient agar (NNA) seeded with *Escherichia coli* (Visvesvara et al., 2007b) as a food source or axenically (absence of living organism) in Ac#6 culture medium containing peptone, glucose, L-methionine and yeast extract (Khan, 2006a). The spine-like acanthapodia are essential for parasitic adhesion onto biological or inert surfaces, parasitic locomotion, and capture of prey (Figure 1.3). The trophozoites plasma membrane possesses abundant phospholipid (25%), sterols (13%) and lipophosphonoglycan (29%), but lacks cellulose. The *Acanthamoeba* plasma membrane is distinguishable from mammalian cells by the presence of lipophosphonoglycan with sugars exposed on both sides of the membrane (Korn et al., 1974).
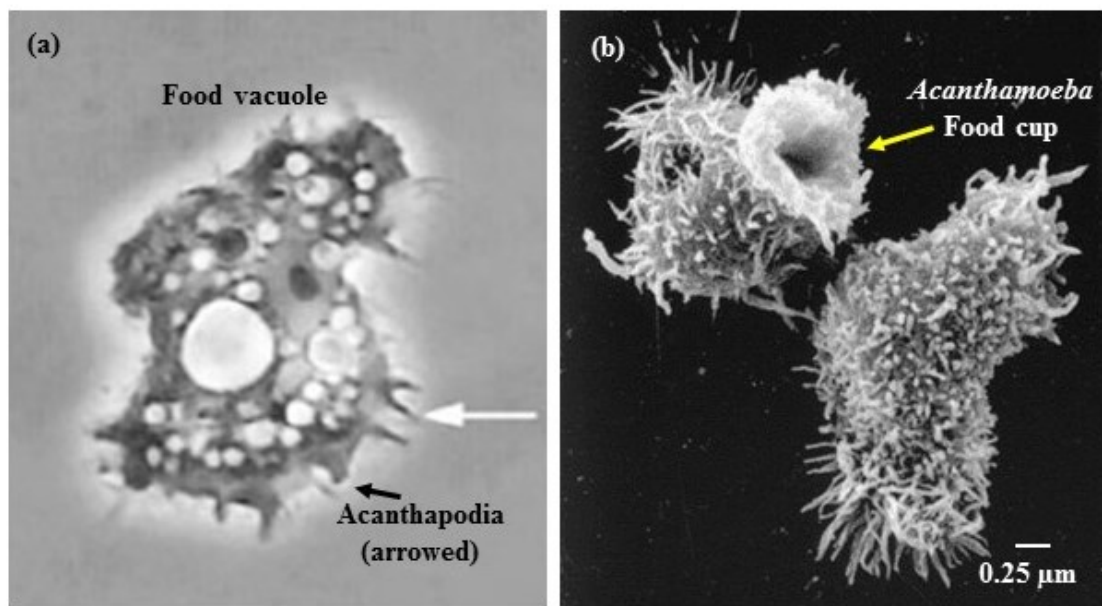
Figure 1-3: Morphology of *Acanthamoeba* (ATCC 50370) trophozoites. (a): Acanthapodium (arrowed) under phase-contrast light microscope. **(b):** scanning electron microscopy of the trophozoites showing the food cup (Scale bar = 0.25 µm). Courtesy: Figure 1.3(a): Dr Simon Kilvington, University of Leicester; and figure 1.3(b): (ChÁVez-MunguÍA et al., 2005).

1.5.1.1 Acanthapodia/Pseudopodia of *Acanthamoeba* trophozoites

The acanthapodia or pseudopodia support both feeding and motility based on chemotactic responses to signals such as concentration gradients of food particles and other substances in the immediate environment. *Acanthamoeba* feeds on organic materials, bacteria, algae, yeasts as food sources (Allen and Dawidowicz, 1990, Bonilla-Lemus et al., 2010, Bonilla-Lemus et al., 2014a) and microscopic organic particles (Marciano-Cabral and Cabral, 2003, Nagyová et al., 2010). The acanthapodia functions in active feeding either by non-specific pinocytosis by membrane invagination and/or by receptor-dependent phagocytosis into the food vacuoles (Allen and Dawidowicz, 1990, Khan, 2006a, Brown et al., 2017). The vegetative *Acanthamoeba* (trophozoites) preferentially feed on non-pigmented, non-encapsulated, non-toxic bacteria, and gram-negative that lack thickened peptidoglycan of Gram positive bacterial thought to be difficult for digestion (Newell et al., 1983, Weekers et al., 1993).

Acanthamoeba (trophozoites) also use their temporary structures formed on their surfaces, termed 'food-cups' (see yellow arrow in Figure 1.3b above) or otherwise called

amebostomes (Khan, 2001) to feed on algae, yeasts (Allen and Dawidowicz, 1990) and microscopic organic particles on surfaces (Pickup et al., 2007, Barker and Brown, 1994) and the air-water interface (Preston et al., 2001). In the presence of bacteria, trophozoites naturally undergo morphological enlargement and clump together in groups of about 10-30 cells when suspended in broth culture (Byers et al., 1991). Nevertheless, certain bacteria such as *Legionella pneumophila* or *Mycobacterium avium* could resist digestion in order to survive within *Acanthamoeba* as either facultative or obligate intracellular bacteria (Barker et al., 1992, Greub and Raoult, 2004a). Apart from its role in feeding, the pseudopodia characterised by cytoplasmic flow of organelles usually alternates extension and retraction of cytoplasmic streaming to accomplish *Acanthamoeba* movement (Marciano-Cabral and Cabral, 2003, Taylor, 1977).

1.5.1.2 Cytoplasmic organelles of *Acanthamoeba* trophozoites

The granulated cytoplasm is comprised of numerous mitochondria, food vacuoles, contractile vacuoles, ribosomes and a single nucleous (Visvesvara et al., 2007a) The abundant mitochondria (genomic DNA size ~ 41,591bp) generate substantial energy required for metabolic activities including motility, nutrition, cell division and other cellular responsibilities via oxidative phosporylation.

Acanthamoeba possess two main types of vacuoles namely the large contractile and smaller digestive vacuoles (Burger et al., 1995). *Acanthamoeba* utilises its large contractile vacuoles to expel water for osmotic regulation, preceding parasitic encystment; while the smaller digestive vacuoles or lysosomes are used for breaking down ingested food particles and to destroy foreign invaders (Siddiqui and Khan, 2012c). Both types of vacuoles are distinguishable by the absence of flocculent content in the digestive vacuole (Neff and Neff, 1969). The haploid genome of *Acanthamoeba* measured by pulse-field gel electrophoresis comprises approximately $2.3 - 3.5 \times 10^7$ bp, with more than 5000 transcripts (Byers et al., 1991). More recently, the entire genome of *Acanthamoeba castellanii* has been shown to contain 15,455 compact intron-rich genes (Clarke et al., 2013).

1.5.1.3 Differentiation of *Acanthamoeba* trophozoites

Glycogen has been implicated as the major source of glucose in *Acanthamoeba;* this is supported by the relative down-regulation of glycogen during parasitic encystment. *Acanthamoeba* trophozoites differentiate by undergoing spontaneous phenotypic

transformation (encystment) into the non-dividing, doubled walled dormant mature cyst form (Tomlinson and Jones, 1962) during harsh environmental conditions such as desiccation, extremes of temperature, pH and nutritional starvation (Martinez and Janitschke, 1985).

The differentiation process of *Acanthamoeba* trophozoites into the mature-cyst wall formation involves degradation of glycogen and synthesis of cellulose, which forms a large part of the inner wall of mature cysts (Clarke et al., 2012, Moon et al., 2017). Cellulose is also major polysaccharide in many bacteria and algae cell walls and consists of linear chain of glucose units joined by β-1, 4 linkages (Mehdi and Garg, 1987, Moon and Kong, 2012, Stewart and Weisman, 1972).

Several efforts to understand the molecular mechanisms underlying *Acanthamoeba* differentiation (Schuster and Visvesvara, 2004) has led to the emerging findings and biological significances of the identities of three genes expressed during *Acanthamoeba* cellular differentiation. These genes include heat shock protein (hsp70), actin-I and EF-1 which were all upregulated in the trophozoites stage as compared to the mature stage. The actin-I is involved in various cellular processes such as differentiation, regulation of cell growth and motility (Pollard and Cooper, 2009). The reoccurrence of favourable conditions such as abundance of nutrition, neutral pH and appropriate temperature (~ 30 °C) triggers mature cysts conversion back into the infective trophozoites form as shown in Figure 1.4 (Henriquez, 2009).

1.5.2 *Acanthamoeba* mature cysts
The mature cysts are formed during a stationary and decline growth phase. They are characterized by the accumulation of increased metabolic waste products with evident morphological changes. This includes the termination of cell growth, expulsion of excess food and water and decreased cytoplasmic mass. These changes eventually cause decreases in the cell volume, weight and diameter followed by condensation of trophozoites to form the resistant double walled cysts (Band and Mohrlok, 1973, Ahmed Khan, 2003). In the laboratory, the presence of metabolic inhibitors and trophozoites in nutrient-free (NNA) encystment medium may also trigger *Acanthamoeba* cysts formation (Figure 1.4).

The immotile *Acanthamoeba* mature-cysts are smaller than the trophozoites, measuring about 5–20 μm in diameter (Khan, 2006a, Marciano-Cabral and Cabral, 2003, Visvesvara et al., 2007b). The double-walled envelope is highly resistant to various biocides, pH and extreme temperature. While fully mature dormant cysts are readily blown away by air currents, the double wall resists desiccation, disinfectants, physical, chemical and radiological challenges (Kilvington and Price, 1990) due to the formation of a dense, impermeable cyst-wall structure that equally reinforces parasitic resistance to anti-amoebic therapeutics (Martín-Navarro et al., 2008, Lorenzo-Morales et al., 2013).

This cyst wall is characterized by irregular (Visvesvara, 1991) outer exocyst and inner endocyst separated by electron-lucent intercyst space of ~850 nm thickness. Both exocysts and endocysts meet at points where they jointly form pores termed ostioles. The ostiole aids the ease of escape of hatching (excysting) trophozoites during return of favourable conditions. These ostioles (three to four) are each closed by an operculum (Mehdi and Garg, 1987, Bowers and Korn, 1969, Neff and Neff, 1969, Krishna Murti and Shukla, 1984, Chávez-Munguía et al., 2013, Moon et al., 2014)

Previous experiments have established the involvement of a catalytic domain of the enzyme--glycogen phosphorylase and cellulose synthetase gene(s) in the encystment process of *Acanthamoeba*, particularly, in the formation of the inner layer of the mature cyst, which consists mainly of cellulose (Lorenzo-Morales et al., 2008).

Earlier studies have also generalised the chemical composition of the matured amoebic cyst as about 33 % protein, 35 % cellulose, D-glucopyranose polymer (Tomlinson, 1967, Blanton and Villemez, 1978), 4-6 % lipid, 8 % ashes (dust) and 20 % unidentified materials (Neff and Neff, 1969). The outer cyst wall is composed of 36 - 45 % acid-resistant protein (Lorenzo-Morales et al., 2008) and 20 to 34 % polysaccharides. However, the inner cyst wall contains cellulose accounting for almost 10 % of the overall cyst dry-weight (Tomlinson and A. Jones, 1962, Neff and Neff, 1969, Hirukawa et al., 1998, Dudley et al., 2009). According to Duarte and colleagues (Duarte et al., 2013) the peculiar morphology and size of the cysts are very indicative of the characteristic *Acanthamoeba species* variation. In addition, the chemical composition of this cyst wall varies between different genotypes of *Acanthamoeba spp* (Neff and Neff, 1969).
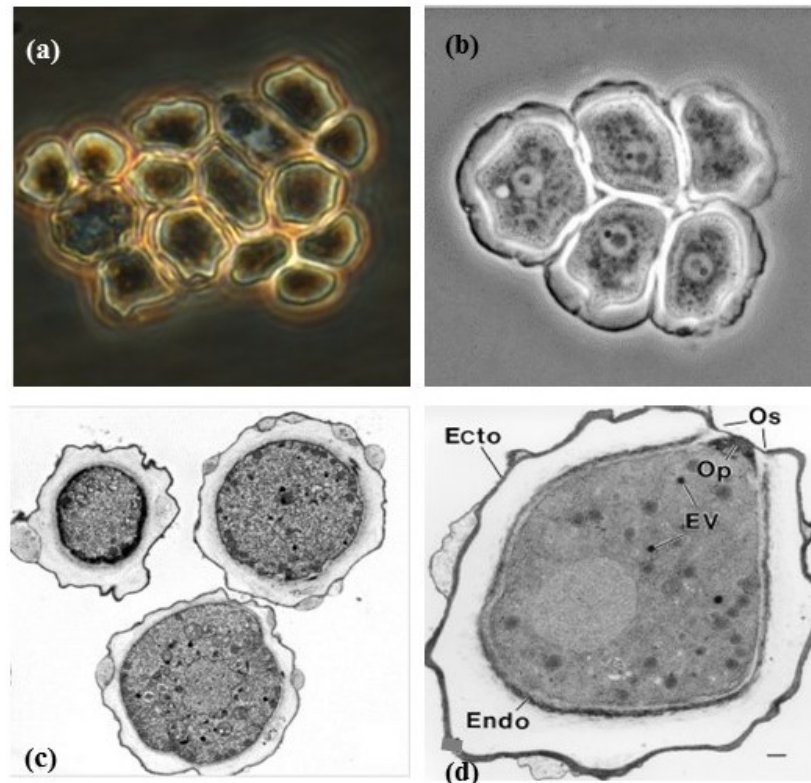
Figure 1-4: Morphology of *Acanthamoeba* (ATCC 50370) mature cysts. Top (a-b): Non-Nutrient Agar (NNA) mature cysts cluster under phase contrast light microscope. Below (c-d): transmission electron microscopy of the double-walled mature cyst with ectocyst (Ecto), endocysts (endo), Ostiole (os), Operculum (Op) and encystation vesicles (EV) within cytoplasm. Scale bar for figure 4d = 0.5 μm. Courtesy: Figure 4(a) Adapted from this study; figures 4(b-c): Dr Simon Kilvington, University of Leicester; and figure 4(d): Chávez-Munguia et al., 2005.

1.5.3 Discovery of *Acanthamoeba* protocysts

Rubin perhaps was the first scientist to have described an additional life stage referred to as an "immature cyst" (subsequently called protocysts) form (Rubin and Maher, 1976). This form is characterised by the presence of a single cell wall rather than the double cell wall of the mature cyst. The protein component of the protocyst cell wall consists mainly of a single peptide (about 70 kDa in size) with eight minor peptides. Unlike the mature cyst, protocysts and trophozoites lack cellulose (Ulsamer et al., 1969, Dearborn and Korn, 1974).

A recent outbreak of AK among contact lens users in the United States led to the recall of the Complete Moisture-Plus® contact-lens solution from the market for suspicion of its contamination with *Acanthamoeba* (Verani et al., 2009). Upon further investigation, it

was found that the propylene glycol in the lens solution induced incomplete encystment, with a morphology similar to the ''immature cysts'' described by Rubin. Kilvington and colleagues (Kilvington et al., 2008) subsequently called these immature cysts protocysts. Subsequent studies by Kliescikova and colleagues (Kliescikova et al., 2011) also described the rapid differentiation of *Acanthamoeba* spp. into non-motile, cyst-like forms (that he termed 'pseudocysts'), using propylene glycol.

In comparison with the mature cysts, protocysts (Kilvington et al., 2008) possess a single-layered coat, which fluoresce green upon staining with calcofluor white dye. The single protocyst wall is inadequate to protect the cell against acidic or encystment media (Kilvington et al., 2008, Kliescikova et al., 2011). Interestingly, propylene glycol has gained wider industrial applications as an ocular lubricant and osmotic agent in contact lens solutions such as MoisturePlus®, MeniCare Soft® (Kilvington et al., 2008). The concept of the protocysts is similar to the rapid internalisation of flagella by *Trichomonas vaginalis*, which does not possess a "true" cell wall (Pereira-Neves and Benchimol, 2007, Pereira-Neves et al., 2003).

1.6 Distribution of *Acanthamoeba* spp.

Acanthamoeba is an opportunistic, eukaryotic protist, ubiquitously distributed worldwide with the unique ability to survive in natural, man-made and/or clinical nichés. Relatively, the abundance of *Acanthamoeba* in nature varies with season, bacterial population, temperature, pH, salinity and temperature (Rodriguez-Zaragoza, 1994). *Acanthamoeba* have been isolated in diverse natural environments including soil, fresh water lakes, ponds, rivers, hot spring resorts (Kao et al., 2012), swimming-pool waters (Landell et al., 2013), spas (Fabres Laura et al., 2016), water-air interface and thermally polluted factory discharges. Other sources include man-made cooling towers, Jacuzzi tubs, humidifiers, air conditioning units (Gomes et al., 2016) domestic water supplies (Lass et al., 2017) bottled mineral water, shower heads, rain-water harvested from roofing materials (Dobrowsky et al., 2017) and sewages.

In most part of United Kingdom, the wide spread use of bathroom storage water tanks and hard water supplies characterised by lime-scale is often implicated with proliferation of *Acanthamoeba* infections (Kilvington, 2004) in the Southern regions of UK unlike in the Northern and/or Midlands (Radford et al., 2002, Casero et al., 2017). But in clinical scenarios, moist areas in hospitals (Muchesa et al., 2017) dialysis units, surgical

equipment, human nasal cavities, pharyngeal swabs, corneal biopsies, cerebrospinal fluids, urine and stool samples of some patients, urinary catheters have been implicated (Barbeau and Buhler, 2001).

Acanthamoeba have been isolated from 20-30% of domestic water supplies and streams of Mexico Basin in Central Mexico (Bonilla-Lemus et al., 2014b, Bonilla-Lemus et al., 2010). The parasites was also found in hospital water networks, and swimming pools, in 68.9% of hot water samples from hot water faucets in Korea; hot water tanks, hydrotherapy bath, dental units, air-conditioning units and soil samples (Jeong and Yu, 2005, Corsaro et al., 2010, Shokri et al., 2016). Further to this, Kilvington (Kilvington, 2004) had implicated household storage water tanks, which promote FLA colonisation in domestic water system. In England alone, he reported FLA colonisation in about 89% homes of patients suffering AK out of which 76 % were recovered from bathroom sink cold-water taps sampled.

The reported cases of AK among immuno-competent individuals in developed nations have been generally characterised by necrotic, oedematous, stromal inflammation of the cornea; and 83-90 % of those affected are contact lens users. The majority display poor contact lens hygiene with bacterial contamination (Dart et al., 2009) and biofilm formation providing a nutrient source for *Acanthamoeba* (Lorenzo-Morales et al., 2010). However difficult it is to estimate the incidence of AK among contact lens wearers, it ranges between 1 - 5 per million daily wear soft contact lens users per year in Europe, USA and Australia (Moore et al., 1987a, Radford et al., 1998, Schaumberg et al., 1998). In the United Kingdom, the incidence rate of AK among contact lens wearer is approximately 0 - 85 per million wearer per year (Kilvington, 1993, Seal et al., 1992, Kilvington, 2004). By contrast, in developing nations, AK is often associated with agricultural-based occupations and ocular trauma (Auran et al., 1987, Moore et al., 1987b, Ma et al., 1990b, Brewitt, 1997).

1.7 The Cornea anatomy and susceptibility to AK

The cornea is a transparent, dome-shaped and avascular membrane of the outer layer of the eyeball. It has a diameter of 10 ± 0.56 mm with a central thickness of about 450 - 600 µm and peripheral thickness of about 650 - 750 µm. It comprises approximately one sixth of the entire ocular structure due to its extension to form the sclera (limbus). The function of the limbus is to support the cornea in accessing oxygen supply from the air. Its anterior

humour is a clear nutrient fluid, which is drained by the network of trabecular meshwork located at the intersection of the cornea, iris and the sclera (Khan and Siddiqui, 2009) (Figure 1.5).

1.8 Histology of the Cornea

The corneal epithelium is a very thin layer of non-keratinised stratified squamous epithelium of fast growing and readily regenerating cells that are often moistened by tears to enable adequate protection and water regulation around the eyes. It is shielded from the external environment by its basal layer.
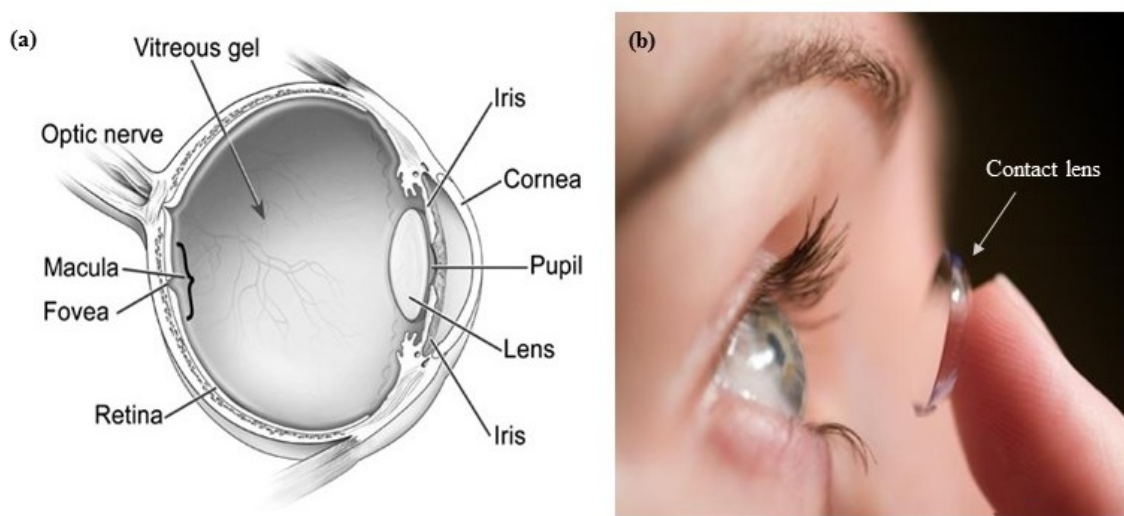
Figure 1-5: The Cornea. (a) The schematic illustration of the human cornea. (b) Application of a soft hydrogel contact lens unto the cornea. (Source: Figure 1.5 (a and b) were modified and adapted from National Eye Hospital, National Institute of Health, USA (2012).

Other histological features of the cornea include the cornea stroma, which constitutes 95% of the thickness (0.5 – 0.6 mm at the centre; 0.6 – 0.8 mm at the periphery) of the cornea and is a transparent middle layer composed of collagen fibres and keratocytes. The stroma serves to repair and regenerate damaged cells (Khan and Siddiqui, 2009). The corneal endothelium (Figure 1.6) is the modified basement membrane from where corneal cells are derived and functions as regulator of fluid and solute transport.

Contact lenses rest on the surface of the cornea thereby assisting the lens to focus light on the retina (Cao et al., 1998). Although the cornea is defended against infections by tear films, it is still inadequately shielded from invading *Acanthamoeba spp*. Perhaps, it is the

agitation and disruption of the tear film by the contact lenses that encourages hypoxia of the corneal epithelium, which lead to increasing adhesion of microorganisms to the eyes surface (Cao et al., 1998).
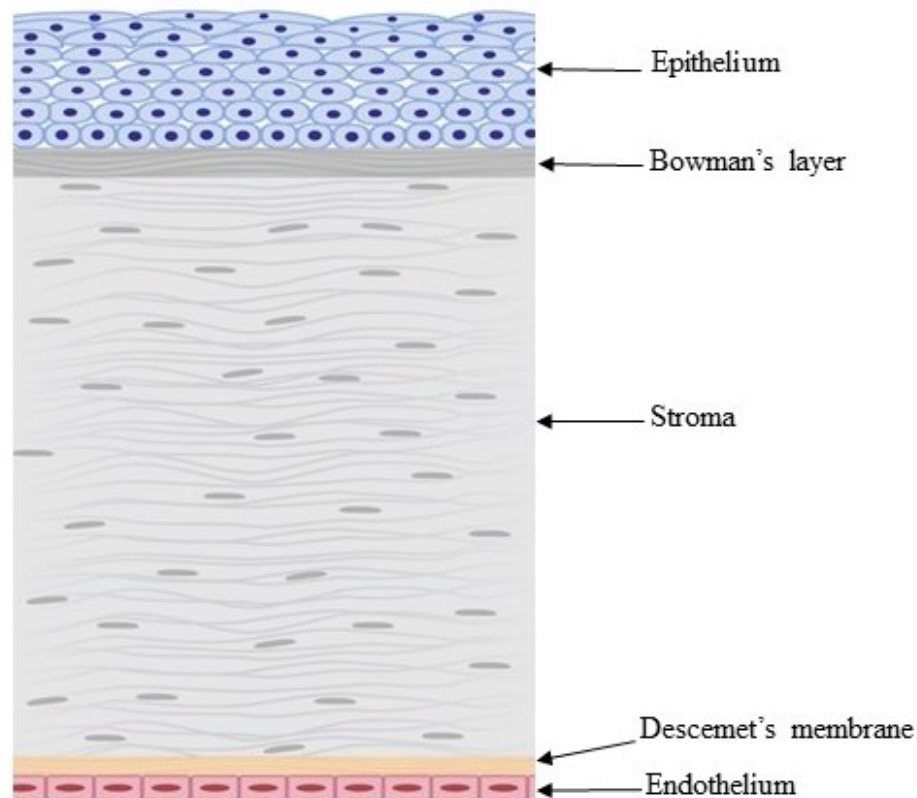
Figure 1-6: The cross-section of the cornea: The basis of the structured layers of the cornea is a reflection of its combined histological morphology and chemical composition. The anterior border is made of non-keratinised squamous epithelium whose basal membrane rests on the Bowman's layer. The Bowman's layer is $8 - 14$ µm thick, tough mass of condensed acellular (non-regenerative) collagen fibril that is resistant to mechanical injuries, and sited superficially above the stroma. The stroma consists of ~ 75 % water, mucopolysaccharide ground substance with numerous collagenic lamellae and parallel arrangements of elastic fibrils to the corneal surface. The Descemet's membrane forms the posterior border towards the anterior chamber. Eventually, this Descemet's membrane transits into endothelial cells that are formed from the homogenous layer of amorphous lamellae (Adapted from Parker et al., 2017).

Kilvington and colleagues first showed that a traumatised cornea facilitates *Acanthamoeba* infection leading to AK in 1990 (Larkin et al., 1990, Kilvington, 2004). However, Omana-Molina (Omaña-Molina et al., 2010) have challenged this idea arguing that accumulation of mature cysts leads to re-infection without the necessity of cornea damage. Other scientists have made it clear that the abundance dormant mature cysts in

the cornea, perhaps remains the most important sources of recurrent AK in clinical patients because the cysts rapidly reconvert to trophozoites under favourable conditions (Mathers et al., 1987, McClellan et al., 2002, Hurt et al., 2003, van Klink et al., 1996); and (Leher et al., 1998).

1.9 *Acanthamoeba* infection of the Cornea

As a result of the cooler temperature of the cornea (about 32-35 °C), the cornea is probably the only recognised human tissue which is sufficiently susceptible to effective colonization of pathogenic *Acanthamoeba* (Hurt et al., 2003) (Schuster and Visvesvara, 2004) in both healthy and immuno-compromised individuals. This low temperature is important for infection. For example, Schuster and Visvesvara (Schuster and Visvesvara, 1998) found that clinical strains of *Acanthamoeba* could not adapt at 37°C until such temperature was otherwise reduced to 30°C. Although, in the absence of any trauma to the corneal epithelial tissue, the host non-specific defences such as tears and eye blinking readily wash off most microbial agents from the ocular surface. However, contact lens wear has the tendency to act as a mechanical vector derived from either human handling, contaminated environment, water supplies or contact lens storage cases (Casero et al., 2017). Perhaps, *Acanthamoeba* adhesion serves the role of prolonging parasitic retention time; upregulate surface expression of corneal mannosylated glycoprotein receptors to which the trophozoites mannose-binding glycoprotein binds and consequently, allowing for a deeper tissue invasion that leads to cytopathology (Jaison et al., 2009).

1.10 *Acanthamoeba* keratitis

AK is a very painful, slowly worsening, vision-threatening corneal infection caused by *Acanthamoeba* following exposure of the traumatised cornea and/or contact lens (Tomlinson et al., 2000, Zimmerman et al., 2016) to *Acanthamoeba*-contaminated water sources. Although AK is common in immunocompetent individuals and it can affect any age group, the infection does not confer immunity despite persistent parasitic re-infection. In the developed countries, the use of contact lens is thought to be a predominant risk factor of AK while ocular trauma has being implicated in the many developing countries (Page and Mathers, 2013). However, AK may occur as a unilateral eye disease, it may also be presented bilaterally characterised by early symptoms such as pain, photophobia, watering and punctate keratopathy often confined to the epithelium. In later stage of the

infection, there may be a characteristic breakdown of the epithelium with recurrent course of stromal inflammation as it progress into the stroma. This may present a sterile inflammatory reaction that manifests as immune ring ulcers and scleritis associated with a severe and persistent pain. The later stage of AK is characterised by the thinning of the stroma, corneal opacity, hypopyon, corneal perforation, cataract, glaucoma and posterior segment inflammation (Blackman et al., 1984, Bacon et al., 1993a, Yang et al., 2001) (Figure 1.7).
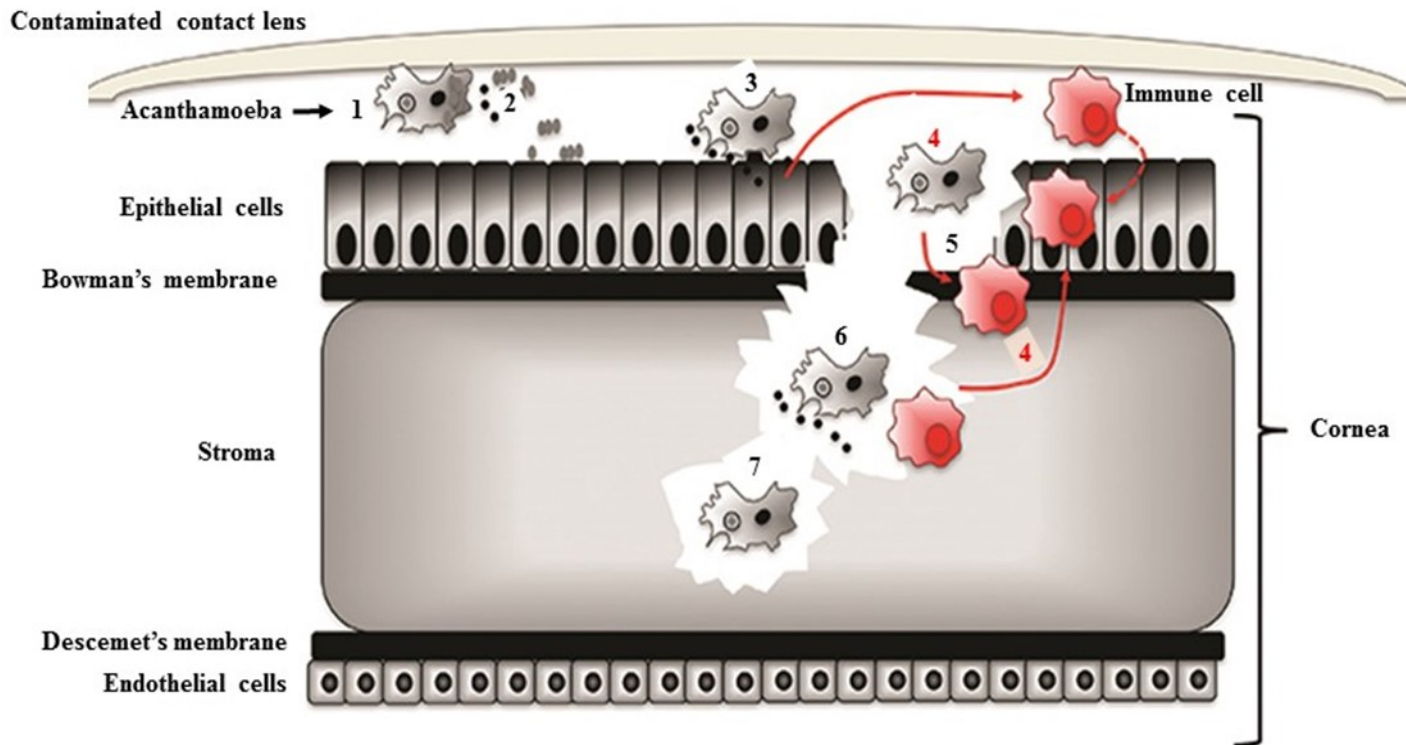
Figure 1-7: Mechanism of *Acanthamoeba* keratitis-related corneal infection from contaminated water source in contact lens wearer. The early infection comprise of (1) *Acanthamoeba* (arrowed) attachment to soft silicone hydrogel or gas-permeable rigid contact lens (2) *Acanthamoeba* phagocytises microbial agents (bacterial/yeast—grey rods) on corneal surface. (3) Simultaneously, *Acanthamoeba*-MBP triggers *Acanthamoeba* adherence onto corneal epithelial cells-glycoprotein and the secreting proteases (black dots) to support phagocytosis and continuous digestion and destruction of the corneal tissue.(4) Tissue damage release signals to recruit immune response by releasing cytokines (red) and with the characteristic ring-shaped neutrophil infiltration of corneal opacity. Late infection is characterised by (5) severe corneal tissue (epithelium, bowman's membrane) damage (6) destruction of the stroma and (7) finally radial keratoneuritis in the event of therapeutic unresponsiveness. (Figure adapted from Henriquez, (2017).

1.11 Risk factors of *Acanthamoeba* keratitis

Related risk factors for AK include extended contact lens wear, lack of personal hygiene, biofilm formation and build-up of carbohydrate moieties on either soft gel (SG) or gas permeable (GP) contact lens. (Sharma et al., 1995) had reported a higher binding tendency of *Acanthamoeba* to soft gel (SG) contact lenses compared to rigid (GP) contact lenses due to the higher water content of the former. According to Beattie and colleagues (Beattie et al., 2003), *Acanthamoeba* has been reported to exhibit higher binding affinity to worn contact lens compared with unworn contact lens. AK is mostly unresponsive to treatment as it progressively leads to blindness (Beattie et al., 2003, Patel and McGhee, 2009).

1.12 Diagnostic techniques for *Acanthamoeba* keratitis

The standard diagnostic approach for *Acanthamoeba* remains the corneal culture (Patel and McGhee, 2009, Casero et al., 2017) as well as slit lamp signs, patient history, symptoms and laboratory results (Bacon et al., 1993b, Tu et al., 2008). Despite various rapid and sensitive diagnostic techniques to help identify progressive AK, visual impairment remains a huge challenge. The most available diagnostic techniques adopted for AK include corneal scraping for histopathology identification of amoeba trophozoites and mature cysts; wet preparation of cerebro-spinal fluid (CSF) samples stained with Giemsa stain or Haematoxylin & Eosin dyes; confocal microscopy, tissue culture (Maycock and Jayaswal, 2016).

Other diagnostic techniques include tissue biopsy of patient samples that are formalin-fixed with immune-histochemistry visualised by fluorescence microscopy (da Rocha-Azevedo et al., 2009); semi-nested-polymerase chain reaction (snPCR) targeting the 18S rRNA gene (Costa et al., 2017) and evaluation of loop-mediated isothermal amplification assay (Mewara et al., 2017) of *Acanthamoeba* life stages. Useful molecular techniques utilised for the determination of *Acanthamoeba* infection include restriction fragment length polymorphisms (RFLP), nuclear and mitochondrial rRNA (Kilvington, 1991, Kilvington, 2004) and fluorescent probes for hybridising *Acanthamoeba* DNA (Stothard et al., 1999).

1.13 Evaluation of sporadic outbreaks of *Acanthamoeba* keratitis

Over the last 20 years, there has been an increasing international reports and diagnosis of AK cases. This increase is partly due to a growing tendency of unhygienic contact lens practices (Joslin et al., 2006, Thebpatiphat et al., 2007, Por et al., 2009) such as cleansing procedures using contaminated domestic water supply and/or home-made saline solutions and ocular trauma (Page and Mathers, 2013, Casero et al., 2017). Subsequent to reports of elevated outbreaks and clusters of AK infections in the USA, the Centre for Disease Control (CDC) responded with major investigations of AK in 2007 and 2011 to identify common risk factors for AK and preventive measure to avert re-occurrence of AK outbreaks (Verani et al., 2009). This follows the increasing populations of contact lens wearers (Na et al., 2001).

1.13.1 *Acanthamoeba* as a reservoir for other microbial pathogens
Bacterial growth in the FLA tends to increase bacterial virulence and bacterial resistance to either antibiotics or biocides (Harb et al., 2000, Byers et al., 1991) consequently *Acanthamoeba* infection can acts as a crucial biological vector or reservoir for infection by several human pathogens. The recognition of the potential of *Acanthamoeba* as reservoir/host for microbial pathogens is well documented (Thomas et al., 2010). By acting as a 'Trojan Horse', *Acanthamoeba* potentially shields most of its engulfed intracellular pathogens termed amoeba-resistance bacteria (ARB) from amoebic digestion in deleterious environmental conditions (Thomas et al., 2010, Guimaraes et al., 2016). This is either thought to be due in part to escape or survival mechanisms possessed by these pathogens to subvert the phagocytic function of the *Acanthamoeba* (Greub and Raoult, 2004b, Siddiqui and Khan, 2012c).

Acanthamoeba do serve as a source of nutrients to microorganisms because it synthesises most amino acids, co-factors and nucleotides de-novo. It possesses cellulase to break down cellulose and is the only protozoan known to possess alginate lysate for degradation of alginate found in the cell walls of brown algae (Aksozek et al., 2002a, Khan, 2006b, Pérez-Irezábal et al., 2006, Marciano-Cabral and Cabral, 2003, Aksozek et al., 2002b). Such bacterial pathogens include *Legionella pnuemophila*, *Helicobacter pylori*, *Escherichia coli* O157:H7, *Vibrio cholera* and *Pseudomonia aeruginosa* (Marciano-Cabral et al., 2004, Thomas et al., 2010). Other pathogens include viruses such as enterovirus (Greub and Raoult, 2004b) and adenovirus (Scheid, 2014). Hence, most of

these microbes tend to survive the encystment of the host *Acanthamoeba* in either culture medium or nature when released from the mature cysts (Ly and Muller, 1990) to facilitate secondary infections (Figure 1.8).
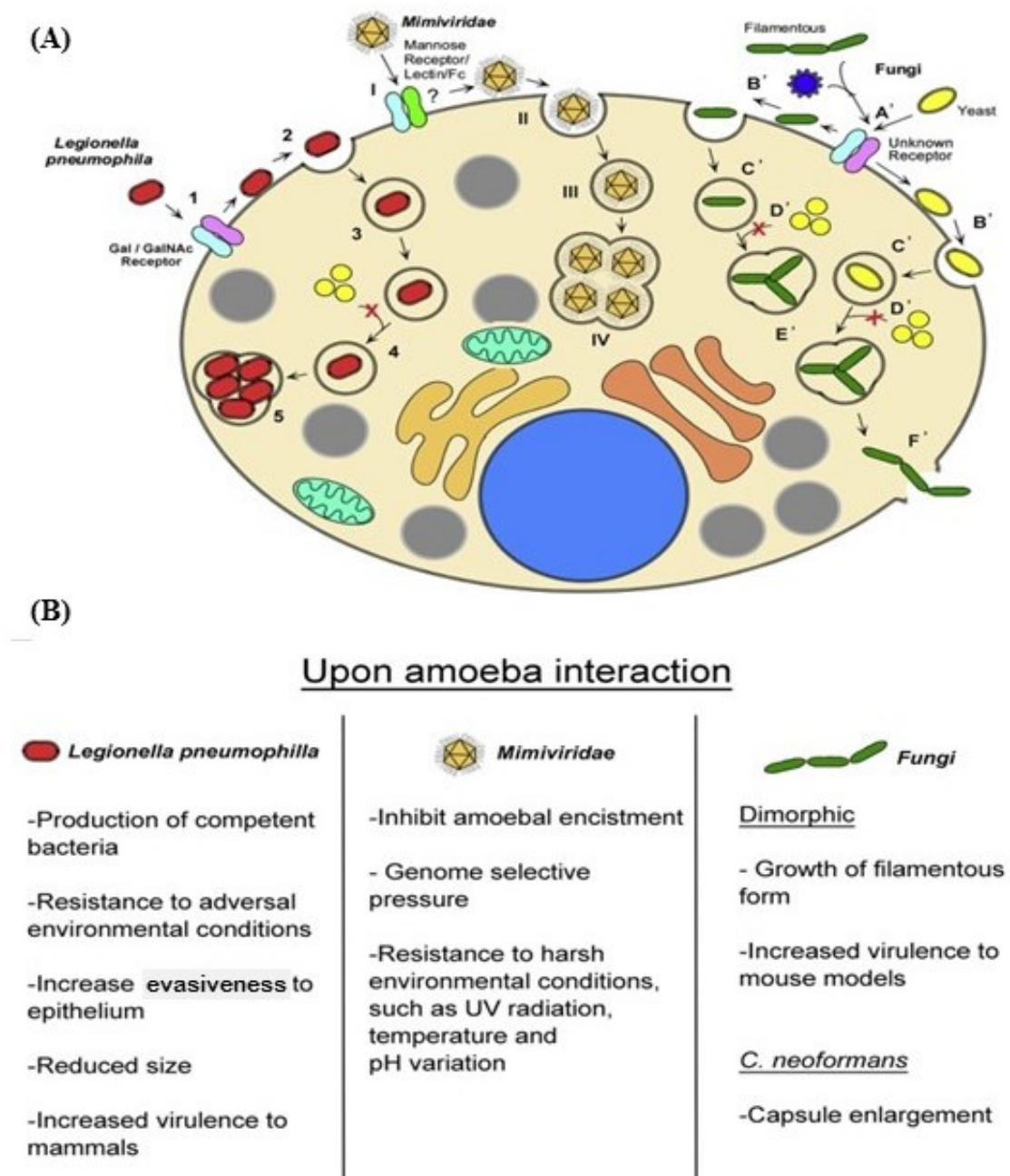
Figure 1-8: *Acanthamoeba castellanii* **interaction with bacteria** *(Legionella spp),* *giant viruses (Mimiviridae), fungi (Filamentous fungi/yeast) and their host* *intracellular fate.* (A)(i) *Legionella spp* (1) attachment of Legionella to *A. castellanii* by mannose or Gal/GalNAc receptor (2) internalization via "coiling" phagocytosis; (3)

avoidance of lysosome fusion and high resistance to biocidal activity; (4) re-modelation of the Legionella containing vacuole (LCV) disseminated all over the cytoplasmic space. (5) Legionella intracellular replication within LCVs. (ii) Mimiviridae (I) viral attachment to *A. castellanii* surface via a mannose receptor, lectin or Fc; (II) internalization of capsid in phagosome; (III) liberation viral DNA; (IV) formation of viral factory for replication and production of newly synthesized viral particles. (iii) Fungi (A') filamentous fungi and yeast attachment to *A. castellanii* surface via an unknown receptor (B') internalization via "coiling" phagocytosis; (C') dissemination of fungi filled-phagosome throughout the cytoplasm; (D') inhibition of phagolysosome formation and high resistance to biocidal activity. (E') Conversion of yeast into intracellularly replicating filamentous form (exemplified by dimorphic fungi) (F') Filamentous phase overgrows and disrupt the Acanthamoeba surface. (B) The main observable characteristics of *Legionella sp.,* mimivirus and fungi upon interaction with Acanthamoeba. The selective pressure from Acanthamoeba changed these pathogens, thus enables higher environmental resistance and frequently enhances their virulence (Adapted from Guimaraes et al., 2016).

1.13.2 Misdiagnosis of *Acanthamoeba* infections

Currently, there is a growing interest in studying the sporadic outbreaks of AK following challenges of persistent misdiagnosis and limited strategies to manage AK cases (Carnt and Stapleton, 2016). Mis-diagnosis of *Acanthamoeba* infection (Siddiqui et al., 2016) are attributed to the diverse microbial ocular infections that share similar clinical symptoms of AK and the swift transition of the trophozoites into dormant drug-resistant mature cysts. Quite often, the persistence of the mature cysts in infected corneal tissue can be readily confused with either neutrophils or macrophages, which are cells of the host immune system (Tu et al., 2008, Hau et al., 2010).

Many cases of AK has been wrongly diagnosed as herpes simplex keratitis (HSK). This is often followed by wrongly prescribed topical corticosteroids instead of prompt anti-amoebic treatment (Illingworth and Cook, 1998, El-Sayed et al., 2014, Sticca et al., Patel and McGhee, 2009, Tabin et al., 2001). Although, the use of polymerase chain reaction (PCR) as a molecular technique for the identification of *Acanthamoeba* ribosomal DNA from swab or epithelial sample gives about 85% diagnostic sensitivity (Lehmann et al., 1998, Dart et al., 2009) nonetheless, it is limited by the inability to distinguish between live and dead organisms. Therefore, PCR diagnostic techniques cannot establish if the corneal tissue is sterile or remain actively infected. These problems can cause a delay in prophylactic treatment and as a result, about 20 % of patients with AK may lose significant vision (Robaei et al., 2014).

1.13.3 Current therapeutics for *Acanthamoeba* infections

As well as misdiagnosis in the early stages of AK infection, most of the existing drugs comprising topical ophthalmic biocides are grossly ineffective against the drug-resistant mature cysts (Carrijo-Carvalho et al., 2017). Furthermore, treatments are scarce in many countries of the world (Lorenzo-Morales et al., 2015, Carrijo-Carvalho et al., 2017) so AK often goes untreated.

Current medical therapies are aimed at eradicating viable parasitic agents through rapid application of effective anti-amoebic drugs and suppression of the inflammatory response. However, existing treatments of AK and contact lens care solutions are not completely effective against the pathogenic *Acanthamoeba* spp (Figure 1.9). Therefore, there is an urgent need to determine the best therapeutic strategies and to identify novel therapeutic targets against the *Acanthamoeba*.

Some of the most effective cystocidal agents used against AK includes biguanides (polyhexidine biguanide, PHMB 0.02 – 0.06 %, and chlorhexidine 0.02 – 0.2 %) and diamidines (propamidine isethionate 0.1 %, Brolene, May and Baker, U.K., and Hexamidine 0.1 % (Elder et al., 1994) in combination with neomycin 1%. These drugs are antiseptic disinfectants often used for treating topical infections. The majority of patients (approximately 90 %) still experience therapeutic failures using these treatment regimes particularly in late-diagnosed cases of AK, due to either resistant strains and/or the persistent, deep stromal infections by *Acanthamoeba*. Because of this resistance, monotherapy is strongly discouraged and recommended treatment regime starts with hourly drops within the first 48 hours; then reduced to 2 – 4 hourly drops in order to reduce the likely consequence of epithelial toxicity. However, treatment may continue beyond 6 months due to persistent amoebic encystment (Clarke et al., 2012).

Meanwhile, Martin-Navarro (Martín-Navarro et al., 2017) had claimed that caffeine and maslinic acid were both amoebicidal and cysticidal, though caffeine had higher activity than maslinic acid against the trophozoites stage of different strains of *Acanthamoeba*. They argued that both products seemed to have a lower activity than chlorhexidine, but higher than that of amphotericin B. In 2014, Lovieno and colleagues (Iovieno et al., 2014) have proposed the use of antifungal drugs as a novel treatment for *Acanthamoeba* keratitis. The authors have tested several cysticidal activities of selected antifungal compounds targeted against different genotypes of culture collection and clinical isolates

of *Acanthamoeba*. However, only voriconazole and posaconazole were found to be cysticidal, with no significant differences in their activities observed between clinical and culture collection isolates. Overall, prompt target of the *Acanthamoeba* in the trophozoites stage is essential for effective treatment of AK.

Cytoskeleton (Actin, myosin, α & β tubulin)
Inhibitors: unknown (current known inhibitors have no effect)

Membrane
Inhibitors: chlorhexidene, polyhexamethylene biguanide, acriflavine hydrodrochloride and proflavin, polymyxin B, amphotericin B, ketoconazole, miconazole, clotrimazole, fluconazole target sterols.
Phospholipid analogues (alkylphosphocholines [APCs] & alkylglycerolphosphocholines [AGPCs]*

Nucleic Acid
Inhibitors: 5-fluorocytosine (5-FC), RNAi

Polyamines biosynthesis (ornithine decarboxylase), effects on protein translation
Inhibitors: DFMO

Alternative oxidase (AOX) and mitochondrial respiration
Inhibitors: SHAM, Ascofuronone,

Differentiation to cysts
Cellulose Biosynthesis and Proximal Biochemical (e.g. glycogen metabolism) affect encystment
Inhibitors: 2,6-bichlorobenzonitrile

Cell membrane
nucleus
ribosomes
mitochondria

Figure 1-9: Diagrammatic representation of the various drug targets and corresponding inhibitors of *Acanthamoeba*. Existing drug targets for *Acanthamoeba* infection include cytoskeleton (actin, myosin, α & β tubulin), *Acanthamoeba* membrane, nucleic acid, polyamines biosynthesis, Alternative oxidase (AOX) and mitochondrial respiration and the trophozoites differentiation into the cysts form through cellulose synthesis. The modes of actions of existing therapeutic agents (indicated as inhibitors of selected drug targets) included the remodelling of lipid inhibition, phospholipid biosynthesis, interference of intracellular signalling, disruption of cellular membrane and induction of apoptosis (Adapted from Roberts and Henriquez, 2010).

1.13.4 Why current *Acanthamoeba* drugs fail

Being eukaryotic, *Acanthamoeba* shares many similar biochemical processes with humans (Roberts and Henriquez, 2010). This coupled with the swift parasitic

differentiation are attributed to the recurrent therapeutic failure. Considerable difficulties in treating *Acanthamoeba* cases is also likely to be related to the similarity of clinical symptoms AK shares with other microbial keratitis (bacterial, herpetic and fungal) leading to late diagnosis whereby the trophozoites swiftly transforms into the drug-resistant mature cysts (Mathers et al., 1997, Marchenko and Kasparova, 2016). The use of corticosteroids have been largely attributed to wrong/lack of accurate diagnosis of AK and are linked to AK cases that developed inflammatory complications, especially following earlier exposure to prior steroids.

Several studies have suggested that *Acanthamoeba* can be effectively killed if they are retained in the trophozoites stage (Turner et al., 2000). However, the cellulose shell of the dormant, inactive mature cysts resist most physiological concentrations of either physical, chemical, radiological conditions or therapeutic agents (Lakhundi et al., 2015). Cysts can persist for several years making elimination extremely difficult. The presence of propylene glycol as a major constituent of contact lens cleansing solutions induces the encystment of *Acanthamoeba* trophozoites, potentially rendering the parasite more resistant to the disinfectants and biocides (Kilvington et al., 2008, Kliescikova et al., 2011, Imayasu et al., 2013).

1.14 Pathogenesis of *Acanthamoeba* infection

Quite often, the ocular surface is exposed to potential pathogens from the external environment. The *Acanthamoeba* is attracted to the corneal endothelial cells by chemotaxis (van Klink et al., 1993). This is an essential pre-requisite for the parasitic adhesion (Yang et al., 1997). The surface protein that is implicated in *Acanthamoeba* adhesion is a mannose-binding protein (AcMBP) that specifically binds the mannose-containing glycoproteins of the *Acanthamoeba* potentially to carbohydrates expressed by the ocular surface epithelial cells. Any further corneal injuries due to inappropriate contact lens application have been shown to enhance the AcMBP expression (Garate et al., 2006, Panjwani, 2010).

Acanthamoeba pathogenesis arises by an extracellular killing mechanism of target corneal cells (Huth et al., 2017). There are three stages to *Acanthamoeba* pathogenesis namely **(i)** the parasitic adhesion onto the cornea tissue (Yang et al., 1997) followed by **(ii)** secretion of proteases and eventually **(iii)** phagocytosis (Khan, 2001) which leads to cell death.

1.14.1 Parasitic adhesion of *Acanthamoeba* onto corneal tissue.

Parasitic adhesion is the primary stage in the pathogenesis of *Acanthamoeba* infection. Significant developments have been made towards understanding the mechanism(s) by which *Acanthamoeba* adhere to the host cells. The first critical step of *Acanthamoeba* infection is the parasitic adhesion (attachment) onto the surface of the target host tissue, which is triggered by AcMBP. The AcMBP-cell adhesion also initiates the secretion of proteases required for tissue invasion which essentially elicits further cytopathology and eventual cornea tissue death (Khan, 2001, Marciano-Cabral and Cabral, 2003), a clinical condition termed A*canthamoeba* keratitis (AK).

1.14.2 *Acanthamoeba* MBP-dependent secretion of proteases and corneal tissue invasion

Subsequent to successful parasitic adhesion, *Acanthamoeba* produces and releases potent pathogenic proteases into the extracellular matrix for degrading cornea basement membranes and the induction of cytolysis and apoptosis (Clarke and Niederkorn, 2006a, Clarke and Niederkorn, 2006b, Clarke et al., 2006). This process involves both contact dependent and contact independent processes. The contact-dependent mechanisms of *Acanthamoeba* adhesion involve direct virulence factors such as AcMBP, which subsequently secretes toxins mediated via the acanthapodia; while indirect virulence mechanisms of contact independent process involve the host factors, changes in *Acanthamoeba* (protists) morphology, biofilm formation and drug resistance (Khan, 2009) (as detailed in section 1.15 below). Studies on *Acanthamoeba castellanii* have implicated secreted three serine proteases, five cysteine proteases and metalloprotease (Cao et al., 1998; Hurt et al., 2003). The serine protease has active serine residue that assisted in catalysis by histidine and aspartate residues while the five-cysteine proteases have active cysteine residue site possessing thiol side chain that are prone to oxidation and involved in covalent catalysis. The metalloprotease possess a metal ion active site that is involved in a catalytic cycle; it is distinguished from other categories of proteases by treatment with metal chelating agents such as EDTA that triggers metal ion co-factor and inactivation (Bugg, 2012).

1.14.3 Cytopathology causing AK

The induction of cytolysis and apoptosis by *Acanthamoeba* results in the dissolution of the collagenous corneal stoma culminating in target cell death, called cytopathic effect

(CPE). The course of AK infection is characterised by varying pathological changes evident during the acute stage of the corneal infection. Within a month of AK infection, the corneal tissue is characterised by superficial infection and perineural infiltration. With time, this progress to the intermediate stage (1-2 months) depicted by neutrophilic ring-like infiltration and ulceration with stromal lysis (Figures 1.7 & 1.10). Thereafter, at a later stage (after 2 months), AK presents a progression into hypopyon, scleritis, glaucoma and cataract (Bacon et al., 1993a). However, therapeutic unresponsiveness often leads to irreversible ocular blindness. Surprisingly, there is still an incomplete understanding of how *Acanthamoeba* adhere to and destroy infected cornea tissues (Lorenzo-Morales, Khan and Walochnik, 2015).
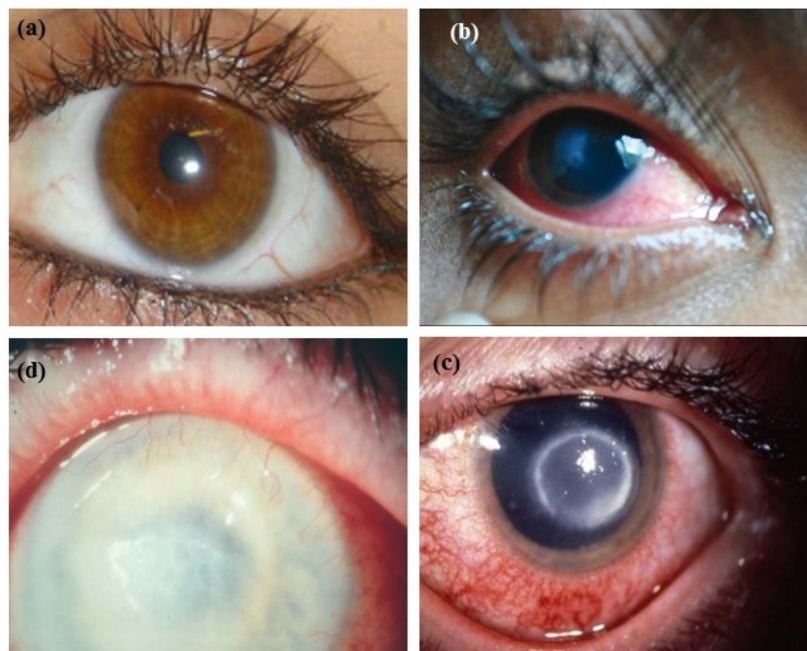
Figure 1-10: Clinical stages of *Acanthamoeba* infection. (a) A normal eye (b) early stage of AK infection in a contact lens wearer following corneal trauma (c) infected eye presenting recurrent *Acanthamoeba* infection (d) Progressive uncontrollable *Acanthamoeba* keratitis infection following unresponsive treatment leading to blindness. Sources of figures **(a)** (Siddiqui and Khan, 2012c); **(b)** (Baradkar et al., 2011); **(c)** and **(d)** (Seal, 2003).

1.15 Virulence factors of *Acanthamoeba spp.* in AK

A combination of factors such as host immune system, biofilm formation on contact lenses, parasitic adaptability to changing environments, *Acanthamoeba* AcMBP and secreted proteases have been attributed to the persistence of *Acanthamoeba* infection (Khan, 2001). According to Khan (Khan, 2001) the extent of host factors in the pathogenesis and outcome of *Acanthamoeba* infection is unclear. Biofilms are microbial-derived sessile communities formed within either aqueous environment, or on medical devices like an intravenous catheter and/or contact lenses (Oldenburg et al., 2011, Toutain et al., 2007). Biofilms provide attractive niches for *Acanthamoeba* survival, nutritional supplies and resistance to disinfectants (Zegans et al., 2002, Beattie et al., 2003). Other suggested virulence factors include alginate lysate, which breaks down the biofilm matrix by providing *Acanthamoeba* with direct access to bacterial food supplies; and trehalose-6-phosphate synthase, which release trehalose that is essential in *Acanthamoeba* stress adaptation (Anderson et al., 2005). *Acanthamoeba* trehalose is thought to protect AcMBP and cellular membrane from denaturation caused by stress conditions such as desiccation and heat (Potter and Weisman, 1971, Bínová et al., 2017).

Several studies have implicated *Acanthamoeba* AcMBP as a major virulence factor (Sun et al., 2006, Ku et al., 2009) that initiates parasitic adhesion to corneal cells. In separate *in-vitro* experiments by Garate and colleagues; and Panjwani (Garate et al., 2006, Panjwani, 2010) the pathogenic potential of *Acanthamoeba* was directly correlated with the AcMBP expression. The most pathogenic strains of *Acanthamoeba* produced robust amounts of AcMBP, which binds to the host tissue and cause cytopathogenecity in contrast to the non-pathogenic strains, which produce little or no AcMBP (Garate et al., 2006, Panjwani, 2010).

AcMBP is essential for parasitic colonisation and persistence at the onset of infection (Khan, 2000) and is responsible for the primary interaction of the parasite to the host tissue. It anchors the parasite to tissues thus avoiding been washed off during adhesion and leads to secondary processes such as the release of proteases, phagocytosis and tissue necrosis. This is a crucial step in AK pathogenesis (Cao et al., 1998, Imbert-Bouyer et al., 2004, Sanchez et al., 2016) because parasitic adhesion is a pre-requisite for the signal transduction pathways that eventually lead to the release of proteases (Leher et al., 1998) that permeates, invades and destroys the host corneal tissue.

Importantly, *Acanthamoeba* infectivity correlates directly with the degree of AcMBP expression; and AcMBP serves as a potential biomarker for the determination of *Acanthamoeba* virulence (Khan, 2006a). Hence, an understanding of the molecular basis of AcMBP in triggering the pathogenesis of *Acanthamoeba* is crucial to the development of therapeutic intervention. In the near future, I envisage the development of new generation of smart contact lenses with technologies capable of detecting *Acanthamoeba* parasitic signal sufficient enough to trigger the dispense of topical anti-MBP targeted at the infective stages. This would require more advanced research in a similar direction to the technology giant (Sony) patented (United States Patent Application 20160097940) smart contact lens in 2014. (https://www.theverge.com/2014/1/16/5317210/google-x-building-smart-contact-lens-to-measure-glucose-levels-for).

1.16 *Acanthamoeba* Mannose-binding protein (AcMBP) gene

The *Acanthamoeba* MBP is a type I trans-membrane protein (Garate et al., 2004) of 830 amino acid residues. It is synthesised with a signal sequence, which is cleaved during biosynthesis. The extracellular portion comprised of 712 residues followed by a short membrane-spanning region of 78 residues towards the C-terminal intracellular domain. Previous studies have suggested that the native protein is ~400 kDa and it is composed of three 130-kDa subunits (Garate et al., 2004). The extracellular region is glycosylated and contains a large cysteine-rich domain with 14 CXCXC repeats near the membrane. AcMBP shares little sequence identity with other characterised proteins, with the exception of a small DUF 4114 domain, (DUF--domain of unknown function). This domain, which is found towards the C-terminus of many different bacterial proteins, possesses highly conserved glutamate and aspartate residues leading to the suggestion that it might possess enzymic activity. The AcMBP gene comprises 6 exons and 5 introns regions **(**Figure 1.11) and spanning almost 3.6 kb of the amoeba's genome (Garate et al., 2004).
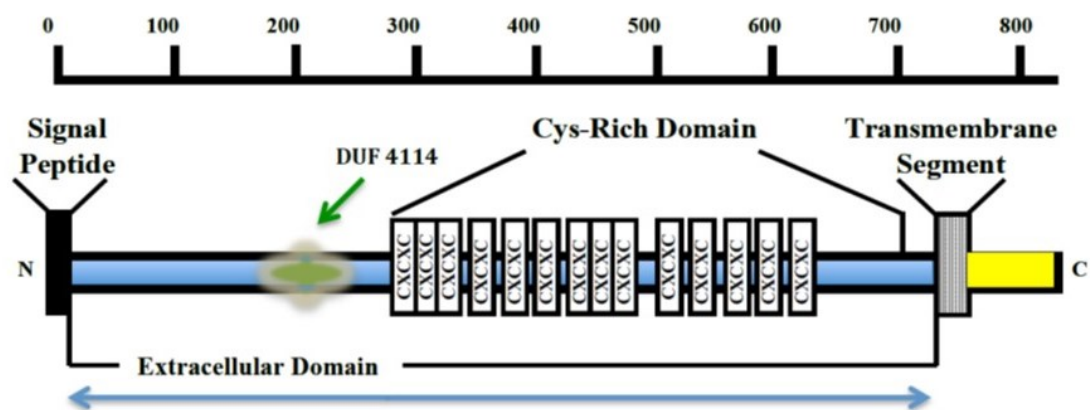
Figure 1-11: *Acanthamoeba* **MBP gene** is composed of 6 exons and 5 introns and encodes a precursor protein of 833 amino acids in length. AcMBP is a trans-membrane receptor with a signal sequence (residues 1-21); a 712 residue extracellular region (blue arrow, residues 22-733); a 22 amino acid long trans-membrane domain (residues 734-755); and a short 78 amino acids C-terminal intracellular domain (residues 756-833). The extracellular domain includes a cysteine-rich region containing 16.4% cysteine and with 14 CXCXC repeats (residues 282-701) and a 73 amino acids domain of unknown function termed DUF 4114 (green arrow, residues 178-250). Other than the DUF 4114 domain, the AcMBP sequence shares no obvious homology with any protein of known function (Garate, et al., (2004)).

1.17 Biological roles of Mannose-binding protein

The Mannose-binding protein of *Acanthamoeba* is thought to play a crucial role in the pathogenesis of *Acanthamoeba* infection by mediating parasitic adhesion, enabling parasitic colonisation and persistence at the onset of infection (Khan, 2000). This is responsible for the primary interaction of the parasite to the infected host tissues including either the cornea, brain or other tissues. Essentially, AcMBP anchors the parasite to host tissues thus avoiding parasitic wash-off during adhesion and leads to secondary processes for the release of proteases, phagocytosis and tissue necrosis. In addition, AcMBP serves as a potential biomarker for the determination of *Acanthamoeba* virulence.

Although, AcMBP is a calcium-dependent like any other known MBL, the latter exists as an acute phase protein produced by the liver. MBL belongs to the "pattern recognition molecules" or collectin family that deploys a variety of antimicrobial activities in the

innate immune system. MBL recognizes and binds various pathogens (including bacteria, viruses, fungi, and parasites) by providing protection against the microbial invasion of the host. This direct MBL interaction with cell surface receptors of these microorganisms triggers agglutination and phagocytic clearance of pathogens as well as activation of lectin-complement pathway, through MBL-associated proteases (LAU et al., 1995, Eisen et al., 2006). Yet, the large number of studies, investigating the role of MBL, the exact clinical relevance of MBL is still poorly understood; and needs to be further elucidated especially in response to infections (De Pascale et al., 2013).

1.18 Aim and objectives of the current study:

1.18.1 Aims of this study:

In this study, I aimed to understand conditions that trigger *Acanthamoeba* switching between different life forms and characterize the AcMBP that enables adhesion/CPE onto the corneal tissues.

1.18.2 General objectives:

The specific Objectives include:

i.   Characterization of the three life forms of *Acanthamoeba castellanii* and establish conditions that induces their differentiation.

ii.   Screening *Acanthamoeba* adhesion and cytopathic effect on monolayer of selected epithelial cell lines using various cell lines including human corneal epithelial cells (HCEC).

iii. Characterize AcMBP with respect to its structure, carbohydrate specificity and biological properties.

1.19 Study hypothesis:

Molecular characterisation of the extracellular AcMBP is crucial to the development of anti-MBP, a potential drug target against the persistent therapeutic unresponsiveness of *Acanthamoeba* keratitis.

2. *Acanthamoeba* life forms, differentiation, adhesion & cytopathology

2.1 Introduction and Objectives

Acanthamoeba keratitis (AK) infections are thought to follow exposure of traumatised corneal tissue and/or scratched contact lens to *Acanthamoeba*-contaminated water sources (Tomlinson et al., 2000, Zimmerman et al., 2016). Quite often, *Acanthamoeba* switches between the two existing life forms either to evade the host immune response or therapeutic interventions. In hostile environments, trophozoites differentiation has been demonstrated by morphological changes, termination of cell growth and biochemical changes to form the dormant mature cysts (Khan and Siddiqui, 2009). During encystment, adenylate cyclase activity increases, resulting in increases in the levels of cyclic AMP. As a result, glycogen is broken down to generate glucose for synthesis of cellulose, which forms the cell wall of the cysts (Weisman, 1976, Weisman et al., 1970, Krishna Murti and Shukla, 1984). How *Acanthamoeba* senses and responds to its changing environment is not fully understood. *Acanthamoeba* adhesion remains a pre-requisite condition for parasitic colonisation of the corneal epithelium and subsequent invasion of the corneal stroma tissue.

This process of *Acanthamoeba* adhesion onto the corneal glycoprotein is usually initiated by AcMBP, which remains the first critical step into AK pathogenesis. Subsequent to successful adhesion, AcMBP triggers the release of proteases, which initiate the invasion of target cells followed by extensive tissue damage. This is characterised by *in-vitro* cytopathic effects (CPE) in monolayer epithelial tissue culture or *in-vivo* destruction of infected corneal tissue. Given the correlation between contact lens use and AK, it is important to understand how the different life forms of *Acanthamoeba* exist in *in-vitro* conditions that closely resemble the natural parasitic attachment onto universal vectors (contact lenses and storage casings). According to previous findings by Beattie (Beattie et al., 2003), *Acanthamoeba* has been reported to exhibit higher binding affinity to worn contact lens compared with unworn contact lens.

In this chapter, *in-vitro* experiments are described to measure the adhesion and cytopathic effects of *Acanthamoeba* life forms on selected epithelial cells. To achieve these objectives, I first sought to study the morphological characteristics of the different life forms of pathogenic *Acanthamoeba* by direct observation using phase contrast and

fluorescence microscopy; establish conditions that induce their differentiation; screen *Acanthamoeba* adhesion and interactions with inert and biological surfaces; and measure the consequential cytopathic effects on selected monolayer epithelial cells. The overall aim of this Chapter is to better understand the changes that occur during *Acanthamoeba* infection and the conditions that trigger these changes.

2.2 Materials and Methods

2.2.1 Materials

2.2.1.1 *Acanthamoeba* strains, bacterial and epithelial cell lines

The culture collection of all strains of *Acanthamoeba* used in this study were obtained and researched in the reference laboratory of Dr Simon Kilvington, Department of Infection, Immunity and Inflammation, University of Leicester, Leicester, United Kingdom. The collection include *Acanthamoeba castellanii* (ATCC 50370)—study model, *Acanthamoeba polyphaga* (ATCC 30461), obtained from the American Type Culture Collection (ATCC, Manassas, VA) and Buller-1*,* a recent clinical strain of *Acanthamoeba* obtained from keratitis patients receiving treatment at Moorfields Eye Hospital, London, U.K. All the *Acanthamoeba* strains were isolated from *Acanthamoeba* keratitis patients and were all of T4 genotypes. In addition, *Escherichia coli* (ATCC 8739) and epithelial cell lines (Vero, Human Hep-2, HT-29) were also kindly provided as gifts from Dr Simon Kilvington, University of Leicester, United Kingdom. Human corneal epithelial cells were purchased from Merck Millipore, England.

2.2.1.2 Chemicals, media and reagents

Most of the chemicals used in this study including monosaccharides sugars like D-(+)-Mannose, D-(+)-Glucose, D-(-)-Fucose, D-(+)-Galactose, D-(+)-Xylose, N-Acetyl-D-Glucosamine were obtained from Sigma-Aldrich (Gillingham, UK), D-(+)- Mannose (Fluka, UK). A variety of artificial surfaces were tested including Non-tissue culture plates (351172, Falcon, Becton Dickinson, USA), tissue culture plates (92096, TPP®, Switzerland); branded disposable contact lenses such as Pure-vision™ (Lot # R28526194, Bausch Lomb, USA), Pure-vision-2® (Lot # R28526194, Bausch Lomb, USA), Bioffinity® (Lot # 6137553912, Cooper Vision, UK), Acuvue® (Oasys™) (Lot # 001WWR, Johnson & Johnson, Vision care Inc., UK).

The media and reagents included semi-defined *Acanthamoeba* axenic growth (Ac#6)

medium (Appendix IV) supplemented with 40 U/ml penicillin and 40mg/ml streptomycin (Hughes et al., 2003c, Hughes et al., 2003a, Hughes et al., 2003b), bovine serum albumin (BSA), Mannan, Ethylene-diamine-tetra acetic acid (EDTA) from Sigma. 2.5% Non-nutrient Agar (NNA), Dulbecco phosphate buffer saline (DPBS, Thermo Fisher Scientific, England), ¼ strength Ringers solution, amoebic saline (PAS) solution.

Disposable haemocytometers were from C-Chip, Fuchs-Rosenthal/DHC-F01, Nano-Entek, USA Inc.

Chemicals, buffers, media, reagents and solutions were prepared in sterilized glassware with deionised water (dH_2O) and were sterilised by autoclaving at 121°C for 15 minutes. Media and reagents that were heat labile, including Neff + 0.5% Propylene glycol (PG) and calco-fluor white reagents were filter-sterilised through a 0.2 μm pore-size of 50 ml Nalgene™ filter unit (Thermo-scientific, India) or sterile 0.2 μm pore-sized Acrodisc® syringe filters (Pall Life Sciences, Portsmouth, U.K.) in a class II safety cabinet before usage.

2.2.1.3. Laboratory equipments

I used the following laboratory equipment: Ultra safe (Class II) biohazard safety cabinet (Faster®, UK); incubators with temperature ranges between 28 °C and 44 °C (Leec, UK); 36°C CO_2 incubator (Sanyo, UK); and phase contrast (Olympus CKX41, Japan)/fluorescence light microscope (U-RFLT50, Japan) connected to micropublisher 5.0 RTV camera (Q-imaging, UK). Others include IKA MS 3 basic digital shaker 32 °C, 110 rpm Sanyo® shaker incubator (Camlab, England), Allegra™ / X-22R refrigerated Beckman Coulter™ centrifuge (Primus Scientific ltd., UK); weighing scale (VWR, UK); Mettler Toledo pH meter (Seven-Easy ltd., UK); micro-pipettes holders (varying sizes-20μl, 200μl, 1000μl & 5000μl) and multi-channel micropipettes holders (1000μl). Additional equipments include -80°C freezer (Sanyo® Gallenkamp, Loughborough, U.K.); water bath (Grant JB series), PCR machine (GeneAmp® PCR System 9700, Applied Biosystem Ltd, UK) and Column chromatography.

2.2.2. Methods

2.2.2.1 Cultivation of *E. coli* and *Acanthamoeba*

2.2.2.1.1 Cultivation and harvesting of *E. coli* (ATCC 8739) as *Acanthamoeba* food source

To prepare a stock suspension of bacterial food source for the purpose of subsequent isolation and culture of free-living *Acanthamoeba*, I streaked *Escherichia coli* onto Luria-Bertani (LB) agar plates using a sterile disposable plastic loop (Fischer Scientific, U.K.). Plates were prepared by cooling the agar to ~ 50 °C before pouring on to Petri-dishes. They were left to dry overnight at room temperature while plates stored at 4 °C remain useable for approximately 2 weeks.

When ready for use, I picked distinct single bacterial colonies of *E. coli* with a sterile disposable plastic loop (Fisher Scientific, U.K.). This was transferred into a 175 cm^2 filtered-lid tissue culture flask (Nunc-Fisher Scientific, U.K.) containing 100 ml of sterile LB broth [12.5 g of Difco LB powder (BD Biosciences) in 500 ml of distilled water] and propagated in a shaking incubator (Sanyo®, U.K.) at 37 °C, 110 rpm overnight.

A turbid suspension of *E. coli* was carefully harvested under strictly aseptic conditions within the perimeter of a Bunsen flame into two 50 ml polypropylene tubes (Falcon®, U.K). Cells were pelleted by centrifugation at 3,000 x g for 30 minutes and the supernatant was discarded. Bacterial pellets were washed by multiple (at least thrice) re-suspension in ¼ strength Ringer's solution [(NaCl (2.25 gm/L), KCl (0.105 gm/L), CaCl$_2$.6H$_2$O (0.12 gm/L and NaHCO$_3$ (0.05 gm/L), pH 7.3 − 7.4 due to the low ionic strength of the medium, (Thermo Scientific, UK)]. One tablet of ¼ strength Ringer's was dissolved in 500 ml of de-ionised water, sterilised by autoclaving at 121 °C for 15 minutes. Afterwards, the final pellet was re-suspended in 10 ml of ¼ strength Ringer's solution. The bacterial stock suspension was stored at 4 °C for ~ two weeks as a ready food source for monoxenic cultures of *Acanthamoeba*.

2.2.2.1.2 Monoxenic culture of *Acanthamoeba* trophozoites

To obtain and maintain steady fresh monoxenic cultures of *Acanthamoeba* trophozoites, I adopted the method of Page (Page, 1967, Schuster, 2002) by seeding non-nutrient agar plates with a bacterial lawn of *E. coli* (NNA-*E. coli*). Prior to the bacterial seeding, the NNA media was prepared from 1.5% plain agar (Agar No. 1, Lab M®, Bury, U.K.) and one tablet of ¼ strength Ringer's solution suspended in 500 ml of deionised water and

autoclaved at 121 °C for 15 minutes. This was allowed to cool down to 50 °C before pouring the plates, which were left to dry overnight at 37 °C in a sterile environment. The NNA plates were seeded with *E. coli* by adding 2 - 3 drops of dense *E. coli* (ATCC 8739) suspension onto the middle of dried NNA, evenly spread over the plate with a sterile disposable spreader, and left to dry at room temperature, later stored at 2 - 8 ° C prior to use. I used sterile scalpel blade for weekly excision of one cm^2 slice of NNA agar containing numerous *Acanthamoeba* trophozoites. This was placed faced down in the centre of a freshly prepared NNA-*E. coli* plate for further incubation, as described above.

2.2.2.1.3 Axenic culture of *Acanthamoeba* trophozoites on semi-defined Ac#6 medium

All clinical strains of *Acanthamoeba* isolated from keratitis patients belonging to the T4 genotype, (American Type Culture Collection, ATCC 50370 and ATCC 30461) and Buller-1 were used in this study. To produce mature *Acanthamoeba* trophozoites that are void of bacterial contamination (axenic) under strictly sterile laboratory procedures, I inoculated *A. castellanii* trophozoites without shaking in 30 ml of Ac#6 medium (a semi-defined medium for cultivating *Acanthamoeba* spp.). This was based on the formulation of Hughes & Kilvington (Hughes and Kilvington, 2001): [20g Biosate (BBL:BD-211862), 5g Glucose, 0.3g Potassium di-hydrogen-orthophosphate (KH_2PO_4), 10mg Vitamin B_{12}, 15mg L-Methionine per 900ml distilled water and pH meter (Mettler Toledo, UK) was adjust to 6.5 - 6.6 using 1M sodium hydroxide (NaOH)]. Prior to usage, two millilitres of a final concentration of 100 IU/ml penicillin and 0.1 mg/ml streptomycin were added into each of the aliquot media in four 225 ml Durham bottles (Hughes and Kilvington, 2001, Hughes et al., 2003a) in order to eliminate bacterial contamination. The complete media was stored at 4°C until ready to use within one month of the media preparation. Meanwhile, a logarithmic growth phase of confluent *Acanthamoeba* trophozoites (>95% parasites) was cultured in a 175 cm² flask (Corning, Corning Incorporated, NY), and incubated at 28ºC (±2ºC) and microscopically confirmed by phase-contrast microscopic examination.

To maintain the axenic culture, it was essential to remove the superfluous bacterial population around *Acanthamoeba* cysts by treatment with 2 % (v/v) hydrochloric acid (HCl) for 24 hours (Kilvington and White, 1994). HCl was removed by washing the cysts in sterile deionised water and pelleting by centrifugation at 1,000 × g for 3 minutes. This step was repeated thrice under sterile conditions within the perimeter of a Bunsen flame.

2.2.2.2 Encystment of *Acanthamoeba*

2.2.2.2.1 Xenic cultivation of mature cysts on encystment Non-Nutrient Agar (ENNA)

To induce *Acanthamoeba* mature-cysts formation, 30 ml suspension of confluent *Acanthamoeba* trophozoites at logarithmic growth phase in a 175 cm² flask (Corning, Corning Incorporated, NY) at 28°C (±2°C) were centrifuged (Allergra X-22R) at 500 x g for 5 minutes. After discarding the supernatant, the pellet was washed, and re-suspended in 30 ml of ¼ strength Ringer's solutions (repeated thrice). Afterwards, 200 µl aliquots of trophozoites pellets were re-suspended in 1 ml of ¼ strength Ringer's solutions, and then gently spread over five separately labelled ENNA plates and left to dry onto the agar surface. Next, the plates were incubated at 28°C (±2°C) for 48 hours before sealing inside polythene bags for continued incubation until 7 days before mature cysts were ready for harvesting.

Following completion of encystment, any mature-cysts that had been formed were harvested by carefully scrapping the surface of the agar plates with a sterile cotton bud into 5 ml of DPBS. The cysts suspension was then centrifuged (Allergra X-22R) at 1200 x g for 10 – 15 minutes and washed twice in 5 ml of ¼ strength Ringer's solutions, removing supernatant after each wash to eliminate any possible bacterial contaminations. I then manually counted the mature cysts using a modified Fushs-Rosenthal haemocytometer as earlier described. The image of the amoeba cysts were captured with a phase contrast (Olympus CKX41, Japan)/fluorescence microscope (U-RFLT50, Japan) viewed through the ×10 or ×40 objective lenses connected to a micropublisher 5.0 RTV camera (Q-imaging, UK).

2.2.2.2.2 Preparation of *Acanthamoeba* mature cysts on Neff's medium

To induce *Acanthamoeba* mature-cysts formation by an alternative method, I adopted the use of Neff's medium according to the methods of Kilvington and colleague (Kilvington and White, 1994). *Acanthamoeba* trophozoites pellets were washed in 30 ml of ¼ strength Ringer's solution, vortex and centrifuged (Beckman coulter, High Wycombe, U.K.) at 500g for five minutes. The supernatant was carefully removed while the pellets were re-suspended in 30 ml of ¼ Ringer's solution (repeated twice). Thereafter, 30 ml of Neff's encystment medium [(KCl (Sigma P-9541) (0.1 M), MgSO4 (0.008 M), NaHCO3 (0.02 M) phenol red (sodium salt: 1.5 %) (25 µl) and nanopure water to 1000 ml, adjusting pH

to 8.9 at 20 - 25°C; a defined solution for encystment of *Acanthamoeba* trophozoites (Adam, 1964) were used for the last wash of the pellet. Finally, the aliquot was re-suspended in 20 ml of Neff's medium. The *Acanthamoeba* trophozoites gradually differentiated into the characteristic mature cysts over a period of 2 - 4 days post inoculation.

2.2.2.2.3 Harvesting of mature cysts

Mature cysts that were formed on five separate ENNA plates (multiple plates were used in order to increase the number of cysts) and were confirmed after 7 days post-inoculation using an inverted microscope (Olympus CK-30) at ×10 objective lens magnification (Khan, 2001). I moistened a sterile swab in ¼ Ringer's solution and then rubbed the swab by rotating it across the plates to harvest the mature cysts. The swabs containing the mature cysts were innoculated into 30 ml of ¼ Ringer's solution in a 50 ml polypropylene conical tube (Falcon 352070; Corning Science Mexico S.A.). After centrifugation at 1200g for 10 minutes, the supernatant was carefully removed. Finally, I re-suspended the pellet in 5 ml of ¼ Ringer's solution and stored at 2 - 8°C for use within two weeks.

2.2.2.3 Preparation of *Acanthamoeba* protocysts on Neff's in 0.5% Propylene glycol medium

To prepare *Acanthamoeba* protocysts, the *Acanthamoeba* trophozoites pellet that was earlier washed in 30 ml of ¼ Ringer's solution were vortex and centrifuged at 500 x g for five minutes. The resulting supernatant was carefully removed but the pellet was re-suspended in 30 ml of ¼ Ringer's solution and washed three times. Afterwards, 30 ml of Neff's + 0.5% propylene glycol (Neff's-PG) were used for the final wash. Subsequently, pelletized trophozoites were re-suspended in 20 ml of the Neff's-PG medium in a 250 ml storage bottle (Corning 430281 non-pyrogenic, Corning Incorporated, NY). Within two hours, the *Acanthamoeba* trophozoites rapidly differentiated into protocysts, as confirmed by fluorescence light microscopy. The preparation was stored in an orbital shaking incubator at 32°C, 121 rpm until the protocysts are ready for use within the seven days of production.

2.2.2.4 Microscopic study of *Acanthamoeba* encystment/excystment assays

To investigate the *Acanthamoeba* differentiation (encystment/excystment), I examined the morphologies of *Acanthamoeba* mature cysts or trophozoites in T-75 flasks using

phase contrast/fluorescence microscopy (U-RFLT50, Japan) with ×10 - ×40 objective lenses (Olympus CKX41, Japan). The encystment assay required the addition of 10 µl of 20 µg/ml calcofluor-white fluorescence dye (Lot # 18909, Sigma Aldrich, now Merck, United Kingdom) (Marines et al., 1987) into one millilitre aliquots of trophozoites. Samples were monitored for protocyst and mature cysts formation. Samples were aliquoted from 25cm² tissue culture flasks at hourly interval from a shaker at 32 °C and 100rpm. At intervals of 0, 30, 60, 90, 120, 150, 180, 210, 240 minutes, one ml aliquots was taken out using sterile disposable pipette into ependorf tube into which ~25µl of 10µg/ml calcofluor-white was carefully introduced for examination using the fluorescence microscope and for cell counting using a Fushs-Rosenthal (DHC-F01, NanoEnTek Inc. Korea) disposable haemocytometer. Trophozoites encystment into protocysts were examined and confirmed by their fluorescence cell walls. The percentage of encysted *Acanthamoeba* trophozoites (into the newly formed protocysts) was recorded over time.

2.2.2.5 Cultivation and harvesting of Hep-2 cells, HT-29 and Vero epithelial cell lines

To carry out *in-vitro* studies of *Acanthamoeba* adhesion and cytopathic effects on cell monolayers, I cultivated and harvested monolayers of human epithelial cells including Hep2, HT-29 and Vero cells. These cells were grown on separately labelled 25 cm² tissue culture flasks (Corning, Corning Incorporated, NY) in 5 ml Dulbecco's modified Eagle's medium (DMEM) (Microlab, Mexico), supplemented with 10 % foetal calf serum (FCS—heat activated) (Gibco, Grand Islands, NY); 10 ml of L-glutamine and 2 ml of Penicillin-streptomycin and incubated in a 5 % CO_2 atmosphere Sanyo® incubator at 36 °C until it reached 80 % confluence. The growth media was then replaced with maintenance media containing 2 % foetal bovine serum in 75 cm² tissue culture flasks (Corning, Corning Incorporated, NY) until ready for seeding with *Acanthamoeba* cells.

Spent media was decanted from epithelial cells and cells were gently washed with Dulbecco's Phosphate Buffered Saline (DPBS) before reconditioning and splitting epithelial cells. 2.5 ml of 1× trypsin-EDTA solution was added and incubated at 32 °C for 4 minutes to detach the cells and 32.5 ml of pre-warmed (37 °C) DMEM were added to neutralise the trypsin. Media re-conditioning and media preparation were all carried out in a digital class II fume chamber (Faster® ultrasafe, Italy) while incubation was

carried out in a humidified incubator with 5 % CO_2 incubator at 36 °C, until 85 – 100 % confluence is achieved.

2.2.2.6 Adhesion assays of *Acanthamoeba* on inert and biological surfaces

In order to evaluate the implication of mechanical vectors such as contaminated contact lens and storage cases in the spread of AK, I studied the adherence of *Acanthamoeba castellanii* onto selected inert surfaces—branded contact lenses (Pure-vision™, Pure-vision-2®, Bioffinity® & Acuvue®), non-tissue culture plates (NTCP), tissue culture plates (TCP) and biological surfaces--Hep2, HT-29 and Vero cells.

2.2.2.6.1 Adhesion assays of *Acanthamoeba* on selected contact lenses

The difference between the numbers of cells still in suspension and the numbers of cells in the primary inoculum was used to calculate the percentage of cells that had bound to the contact lenses for each preparation. Cells were counted manually using a handheld tally counter (4 digit Ref # 160, BDS, England) and disposable modified Fushs-Rosenthal/DHC-F01 haemocytometer and percentage protocysts adherence were observed/recorded (Connell et al., 2001).

2.2.2.6.2 Adhesion assays of *Acanthamoeba* on tissue culture & non-tissue culture plates

The difference between the numbers of cells still in suspension and the primary inoculum for each preparation was used to calculate the percentage of cells that had bound to the non-tissue culture plates (NTCP) and tissue culture plates (TCP). Cells were counted manually using a handheld tally counter (4 digit Ref # 160, BDS, England) and disposable modified Fushs-Rosenthal/DHC-F01 haemocytometer and percentage protocysts adherence were observed/recorded (Connell et al., 2001).

2.2.2.6.3 Adhesion assays of *Acanthamoeba* on Hep-2, HT-29 and Vero cell lines

After replacing spent growth media with 3 ml of fresh maintenance media, one ml of freshly prepared trophozoites, mature-cysts (< 2weeks old), and protocysts (< one week old) were adjusted to 1×10^6 parasites/ml and inoculated separately into labelled 75 cm² tissue culture flasks containing either confluent Hep2, HT-29 or Vero epithelial cells. 25μg/ml of calcofluor white dye was gently mixed with the each preparation. The cells were counted at hourly intervals until no more cells were found in the suspension. The difference between the numbers of suspended cells and the numbers of cells in the

primary inoculum was used to determine the number of cells that were bound to the studied epithelial monolayer. As before, parasites were counted manually using a handheld tally counter (4 digit Ref # 160, BDS, England) and disposable modified Fushs-Rosenthal/DHC-F01 haemocytometer and the percentage of protocysts adherence were observed/recorded (Connell et al., 2001).

2.2.2.7 Cytopathic effect (CPE) of *Acanthamoeba* on Hep2, HT-29 & Vero cell lines

To study the cytopathic effects of *Acanthamoeba* on Hep2 and Vero epithelial cells, I used the modified methods of (De Jonckheere, 1980, Khan, 2001, Garate et al., 2006). I gently tipped the media, washed off any unbound epithelial cells with DPBS (thrice), and added 3ml of fresh maintenance media. Then, I added 2×10^5 parasites per ml of *Acanthamoeba* trophozoites or protocysts to each flask and incubated the flasks in the CO_2 incubator at 36 °C for assessment at 1, 6, 24, 48, 72 & 96 hours post infection. The cytopathology assay involved the observation of degradation of Hep2, HT-29 or Vero monolayer epithelial cells by *Acanthamoeba* trophozoites and where applicable, the hatching of protocysts into trophozoites that eventually destroys the monolayer epithelial cell types under investigation.

Acanthamoeba trophozoites or protocysts were grown as earlier described in 2.2.2.1.3, in 5 ml of semi-defined (Ac#6) culture medium in labelled 25 cm^2 tissue culture flasks, to ~ 85% confluence. The protozoon parasites were pooled and harvested, following centrifugation (500 x g for 1 minutes at room temperature), washed in ¼ strength Ringer's solution thrice before quantifying using modified Fushs-Rosenthal haemocytometer as earlier described. 20µl of cell suspension was aliquot and filled into the chamber of a modified Fushs-Rosenthal haemocytometer. Cells were counted in five out of the nine large squares of the chambers using the 20x objective lens of the CKX41 phase contrast microscope (Olympus, Essex, U.K.). Cell counts were multiplied by the dilution factor times one thousand and expressed as count per millilitre.

The cytopathogenic effects (CPE) of *Acanthamoeba* were identified as clear area of studied epithelial cells otherwise described as the destruction of epithelial monolayer, confirmed by visible plaques, and established using phase contrast microscope at magnification ×200. The plaques were caused by the phagocytic action of the earlier excysted protocysts on the monolayer. Control experiments were conducted with epithelial cells incubated and sustained alone in 30 µl of either ¼ strength Ringer's

solution or culture medium (devoid of *Acanthamoeba* parasites) while other experimental conditions remains the same for comparison. The pictographs were taken and CPE documented as percentage CPE.

2.2.2.8 Thermo-tolerance of *Acanthamoeba*

Acanthamoeba have adapted to withstand diverse conditions by inter-switching life forms. However, Martinez (Martínez and Visvesvara, 2002), Khan (Ahmed Khan, 2003) and De Jonckheere (García et al., 2011) have shown that pathogenic *Acanthamoeba* are often characterised by high temperature tolerance both on the infected corneal tissue and/or outside of host environment for successful parasitic transmission. To explore the thermo-tolerance of *Acanthamoeba* trophozoites' adhesion and CPE on Vero, and HT-29, varying temperatures of 25 °C, 32 °C and 36 °C were used and incubated at 5 % CO_2 using the methods described in 2.2.2.6 – 2.2.2.7.

2.2.2.9 The effect of pre-conditioned media on *Acanthamoeba* differentiation

Metoprolol and propranolol are non-cardio-selective β-blockers used in the treatment of heart conditions such as angina. Previous studies have shown that such β-blockers affect the growth and differentiation of *Acanthamoeba* through their action on G protein coupled receptor-mediated signaling (Aqeel et al., 2015). The aim of the next series of experiment was to test whether pre-conditioning of trophozoites and/or protocysts in various growth media containing non-cardio-selective β-blockers would affect their differentiation. I established in previous experiments that Neff's encystment media induces the conversion of trophozoites into mature cysts over a period of 2 - 4 days. Here, trophozoites were pre-conditioned in Neff's media supplemented with either 1M Metoprolol or Propanolol. After 24 hours, the pre-conditioning media was removed and cells were re-suspended in Neff encystment media.

2.2.2.10 Cryopreservation and storage of cultures

Vero, Hep2, and HT 29 epithelial cell lines cultures were stored at -80 °C or in liquid nitrogen as described by Grout, Morris and McLellan and Bolton and colleagues (Grout et al., O'Brien and Bolton, 1995). Throughout this study, I ensured the absolute maintenance of cells integrity and avoidance of cross-contamination of the sub-cultures.

2.2.2.10.1 Cryopreservation of *E. coli*

To cryopreserve *E. coli,* I harvested the pure culture of the bacteria from Trypticase Soy Agar (TSA) plate. They were re-suspended into 5ml of Trypticase Soy Broth (TSB) using 15ml propylene centrifuge tube (Corning 430791, Corning Incorporated, NY) and grown overnight at 37 °C in an orbital shaking incubator (Sanyo®, U.K.) at ~200 r.p.m. Afterwards, the culture was centrifuged at 2,000 x g for 20 minutes to harvest the bacterial cells pellet while the supernatant was discarded. Next, the pellets were re-suspended in fresh medium at a concentration of $~10^9$ CFU/ml. Then, the preparation was vortexed and 5 ml of broth media containing 15% Dimethyl-sulfoxide (DMSO) (D2650, Sigma Aldrich, U.K.) was added. The mixture gently inverted six times and one ml aliquots were prepared in labelled 1.2ml cryopreservation tubes (Nalgene 5000-0012) at -80 °C in the freezer or in liquid nitrogen. The viable of *E. coli* cells was tested after 2- 4 days of storage by scraping a little of the frozen culture and plating onto on TSA agar plates (using an inoculating loop).

2.2.2.10.2 Cryopreservation of *Acanthamoeba*

To cryopreserve the protozoa culture, axenically grown cell suspensions ($~1 \times 10^6$ trophozoites /ml) in the growth medium recovered from late growth log phase was placed in 15 ml propylene centrifuge tube (Corning 430791, Corning Incorporated, NY) and centrifuged at 500 x g for 5 minutes. The pellets were re-suspended into fresh Ac#6 culture medium and counted using disposable modified Fushs-Rosenthal/DHC-F01 haemocytometer and adjusted to approximately 2×10^6 trophozoites/ml. 0.5ml aliquots (2×10^6 trophozoites/ml) in growth medium were transferred into cryovials (Nalgene Lot # 5000-0012, Nalgene-Fisher Scientific UK).

About 0.5ml of cryoprotectant containing 10 % (v/v) of dimethyl-sulfoxide (DSMO) and 10 % (v/v) foetal bovine serum (FBS) (Gibco®, Invitrogen, UK) was added to the vial and mixed by inversion. Labelled tubes were placed in a Nalgene freezing box manufactured to provide a steady cooling at a rate of 1 °C per minute. Thereafter, the samples were transferred immediately into a -80 °C freezer (Sanyo® Gallenkamp, Loughborough, U.K.) for a minimum of four hours or overnight. Thereafter, the vials of the sample strains were catalogued stacked in the liquid nitrogen storage tank at -196 °C for long-term preservation.

For sample recovery, the frozen stock was readily reconstituted by thawing in a 37 °C water bath. Once thawed, samples were immediately transferred into a tissue culture flask containing required growth medium supplemented with antibiotics and incubated at 28 °C. Any possible toxic effects of DSMO were reduced by replacement of the culture medium with a fresh medium six hours after innoculation.

2.2.2.11 *In-vitro* activities of *Acanthamoeba* MBP on Corneal epithelium

In this chapter, I established conditions for maintaining the different life forms, and measuring adhesion and CPE of *Acanthamoeba.* In these experiments, I explored the *in-vitro* impact of *Acanthamoeba* mannose-binding protein (AcMBP) on *Acanthamoeba* adhesion and its cytopathology on human cornea epithelial cells (HCEC) by direct microscopic observation. Although, carbohydrates have been shown to inhibit amoebic attachment to biological surfaces (Yang et al., 1997, Cao et al., 1998), the design of these experiments commenced with an initial comparative determination of *Acanthamoeba* adherence onto inert surfaces in the presence of monosaccharides: N-acetyl-D-glucosamine, galactose, mannose, glucose and xylose using adhesion and CPE assays that I have already established. The selected sugars were serially diluted starting from 1M to 0.015mM to enable me to determine the concentration required to inhibit 50 % of *Acanthamoeba* adhesion onto the polystyrene plates at time intervals of 60, 120 and 180 minutes. The experiment was carried out at least twice.

Next, I tested the effects of metal ion chelators (EDTA, EGTA) on adhesion, because many lectins (including AcMBP, see Chapter 3, and extracellular receptors) depend on metal ions for their adhesion activities (Wang et al., 1994).

2.2.2.12 Investigation of the *Acanthamoeba* surface proteins

The search for a novel AK therapeutics is sequel to the evolutionarily conservation of phospholipids analogs (miltefosine) though effective therapeutic target for *Acanthamoeba* but remains toxic to humans (Aichelburg et al., 2008, Roberts and Henriquez, 2010, Lorenzo-Morales et al., 2013). In the interest of finding an alternative drug target specific to *Acanthamoeba* without affecting the host, I sought to establish and characterise the *Acanthamoeba* surface lectin sugar binding activities, by designing a solid-phase surface protein assay. I coated wells of microtitre plates with Bovine Serum Albumin (BSA)-mannose, BSA-mannan and Mannan-Mannose in Sodium bicarbonate

buffer, pH 9.6, 4°C, overnight. Thereafter, I blocked non-specific binding with 1 % BSA in DPBS, incubated at room temperature for 1 hour.

2.2.2.13. *Acanthamoeba* strains and Human corneal epithelial cell (HCEC) lines

To gain define insight into the mechanism of *Acanthamoeba* pathogenesis, I sought to explore the effect of mannose on *Acanthamoeba* adhesion and cytopathic effects on HCEC. Here, I used *Acanthamoeba* strain (ATCC 50370) of T4 genotypes that was isolated from *Acanthamoeba* keratitis patient. Dr Simon Kilvington, University of Leicester, United Kingdom, kindly provided this strain from American Type Culture Collection (ATCC, Manassas, VA). Meanwhile, I procured the human corneal epithelial cells (HCEC), corneal epithelial cell growth-kit components and the basal medium (485 ml) from Merck Millipore, England. The kit components included 5 mg/ml Apo-transferrin, 1.0 mM Epinephrine, 0.4 % Extract-P, 100 ng/ml hydrocortisone hemisuccinate, 6mM L-Glutamine, 5 µg/ml rh Insulin, proprietary formulation of CE growth factor, 10 units/ml Penicillin, 10 µg/ml Streptomycin and 25 ng/ml Amphotericin B (ATCC® PCS-700-040™).

2.2.2.13.1 Reconstitution of the Human Corneal Epitelial Cells (HCEC) growth kit components

The protocol for Human Corneal Epithelial Cells by Millipore was adopted to reconstitute the 5×10^5 cells/vial corneal epithelial cells. A tightly sealed set of HCEC growth kit components obtained from the -150 °C freezer was allowed to thaw while the L-glutamine component was warmed in a 37 °C water bath and shaken to dissolve any possible precipitate just prior to mixing them to the 485 ml basal medium from cold storage. I de-contaminated the external surfaces of all the components with 70% ethanol spay in aseptically cleaned bio-safety cabinet. Using separate sterile pipette to mix each component in the hood, the final preparation was wrapped in a sterilised kitchen foil paper to shield it away from oxidative reaction of light source.

2.2.2.13.2 Cultivation of Human Corneal Epitelial Cells (HCEC)

During this experiment, I took adequate precautions to avoid unforeseen distortion of primary HCEC cellular morphology by avoiding prolong culture of limited life-span-HCEC. To establish confluent monolayer of HCEC, I grew the primary HCEC on separately labelled 25cm² tissue culture flasks (Corning, Corning Incorporated, NY) in reconstituted HCEC supplemented-basal medium. Then, it was incubated in a 5% CO_2

atmosphere Sanyo® incubator at 36 °C until ready for seeding with *Acanthamoeba* cells. Media re-conditioning and media preparation were all carried out in a digital class II fume chamber (Faster® ultra-safe, Italy) while we exercised cautious not to trypsinize the HCEC at any point in time during the experiment.

2.2.2.14 Mannose-mediated *Acanthamoeba* interaction (adhesion) with HCEC

To determine whether or not *Acanthamoeba* interacts with corneal epithelium by mannose-mediated pattern, I studied the role of mannose in *Acanthamoeba* trophozoites (ATCC 50370) adhesion on HCEC monolayer cells, as we adopted the modified methods of Leher and colleagues (Leher et al., 1998, Khan, 2001, Hurt et al., 2003, Garate et al., 2006, Kim et al., 2012b). I grew the corneal epithelial monolayer to confluence in HCEC supplemented basal medium (as previously described in section 2.2.2.5 above). Between 24 – 48 hours preceeding adhesion assay, the spent medium was replaced with a fresh 5 ml medium, each supplemented with either 100mM of Mannose, or 100mM of galactose (positive control) or HCEC medium only (negative control). Next, I prepared *Acanthamoeba castellanii* that was inoculation into the conditioned monolayer HCEC. After replacing spent Ac#6 medium with 3 ml of fresh maintenance media, one ml of fresh axenic trophozoites cultured in Ac#6 medium was washed in DPBS. The trophozoites count adjusted to 1×10^4 parasites/ml of HCEC basal medium was seeded into separately labelled 75cm² tissue culture flasks containing the confluent supplemented HCEC, incubated at 36 °C, 5% CO_2.

Then, 30 µl samples were removed at approximately every one hour through duration of eight hours for the different conditions. The samples were immediately examined for trophozoites in suspension by direct haemocytometer count using a phase-contrast microscopy. Cells were counted manually according to the methods of Cornell (Connell et al., 2001). The cells suspension was counted on hourly intervals until no more cells were found in the suspension over time. The percentage of the difference between suspended cells and the primary inoculums divided by the original primary inoculums for each preparation indicated approximate percentage of adhered cells to the confluent HCEC. The assay was carried out in duplicates.

2.2.2.15 Mannose-mediated *Acanthamoeba*–induced Cytopathic effect (CPE) on HCEC

To study the cytopathic effects of *Acanthamoeba* trophozoites on HCEC monolayer, I used the modified methods of (De Jonckheere, 1980, Khan et al., 2000, Hurt et al., 2003, Garate et al., 2006, Kim et al., 2012b). The existing HCEC medium in the corneal monolayer epithelium cells has recently been decanted by careful pipetting; and rinsed with 5 ml DPBS and subsequently pre-incubated in freshly prepared conditioned HCEC maintenance medium suspended in 100mM Mannose, 100mM Galactose or the untreated HCEC medium (as control) for 24 hours.

The >95% confluent human corneal epithelial cells culture in each of the separately labelled 75cm² tissue culture flasks was seeded with *Acanthamoeba* trophozoites adjusted count to 1×10^4 parasites/ml in HCEC conditioned medium and incubated at 36 °C, 5% CO_2. I estimated the CPE using the phase contrast microscope and expressed as the percentage of the clear zones (plaques) formed due to cellular destruction relative to the control cells. This plaques reading were periodically observed as destruction of epithelial monolayer, confirmed as visible plaques, by phase contrast microscope at 36 °C periodically at 1, 6, 24, 48 hours. Meanwhile, assays were re-incubated in CO_2 incubator at 36 °C until the remaining corneal monolayer was completely lifted off the flask basement. The plaques were caused by the phagocytic action of the trophozoites on the HCEC monolayer. The pictographs were taken and CPE documented as percentage CPE.

2.3 Results

2.3.1 Differentiation of *Acanthamoeba castellanii* into the three life forms

Relatively few studies have described *Acanthamoeba* excystment compared to the encystment (Fouque et al., 2012). To determine how *Acanthamoeba* switches between its different life forms and to compare excystment patterns of protocysts and mature cysts into trophozoites and vice-versa, *Acanthamoeba* trophozoites were suspended onto Neff's encystment media-containing 0.5% propylene glycol (Neff + 0.5 % PG) to produce protocysts. The trophozoites rapidly differentiated (encystment) into protocysts within 120 minutes of inoculation irrespective of the strains studied (Figure 2.1). Upon removal of the PG, the protocysts converted back to trophozoites over the course of 8-10 hours.
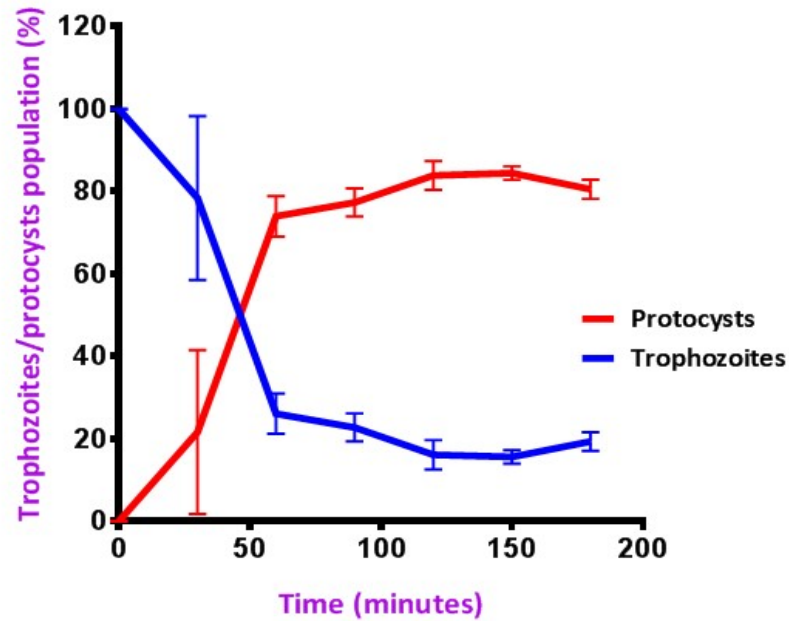
Figure 2-1: Antigenic variation of *Acanthamoeba* trophozoites into protocysts stages: A culture of 3.42 x 10^{5}cells/ml of *Acanthamoeba* trophozoites swiftly differentiated into the protocysts within 120 minutes upon axenic culture in Ac#6 medium containing 5% propylene glycol (PG). The removal of PG caused a rapidly reversible transformation of protocysts back into actively dividing trophozoites within 8-10 hours (not shown). In-vitro, differentiation into protocysts was carried out by incubating cells in Neff's media + 0.5% PG incubation at 32°C with shaking for 2 – 4 hours. About 50 % differentiation occured within ~ 60 minutes of induction. Differentiation was complete 2-3 hours post-innoculation.

A similar pattern of excystment was seen using *Acanthamoeba polyphagia* (Figure 2.2) and the clinical strain of *Acanthamoeba*, Buller-1 strain (not shown here).
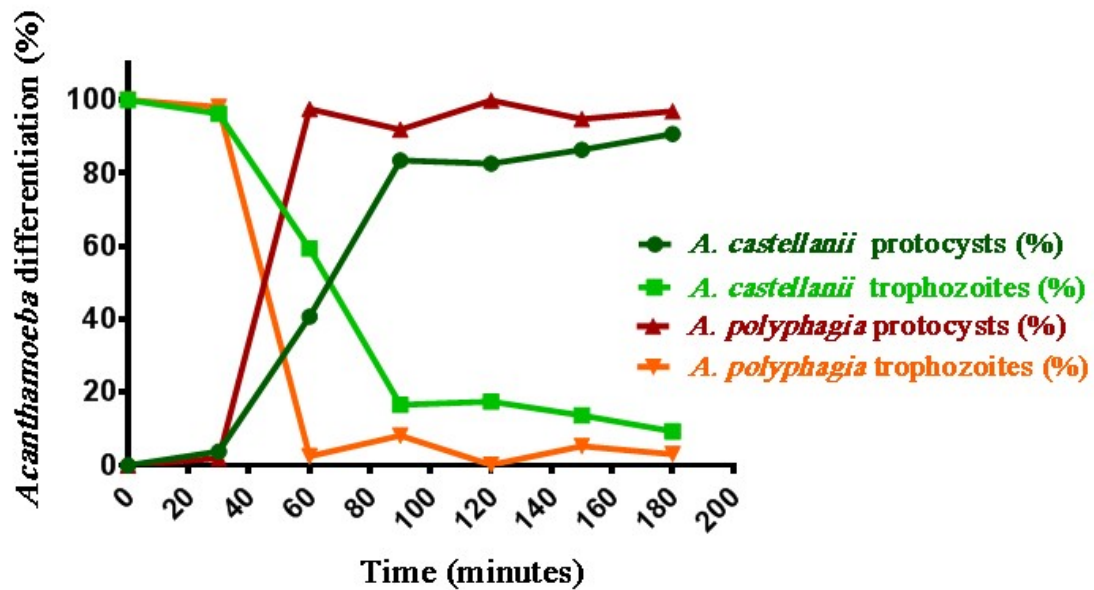
Figure 2-2: Encystment of *Acanthamoeba polyphagia* (ATCC 30461) and *Acanthamoeba castellani* (ATCC 50370) in PG. The experiment was carried out at least twice as described in sections 2.2.3 and 2.2.2.4 above.

Two different methods were used to produce mature cysts from *Acanthamoeba* trophozoites. Firstly, trophozoites were incubated in axenic culture (i.e. in the absence of bacteria as a food source) in Neff's encystment media (without 0.5 % propylene glycol), and encystment into mature cysts was observed over 2-4 days. The second method required seeding of trophozoites onto 2.5 % ENNA plates. Mature cysts were harvested 7 - 10 days after-inoculation. Reversal (excystment) of mature cysts into trophozoites occurred when *E. coli* was added to the culture (xenic culture). This process was also slow taking 7-10 days. Thus, both protocysts and mature cysts could convert into trophozoites and vice-versa depending on the environmental conditions and/or type of culture media used *in-vitro*.
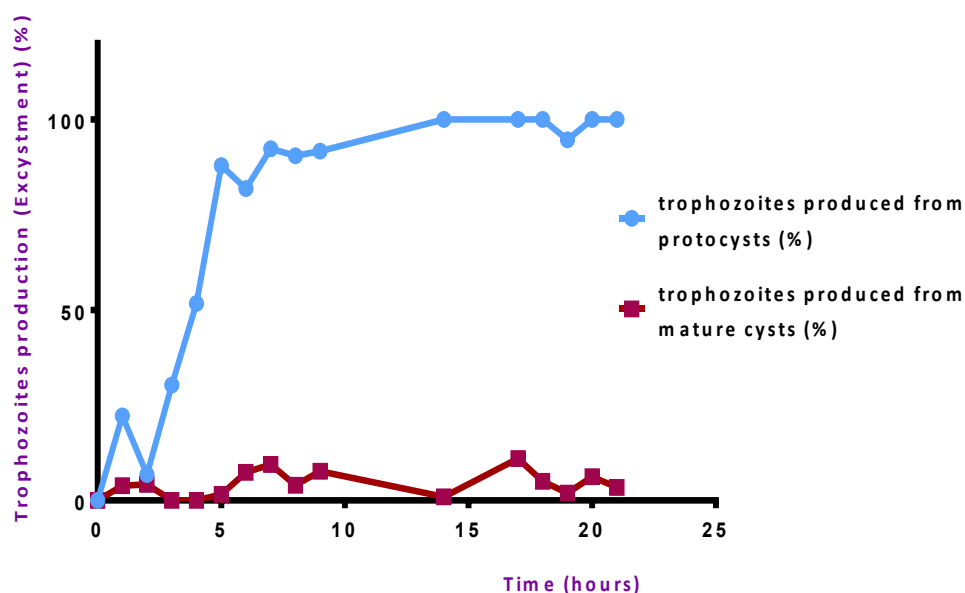
Figure 2-3: *Acanthamoeba* **differentiation of protocysts and mature cysts to trophozoites.** Trophozoites encystment into mature cyst was carried out by adding ~5 drops of washed pelleted trophozoites in ¼ Ringer's solution and spreading the culture onto 2.5% ENNA plates, incubated at 28°C for 5 – 7 days. Excystment back to trophozoites was achieved by overlaying the cysts with *E. coli* (ATCC 8739). No excystment of mature cysts was detected over 22 hours but excystment did occur after 7-10 days (not shown). By contrast, transformation of protocysts back into actively dividing trophozoites occurred within 8-10 hours after removal of PG from the culture medium.This graphical illustration represents an average of two repeated experiments.

Although both protocysts and mature cysts could reversibly convert to trophozoites, they did not themselves intercovert without first passing through the trophozoite stage in any of the experiments/conditions tested. This supports the work of Kilvington (Kilvington et al., 2008). Protocysts do not transit into mature cysts hence confirming the protocysts as a third life form of *Acanthamoeba* spp rather than simply reflecting an intermediate on the process of encystment.

Overall, these experiments show that trophozoites can convert to protocysts or mature cysts but the two cyst forms cannot directly convert. In addition, conversion of trophozoites to protocysts and *vice-versa* is much more rapid than conversion of trophozoites to mature cysts and *vice-versa* (figure 2.3).

The difference in timescales of encystment and excystment of protocysts and mature cysts probably reflects the morphological changes involved in these processes most

notably formation (and breakdown) of the double cell wall of the mature cyst form. In the mature cysts, stress conditions triggers formation of trehalose, which is a major source of energy, carbon reserve, stabilizer and protectant of membrane proteins from dehydration, heat, causing encysted *Acanthamoeba* to remain in a state of 'anhydrobiosis' for decades until water/nutrient is available (Elbein et al., 2003).
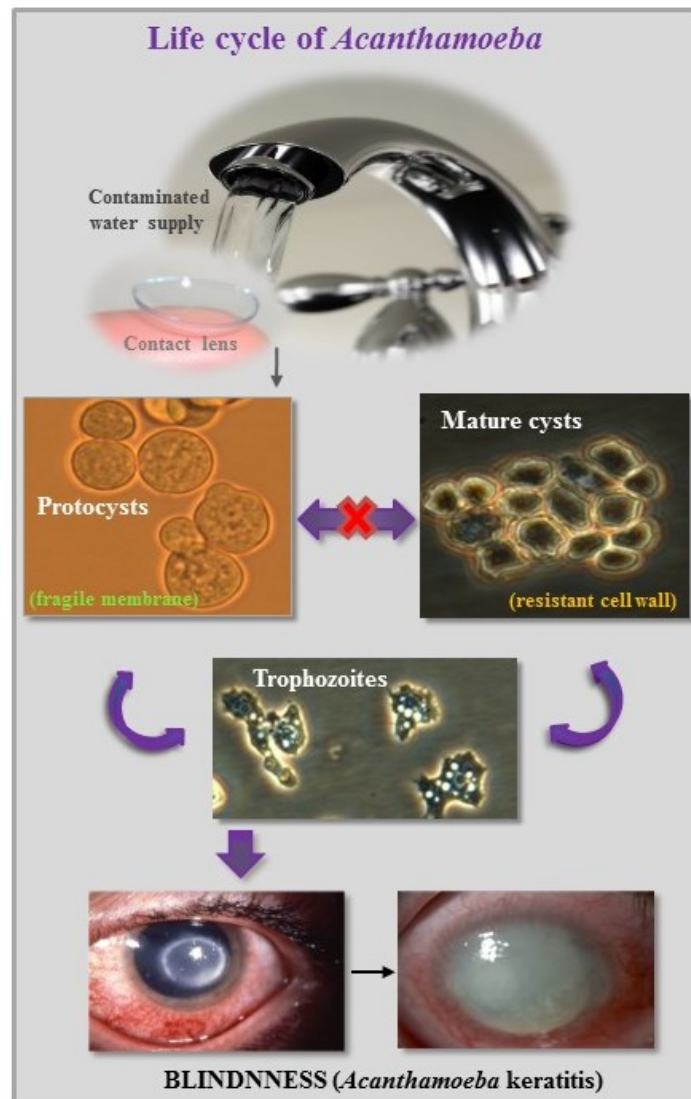
Figure 2-4: Revised life cycle of *Acanthamoeba*. (Top): *Acanthamoeba* keratitis is caused by free-living, eukaryotic, amoebae from contaminated domestic water supplies, promoted by bio-film-ladden water-supply pipes/taps and pre-existing damage to the cornea prompted by contact lens application **(Middle):** Three different life forms exists namely fragile-membrane protocysts (newly discovered) which cannot interconvert directly to dormant mature-cysts and the actively virulent trophozoites. **(Bottom):** Progression of *Acanthamoeba* keratitis in a pre-traumatised corneal tissue already infected by *Acanthamoeba*. Parasitic adhesion is followed by cytopathology and in most cases is unresponsive to treatment and eventual blindness.

2.3.2 Colonial morphology and microscopic characterization of the *Acanthamoeba* life stages

Having established conditions for differentiation of the life forms, I then went on to characterise these life stages of *Acanthamoeba castellanii* (ATCC 50370) morphologically using confocal microscopy. The three different life stages: trophozoites, mature cysts and recently discovered protocysts could be stably maintained and exhibit distinct morphological features. The life-forms of *Acanthamoeba* are shown in Figure 2.5. *Acanthamoeba* trophozoites possess irregular-shaped acanthapodia with numerous vacuoles; the mature cysts form clumps and have a ringed-shaped double-cyst wall and the protocysts is spherical with a single-wall (confirmed with fluorescence calco-flour-white stain) respectively**.**
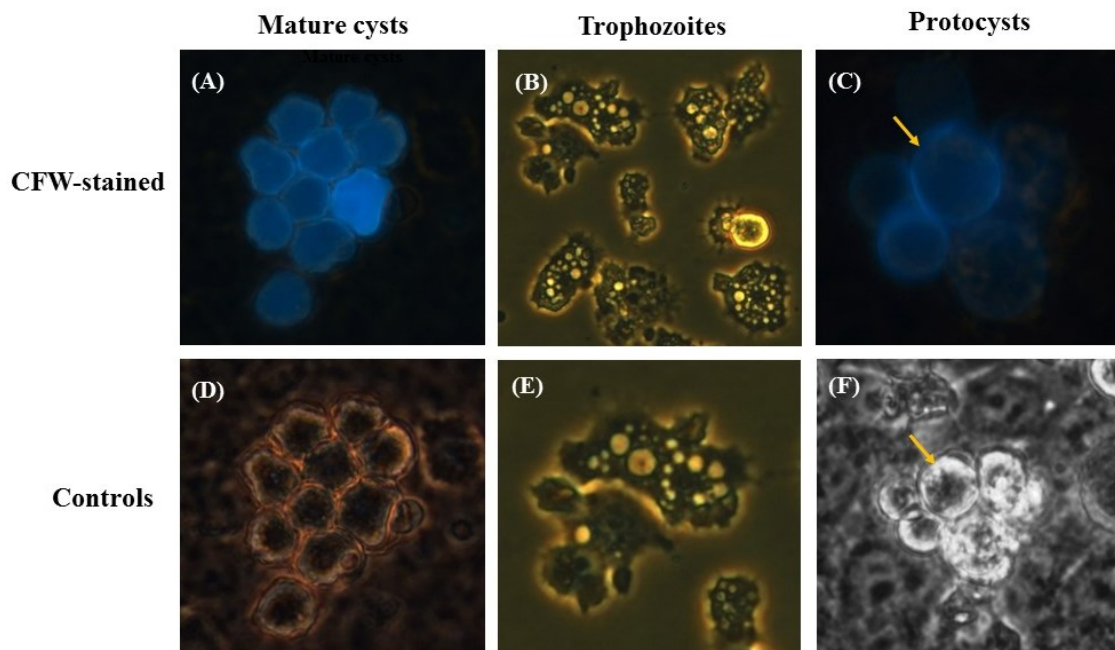
Figure 2-5: Morphologies of the three life forms of *Acanthamoeba*. (Top): (a-c) Flourescence micrographs of polygonal-shaped mature cysts; irregular-shaped trophozoites (not stained as it lacks cellulose membrane), spherical-shaped protocysts (arrowed) stained with calco-fluor white (CFW) dye and examined under 400x magnification by fluorescence microscopy.**(Bottom):** (d-f) Phase-contrast images of corresponding mature cysts, trophozoites and protocysts (arrowed)). All micrographs were obtained from this study.

Mature cysts were produced from differentiated trophozoites on NNA plates seeded with *E. coli* (Greenfield et al., 2009). The characteristic appearance of mature-cysts is irregular

polyhedral (angular) shaped structures, composed of thicker ectocysts and endocysts (Khunkitti et al., 1998, Kilvington and Lam, 2013). To enable the propagation for the large-scale harvest of mature cysts required for quantitative assays, I adopted a controlled axenic cultivation of trophozoites grown in Ac#6 medium at exponential phase. I took adequate caution to avoid microbial contamination of the cultured *Acanthamoeba*, which might hinder both the growth and encystment of *Acanthamoeba* (Glaser et al., 2011). The presence of propylene glycol transformed *Acanthamoeba* trophozoites into the immature cysts (protocysts) that did not develop further into the mature cysts (Figure 2.6). Because they lack a cellulose cell wall, trophozoites and protocysts are more likely to be susceptible to anti-parasitic agents compared to the resistant dormant mature cysts (Bínová et al., 2017).
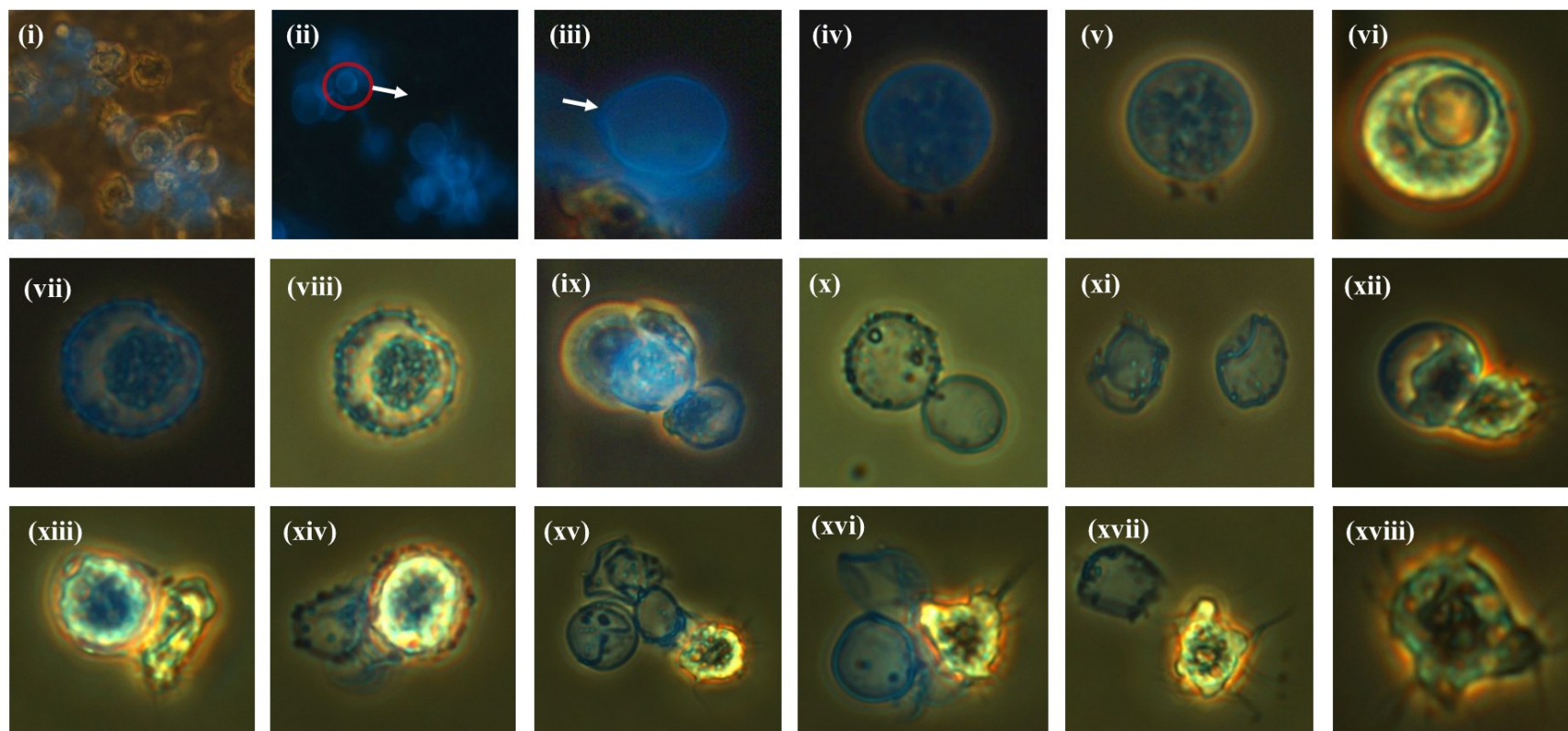
Figure 2-6: Differentiation of *Acanthamoeba* protocysts into trophozoites. (i) Fluorescent image of protocysts in calca-fluor stain against a monolayer of vero epithelial cells (ii) Protocysts alone (red circle) (iii) 10x magnified image of ii. (iv and v) Fluorescent and non-fluorescent images of a protocyst. The granular chromatin and cell membranes are visible. (vi) Development of a marginal ringed-nucleus. (vii – viii) The remnant of the cell membrane was detected by faint CFW fluorescence. Dissolution of both the nuclear and membrane proteins. (ix - x) Eruption of the membrane to release the nuclear material. (xi) Separation of the nuclear material from the membrane protein. (xii - xvii) Further development of trophozoites and development of the acanthapodia. (xviii) Hatched trophozoites freed from the casing shell. (All micrographs were obtained from this study).
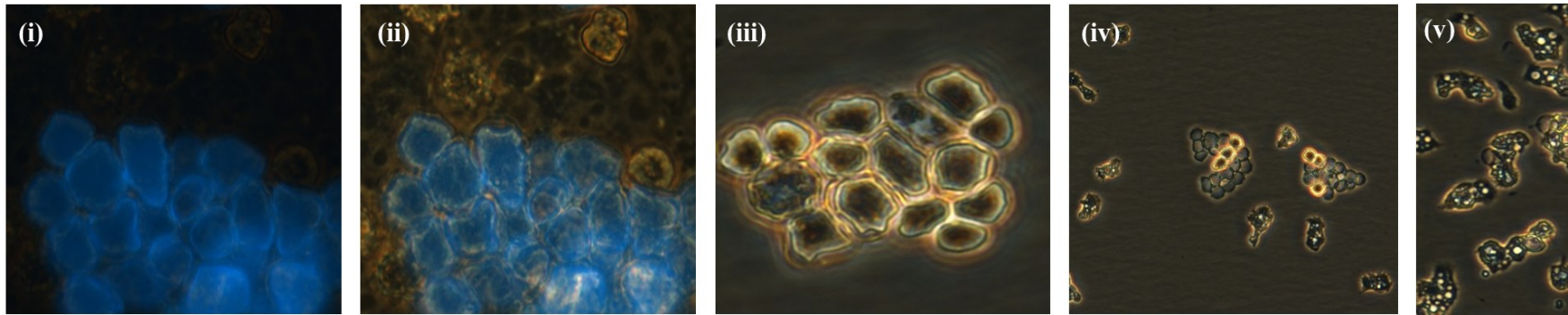
Figure 2-7: Stages of excystment from *Acanthamoeba* mature cysts into trophozoites. (i) Fluorescent image of mature cyst in calcafluor white stain against a monolayer of vero epithelial cells (ii) Contrast of fluorescent mature cysts in (i) against vero epithelial cells (iii) Non-fluorescent image of mature cysts (iv) Mature cysts slowly excyst into the trophozoites without transiting through the protocysts stage. Mature cyst differentiation into the trophozoites was slower and not very detailed as compared to the protocysts. Empty clustered shells were left after excystment of hatched trophozoites. (v) Further development of trophozoites and development of the acanthapodia. (All micrographs were obtained from this study).

2.3.3 Adrenergic signalling of *Acanthamoeba*

Previous studies have shown that β-blockers can inhibit differentiation of *Acanthamoeba* (Heaselgrave and Kilvington, 2016). To test the effects of β-blockers on the encystment of trophozoites to protocysts, the proportion of the different *Acanthamoeba* life forms were counted in the presence and absence of Propanolol, under conditions that induce differentiation.
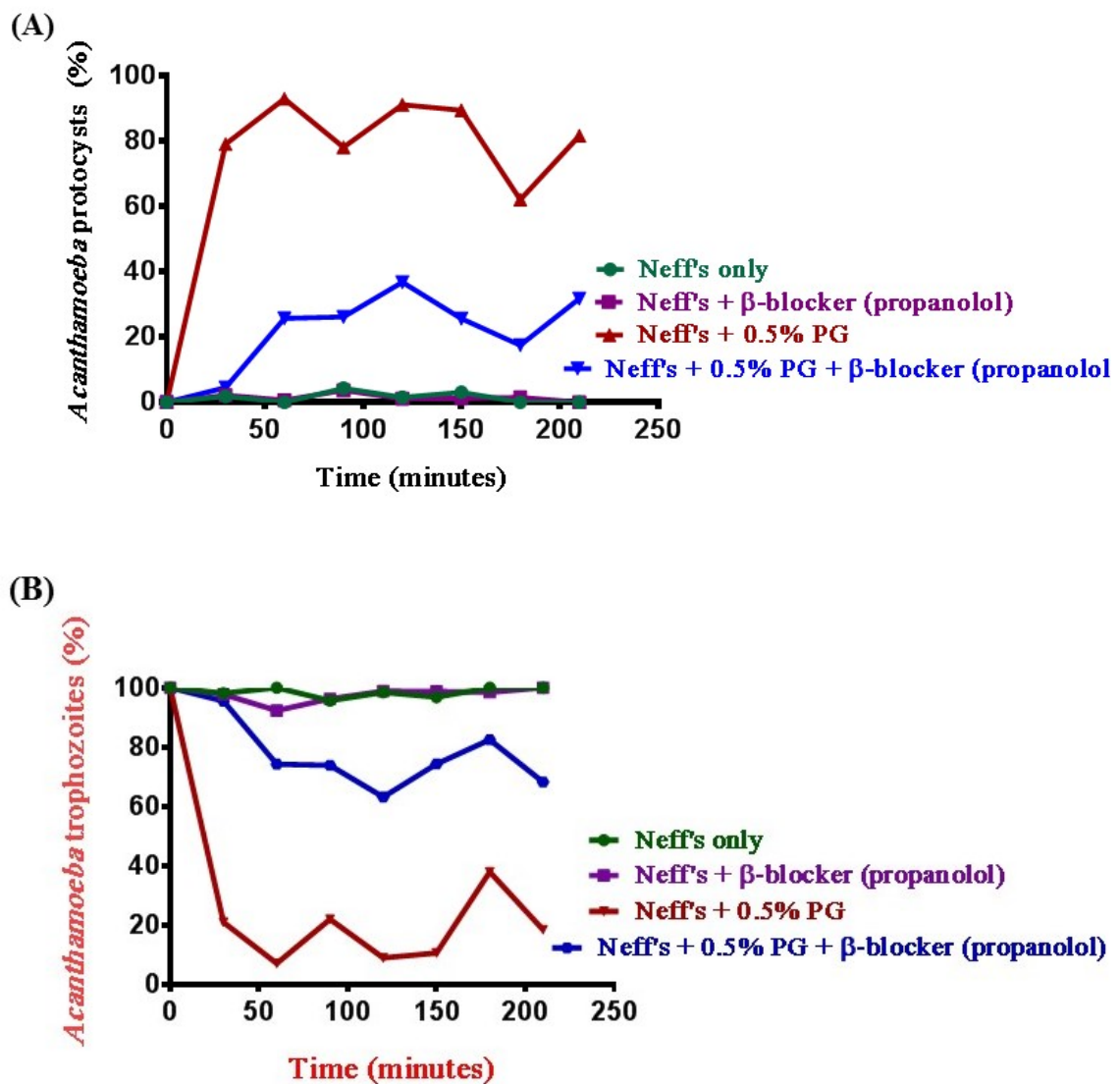
Figure 2-8: Inhibitory effect of ß-blockers (Propranalol) on *Acanthamoeba* differentiation. Differentiation was induced by addition of 0.5% PG. The concentration of propranolol was 1M. **(A)** Only trophozoites in PG differentiate into protocysts, those in Neffs alone did not differentiate. **(B)** Only protocysts in PG differentiate into trophozoites, those in Neffs alone did not differentiate.

Having established the conditions for trophozoites encystment, I sought to investigate the inhibitory effects of β-blockers on either protocysts or mature cysts formation. First, we incubated trophozoites with Neff media or Neff + propylene glycol + serial dilutions of β-blockers (Propanolol or Metoprolol) for 24 or 48 hours. Sterile nanopure water was used as a control. The numbers of mature cysts (in Neff media) or protocysts (in Neff + propylene glycol) was counted at each concentration. At the highest concentration of β-blocker, encystment was completely inhibited.

Figure 2.8 shows that there was no significant difference in the pattern of trophozoites encystment after pre-conditioning. All protocysts were rapidly converted to trophozoites. As expected, no mature cysts were observed in the Neff media over the relatively short timescale observed. In a separate experiment, protocysts were pre-conditioned as before, washed and re-suspended in Ac #6 media (which causes excystment). All converted to trophozoites with no apparent differences in the timescale. Thus, the pre-conditioning had little effect on differentiation.

As shown in Fig 2.9, trophozoites differentiated to protocysts in the presence of PG and differentiation was inhibited by propranolol. The IC_{50} for propranolol (~20 μM) on protocysts differentiation was measured by titrating the amount of propranolol and measuring encystment via numbers of protocysts.
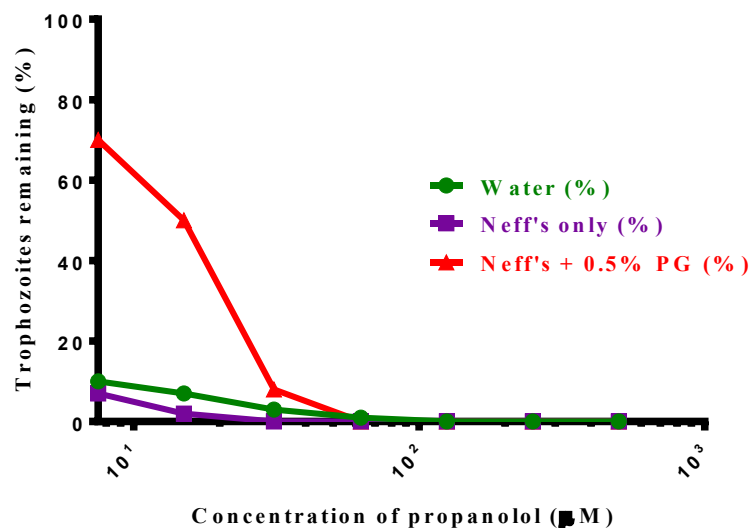
Figure 2-9: Inhibitory effect of propanolol on encystement of trophozoites to protocysts. Two-fold dilutions of propranolol starting at 500 μM were added to 1 x 10^6 trophozoites/ml and incubated at 28 °C for 24 hours post inoculation. To distinguish

encystment from the toxic effect of propanolol, 1 ml of calcoflor white (CFW) was added to each of the preparations in the control. Florescence protocysts indicated encystment while absence of florescence cells indicates cellular toxication.

At 24 hours post-treatment, the IC_{50} values (concentration of β-blockers that leads to 50% inhibition of encystment) were 18 and 250 µM for protocysts formation (Neff + propylene glycol) in Propranolol or Metoprolol respectively and 5 and 50 µM for mature cyst formation. At 48 hours after treatment, IC_{50} values (concentration of β-blockers that leads to 50% inhibition of encystment) were 25 and 220 µM for protocysts formation (Neff + propylene glycol) in Propranolol or Metoprolol respectively and 5 and 75 µM for mature cyst formation. Thus, β-blockers are more active at inhibiting mature cyst versus protocysts formation and Subsequent experiments were preferentially conducted using propranolol that was more effective than metoprolol at inhibiting *Acanthamoeba* encystment; although, there was little difference at the different time points (24 vs. 48 hours).

Initially, I set the concentration at 10 µM while we observe the conversion of trophozoites to protocysts or mature cysts over the time frame of about ~200 minutes. My findings revealed a rapid trophozoites encystment into protocysts with a half time of < 40 min in the absence of propanolol. However, encystment was inhibited (with only ~30% of protocysts in the population after 200 minutes) in the presence of Propanolol. Expectedly, the mature-cysts were not formed within this short time course of observation.

2.3.4 Adhesion of the different life forms of *Acanthamoeba* onto inert and biological surfaces

2.3.4.1 Adhesion to tissue culture and non-tissue culture plates

Most reported cases of AK have been attributed to either contaminated contact lens, contact lens-storage cases (plastic/polymer) or traumatised corneal tissue (Yang et al., 1997, Tomlinson et al., 2000) raising the possibility that *Acanthamoeba* may bind directly to contact lenses and contact lens cases. I therefore compared adhesion of the different life forms to surfaces. *Acanthamoeba* were inoculated onto the different selected surfaces and the numbers of cells still in suspension were counted at intervals using a haemocytometer. The number of cells stuck to the surface was calculated from the

starting numbers minus those still in suspension. Figure 2.10 shows binding to tissue culture (TCP) and non-tissue culture plates (NTCP).
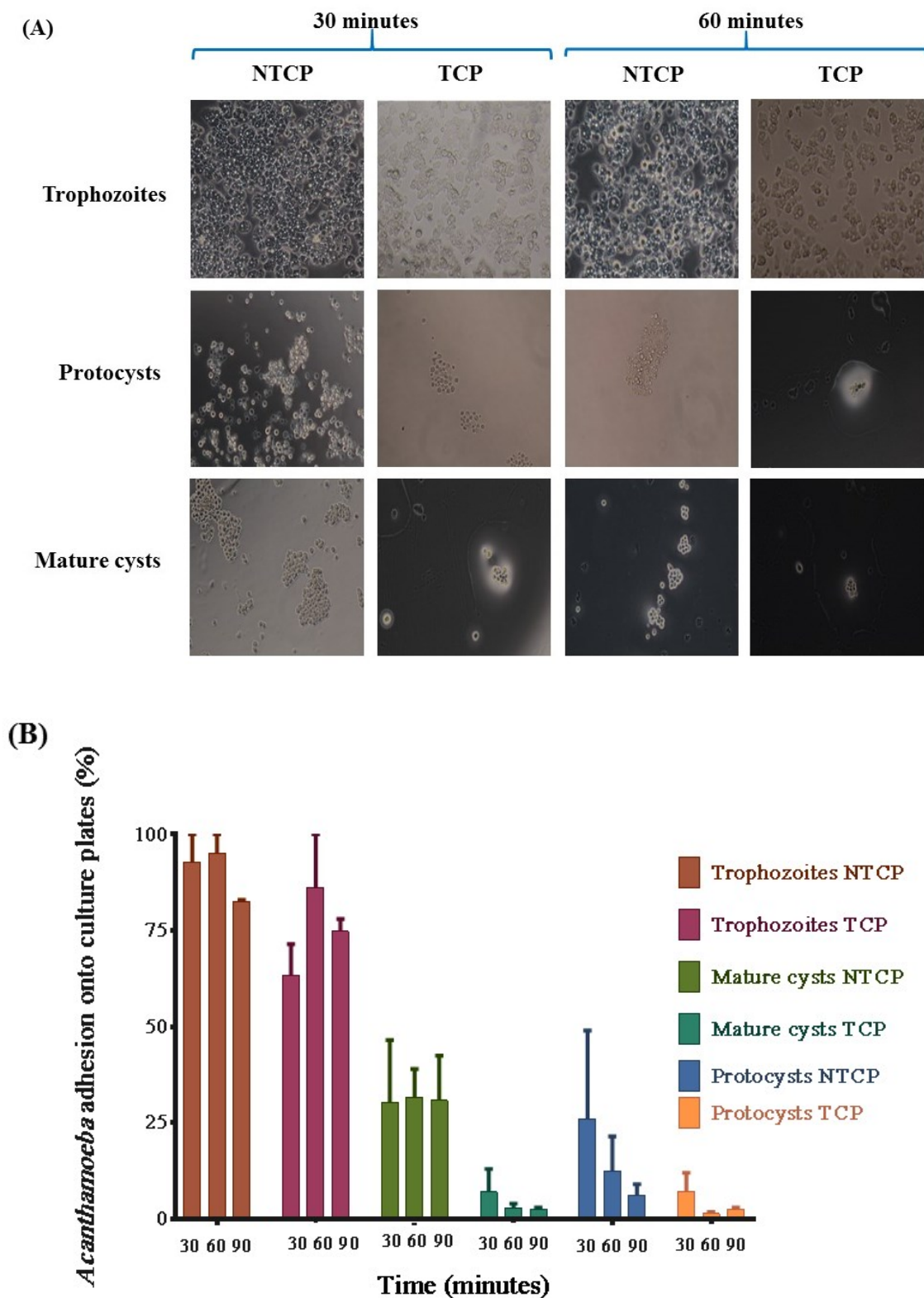
Figure 2-10: Adhesion of different life-stages of *Acanthamoeba*. (Top): Culture plates were inoculated with 2 x 10^4 cells/ml of *Acanthamoeba*. Two types of plates were used

tissue culture plates (TCP) & non-tissue culture plates (NTCP). The TCP are hydrophobic, negatively charged polystyrene plastics while NTCP are neutral surfaces. **(Bottom):** For each life form, the number of cells stuck to the surface was calculated from the starting number minus those still in suspension. Error bar signifies the standard error of mean (SEM). Experiments were repeated at least twice.

All life stages of *Acanthamoeba* bound to plates. Trophozoites bound best with lower binding by protocysts and mature cysts. Binding occurred within 30 mins of addition of *Acanthamoeba* and similar levels of binding were observed over the time course of the experiment. There was little difference in binding to TCP and NTCP indicating that *Acanthamoeba* can adhere to a wide variety of surfaces.

2.3.4.2 Binding to mannan-coated ELISA plates

To test if *Acanthamoeba* could bind to mannan, a polymer of mannose, isolated from yeast cell walls was used. ELISA plates were coated with mannan and inoculated with trophozoites. Plates were also coated with BSA (a serum protein lacking carbohydrate) as a control. As shown in figure 2.11, trophozoites adhered to both surfaces with little difference in the amount of adhesion. Addition of EDTA to the buffer reduced but did not abolish binding in each case. EDTA chelates divalent metal ions, which in turn are often important for function of adhesion proteins (Wang, Asem and McLaughlin, 1994).
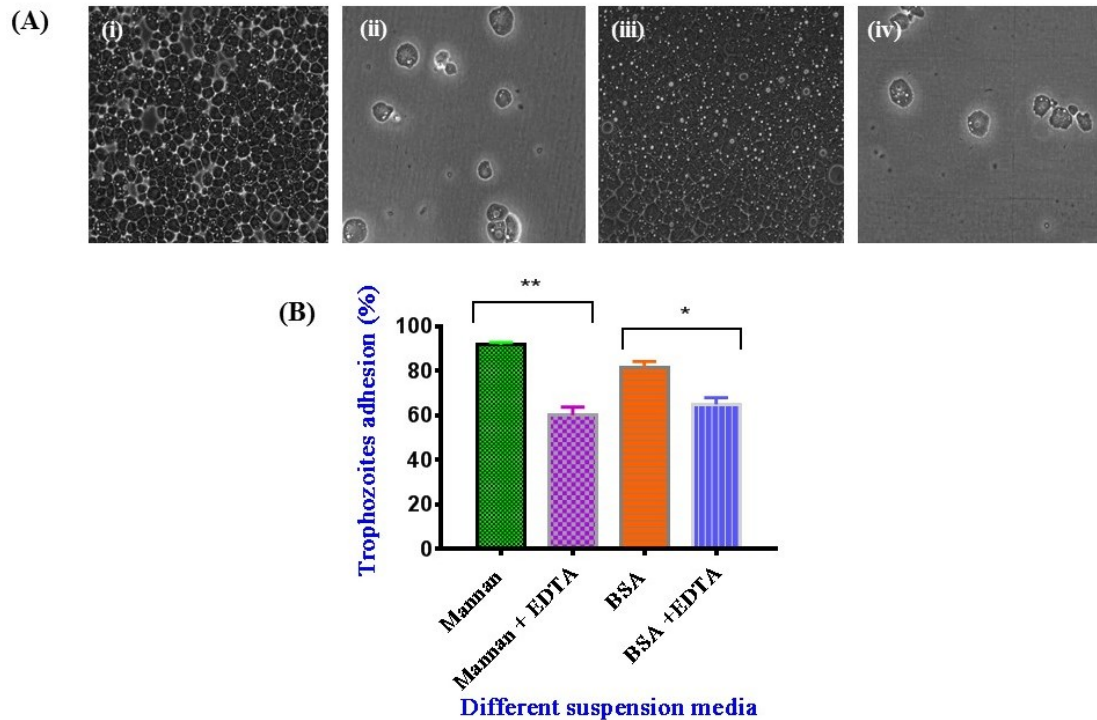
Figure 2-11: *Acanthamoeba* **adhesion on mannan-coated ELISA plates.** The primary inoculum of *Acanthamoeba* was ~ 3 x 10^5 cells/ml. (**A**): Micrographs of trophozoites at 120 minutes post-inoculation at magnification of 200x on wells on an ELISA plate coated with (i) Mannan (ii) Mannan in the presence of EDTA (iii) BSA (iv) BSA with EDTA. (**B**): Graph showing adhesion of trophozoites under the different binding conditions. Using Paired t-test (two tailed), n = 3, Mannan + EDTA versus Mannan only, p value = 0.0088, t = 10.62, df = 2 compared to unpaired t test of data (two tailed): BSA + EDTA versus BSA only, p value = 0.0153, t = 4.063, df = 4. Overall analysis of the four conditions using ordinary one-way ANOVA, F = 27.13, P value = 0.0002, p value summary = ***, R square = 0.9105. There was a significant difference among means (P < 0.05). This confirms the relative significance of both mannose (mannan) and Ca^{2+} (absence of EDA) in *Acanthamoeba* adhesion. Error bars indicates the SEM. Experiments was repeated thrice.

Overall, the data show that *Acanthamoeba* bind to both BSA and mannan-coated plates to approximately similar extents. EDTA reduced the level of binding to both surfaces, indicating that divalent metals ions are important but not essential for binding.

2.3.4.3 Adhesion to Contact lenses

I also measured adhesion of *Acanthamoeba* to contact lenses. Most contact lens solutions contain PG, which maintains *Acanthamoeba* as protocysts. It was therefore of interest to see if these protocysts bound to contact lenses. Adhesion was measured in standard water

containing 0.5% propylene glycol (PG). Assays were carried out at room temperature in non-tissue culture plates (NTCP) to mimic a contact lens plastic storage case.
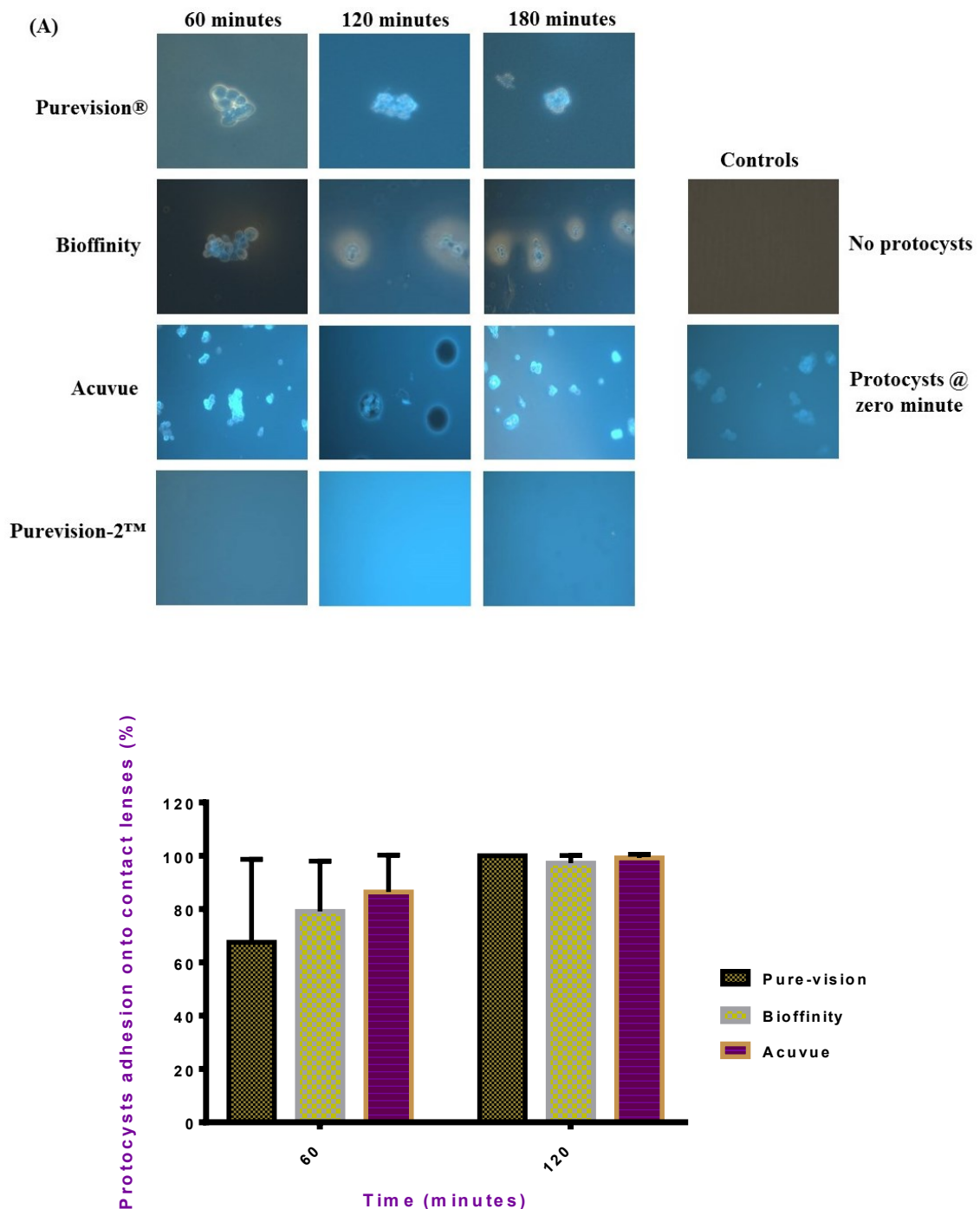
Figure 2-12: Adhesion of *Acanthamoeba* protocysts onto selected contact lenses. *Acanthamoeba* protocysts (3×10^4 cells) were inoculated onto four popular brands of sterile contact lenses, which were twice pre-washed in DPBS at room temperature for 10 minutes. Two brands of Purevision lenses were tested namely Purevision® (row 1) and

Purevision 2™ (row 4). **(A)** Binding of protocysts to contact lenses at 60, 120 and 180 minutes. Adhesion was confirmed by fluorescence microscopy after addition of calcoflor white stain. Over 24 – 48 hours protocysts differentiated to active trophozoites. Negative and positive control experiments showed no protocysts (top micrograph) and presence of protocysts at zero minute (bottom micrograph) respectively. **(B)** Protocysts adhesion onto the selected contact lenses at 60 and 120 minutes. No adhesion of protocysts was detected on Purevision-2 lenses. n = 2, error bars indicates the SEM.

As shown in Figure 2.12, protocysts bound to three of the four contact lenses tested: Purevision, Bioaffinity, Acuvue, and binding increased over the 120 minutes of the experiment. Interestingly no binding was detected to Purevision-2 lenses. Both Purevision lenses are made from a silicon hydrogel material called balafilconA, with a 36% water content. It is not clear why no adhesion was detected to Purevision-2 lenses because the manufacturers do not provide details of the production process. Adhesion of protocysts to contact lens cases and to contact lenses themselves is likely to be a mechanism for transfer to the eye leading to infection. Once in the eye, the protocysts can rapidly differentiate into trophozoites.

2.3.4.4 Adhesion to epithelial cell lines

Previous studies have focused on adherence of *Acanthamoeba* to primary corneal cells, but it was of interest to see if *Acanthamoeba* can adhere to other epithelial cell lines. Three different cell lines were tested namely Hep2 cells, Vero cells and HT 29 cells. Hep2 cells are an immortalized Human epithelial type-2 cell line derived from human laryngeal carcinoma cells whereas Vero cells are derived from kidney epithelial cells extracted from an African green monkey. The HT-29 cell lines were derived from human Caucasian colon adenocarcinoma grade II (Eklöv et al., 1992, Ammerman et al., 2008, Martínez-Maqueda et al., 2015).
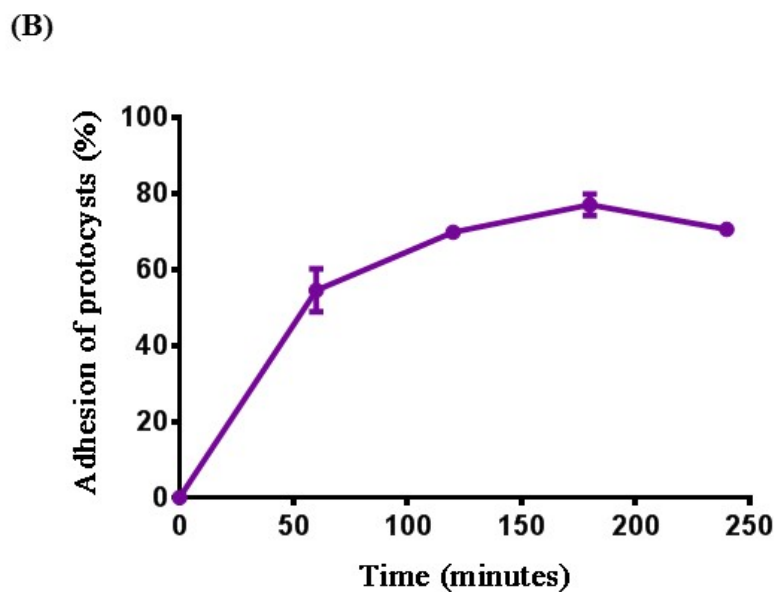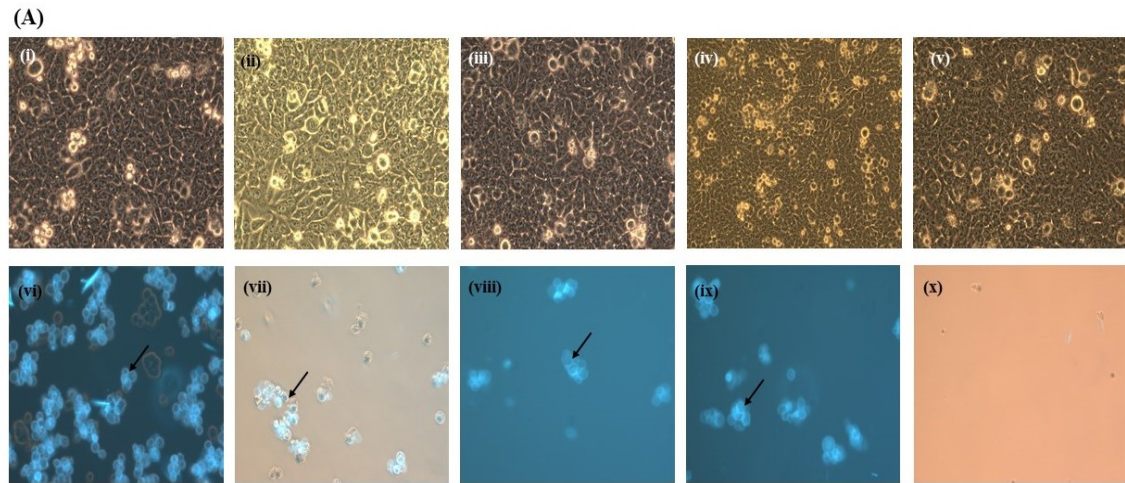
Figure 2-13: Adhesion of protocysts to a confluent lawn of Vero cells. (A) Top row phase contrast micrographs of protocysts adhesion onto vero monolayer cells at: **(i)** 60 mins **(ii)** 120 mins **(iii)** 180 mins **(iv)** 240 mins **(v)** 300 mins. Bottom row fluorescence micrographs of protocysts adhesion (arrowed) onto vero monolayer cells at equivalent time points: **(vi)** 60 mins **(vii)** 120 mins **(viii)** 180 mins **(ix)** 240 mins **(x)** 300 mins. Only protocysts are visible by fluorescence microscopy. Over the time course of the experiment, protocysts differentiate to trophozoites (not visible). In (x) all protocysts have differentiated to trophozoites **(B)** Graph of adhesion of *Acanthamoeba* to Vero cells. The number of cells bound to the monolayer was calculated from the amount still in suspension. The apparent decrease in binding observed after 200 mins is likely to be due to differentiation to trophozoites, which are not detected by the fluorescent microscopy. Experiments were repeated at least twice.

As shown in Figure 2.13, protocysts adhere to the Vero cells over ~ 200 mins. The decrease observed at longer timepoints is due to differentiation of protocysts to trophozoites (beyond 400 min, no protocysts were detected). A similar patter of adhesion was observed towards Hep2 cells (Fig. 2.14)
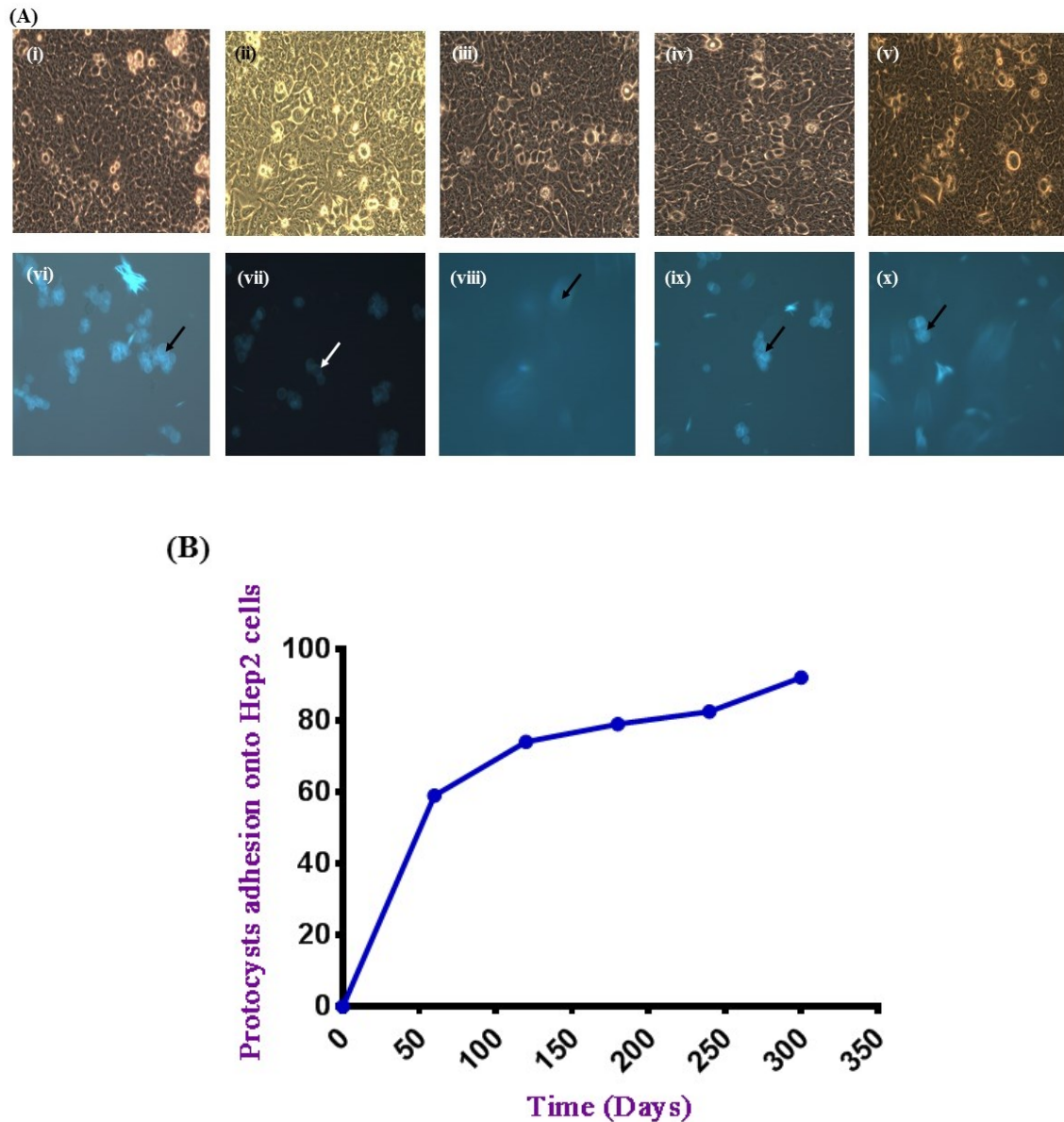
Figure 2-14: Adhesion of protocysts to Hep2 cells. (A) Micrographs: Top row phase contrast micrographs of protocysts adhesion onto Hep2 monolayer cells at: **(i)** 60 mins **(ii)** 120 mins **(iii)** 180 mins **(iv)** 240 mins **(v)** 300 mins. **Bottom row** fluorescence micrographs of protocysts adhesion (arrowed) onto Hep2 monolayer cells at equivalent time points: **(vi)** 60 mins **(vii)** 120 mins **(viii)** 180 mins **(ix)** 240 mins **(x)** 300 mins. Only protocysts are visible by fluorescence microscopy. Over the time course of the experiment, protocysts differentiate to trophozoites (not visible). **(B)** Graph of adhesion of *Acanthamoeba* to Hep2 cells. The number of cells bound to the monolayer was calculated from the amount still in suspension. The apparent decrease in binding observed

67

after 200 mins is likely to be due to differentiation to trophozoites, which are not detected by the fluorescent microscopy. Experiments were repeated at least twice.

To examine the effects of mannose on adhesion, experiments were carried out in the presence of mannose or glucose as a control. Mannose has previously been shown to inhibit AcMBP and affect adhesion and CPE (Hurt et al., 2003, Garate et al., 2005, Garate et al., 2006). As shown in Fig 2.15 the presence of mannose (100 mM) did not prevent adhesion to Vero cells by protocysts or trophozoites, implying that AcMBP is not essential for the adhesion of either life form to Vero cells. Adhesion of trophozoites was slower in the presence of mannose, however, suggesting that AcMBP may play a role in the adhesion process.
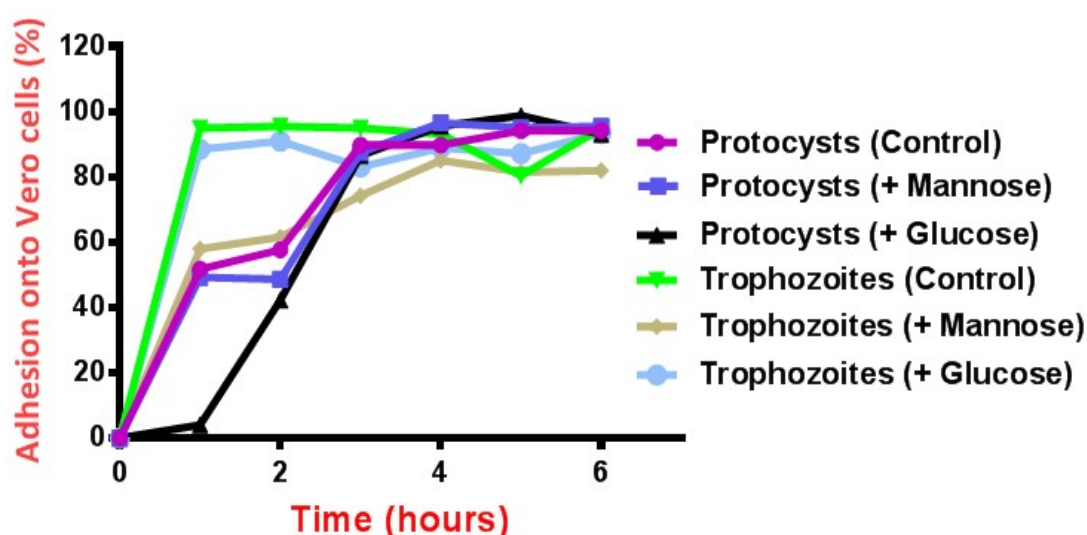
Figure 2-15: Effects of mannose on *Acanthamoeba* adhesion. *Acanthamoeba* trophozoites adhere faster than protocysts within the early three hours of inoculation onto vero cell line. The process of protocysts excystment into trophozoites prior to attachment was responsible for the difference. Mannose delayed trophozoites attachment onto vero cell lines while there was no significant inhibitory effect on protocysts adhesion to vero epithelial cells, n = 2.

2.3.5 Cytopathic effects of *Acanthamoeba* on Hep2 and Vero cells

To establish and characterise the pathogenic behaviour of *Acanthamoeba*, I carried out separate experiments to measure the cytopathic effect (CPE) of trophozoites and protocysts against monolayers of epithelial cell lines. In this experiment, the area of

monolayer destroyed (plaques) was estimated at hourly intervals using phase contrast microscopy (González-Robles et al., 2014). Protocysts themselves are not able to kill cells but must first excyst into trophozoites. The half time for CPE was ~2 days and ~4 day for excysted protocysts on Vero and Hep2 epithelial cell monolayers, respectively (Figures 2.16 – 2.19).
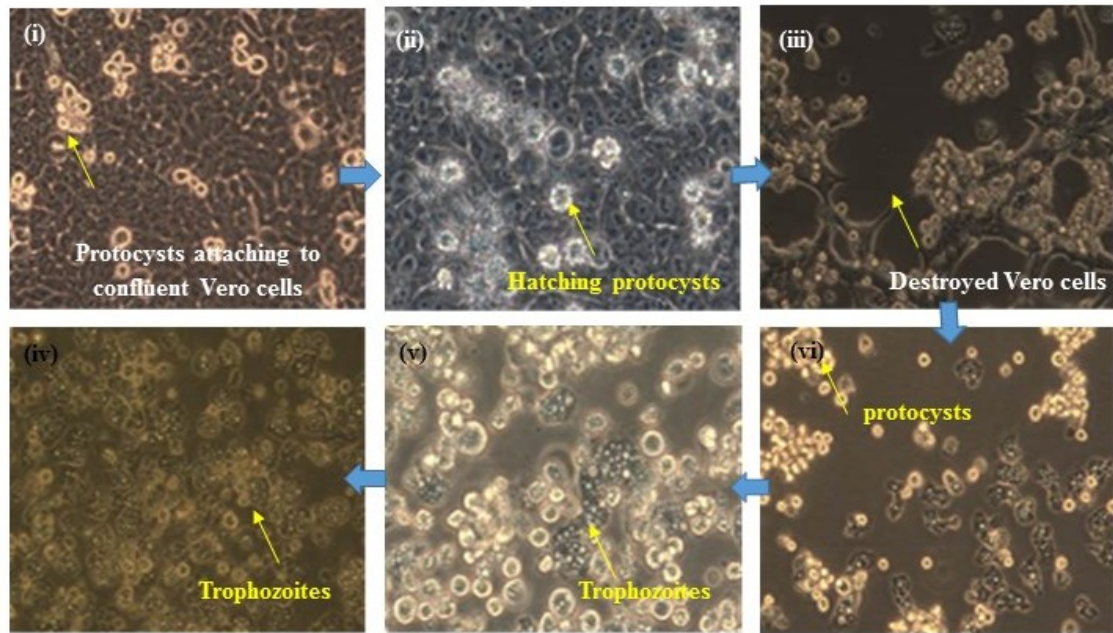
Figure 2-16: Micrographs of *Acanthamoeba* adhesion and cytopathic effects on Vero epithelial cell monolayer. Clockwise direction **(i)** Protocysts attaching to a confluent monolayer of Vero cell **(ii)** Protocysts hatching on Vero cell lines **(iii)** Destruction (CPE) of Vero cell lines by resulting trophozoites **(iv - vi)** further destructions of Vero cell lines as the trophozoites population increases, n = 3).
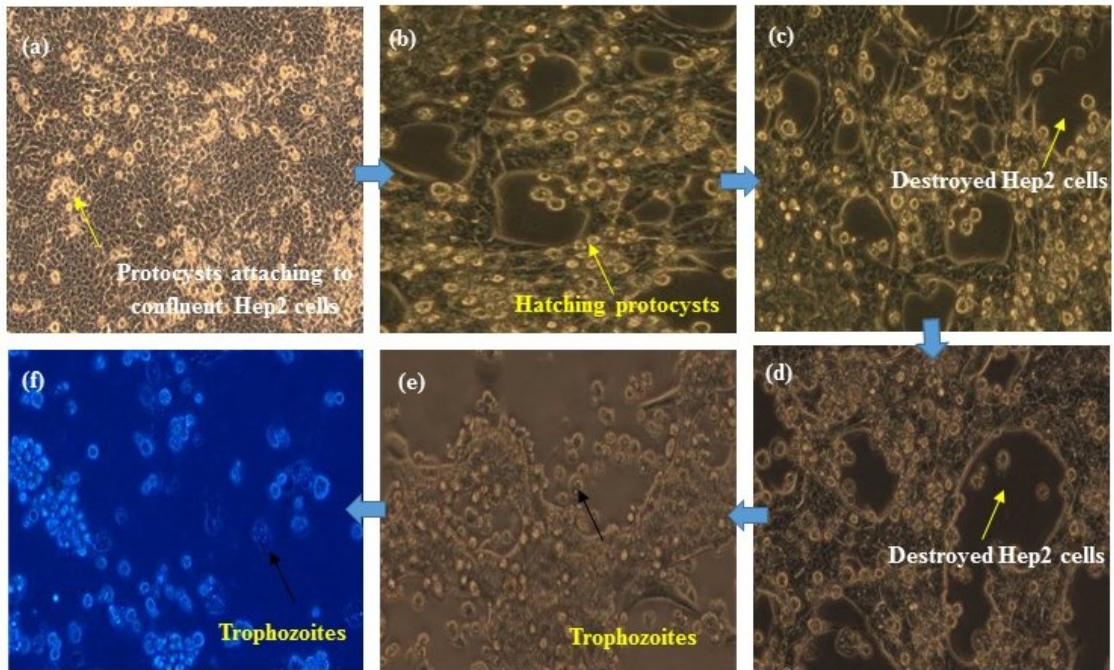
Figure 2-17: cytopathic effects of *Acanthamoeba castellanii* protocysts on Hep2 epithelial cells: Clockwise direction **(a)** Protocysts attaching to a confluent monolayer of Hep2 cells **(b - c)** Protocysts hatching on Hep2 cell lines and destruction (CPE) of Hep2 cell lines by resulting trophozoites **(d - f)** further destructions of Hep2 cell lines as the trophozoites population increases, n = 3).
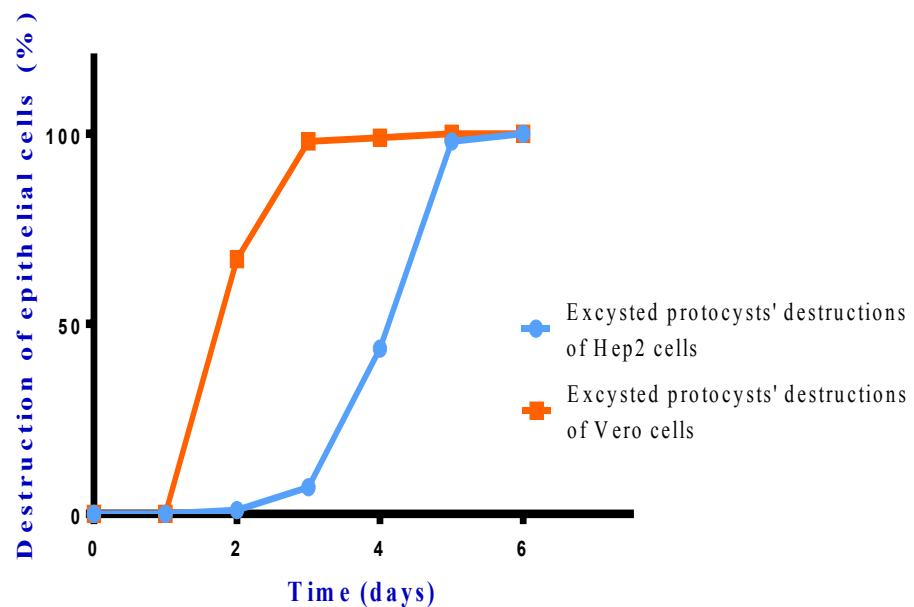
Figure 2-18: Comparison of the CPE of protocysts on Hep2 and Vero cells. Representative experiments showing CPE measured by estimating the size of the clear zones. There was a ~ 24 hour difference in half time of the CPE on Vero and Hep2 cell lines.
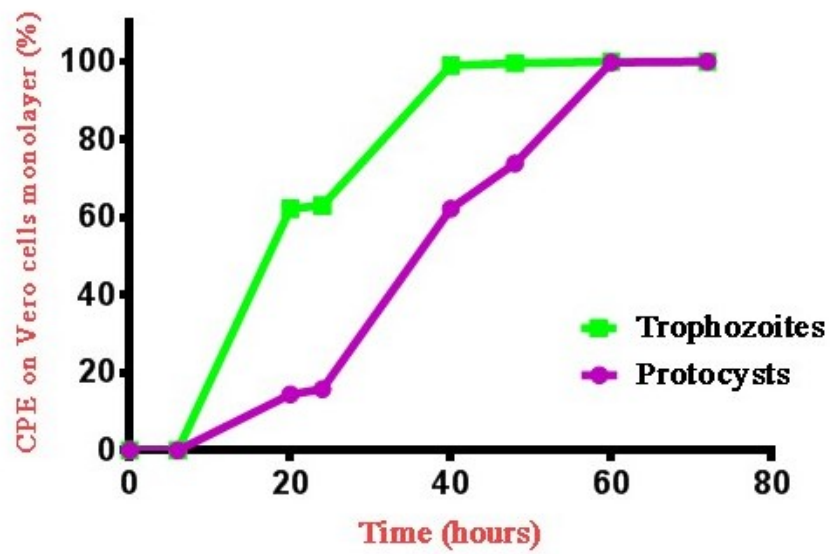
Figure 2-19: Comparison between CPE produced by trophozoites and protocysts.
The difference of ~20 hours in eliciting 50 % CPE between trophozoites and protocysts
is likely to be due to the lag period of protocysts excystment into trophozoites before
triggering CPE.
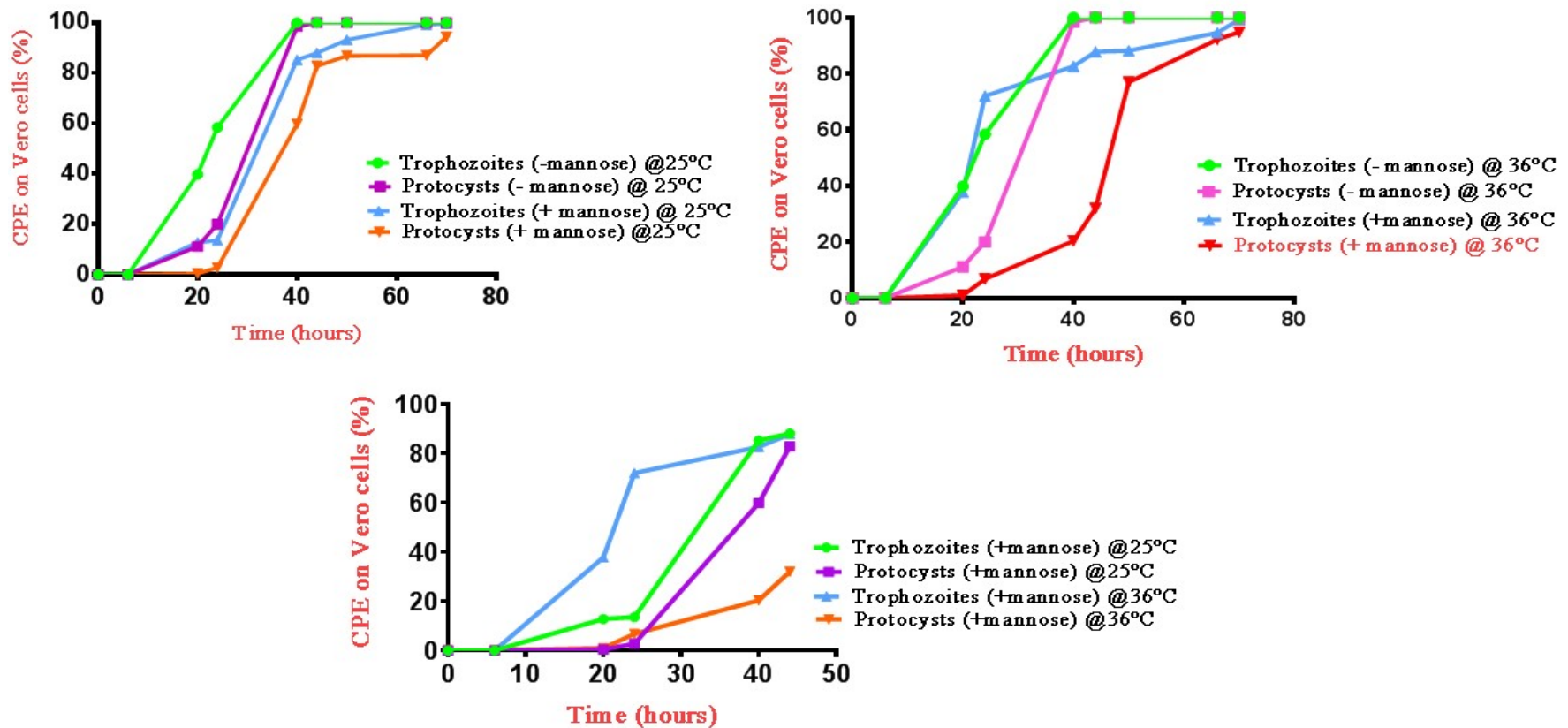
Figure 2-20: Thermo-tolerance and cytopathic effect of either trophozoites or protocysts in the presence or absence of mannose. (a) No apparent difference in the cytopathic effects of either trophozoites or protocysts on vero epithelial cells in the presence or absence of mannose at 25 °C. **(b)** However, the presence of mannose caused an approximately 20 hours delayed CPE of protocysts on vero cells line compared to the absence of mannose at 36 °C. **(c)** Although, trophozoites is more virulent at 36 °C (body temperature) compared to 25 °C (room temperature), there was no difference in the trophozoites cytopathic effects on either the presence or absence of mannose on vero cell lines at 36 °C.

To test the effect of mannose on CPE, experiments were set up in the presence and absence of mannose. As shown in Figure 2.20, mannose had little effect on the onset of CPE by mature trophozoites; however, CPE was delayed when Vero cells were inoculated with protocysts. Interestingly, CPE was delayed more at higher temperature (36º C vs 25 ºC). Overall the data suggest that mannose delays but does not prevent the onset of CPE against vero cells, consistant with AcMBP playing a role but not being essential for the infection process.

CPE was also measured starting with mature cysts. As for protocysts mature cysts must first differentiate to trophozoites before infecting cells. CPE was induced at 25 ºC and 36 ºC with a delay of ~50 hours in each case.
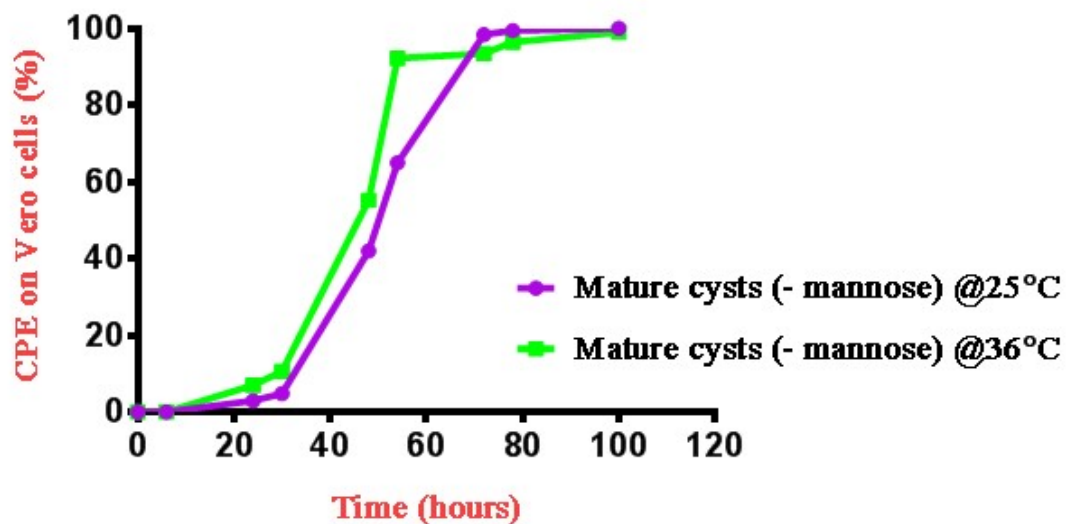
Figure 2-21: Thermo-tolerance and cytopathic effect of mature cysts on vero cells in the absence of mannose at 25 °C and 36 °C.

Figure 2.22 provided evidence that *Acanthamoeba* may destroy different cell types other than corneal epithelial cells. Meanwhile, figures 2.23 – 2.25 establish that mannose presented an earlier inhibitory effect on *Acanthamoeba* adhesion onto HCEC compared to either the galactose or the control experiment. However, there was no apparent inhibition of *Acanthamoeba* CPE on HCEC.
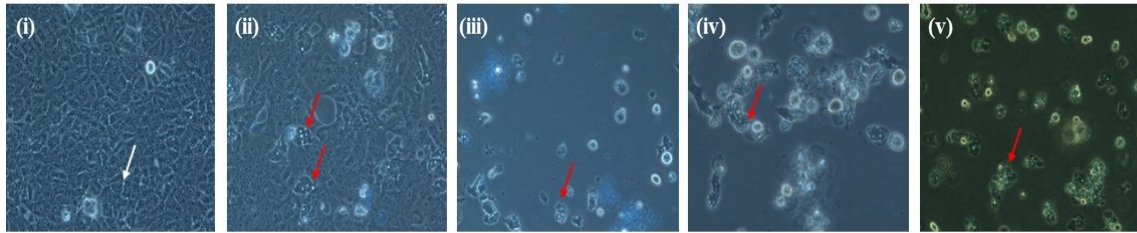
Figure 2-22: Adhesion and subsequent CPE of excysted protocysts (red arrow) to confluent HT-29 cells. (i) Protocysts (invisible without CFW stain, white arrow) attached onto confluent monolayer HT-29 cells at 60mins. (ii) Protocysts differentiate into trophozoites to destroy HT-29 cells at 24 hours. (iii) Differentiated protocysts (hatched trophozoites (red arrows)) continues to destroy HT-29 cells at 48 hours. (iv) Hatched trophozoites destroy HT-29 cells at 72 hours post inoculation with protocysts. (v) Fluorescence micrographs of hatched trophozoites and completion of CPE. Evidence of *Acanthamoeba* destruction different cell types other than corneal epithelial cells.
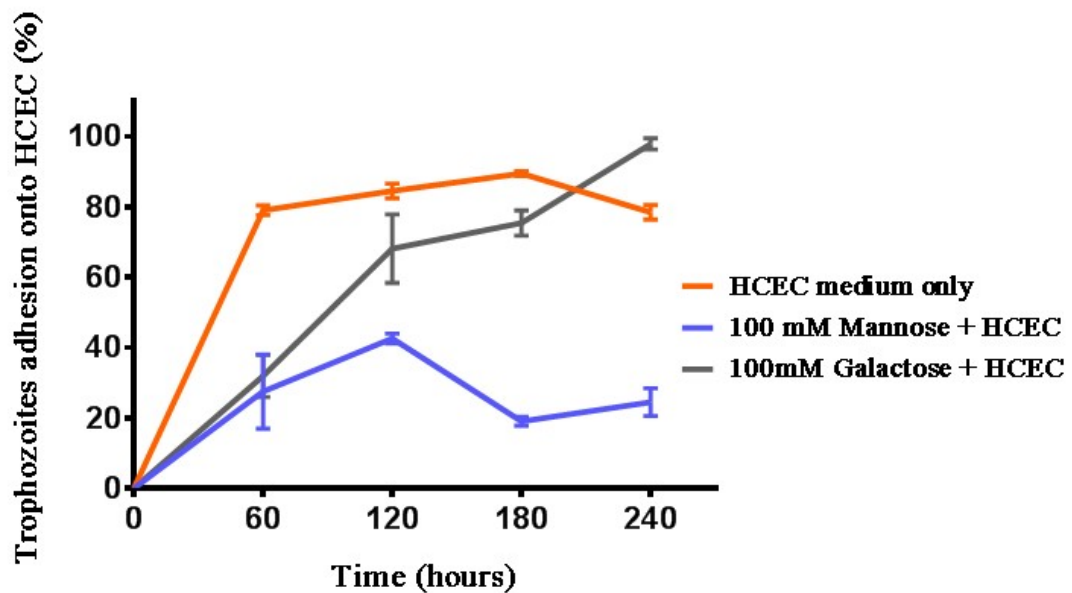
Figure 2-23: Effect of mannose on adhesion of *Acanthamoeba* trophozoites onto HCEC monolayer. Either 100 mM of mannose or galactose and HCEC medium only (control) were used in this study. Corresponding graphical illustration depicts differential inhibitory effects of selected sugar on Acanthamoeba trophozoites adhesion onto the HCEC monolayer cell lines. Mannose presented an earlier inhibitory effect compared to either the galactose or the control experiment. (Mag. x400). This experiment was repeated twice.

(A)
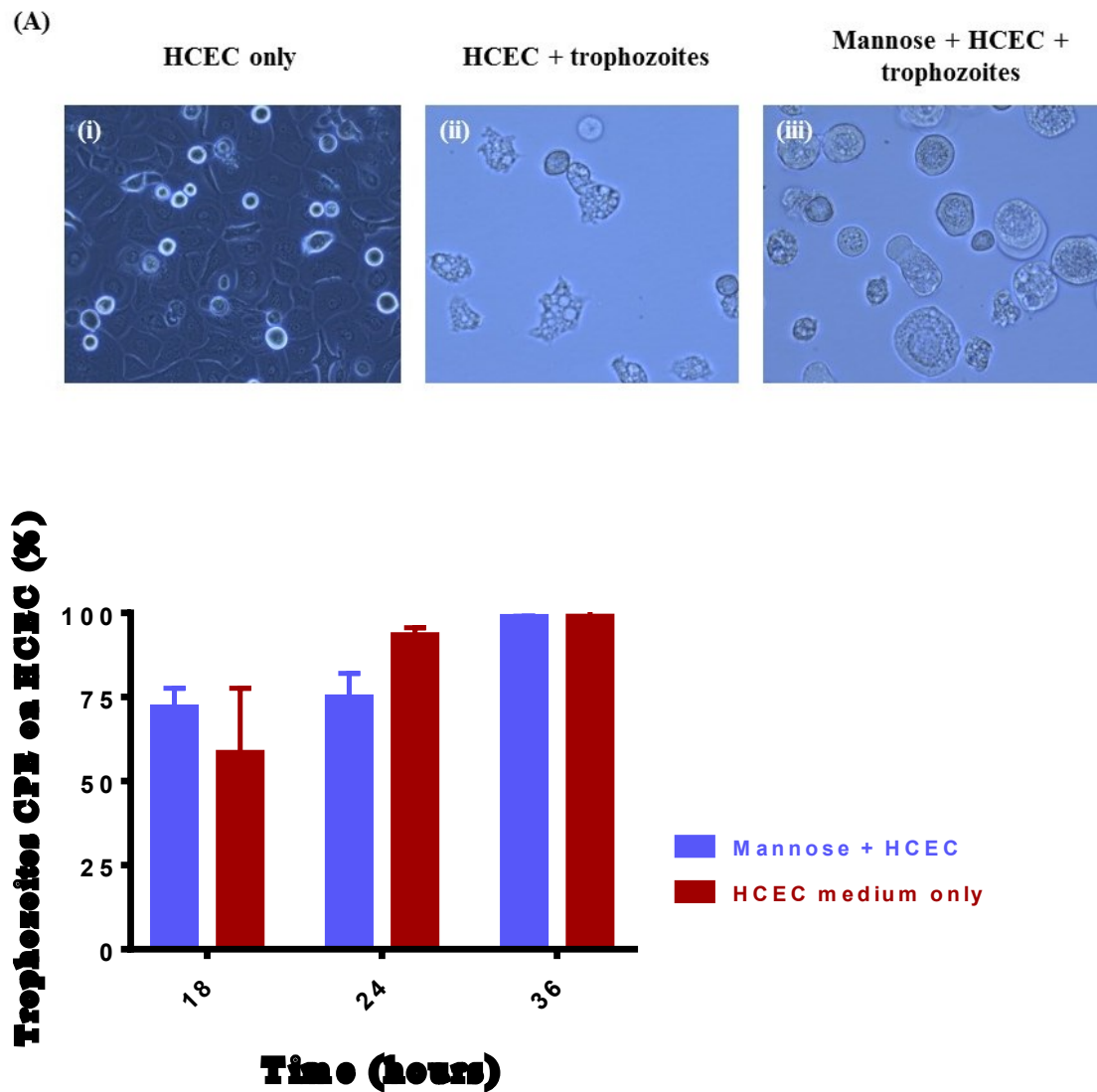
Figure 2-24: CPE of *Acanthamoeba* trophozoites on HCEC treated with or without 100 mM mannose at 36 hours post inoculation. Either 100 mM of mannose or HCEC medium only (control) at 36 °C, 5% CO_2 was used in this CPE study. Corresponding graphical illustration depicts HCEC monolayer destruction (CPE) by the trophozoites in the presence or absence of 100 mM mannose (Mag. x400). This experiment was repeated at least twice.
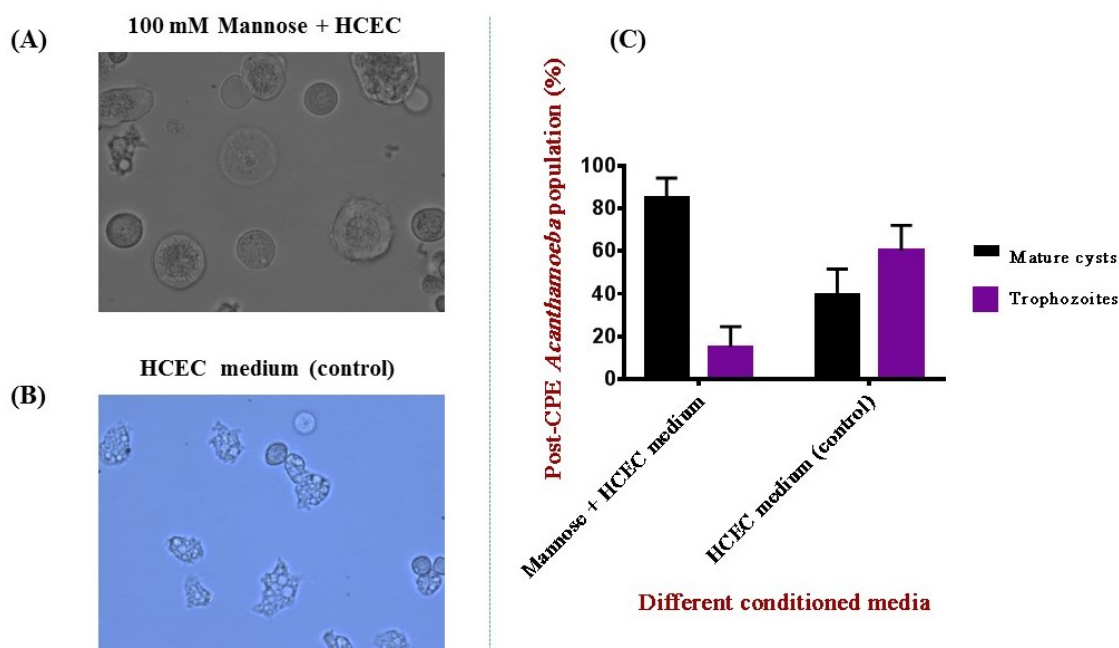
Figure 2-25: Post-CPE of *Acanthamoeba* trophozoites on infected HCEC monolayer. Either 100 mM of mannose or HCEC medium only (control) at 36 °C, 5% CO_2 were used in this study. Corresponding graphical illustration depicts the percentage ratio of trophozoites: mature cysts at day 18 of post inoculation with Acanthamoeba trophozoites. After completion of monolayer destruction (CPE), the trophozoites transforms into mature cysts. This in-vitro study mimics the pattern of persistent infection (in-vivo) due to cumulative mature cysts that may trigger potential re-infection in most clinical cases (mag. x400). This experiment was repeated six times.

2.4 Discussion

In this Chapter, I established conditions to maintain *Acanthamoeba* in its three different life stages: trophozoites, protocysts and mature cysts. Protocysts and mature cysts represent two different encysted forms and did not interconvert without first differentiating into trophozoites. Because they lack the double cell wall structure of mature cysts, protocysts are a candidate for drugs targeted towards *Acanthamoeba*. PG could potentially be used to maintain *Acanthamoeba* in the protocyst stage.

The data described show that *Acanthamoeba* bind to a wide variety of surfaces. Mannose did not inhibit binding to plastic surfaces indicating that receptors other than AcMBP are important for adhesion. Adhesion was inhibited to a certain extent by EDTA, indicating that divalent cations are important. Adhesion molecules such as cadherins and integrin

are likely to be involved in adhesion to different surfaces. Both of these adhesion families require Ca^{2+} to function (Alswied and Parekh, 2015). Cytopathic effect was observed on Vero cell and Hep2 cells. Mannose did not prevent CPE, but did delay the onset of CPE, particularly when cells were inoculated with protocysts. Protocysts must differentiate into trophozoites before they can kill cells, so AcMBP may play a role in the early stages of adhesion and CPE.

3. Structure & Ligands of *Acanthamoeba* MBP

3.1 Introduction and Objectives

Several studies have implicated *Acanthamoeba* mannose-binding protein (AcMBP) as an important virulence factor in AK (Sun et al., 2006, Ku et al., 2009). It triggers parasitic adhesion that in turn leads to destruction of target cells. Currently, relatively little is known about the properties or ligand binding by *Acanthamoeba* MBP. I therefore sought to overexpress and characterise recombinant AcMBP.

Blast searches reveal no sequence identity with any known protein domains, with the exception of a small DUF 4114 domain of ~10 kDa within the extracellular region. The DUF domain is a domain of unknown function found in many different types of protein. There are highly conserved glutamate and aspartate residues suggesting that this domain might carry enzymic activity. The strategy used was to generate a synthetic cDNA encompassing the entire extracellular region of AcMBP that was codon optimised for expression in Chinese hamster ovary cells.

3.2 The structural organisation of AcMBP

The gene for AcMBP is 3.6kb with 6 exons. The coding region is 2.5 kb encoding a protein of 833 amino acid residues. The polypeptide is synthesised with a signal sequence that is cleaved during biosynthesis. The N-terminal 700 residues form the extracellular region. This is followed by a transmembrane region and a short C-terminal cytoplasmic region (78 residues) (figure 3.1).
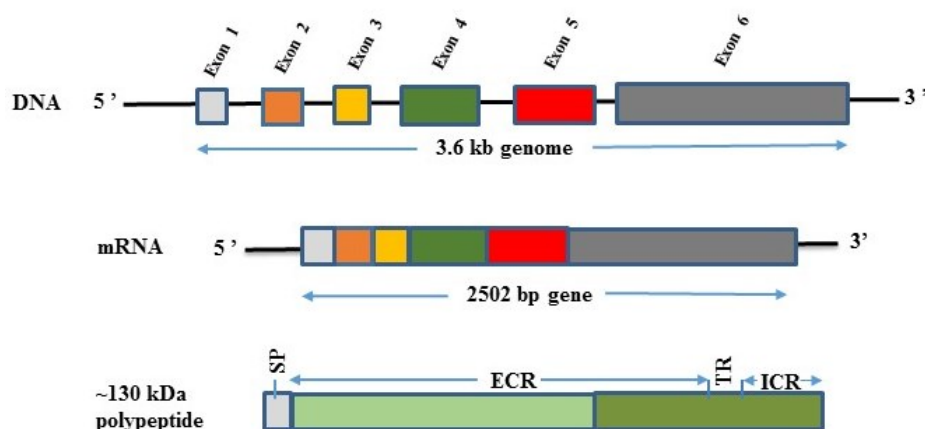
Figure 3-1: Organisation of AcMBP Gene. (Top): Schematic illustration of the organisation of the 3.6 kb *Acanthamoeba* gene comprising 6 exons and 5 introns. The

exons are represented as coloured boxes and are connected by introns (not shown to scale). (Middle): spliced mRNA, the introns are removed and the exons joined; (Bottom): The precursor protein is 833 amino acid residues. The signal peptide (SP) is derived from exon 1, the extracellular region (ECR) is derived from exons 1 – 6 and the transmembrane (TM) and intracellular regions (ICR) are encoded by exon 6 (Adapted and modified from Garate et al., 2004).

(A)

(B)

(C)

```
          10         20         30         40         50         60
MRSLPVFVVL MVALFAAVAS AGTCNLSGAI KQPGLDCSST SCSITSGTFP FPLPQGETYD

          70         80         90        100        110        120
SFYSWILGVI GTDGATVNAQ YVDYTKADPN IYFTAGQTNC MVNLTFVYEV AFYRNSMGYF

         130        140        150        160        170        180
TFTRDSKPTS VGSVTLKPVF SETTVDCSRT SSQPLPGTSC LAPGSTISLG PFSSTQAVGF

         190        200        210        220        230        240
YLKQDSICSG TTTFYSVDAL NKVTSRWKPI PAAHGRMIAV LRDPNTLRAY LGFEDSPDGS

         250        260        270        280        290        300
DSDYNDNVFS VTSNCEIDTS LLPCATVTTC RNSKQTFDSS KCTCSCPNPV TCTAPQVYST

         310        320        330        340        350        360
DLCACTCPNA TQTCTAPLTW NSATCQCDCP STKPSGVTCS NLQQWSNVVA TCGCKCPDPA

         370        380        390        400        410        420
TYTCSDNRFV LRTSDCTCNC PSTGSCSGNL KWNSANSVCG CQCPSTPPTP CSGNLKWNST

         430        440        450        460        470        480
ASKCACECPA TAALAGVTCK DKEVWDTASC SCKCPATASA ADTTCPNVNY QWNYNGKCDC

         490        500        510        520        530        540
VCPATSAEAG INCTALGLGN TVWDTTACNC ACPPTGTCPG NKVWNPSNDP AKCGCSCPAS

         550        560        570        580        590        600
APAGKECKGN FYWNTSDDVC DCYCPLEAPA DDPCIGYTTW NRTECDCYCP LEPPFEGGCP

         610        620        630        640        650        660
GVQVWDRDQC QCVCPDDDPC AAQSTACKQF YCSSSTGECA LVYEDTCASQ KLQFNTTGCL

         670        680        690        700        710        720
SWQCDPDLGC VRKANGSCCD DYKDCPTCAK YDGCDWIGTK CADSGQVLTS PIDQADHPDC

         730        740        750        760        770        780
FPSTGLSAGE TAGITVGIVA GVTVGVGGAA GLFGAGYILY RMLNKPPPPE QLPTIENLDT

         790        800        810        820        830
EAGTDDNPLF HKNEIEMTNP MFSAAGAGGG GDAGAMFAQG GGASAVPADL HTL
```

Figure 3-2: (A) Schematic illustration of *Acanthamoeba* mannose-binding protein showing three different regions: extracellular region (ECR), transmembrane (TM) and cytoplasmic region (CR). The cysteine-rich motifs are in the middle of the extracellular region **(B)** the domain organisation of AcMBP. **(C)** The amino acid sequence of the full-length AcMBP. Different regions are shown in different colours. The signal peptide is in GREY, The DUF4114 domain in BLUE, the cysteine-rich domain is YELLOW, the transmembrane region is DARK GREEN and the intracellular region is in BRIGHT GREEN. Regions of no known function are in PURPLE. (Sources: Figures 3.2a and 3.2b were adapted and modified from Khan, 2015 and Garate, 2005 respectively).

An unusual feature of the AcMBP is the presence of 14 CXCXC motifs in the region N-terminal to the membrane-spanning region (figure 3.2). The DUF4114 domain is towards the N-terminus. The function of the cysteine-rich region is unknown. However, its repeating structure and localisation towards the membrane-spanning region (figure 3.3) suggests that it may form a neck or stem-like structure with the lectin domain furthest from the membrane. The full-length protein is reported as a trimer composed of 130 kDa subunits. The cysteine rich domain may participate in oligomerisation.

```
CRNSKQTFDSSK
CTCSCPNPVTCTAPQVYSTDL
CACTCPNATQTCTAPLTWNSAT
CQCDCPSTKPSGVTCSNLQQWSNVVAT
CGCKCPDPATYTCSDNRFVLRTSD
CTCNCPSTGSCSGNLKWNSANSV
CGCQCPSTPPTPCSGNLKWNSTASK
CACECPATAALAGVTCKDKEVWDTAS
CSCKCPATASAADTTCPNVNYQWNYNGK
CDCVCPATSAEAGINCTALGLGNTVWDTTA
CNCACPPTGTCPGNKVWNPSNDPAK
CGCSCPASAPAGKECKGNFYWNTSDDV
CDCYCPLEAPADDPCIGYTTWNRTE
CDCYCPLEPPFEGGCPGVQVWDRDQ
CQCVCPDDDPC


CRNSKQTFDSSKCTCSCPNPVT
CTAPQVYSTDLCACTCPNATQT
CTAPLTWNSATCQCDCPSTKPSGVT
CSNLQQWSNVVATCGCKCPDPATYT
CSDNRFVLRTSDCTCNCPSTGS
CSGNLKWNSANSVCGCQCPSTPPTP
CSGNLKWNSTASKCACECPATAALAGVT
CKDKEVWDTASCSCKCPATASAADTT
CPNVNYQWNYNGKCDCVCPATSAEAGIN
CTALGLGNTVWDTTACNCACPPTGT
CPGNKVWNPSNDPAKCGCSCPASAPAGKE
CKGNFYWNTSDDVCDCYCPLEAPADDP
CIGYTTWNRTECDCYCPLEPPFEGG
CPGVQVWDRDQCQCVCPDDDP
CAAQSTA
```

Figure 3-3: The sequence of the cysteine-rich domain of AcMBP. Two alternative alignments are shown. Conserved tryptophan residues are shaded in green and equivalent aromatic residues in grey. A conserved proline residue is in cyan.

AcMBP has been shown to bind to mannose-Separose and to D-mannose. It is believed that its lectin activity enables binding to corneal glycoproteins in order to initiate parasitic adhesion, a key step in the pathogenesis of *Acanthamoeba* keratitis (Garate et al., 2005). However, the specific ligands on the corneal surface or the mechanism of binding are not known.

3.3 Materials and Methods

3.3.1 Materials

All the DNA restriction and modifying enzymes were obtained from New England Biolabs. Bovine fetuin, human milk lactoferrin, aldolase, yeast invertase, sweet potato β-amylase and yeast mannan and methotrexate were procured from Sigma–Aldrich Company Ltd (Gillingham, UK). Bovine thyroglobulin was from GE Healthcare (Little Chalfont, UK); Human IgG and IgM were obtained from Anthens Research & Technology, Inc. (Anthens, Georgia, USA); Recombinant AcMBP (AcL1) was produced in Chinese hamster Ovary DHX11 cell line. Minimum essential medium (MEM), serum-free medium (SFM), protein molecular markers for SDS-polyacrylamide gel electrophoresis were from Life Technologies, U.K; pED4 vector kindly provided by Professor Russell Wallis (University of Leicester, UK); and FPLC columns were from GE Healthcare.

3.3.2 Methods

3.3.2.1 Plasmids

The cloning vector containing the extracellular region of the cDNA of AcMBP is shown in Figure 3.4. The mammalian expression plasmid pED4 is shown in Figure 3.5.

3.3.2.2 Expression of full-length AcMBP:

3.3.2.2.1 A synthetic AcMBP cDNA

The *Acanthamoeba* MBP gene (Figure 3.2b) composed of 6 exons and 5 introns (Garate et al., 2004) was used as a template to design a synthetic oligonucleotides encoding the extracellular region of AcMBP. The cDNA was synthesised by Gene Art, (Life technologies) and was codon optimised for expression in Chinese hamster ovary cells (CHO) with a C-terminal hexahistadine tag to enable purification. To produce

recombinant AcMBP, I used PCR to amplify the DNA sequences of interest, using oligonucleotides primers (Eurogentech) shown in Tables 3.1 – 3.3 and Figures 3.6 – 3.8.
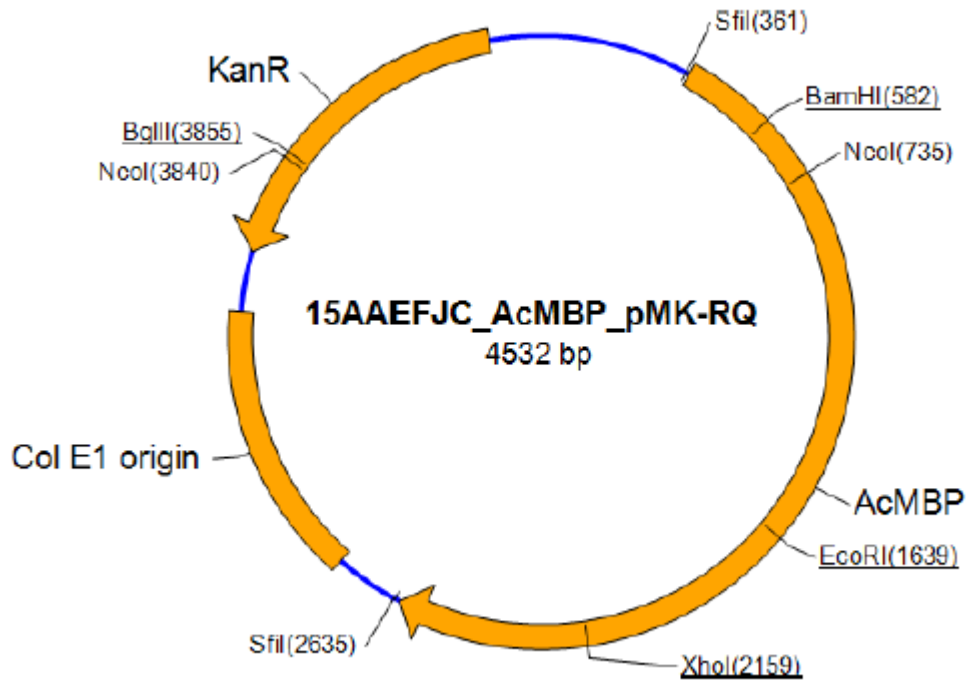
Figure 3-4: Vector containing the full-length extracellular region of AcMBP. The synthetic AcMBP gene (sized 2254 bp) was edited, optimised and assembled from synthetic oligonucleotides and/or PCR product for maximum expression yields by Gene-Art, life-technologies. The fragment was transformed into *E. coli* K12 (dam + dcm + tonA rec-) vector backbone pMK-RQ (KanR) at the cloning sites Sfil / Sfil. The plasmid DNA was purified from the transformed *E. coli*, and its concentration was determined by UV spectroscopy. The sequence was 100% congruent within the insertion site. The final construct (4532 bp) was confirmed by sequencing and approximately 5-µg plasmid DNA was lyophilised at Gene-Art, life-technologies.
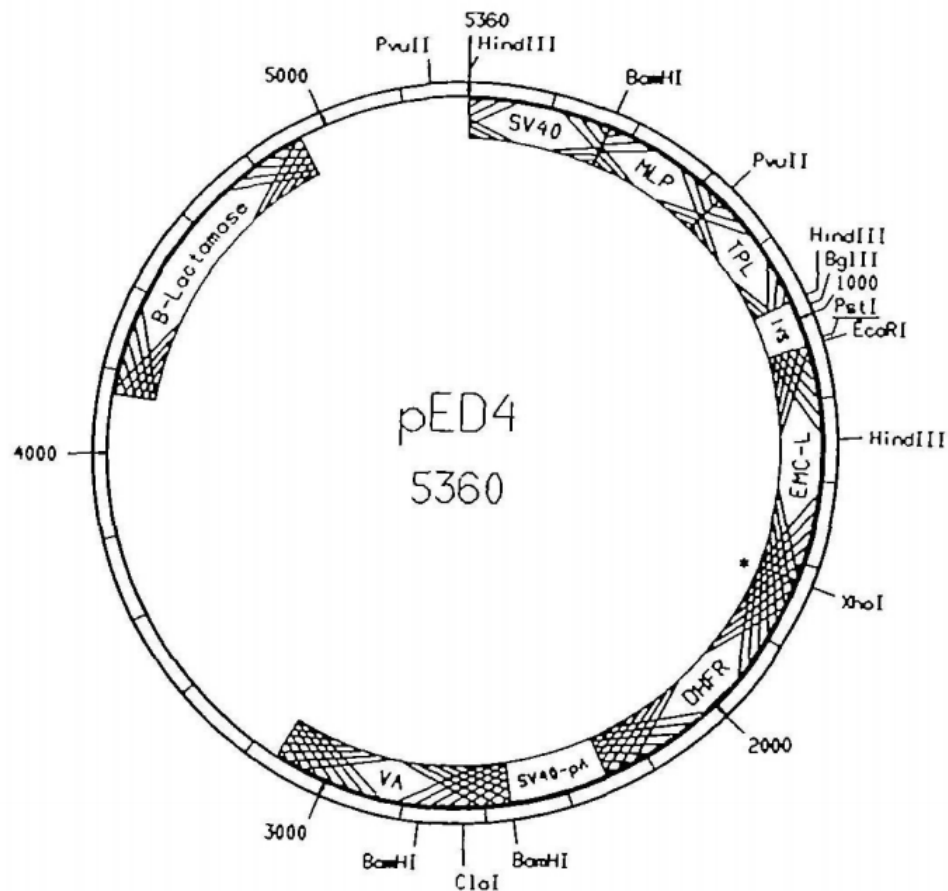
Figure 3-5: The plasmid map of pED4 expression vector. pED4 is an efficient 5360bp dicistronic vector for protein expression in a stably transfected cell lines. It contains plasmid sequences derived from pUC 18 that allow propagation and selection for ampicillin resistance in *E. coli*. It also contain the SV40-Simian virus 40 origin of replication, enhancer elements, Adenovirus major late promoter (MLP), a tripartite leader from Adeno major late mRNA at the 5' end of the mRNA. There is a hybrid of intron composed of 5' splice site from the leader; multiple cloning sites (MCS); an untranslated leader from encephalo-myocarditis; and the dihydrofolate-reductase (DHFR) gene for selection at the 3' end of the transcript. Efficient translation of DHFR is possible from the internal ribosomal entry site derived from encephalomyoarditis virus. There is direct expression of the dicistronic mRNA in cell lines such as Chinese hamster ovary deficient in DHFR (Adapted from Kaufman (Kaufman et al., 1991)).

3.3.2.2.2 PCR amplification of AcMBP cDNA

PCR amplification of AcMBP DNA was performed in a 24-well PCR thermocycler. The PCR mixtures were prepared with ~50 ng of AcMBP DNA with 5 µl 10x reaction buffers, 1.5 µl of $MgSO_4$ (1 mM), 2 µl of dNTPs (0.3 mM), 1 µl of each forward and reverse primer (0.3 mM). Other components of the PCR mix included 5 µl of Enhancer, and 0.5 µl of polymerase (Platinum Pfx DNA (1 U)). The mixture was made up to a total volume of 50 µl with ddH_2O. Thermal cycling conditions were varied according to the oligonucleotides used. A typical cycle comprised of an initial DNA denaturing phase at 94 °C for 60 seconds, primer annealing at 65 °C for 45 seconds, followed by extension at 72 °C for 1.5 min. The extension time was dependent on the size of the product (Sambrook et al., 1989). After 30 cycles, there was a final extension phase at 72 °C for 10 minutes. The reaction was maintained at a soak temperature held at 4 °C, (section 3.2.2.3.2).

Table 3-1: Sequence of oligonucleotides used for site-directed mutagenesis & cloning of full length AcMBP

AcMBP	Oligonucleotides	Primer codes
AcL1 Full length (wild-type)	5'—aggtccaactgcagg**gccaccatg**—3' (FP)	MBPF
	5'—tccccgggtc**tag**agttcagtggt—3' (RP)	MBPR
Start and stop codons are represented in green and underlined; Kosak sequences (orange) were included prior to the start codon to enhance the initiation of translation. FP—forward primer and RP—reverse primer.		

Table 3-2: PCR mix and conditions for full length AcMBP

PCR mix	µl
DNA (10 nmol)	0.5
MgSO$_4$ (1 mM)	1.5
Buffer (1.5 x)	5.0
Enhancer (10 x)	5.0
dNTPs (0.3 mM)	2.0
Primers (F) (0.3 mM)	1.0
Primers (R) (0.3 mM)	1.0
Polymerase (Platinum Pfx DNA) (1 U)	0.5
H$_2$O	33.5
Total volume	**50.0**
The above volume are for a single reaction. Note: 1x = final concentrations of PCR mix relative to the concentration (1 U) of the Pfx DNA polymerase.	

Table 3-3: Polymerase Chain reaction (PCR) conditions for full length AcMBP

PCR conditions	Temperature (°C)	Time (mins/secs)
Pre-denature	94	5 mins
Denature	94	1 min
Annealing	65	45 secs
Extension	72	1 min 30 secs
Final extension/delay	72	5 mins
Soak temperature	4	∞
No of cycles (Denature, Annealing & Extension) = 30 cycles		

3.3.2.2.3 DNA analysis by Agarose gel Electrophoresis

DNA were isolated by separating fragment(s) obtained from either restriction enzyme digestion or PCR by agarose gel electrophoresis. A 1 % agarose-gel was prepared by dissolving 1.2 g of low-melting point agarose into 120 ml of 1× Tris buffer-EDTA solution [1 M Tris-HCl pH 7.5, 0.5M EDTA pH 8.0 and ddH$_2$O] by heating the mixture in a microwave for about 5 mins. Next, 12 µl of DNA safe stain dye was added to the gel

mix, and the mixture was cooled to 45°C and poured into a gel cassette with a comb. 10 µl of 6 x blue DNA loading dye (Thermo-Fisher Scientific) was added to each 50µl PCR DNA sample. Samples were loaded alongside a DNA marker, and the DNA was separated using 90 V and 400 mA for 1 hour.

The gel was visualised using a UV trans-illuminator (305 - 327 nm) and the DNA bands were excised with a sharp scalpel blade. Slices of gel containing the DNA fragments were transferred into labelled Eppendorf tube for purification.

3.3.2.2.4 DNA purification from agarose gels

Extracted DNA was purified using the E.Z.N.A. gel extraction kit using the protocol provided. The DNA concentration was measured using a Nanodrop spectrophotometer at 260 nm. The A_{260}/A_{280} ratio was used to gauge the purity of the DNA, a ratio of ~1.8 reflecting pure DNA.

3.3.2.2.5 Restriction enzyme digestion of Vectors & Ligation of DNA into cloning vectors

Table 3-4: Restriction enzymes used in this project

Restriction enzymes	Sticky & Blunt ends cutting sites	Sticky & Blunt ends digests
*Bam*HI	5'---G↓GATCC---3'	5'---G↓ GATCC----3'
	3'---CCTAA↑G---5'	3'---CCTAA ↑G----5'
H*in*dIII	5'---A↓AGCTT---3'	5'---A↓ AGCTT-----3'
	3'---TTCGA↑A---5'	3'---TTCGA ↑A----5'
*Eco*RI	5'---G↓AATCC---3'	5' ---G↓ AATCC----3'
	3'---CTTAA↑G---5'	3'---CTTAA ↑G----5'
*Sal*1	5'---G↓TCGAC---3'	5' --- G↓ TCGAC ----3'
	3'---CAGCT↑G---5'	3' --- CAGCT ↑G ----5'

Bulk restriction digestion of plasmid DNA (e.g. pED4) was carried out in a 0.5 ml Eppendorf by mixing ~30 µl of pED4 DNA, 13 µl of Smart Cut Buffer (NEB), 2.5 µl *Sal*I high fidelity and H_2O to a final volume of 200 µl. The mixture was incubated at 37 °C for 3 hours. Thereafter, samples were separated by gel electrophoresis. PCR products

were introduced into SalI restriction site within the polylinker of pED4 expression vector by homologous recombination using the GeneArt® Seamless Cloning Kit (Table 3.4).

3.3.2.3 Production of competent *E. coli* cells (XL-10)

Competent *E. coli* XL-10 cells were used for the plasmid amplification and cloning and *E. coli* BL21 (DE3) was used for protein expression. The competent *E. coli* XL-10 cells were prepared using the protocol developed by Promega, (U.K) using rubidium chloride for the production of cells with a transformation efficiency of $> 1.5 \times 10^7$ cfu/µg of plasmid DNA. A single colony from a LB plate was inoculated into 2.5 ml of LB medium and incubated at 37 °C in a 225-rpm shaking incubator overnight. Next day, the entire overnight culture was inoculated into 250 ml of LB medium containing 20 mM $MgSO_4$ and then incubated for 2-3 hours in a baffled flask and grown to an $OD_{600} = 0.6$. Cells were placed on ice for 10 minutes, and then pelleted by centrifugation at 4,5 00 × g for 5 minutes at 4 °C. Cells were re-suspended in sterile ice-cold 20 ml TFB1 (30 mM potassium acetate, 10 mM $CaCl_2$, 50 mM $MnCl_2$, 100mM RbCl and 15 % glycerol and adjusted to pH 5.8 with acetic acid). The re-suspended cells were incubated on ice for 5 minutes, pelleted by centrifugation at 4,500 × g for 5 minutes at 4 °C and finally re-suspended in 4 ml of sterile ice-cold TFB2 (10 mM MOPS, 75 mM $CaCl_2$, 10mM RbCl and 15 % glycerol; the pH was adjusted to 6.5 with KOH).

Cells were incubated on ice for 30 minutes. Aliquot of 0.5 − 1.0 ml quantities were transferred into pre-chilled eppendorf tubes and quick freezed the tubes in liquid nitrogen. The cells were stored at − 80 °C for up to one year. Samples of the XL-10 competent cells were routinely tested for competency using uncut pED4 vector.

3.3.2.3.1 Transformation of competent *E. coli* cells

The DNA sample was mixed with 200 µl of competent cells and left on ice for 30 minutes, with occasional gentle mixing. Cells were then heat shocked at 42 °C for 45 seconds and transferred to ice for 2 minutes. 200 µl of Luria-Bertani (LB) was added and cells were left to recover in a 250 rpm shaking incubator at 37 °C for 1 hour. Then, 200 µl of the transformation mix was spread on LB agar plates containing 100 µg/ml of ampicillin. All plates were incubated overnight at 37 °C. Next day, single distinct colonies were picked and grown in LB broth with ampicillin (100 µg/ml) in a LB culture in a 200 rpm shaking incubator at 37 °C.

3.3.2.4 QIAGEN® plasmid maxi kit

Plasmids were purified using Qiagen® plasmid mini or midi-prep kits (QIAGEN Ltd) based on the alkaline-lysis technique using the protocol provided. Plasmid was resuspended in ddH$_2$O and quantified using a Nanodrop spectrometer as described above.

3.3.2.5 Sequencing and analysis of sequence

All new clones were sequenced by the Protein Nuclear Acid Chemistry Laboratory (PNACL, University of Leicester, U.K.). The sequence data obtained thereof were viewed by chromatogram using Chromas software version 2.4.1 (http://en.bio-soft.net/dna/chromas.html). The primer sites were not included in the sequence meant for this analysis to reduce any possible forced bias.

3.3.2.6 Generation of stable mammalian (CHO) cell lines for transfection

The mammalian (CHO) cell line DXB-11 was chosen to express the extracellular region of AcMBP (AcL1). DXB-11 cells are a dihydrofolate reductase (DHFR)-deficient CHO cell line enabling selection of pED4 that carries a copy of the DHFR gene. The cDNA of interest is transcribed as a dicistronic message together with the DHFR gene. Cells were grown in 25 cm^2 tissue culture flasks in Minimum Essential Media α with nucleosides (MEM α$^+$) supplemented with 10 % dialysed, heat-treated foetal calf serum (DHFCS) and 50 units/ml penicillin and 50 μg/ml streptomycin. Cells were incubated at 37 °C and 5 % CO$_2$.

Transfection was carried out using the calcium phosphate method, developed by Graham and Van der Eb (2005). This method takes advantage of the formation of small, insoluble, calcium-phosphate-DNA precipitates that can be adsorbed onto the cell surface, up taken through endocytosis by cells. It requires the mixing of DNA with calcium ions, followed by the addition of phosphate to the mixture of cells in culture. The calcium phosphate method is a simple, cheap and popular technique.

To transfect AcL1 plasmid DNA into a monolayer of CHO cells, 5 μg of plasmid DNA was precipitated by adding 1/10 volume of 3M acetate pH 5.3 and 2.5 volumes of ice-cold ethanol. The mixture was incubated on dry-ice for 10 – 15 minutes and then centrifuged in an Eppendorf centrifuge for 10 minutes to pellet the DNA. The DNA was washed with 500 μl of ice-cold 70 % ethanol centrifuged and left to dry in a sterile hood. Later, 140 μg of carrier DNA (calf thymus DNA) was treated in a similar way. The DNA and carrier DNA were re-suspended in 1 ml of 200 mM CaCl$_2$. This was added in a drop-

wise approach into bubbling solution of 1 ml of $2\times$ Hepes buffered saline (HBS) [280mM NaCl, 10 mM KCl, 1.5 mM Na_2HPO4, 12 mM Dextrose 50 mM HEPES, pH 7.01 and ddH_2O]. Also, we added 40 µl of $100 \times$ phosphate buffer [8.0 g/L NaCl, 0.2 g/L KCl, 1.42 g/L Na_2HPO4, 0.24 g/L KH_2PO4 and ddH_2O]. The mixture was left at room temperature for 15 – 30 minutes to precipitate. One millilitre of the precipitate mix was added to a tissue culture flask containing CHO cells. The CHO cells were at least ~50 % confluent with a change of medium at least 4 – 5 hours before transfection.

Next day, the medium was replaced with a fresh MEM α^+ medium. Once the cells has grown to confluence, the media was removed and the cells were washed with 2 ml phosphate buffer saline (PBS) pH 7.4, to remove any trypsin inhibitors present in the serum and incubated with 1 ml trypsin-EDTA solution to detach them from the flask. Then, one drop of resulting cell suspension was seeded into the wells of a 96 well plate-containing medium without nucleotides (MEM α^-) supplemented with 10 % DHFCS penicillin/streptomycin. Cells were incubated at 37 °C and 5 % CO_2 for up to two weeks until colonies started to grow. To increase the level of protein expression, single clones were passaged into increasing concentration of methotrexate (MTX), an inhibitor of DHFR (initially at 0.02 µM, then 0.1 µM and finally 0.5 µM MTX) over several weeks, at which point the cells were assessed for production.

3.3.2.7 Production and purification of AcL1

For production of cells, they were grown in 500 cm^2 tissue culture flasks with 75 ml of MEM α^- supplemented with 10 % (v/v) DHFCS) with penicillin/streptomycin and 0.5 µM methotrexate. When the cells reached confluence, the spent media was replaced with 100 ml of CHO serum-free II medium supplemented with 50 mM HEPES buffer, pH 7.55 with penicillin/streptomycin and 0.5 µM methotrexate. Media was replaced every other day for 5 harvests, centrifuged at $3000 \times g$ for 5 minutes, to remove any available cell debris; and stored at -20 ºC for purification.

Protein was purified by affinity chromatography on a nickel-Sepharose column; Generon®. Briefly, 400 ml of culture medium containing recombinant AcMBP was diluted with an equal volume of binding buffer N1 (20 mM Tris-HCl, pH 7.5, containing 1 M NaCl) and loaded onto a 2 ml nickel-Sepharose column (Generon, U.K.) pre-equilibrated with binding buffer (20 ml).

After separate washes with 20 ml each of binding buffer N1 and wash buffer N2 (20 mM Tris-HCl, pH 7.5, containing 1 M NaCl and 20 mM imidazole), the recombinant AcL1 was eluted in 1 ml fractions with elution buffer N3 composed of 20 mM Tris-HCl, pH 7.5, containing 1 M NaCl and 500 mM imidazole. Aliquots of protein fractions were run on a 15% SDS-PAGE gel and were stained with Coomassie blue.

3.3.2.8 Sodium dodecyl-polyacrylamide gel electrophoresis (SDS-PAGE)

SDS-PAGE was a qualitative method carried out by using a BioRad mini protein II gel system for the purification and separation of protein according to their sizes; and the determination of their relative molecular mass. Protein samples were unfolded by boiling in buffer containing β-mercaptoethanol and SDS that reduce any disulphide bridges and negatively charge the resulting polypeptide chain. The resolving gel (375mM Tris-HCl pH 8.8, 15% v/v acrylamide, 0.1% v/v ammonium persulfate, 0.1% w/v SDS and 0.0004% TEMED) was set under isopropanol to eliminate air bubbles until the gel was solidified. The stacking gel (125 mM Tris-HCl pH 6.8, 4% v/v acrylamide, 0.002% v/v ammonium persulfate, 0.1% w/v SDS and 0.0004% TEMED) was cast on top of the resolving gel and the comb was added.

The gel was run using 1× SDS running buffer (25 mM Tris-HCl, 192 mM glycine, 0.1% w/v SDS). Then, I mixed 5 µl of 5× loading buffer (250 mM Tris-HCl pH 6.8, 50% v/v glycerol, 500 mM DTT, 10% w/v SDS, 0.25% Bromophenol blue) with 20 µl of each protein sample. Samples were denatured at 95 °C on heat block for 5 min before running. Electrophoresis was carried out at room temperature at a constant voltage (200 V) and variable current for about 50 minutes until dye front reached the end of the gel. Gels were carefully removed from the cassette mould and stained with Coomassie blue stain (0.4% w/v in 50% v/v methanol and 10% v/v acetic acid) for at least 15 min, then, rinsed with water before being destained in 30% v/v methanol containing 7% v/v acetic acid. Afterwards, gels were scanned with an HP Scanjet G4010.

3.3.2.9 Gel filtration chromatography

AcL1 was further purified by gel filtration chromatography on Superdex 200 column (10mm × 300 mm, GE Healthcare) equilibrated in 25mM TRIS pH 7.5, containing 150mM NaCl and 1mM EDTA at a flow rate of 1 ml/min at room temperature. Fractions were collected across the elution profile of the AKTA system. The AKTA system is a fast protein (or performance) liquid chromatography (FPLC) system that primarily used

lower pressure during preparative purification of proteins at laboratory scale. Unlike the high performance liquid chromatography (HPLC), the AKTA system was operated based on a higher flow rate and lower pressure to avoid sample denaturation, move buffers and protein samples through separating column according to the protocol of GE Healthcare Life Sciences, U.K.

To estimate the molecular mass of AcL1, the gel filtration column was calibrated using Bovine thyroglobulin (8 nm), Horse spleen apoferritin (5.9 nm), sweet potato ß-amylase (4.15 nm), yeast alcohol dehydrogenase (3.72 nm), bovine serum albumin (3.52 nm) and bovine carbonic anhydrase (2.39 nm). Values in brackets are the stoke's radii of protein standards. The molecular mass of AcL1 was determined from a graph of $[-\log (K_{av})]^{\frac{1}{2}}$ against the molecular mass of the protein standards, where K_{av} is the partition coefficient, V_e is the elution volume of the protein while V_o and V_t are the void and total volumes of the gel filtration column respectively.

$$K_{av} = \frac{(V_e - V_o)}{(V_t - V_o)} \qquad\qquad \ldots\ldots\ldots\ldots\text{equation 1.}$$

Yield of full-length AcL1 was ~7 mg per litre of culture medium. Samples were separated by gel electrophoresis on 15% (w/v) SDS-PAGE followed by Coomassie blue staining and gel scanning to confirm the purity of the purified protein. Protein was concentrated by ultra-filtration to >5mg/ml and stored at -80 °C until use.

3.3.2.10 Biotinylation of AcL1

Covalent labelling of AcL1 with biotin (biotinylation) enables the target protein-biotin to bind avidin based on its high binding efficacy for ease of target protein detection without loss of its biological activities. The choice of streptavidin, (MW 60,000), a product of *Streptomyces avidinii,* over avidin was due to its characteristic non-specific binding to ligands and the ease of conjugation with Horseradish peroxidase (HRP) or alkaline phosphatase (AP) for immunodetection. According to the procedure of Z-link sulfo-NHS-LC-Biotin (product No. 21327; Thermo Scientific, U.K.) adopted for biotinylating AcL1, I calculated 42 µl of Biotin as requirement for 0.65 ml of AcL1 (2.73 mg/ml) given the molecular mass of AcMBP as 130,000 using the formula:

$$\text{mmol Biotin} \times \frac{1{,}000{,}000 \ \mu l}{L} \times \frac{L}{10 \ \text{mmol}} = \mu l \ \text{Biotin} \qquad \qquad \text{.......equation 2}$$

3.4 Results

3.4.1 Production of the extracellular region of AcMBP

PCR was used to amplify the cDNA encoding the full-length extracellular AcMBP. To clone the extracellular portion of AcMBP (subsequently called AcL1 in this study), a synthetic cDNA was produced and cloned into the polylinker of the expression plasmid pED4 by homologous recombinantion (a type of genetic recombination that involved the exchange of nucleotide sequences between two similar molecules of DNA or introduction of specific mutation into a gene). Figure 3.6 shows the gel of pED4 Sal 1 digestion prior to the cloning of AcL1.
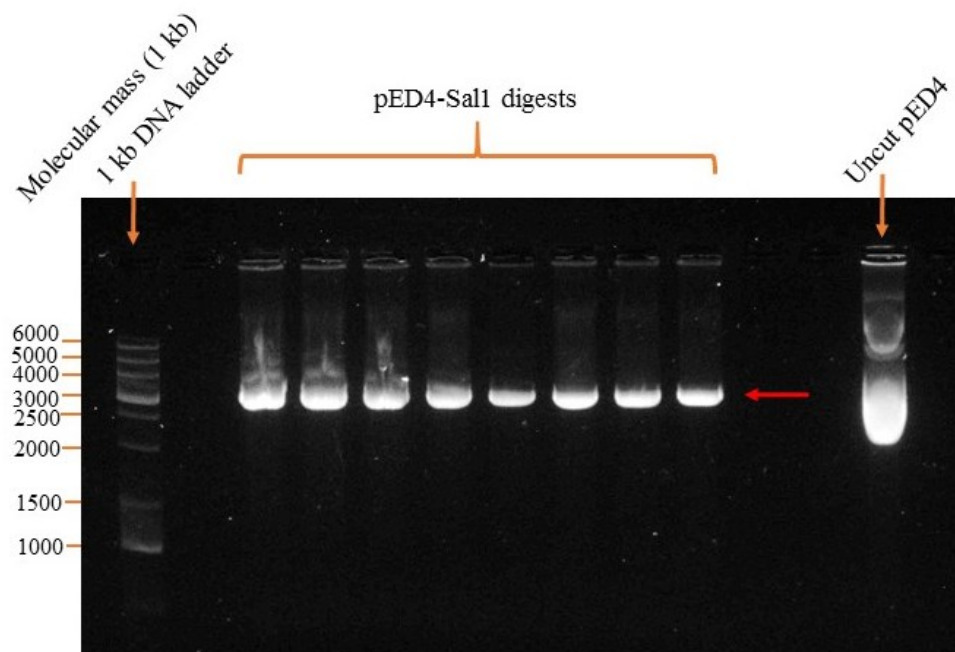
Figure 3-6: Purification of pED4 vector by gel purification. After digestion, the bands of pED4 Sal1 digests (red arrowed) were cut from the gel and purified for the cloning of AcL1. The uncut pED4 appeared as high molecular weight smear on gel measured against a 1 kb DNA marker.

The natural signal sequence of AcMBP was replaced by the signal sequence for interleukin 2 and a Kozak sequence (GCCACC) was introduced immediately 5' of the start codon (Figure 3.7). The cDNA was codon optimised for expression in CHO cells and synthesised to encode a C-terminal hexahistidine tag for purification.
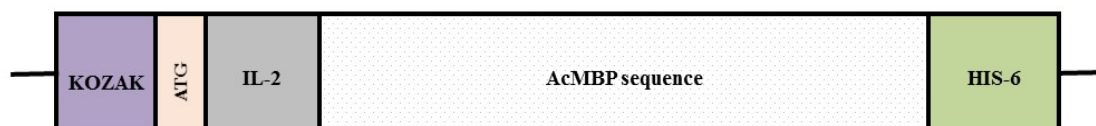
Figure 3-7: The synthetic cDNA encoding the AcL1. KOSAK consencus sequence initiates eukayotic translation process. ATG = start codon, IL-2 = Interleukin 2 signal sequence to control the precise expression of a single gene. The codon optimised AcMBP sequence is the protein of interest in this study. His-6 is the hexahistidine tags for the protein purification by affinity chromatography based on its affinity for Nickel, cobalt or Zinc.

3.4.2 Cloning, expression and production of recombinant AcL1

The cDNA encoding the AcL1 was amplified by PCR (Evans)(Sambrook et al., 1989) using primers shown in Table 3.1. The DNA was separated on a 1% agarose gel (Figure 3.8). The product was excised, purified and then cloned into the *Sal*I restriction site of the mammalian expression vector pED4 by homologous recombination. It is a gap-repairing cloning approach of overlapping ends of PCR product and vector. After transformation, minipreps were prepared and clones containing the insert were identified by PCR. From six clones tested five positive were identified giving products of the expected size for the AcL1 cDNA (~2.5 kb) (Figure 3.9). Two of these clones were sequenced by Protein Nucleic Acid Chemistry Laboratory (PNACL) University of Leicester to confirm that no mutations were induced by the PCR. At PNACL, the DNA plasmid or PCR product were purified by Qiagen 9600 Robot using QIAPrep Turbo kits or QIAquick kits respectively. Afterwards, cycle sequencing reactions were carried out on the samples, cleaning them up using Centrisep columns. Finally, the products were analysed using the 3730 automated sequencer.
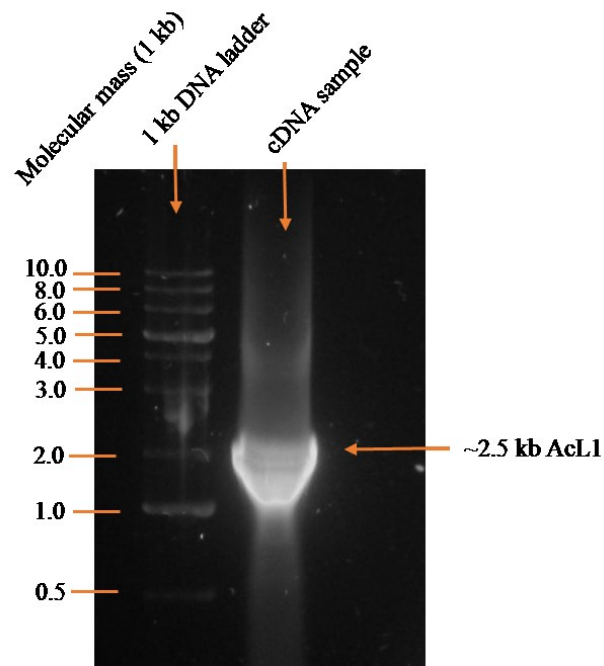
Figure 3-8: A 1 % agarose gel showing PCR amplification of the cDNA encoding AcL1. Lane 1 is 1 kb DNA ladder, lane 2 is the AcL1 DNA (the product size was ~2.5 kb as expected). The primers used were MBPF and MBPR. The fragment was purified from the gel and cloned into pED4 expression vector.
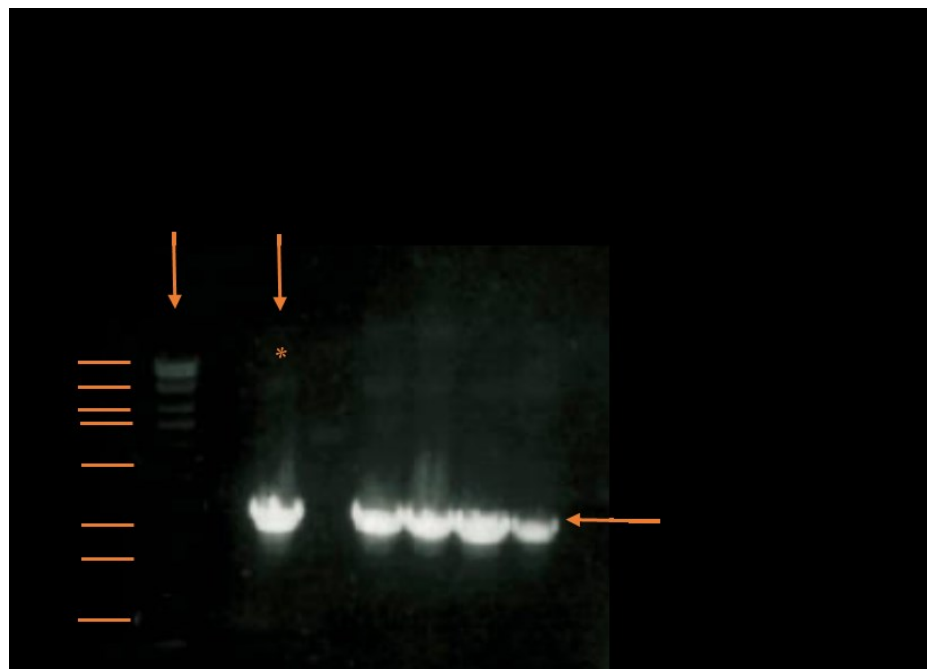
Figure 3-9: Test PCR of six pED4 clones following recombination. Six mini-prep were tested for the presence of the AcL1 cDNA by PCR. A product of the expected size was detected in five out of the six clones.

3.4.3 Protein purification and analysis of recombinant AcMBP

To express the AcL1, CHO cells DXB11 (lacking dihydrofolate reductase) were transfected with pED4 containing the AcL1 cDNA by the calcium phosphate method. The expression plasmid encodes a dicistronic message with the cDNA of interest followed by the dihydrofolate reductase gene. Clones containing the plasmid were selected on media lacking nucleosides and production was increased over several months by passaging cells into increasing concentrations of methotrexate (an inhibitor of dihydrofolate reductase) up to a concentration of 0.5 µM. Protein was isolated from CHO cells in serum-free medium as described (Wallis and Drickamer, 1999). The media was harvested every other day for five (5) harvests.

Recombinant AcL1 was purified by affinity chromatography on nickel-Sepharose, followed by gel filtration chromatography on a Superdex 200 10/300 column (GE Healthcare) (Figures 3.10 & 3.11). A small proportion of AcL1 eluted from the nickel column with 20 mM imidazole, but most was found in the elution fractions. The AcL1 protein concentration was quantified using nanodrop spectrophotometer for direct measument of UV absorbance of protein at 280 nm divided by extinction coefficient. Yields of protein were high with ~ 7mg of pure AcL1 per L of culture medium.
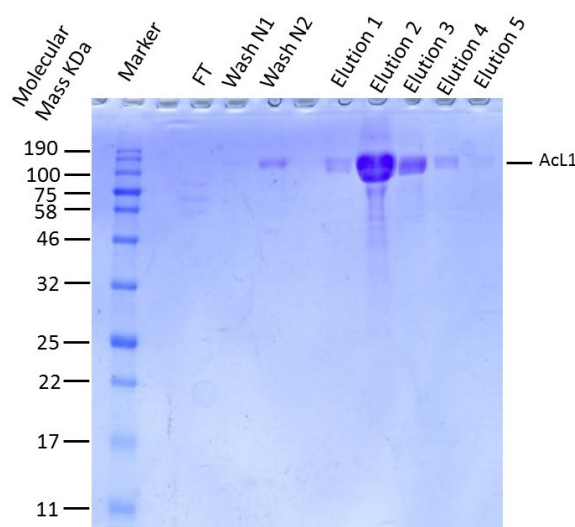
Figure 3-10: SDS-PAGE of AcL1 purified by affinity chromatography on a nickel-Sepharose column. AcL1 was expressed in CHO (DBX-11) cells line and purified by affinity chromatography on Nickel column. The first lane is the 11 – 190 kDa protein ladder. FT is the flow through. The elution fractions were shown in Wash buffer N2 and elution buffers 1 – 4 after chromatography. The minor bands in elution lane 2 are possibly protein aggregates as impurities. A 15% SDS gel was run under reducing condition (with ß-mercaptoethanol) and stained with Coomassie blue. A 15% SDS gel was the optimum

weight percentage of gel (cross-linker) pore-size required to yield the best protein separation and resolution for AcL1). The apparent molecular mass was ~120 kDa. The experiment was repeated at least eight times.
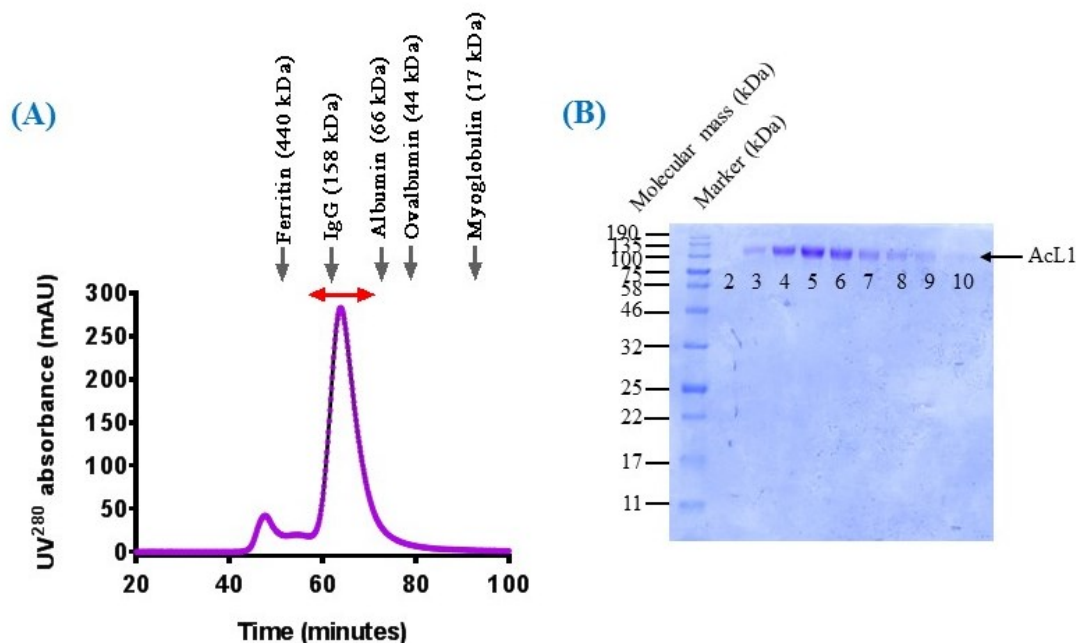
Figure 3-11: Purification of AcL1 by size-exclusion chromatography. (A) Elution profile of pooled AcL1 protein fractions of about 5.5ml volume sample (0.83mg/ml), collected following His-tag protein elution from affinity chromatography was analysed on a Superdex 200 16/60 gel filtration column at a flow rate of 0.8 ml/min to reveal protein peak. The main peak labelled with arrow is AcL1 ~ 120 kDa. The first smaller peak is aggregate. The molecular weight of AcL1 was extrapolated from the approximate molecular weight standards (grey arrows) of eluted profile (not shown) of: (i) Ferritin, 0.24 mg/ml, M_r 440 000 (ii) IgG, 0.2 mg/ml, M_r 158 000 (iii) Albumin, human 5 mg/ml, M_r 66 000 (iv) Ovalbumin, 5 mg/ml, M_r 44 000 (v) Myoglobulin, 1.5 mg/ml, M_r 17 000 on Superdex 200 column. **(B)** A 15% SDS-PAGE gel under reducing condition (with ß-mercaptoethanol) showing fractions collected across the gel filtration peak that corresponded with the red arrow in part A). Protein was stained with Coomassie blue. The protein runs as a single band of molecular mass ~100kDa (lanes 3 – 9). Lane 2 is a blank space in between the protein marker and AcL1 protein samples. Lane 1 is the molecular mass standard represented as blue-pre-stained protein standard broad-range 11-190 kDa. Experiment was repeated at least eight times.

AcL1 migrated as a single band with an apparent molecular mass of ~120 kDa on SDS-PAGE under both reducing (Figures 3.10, 3.11b, 4.25) and non-reducing conditions (Figure 4.25). The expected molecular mass was 81 kDa, indicating that the protein is

97

likely to be post-translationally modified. Recombinant AcL1 eluted from the gel filtration column with an apparent molecular mass of ~150 kDa. Although the molecular mass is larger than expected, it is too small for a dimer suggesting that AcL1 is monomeric under native conditions. The aberrant migration of the protein by gel filtration probably indicates that AcL1 is asymmetrical. Previous reports of protein isolated from *Acanthamoeba* have shown that full-length AcMBP is a trimer with a molecular mass of ~330 kDa. Taken together these results indicate that the transmembrane region and/or the N-terminal intracellular domain is necessary for trimerisation of AcMBP.

3.4.4 Mass spectrometry of AcL1

Mass spectroscopy is an analytical technique that ionises peptides in the gaseous phase and sorts these ions according to their mass-to-charge ratio and detected. Figure 3.12 shows the fragment ion nomenclature, basis of LC-MS/MS analysis of peptides.
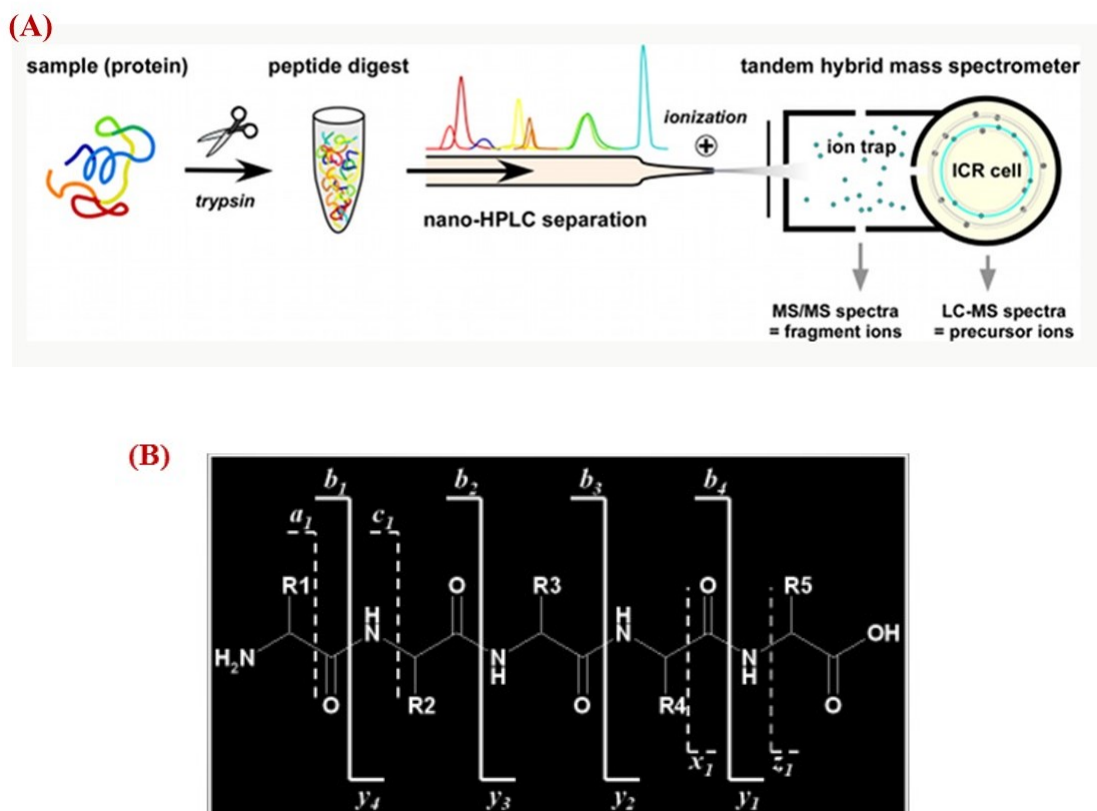
Figure 3-12: (A) Schematics of mass spectrometry instrument. Sample preparation includes excision of gel band, de-staining and reduction, proteolysis of protein sample. Resulting peptide digest were projected through nano-HPLC system for separation of yielded ionised particles, which are analysed by tandem hybrid mass spectrometer. Ion trap uses ESI to produce ions which are trapped (stored); Ion cyclotron resonance (ICR)

cells are detected based on the frequency of ionised particles in a fixed magnetic field and are subsequently analysed. **(B) Fragment ion nomenclature, basis of LC-MS/MS analysis of peptides.** The type of fragment ions detected will depend on the primary sequence, amount of internal energy, how the energy that was introduced and the charge state, provided they carry at least a one charge. The ions are categorised as either a, b or c if the charge is retained on the N terminal fragment while ion types x, y or z is allocated to fragments with charges retained on the C terminal. However, a subscript indicates the number of residues in the fragment. (Figures 3-12a and b were adapted from the Institute of Physiology, University of Freiburg; and Core Biotechnology Services, PNACL, University of Leicester, U.K. respectively).

To verify that the purified protein was full-length AcL1, a sample was excised from an SDS-PAGE gel, digested with trypsin at lysine and arginine residues and analysed by mass spectrometry (Figure 3.13). Peptides identified are shown in red.

(A)

```
   1 GTCNLSGAIK QPGLDCSSTS CSITSGTFPF PLPQGETYDS FYSWILGVIG
  51 TDGATVNAQY VDYTKADPNI YFTAGQTNCM VNLTFVYEVA FYRNSMGYFT
 101 FTRDSKPTSV GSVTLKPVFS ETTVDCSRTS SQPLPGTSCL APGSTISLGP
 151 FSSTQAVGFY LKQDSICSGT TTFYSVDALN KVTSRWKPIP AAHGRMIAVL
 201 RDPNTLRAYL GFEDSPDGSD SDYNDNVFSV TSNCEIDTSL LPCATVTTCR
 251 NSKQTFDSSK CTCSCPNPVT CTAPQVYSTD LCACTCPNAT QTCTAPLTWN
 301 SATCQCDCPS TKPSGVTCSN LQQWSNVVAT CGCKCPDPAT YTCSDNRFVL
 351 RTSDCTCNCP STGSCSGNLK WNSANSVCGC QCPSTPPTPC SGNLKWNSTA
 401 SKCACECPAT AALAGVTCKD KEVWDTASCS CKCPATASAA DTTCPNVNYQ
 451 WNYNGKCDCV CPATSAEAGI NCTALGLGNT VWDTTACNCA CPPTGTCPGN
 501 KVWNPSNDPA KCGCSCPASA PAGKECKGNF YWNTSDDVCD CYCPLEAPAD
 551 DPCIGYTTWN RTECDCYCPL EPPFEGGCPG VQVWDRDQCQ CVCPDDDPCA
 601 AQSTACKQFY CSSSTGECAL VYEDTCASQK LQFNTTGCLS WQCDPDLGCV
 651 RKANGSCCDD YKDCPTCAKY DGCDWIGTKC ADSGQVLTSP IDQADHPDCF
 701 PSTGLSAGET AGHHHHHH
```

(B)
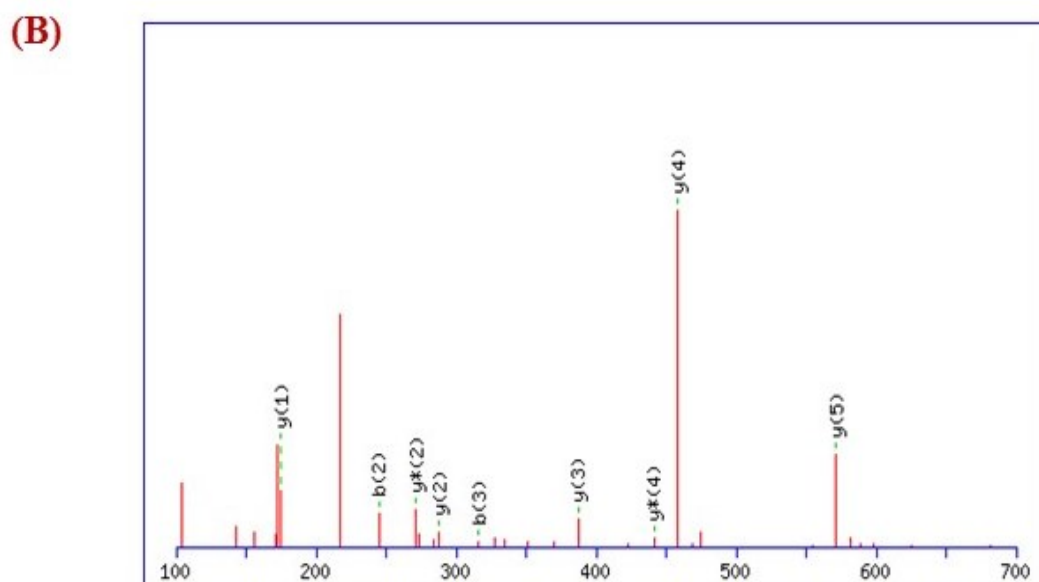
Figure 3-13: Mass spectrometry of AcL1 following trypsin digestion. (A) Sequence of AcL1. Peptides identified by MALDI-MS are shown in **bold red. (B):** LC-MS/MS spectrum of one of the AcL1 peptides with annotated peaks: MIAVLR (701.93Da) where y (1-5) represent peaks corresponding to the loss of amino acid residues R, L, V, A and I, respectively.

As shown in Figure 3.13, peptides were identified throughout the entire sequence of AcL1 (including the hexahistadine tag) indicating that the protein is not degraded.

100

3.4.5 Purification of AcL1 on mannose-Sepharose

To verify that recombinant protein bound to mannose, AcL1 was purified by affinity chromatography on a mannose-Sepharose column. Serum-containing medium harvested from the CHO cells was diluted with buffer containing Ca^{2+} and loaded onto the mannose-Sepharose column. After two wash steps, five elution fractions were collected using buffer 2 mM containing EDTA, pH 7.5 followed by additional elution steps using buffer-containing mannose. As shown in Figure 3.14, all the protein eluted in the buffer containing EDTA. AcL1 migrated at ~120 kDa. Additional bands were observed in the elution fractions (EDTA 3 and 4) at ~46 kDa and ~30 kDa. These are often seen in serum-containing samples following purification by mannose-Sepharose and have been previously identified as bovine collectin-43 and bovine mannan-binding lectin, from the foetal calf serum. Nevertheless, these extraneous proteins could have better been removed from the target AcL1 protein by ion-exchange chromatography which is based on charge-to-charge interactions between sample protein and the immobilised resin structure of the study protein.
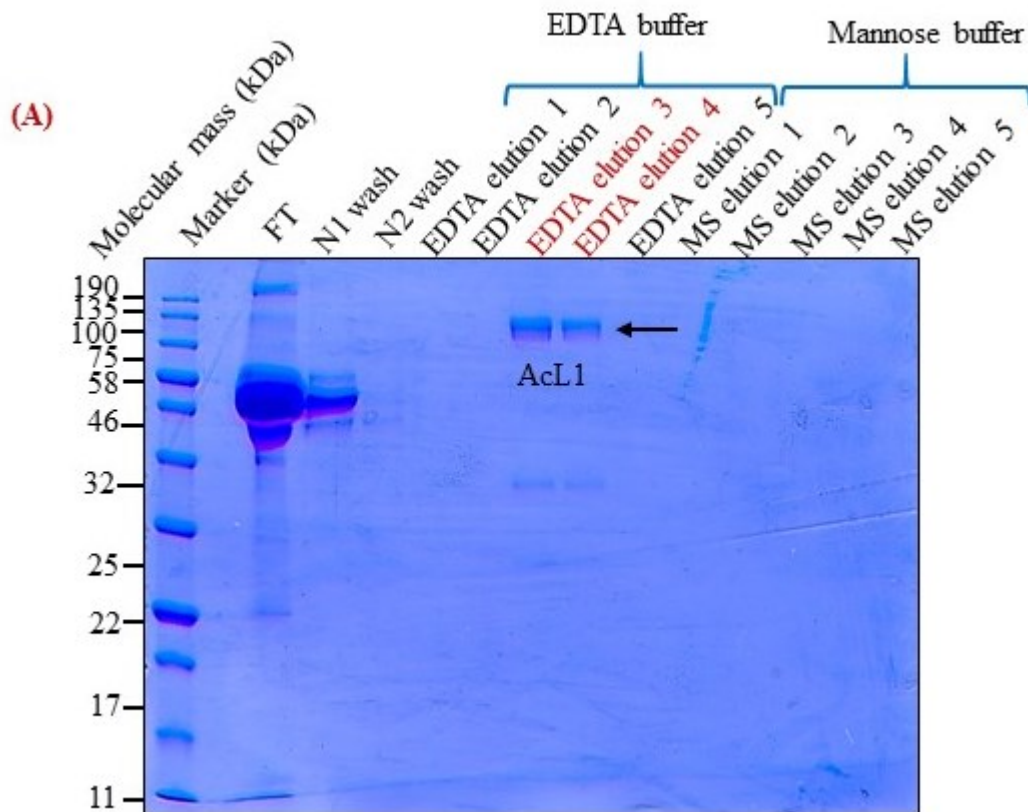
Figure 3-14: Purification of AcL1 by affinity chromatography on a mannose-Sepharose column. Medium from AcL1-producing CHO cells containing 10% foetal calf serum was loaded onto a mannose-Sepharose column. After two wash steps proteins were eluted using buffer containing EDTA followed by buffer containing mannose. The band corresponding to AcL1 is marked with an arrow.

In previous studies (Garate et al., 2005) AcL1 was eluted using mannose, so the finding that mannose binding is Ca^{2+}-dependent is novel. Interestingly, AcL1 shares many of the properties of C-type lectins such as mannose-binding lectin, both with respect to its lectin activity and its requirement for Ca^{2+}. However, AcL1 does not contain a C-type carbohydrate-recognition domain, so both Ca^{2+} and mannose binding must be mediated through a different mechanism.

Purified AcL1 was also tested for binding to mannose-Sepharose. As expected it bound in buffer containing Ca^{2+} and eluted in EDTA, confirming that it binds to mannose in the presence of Ca^{2+} (Figure 3.15).
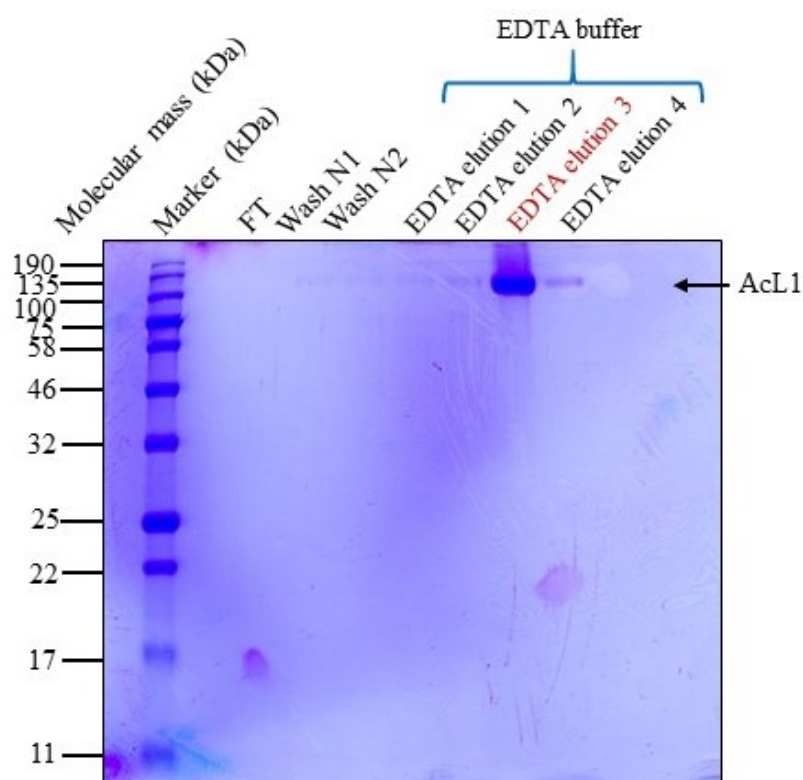
Figure 3-15: SDS-PAGE showing purification of AcL1 by affinity chromatography on a mannose-Sepharose column. AcL1 bound to the column in buffer containing Ca^{2+} and eluted from the column in buffer containing EDTA (Elution 3). This confirms correct protein folding and Ca^{2+}-dependent mannose-binding property of AcL1.

3.4.6 Glycosylation of AcL1

 AcL1 contains nine (9) potential N-linked glycosylation sites, and glycosylation at these positions is likely to account at least in part for the increased mass observed on SDS-PAGE gels (Figure 3.16). To test if the proteins are modified, AcL1 was digested with PNGaseF, which removes N-linked glycans. Reactions were carried out under non-denaturing conditions.

```
GTCNLSGAIKQPGLDCSSTSCSITSGTFPFPLPQGETYDSFYSWILGVIGTDGATVNAQYVDYTKADPNIYFTAGQTNCM   80

VNLTFVYEVAFYRNSMGYFTFTRDSKPTSVGSVTLKPVFSETTVDCSRTSSQPLPGTSCLAPGSTISLGPFSSTQAVGFY  160

LKQDSICSGTTTFYSVDALNKVTSRWKPIPAAHGRMIAVLRDPNTLRAYLGFEDSPDGSDSDYNDNVFSVTSNCEIDTSL  240

LPCATVTTCRNSKQTFDSSKCTCSCPNPVTCTAPQVYSTDLCACTCPNATQTCTAPLTWNSATCQCDCPSTKPSGVTCSN  320

LQQWSNVVATCGCKCPDPATYTCSDNRFVLRTSDCTCNCPSTGSCSGNLKWNSANSVCGCQCPSTPPTPCSGNLKWNSTA  400

SKCACECPATAALAGVTCKDKEVWDTASCSCKCPATASAADTTCPNVNYQWNYNGKCDCVCPATSAEAGINCTALGLGNT  480

VWDTTACNCACPPTGTCPGNKVWNPSNDPAKCGCSCPASAPAGKECKGNFYWNTSDDVCDCYCPLEAPADDPCIGYTTWN  560

RTECDCYCPLEPPFEGGCPGVQVWDRDQCQCVCPDDDPCAAQSTACKQFYCSSSTGECALVYEDTCASQKLQFNTTGCLS  640

WQCDPDLGCVRKANGSCCDDYKDCPTCAKYDGCDWIGTKCADSGQVLTSPIDQADHPDCFPSTGLSAGETAG
```

Figure 3-16: Sequence of AcL1 showing the potential N-linked glycosylation sites.
Sites with the characteristic motif: NXS or NXT are shown in red. The sequence NPS is highlighted but is unlikely to be glycosylated due to the presence of the proline residue, which usually prevents modification. The DUF and cysteine-rich domains are highlighted in blue and yellow respectively.

Upon digestion with PNGaseF, the apparent molecular mass of AcL1 decreased from ~120 kDa to ~100 kDa indicating that it is glycosylated. Increasing the amount of PNGaseF had no additional effect. Notably the apparent molecular mass of AcL1 on the gels was still greater than expected (~81 kDa) from the amino acid sequence suggesting that it might be modified in additional ways (Figure 3.17).
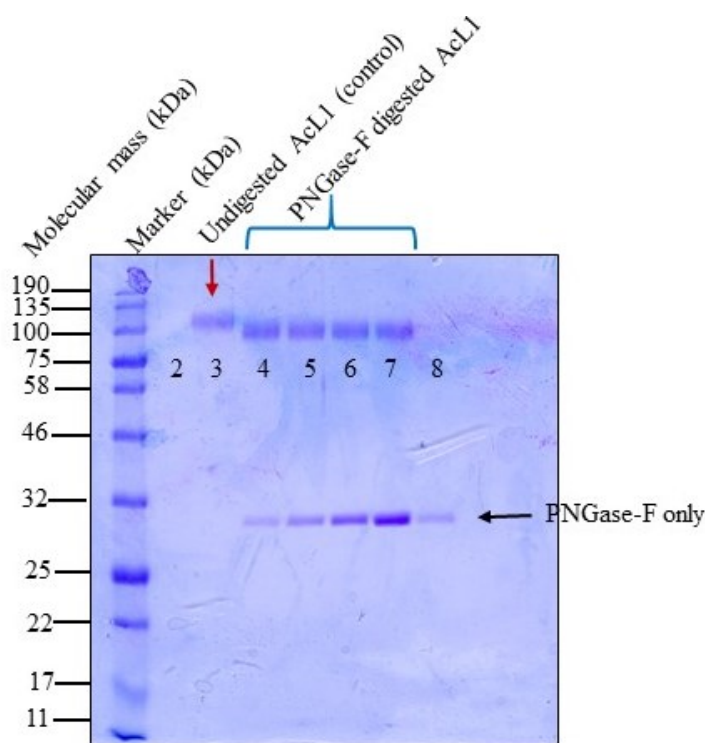
Figure 3-17: Digestion of AcL1 with PNGaseF analysed by SDS-PAGE. Purified AcL1 (~2 μg) was incubated with increasing amounts of PNGaseF (2-fold dilutions with a maximum amount of 1000 U: New England Biolabs). Serially, each of lane 3-7 contained 10μl of protein and 0, 0.25, 0.5, 1.0, 2.0μl of PNGase-F respectively; Lane 8 (control) contained 10μl nH_2O and 2.0μl PNGase-F. Then, a 15% SDS-PAGE analysis of AcL1 digested with PNGase-F incubated at 37°C for 2 hours. Lane 1 was a 1kDa protein ladder of blue-pre-stained protein standard broad-range 11-190 kDa. Lanes 3 (negative controls = undigested AcL1 only: there was no de-glycosylation/denaturation of AcL1 in the absence of heat); lanes 3-7 (serially diluted protein sample with PNGase-F); lane 8 (positive controls, PNGase-F only. This was to monitor posttranslational modification as confirmed by mass spectrometry in **figure 3-16**. Expectedly, the theoretical values of the 712 amino acids forming AcMBP ~123kDa (M_r = 87415.75; pI = 4.41; Ext. coef. = 1.44) is distinct from the actual 718 amino acids-translated AcL1 ~106kDa (M_r = 76143.0; pip = 4.6; Ext. coef. = 1.59) that explains the impact of posttranslational glycosylation. This experiment was repeated at least five times and it confirmed correct protein folding and apparent loss of molecular mass due to post-translational glycosylation of AcL1.

However, complete inhibition of N-glycan formation could result in altered glycoprotein chain and consequently be useful for studying the key functional role of N-glycosylation in the protein folding of the post-translationally modified AcMBP; and subsequently, understanding its therapeutic roles against AK. Tunicamycin is chemical inhibitors of N-

glycosylation (Hall et al., 1990); Esko, Bertozzi and Schnaar, 2017) which blocks glycosylation of glycoproteins entirely in eukaryotes by obstructing the transfer of *N*-acetylglucosamine-1-phosphate (GlcNAc-1-P) from UDP-GlcNAc to dolichol-P (catalyzed by GlcNAc phosphotransferase; GPT), thus reducing the formation of dolichol-PP-GlcNAc. Unlike tunicamycin, other inhibitors include plant alkaloids, which inhibit the processing of glycosidases (α-glucosidases and α-mannosidases) by trimming nascent chains.

3.4.7 Ca^{2+}-binding by AcL1

Mannose binding by AcL1 was Ca^{2+} dependent as described above, yet nothing is known about its binding properties. To see if Ca^{2+} affected the stability of AcL1, protein was incubated with increasing concentrations of trypsin in the presence of Ca^{2+} or EDTA. In C-type carbohydrate-recognition domains, Ca^{2+} stabilises loop regions that form the binding site for the sugar. In the absence of Ca^{2+}, the loops are much more susceptible to proteases such as trypsin (Venkatraman Girija et al., 2015).
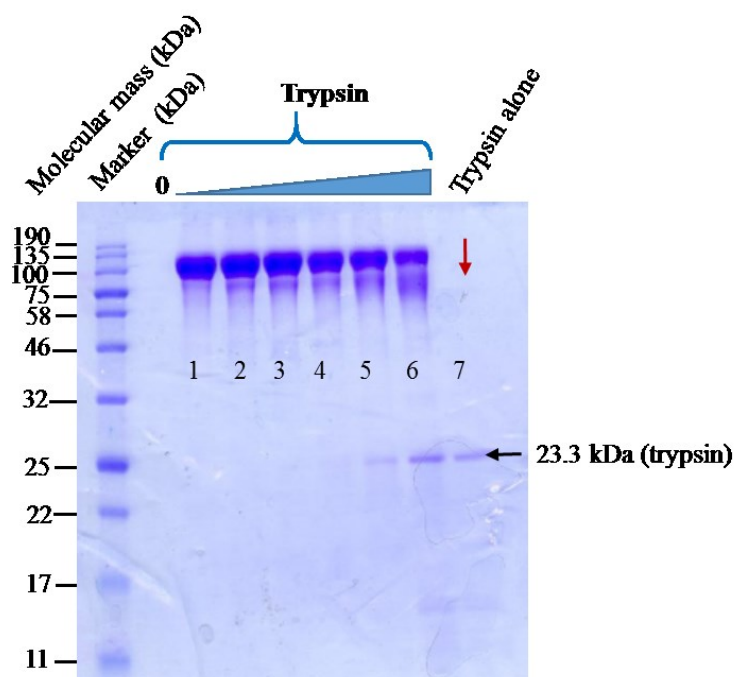
Figure 3-18: SDS-PAGE showing trypsin digestion of AcL1 in the presence of Ca^{2+}. A ~5 µg of AcL1 (7.55 mg/ml) was incubated with decreasing amounts of trypsin (5-fold dilutions starting at 1 µg from a concentration of 2 % (w/w) in the presence of 10 mM CaCl$_2$ at 37°C for 2 hours. Undigested protein (lanes 1 – 5), partially digested protein (lane 6) and trypsin alone, 23.3 kDa (lane 7). Trypsin-proteolysis of AcL1 in the presence of calcium was analysed by SDS-PAGE and gel were scanned to determine the amount

of AcL1 remaining. Folded proteins are relatively resistant to proteolysis. Ladder (L) = Blue-pre-stained protein standard broad-range 11-190 kDa. Experiment was repeated at least thrice.

In the presence of Ca^{2+}, AcL1 was resistant to trypsin, with relatively little digestion even at the highest concentration of trypsin tested (Fig 3.18). By contrast, in the absence of Ca^{2+} (i.e. with of EDTA) and in otherwise identical conditions, AcL1 was cleaved at the lowest concentration of trypsin to generate a fragment of ~80 kDa (Figure 3.19). The remaining fragment was more resistant to further digestion, although some general degradation was observed at the higher concentrations. These data support the previous observation that AcL1 is a Ca^{2+}-binding protein. Furthermore, Ca^{2+} stabilises AcL1 providing protection against proteolysis.
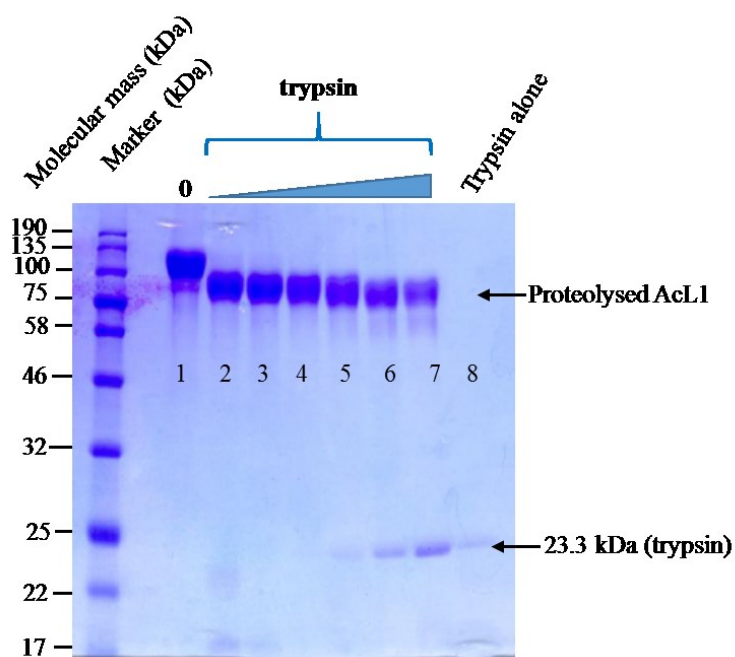
Figure 3-19: SDS-PAGE showing trypsin digestion in the absence of Ca^{2+}. AcL1 (~5 µg) was incubated with decreasing amounts of trypsin (5-fold dilutions starting at 1 µg) in the presence of 2 mM EDTA at 37°C for 2 hours. Trypsin-proteolysis of AcL1 (7.55 mg/ml) in the absence of 10mM Ca^{2+} (1M EDTA was used for protein dialysis to completely eradicate Ca^{2+}): Negative control (lane 1), positive control (lane 8) and absence of Ca^{2+} in AcL1 samples (lanes 2-7). A completely digested full length AcL1 in the absence of ca^{2+} (+ EDTA) was analysed by SDS-PAGE and gel were scanned to

determine the amount of AcL1 remaining. Ladder (L) = Blue-pre-stained protein standard broad-range 11-190 kDa. Experiment was repeated at least thrice.

To further explore Ca^{2+} binding, AcL1 (~5 μg) was incubated with a fixed amount of trypsin (0.1 μg) in the presence of decreasing concentrations of Ca^{2+} (2-fold dilutions starting at 10 mM). After digestion the samples were separated on a SDS-PAGE gel. As shown in Figure 3.20, AcL1 was resistant at 10, 5 and 2.5 mM Ca^{2+} (lanes 1-3); but mostly digested at 1.25 mM and at lower concentration of Ca^{2+}, giving an apparent dissociation constant K_{Dapp} for Ca^{2+} of ~1.25 mM. Typical serum concentrations of Ca^{2+} are ~2 mM, so the K_{Dapp} is within the physiological range.
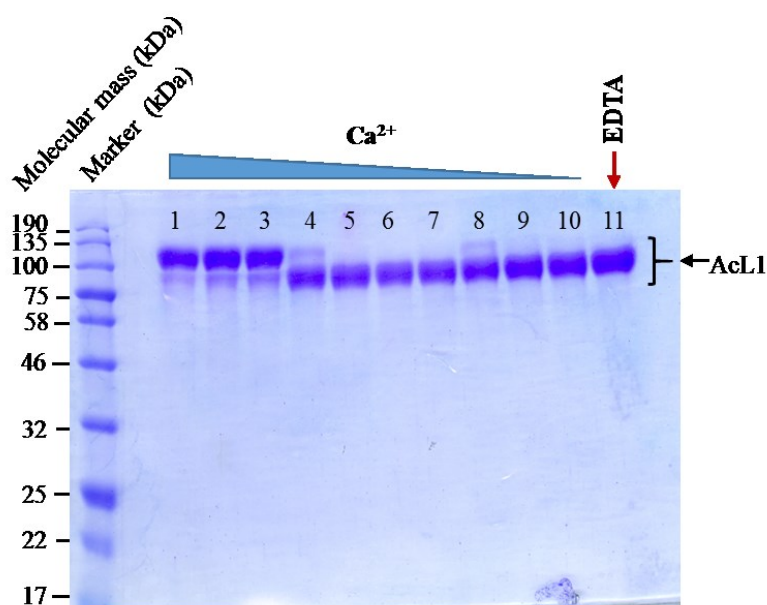
Figure 3-20: SDS-PAGE showing trypsin digestion with decreasing concentrations of Ca^{2+}. A 30μl of AcL1 at a starting concentration of 7.55mg/ml (i.e. ~5 μg) was incubated with a fixed amount of (1:125) trypsin (0.1 μg) in the presence of 2-fold dilutions of Ca^{2+} starting at 10 mM at 37°C for 2 hours. (1M EDTA was used for dialysis of protein sample to completely eradicate Ca^{2+}). AcL1 was resistant at 10, 5 and 2.5 mM Ca^{2+} but mostly digested at 1.25 mM Ca^{2+}. The sample was analysed by SDS-PAGE and gel were scanned and documented as undigested protein sample (lanes 1-3), digested protein (lanes 4-10) and positive control in the absence of Ca^{2+} (lane 11; arrowed). Ladder (L) = Blue-pre-stained protein standard broad-range 11-190 kDa.

3.4.8 Dynamic light scattering of AcL1

Gel filtration analysis indicated that the extracellular region of AcL1 is monomeric but is likely to be asymmetrical. To gain more information about its size and shape, the hydrodynamic radius of AcL1 was determined by dynamic light scattering using a Malvern Zeta-sizer. Dynamic Light Scatterring (DLS) measures the fluctuations of light scattering of solute particles due to the bombardment by solvent as a function of time. The hydrodynamic diameter is calculated from the translational diffusion coefficient based on Stokes-Einstein's equation:

$$d(H) = KT/3\pi\eta D \ ....equation\ 3$$

where d(H) is hydrodynamic diameter, D is transitional diffusion coefficient, K is Boltmann's constant, T is absolute temperature and η is viscosity. From these changes the diffusion coefficients of the particles undergoing Brownian motion can be determined. AcL1 protein sample was filtered purified-buffered in 0.1 μm filtered to eradicate the likelihood of dust particles which may alter its DLS value. AcL1 was monodisperse with a hydrodynamic radius estimated as 5.9 nm (Figure 3.21). Using a molecular mass of 120 kDa and a partial specific volume of 0.73 ml/g (a typical value for protein), this suggests that AcL1 is highly asymmetrical. Assuming a prolate (cigar) shape, the axial ratio would be ~15:1 or 19:1 for an oblate (flattened spheroid) shape (calculated using the Zetasizer software).
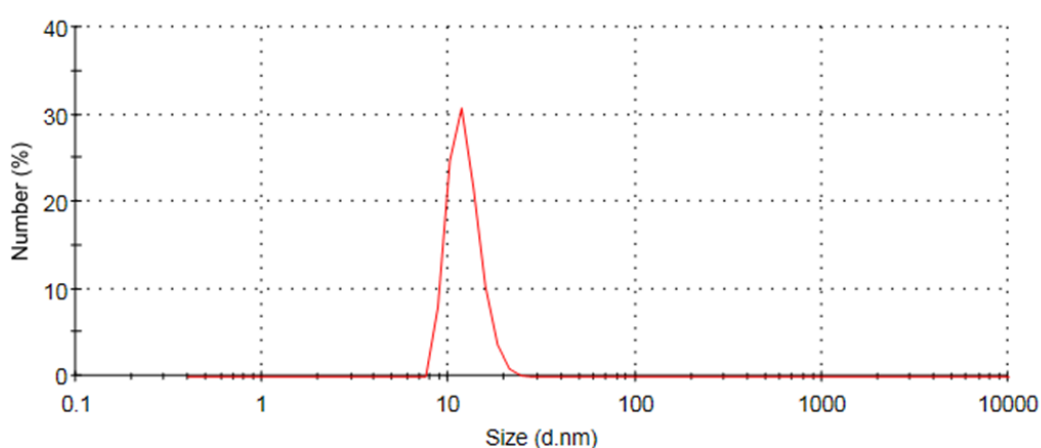
Figure 3-21: Hydrodynamic size of AcL1. Data shows dynamic light scattering using a Malvern Zeta-sizer at 25°C. 90μl of AcL1 (0.25mg/ml) was mixed with 400μl of buffer (in 25mM HEPES pH 7.5, equilibrated in 150mM NaCl and 1mM EDTA) and centrifuged at 10000rpm for 60 seconds to remove any particles. Thereafter, 0.5ml of

protein sample aliquoted into a 1 cm cuvette for DLS which measures the intensity of light scattered at one point; measuring the particle size = 11.8nm approximate estimate of about 800kDa. The d.nm = distribution by numbers. The homogeneity of AcL1 based on similar peak from multiple measurements of 5 trials demonstrated highly purified and homogeneous AcL1 protein preparation.

3.4.9 Secondary structure of AcL1

Given its lack of homology to other proteins, nothing is known about the structure of AcL1. Circular dichroism was used to gain information about its secondary structure. Circular dichroism (CD) measures the relative absorbance of left and right circularly polarised light usually at a frequency of 50 kHz. Because protein secondary structures are chiral as are most of the amino acid residues themselves, CD gives an accurate measure of the composition of secondary structure and monitors the protein unfolding to folding transition as detailed in http://cddemo.szialab.org/.

Figure 3.22 shows the CD spectra of different protein secondary structures. In addition to the choice of a shorter path length, AcL1 protein concentration was adjusted to obtain the best CD signal. Table 3.5 and Figure 3.23 show the CD spectra of AcL1 in the presence and absence of Ca^{2+}. Similar spectra were obtained indicating that Ca^{2+} binding does not substantially alter the secondary structure of AcL1.
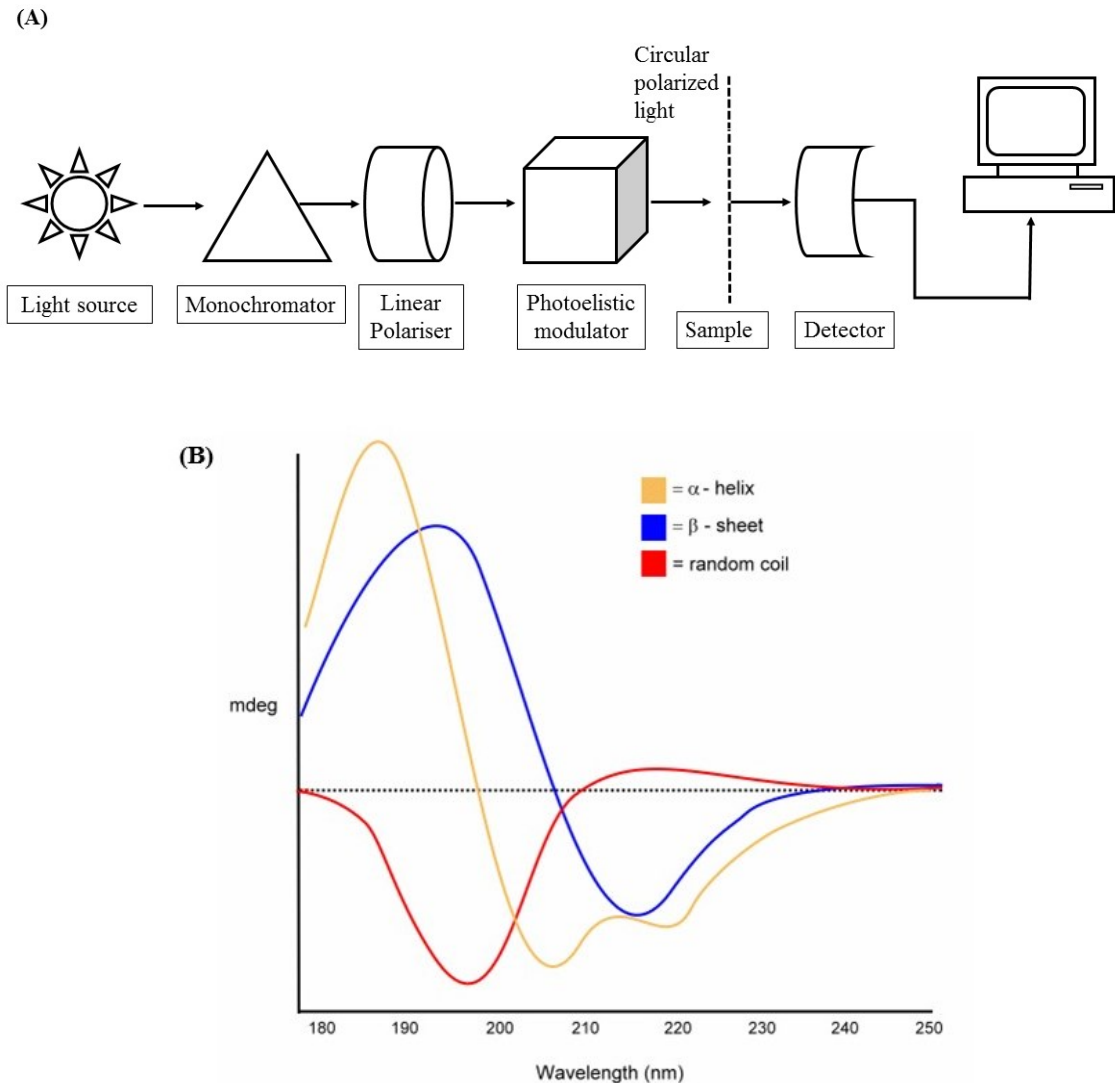
Figure 3-22: (A) Schematics of a CD instrument showing the polarisation of light and differentiatial absoption of LCP and RCP light. A high intensity white unpolarised light source passed through a monochromator to produce a single wavelength light polarised by the linear polariser. The photoelistic modulator transforms the linear light to circular polarised light. The incident light switches directions of polarisation between left circularly polarised (LCP) and right circularly polarised (RCP) lights as it impacts on the sample for absorption.The differentiation of molar absorptivity is detected by the detector and **(B) CD spectra of standard protein secondary structures**. The absorption spectrum of a named folded protein (poly-L-lysine) in a continuous array showing an α-helixes (positive at 192 nm, negative 209 nm); β-sheets (positive at 196 nm, negative at 218 nm) and unordered (random coils, positive at 212 nm, negative 195 nm) in the far UV region (< 250 nm). (Karabencheva and Christov, 2010).
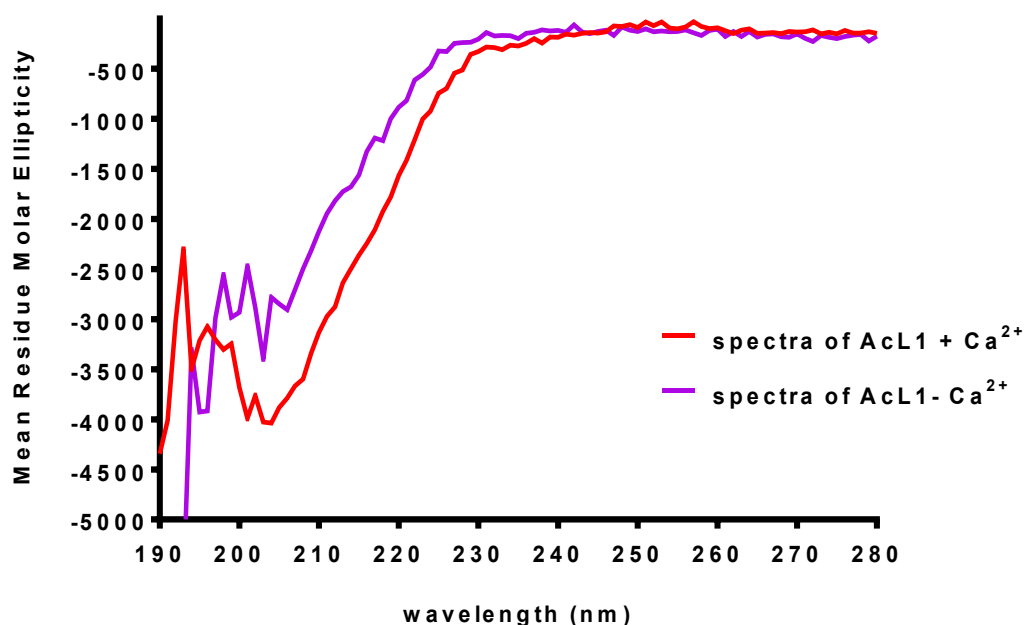
Figure 3-23: CD spectra of AcL1 in the presence and absence of Ca²⁺. AcL1 (0.4mg/ml) in 10mM TRIS/HCl pH 7.4 (± Ca²⁺) was analysed in a 1 mm cell path-length in a Chirascan CD spectrometer (Applied Photophysics). Far UV CD spectra of secondary structures of folded full-length AcL1 in either the presence (in red) or absence (in blue) of calcium. Data from the mean (n = 3) residual ellipticity shows a moderate difference in secondary characteristics of AcL1 due to the presence of Ca²⁺ between 210 – 230 nm while < 210 nm depicts noisy spectra.

Based on the spectra, AcL1 contains appreciable amounts of a β-sheet structure (~30%) but with some α-helix (~13%). A considerable proportion of the protein is random coil (~50%). This is likely to reflect the cysteine-rich domain, which is unlikely to be α-helical or β-sheet.

Table 3-5: The proportion of secondary structure in AcL1 by CD in a Chirascan CD spectrometer.

	CD spectrum of AcL1 + Ca²⁺			CD spectrum of AcL1 - Ca²⁺		
	200-260nm	205-260nm	210-260nm	200-260nm	205-260nm	210-260nm
Helix	14.8%	15.0%	13.9%	13.9%	13.7%	12.8%
Antiparallel	18.7%	14.8%	17.9%	19.5%	15.7%	19.1%
Parallel	16.8%	18.3%	16.6%	17.7%	19.6%	17.5%
Beta-Turn	21.8%	20.9%	22.0%	22.1%	21.3%	22.5%
Rndm. coil	48.5%	51.4%	51.5%	50.3%	53.3%	53.1%
Total sum	**120.5%**	**120.3%**	**121.9%**	**123.4%**	**123.5%**	**124.9%**

(The overall percentage of structures was greater than 100%. The reason for this is unknown).

CD was also used to investigate the stability of AcL1. As protein is heated, it will lose its secondary structure and the CD spectra will more resemble random coil (region of secondary structure that is neither α-helix, β-strands nor turns). Figures 3.24 and 3.25 show the change in the CD spectra of AcL1 at increasing temperatures in the presence and absence of Ca^{2+}. Although the change was relatively small, probably due to appreciable amounts of random coil in the native structure, a change was observed at higher temperatures.
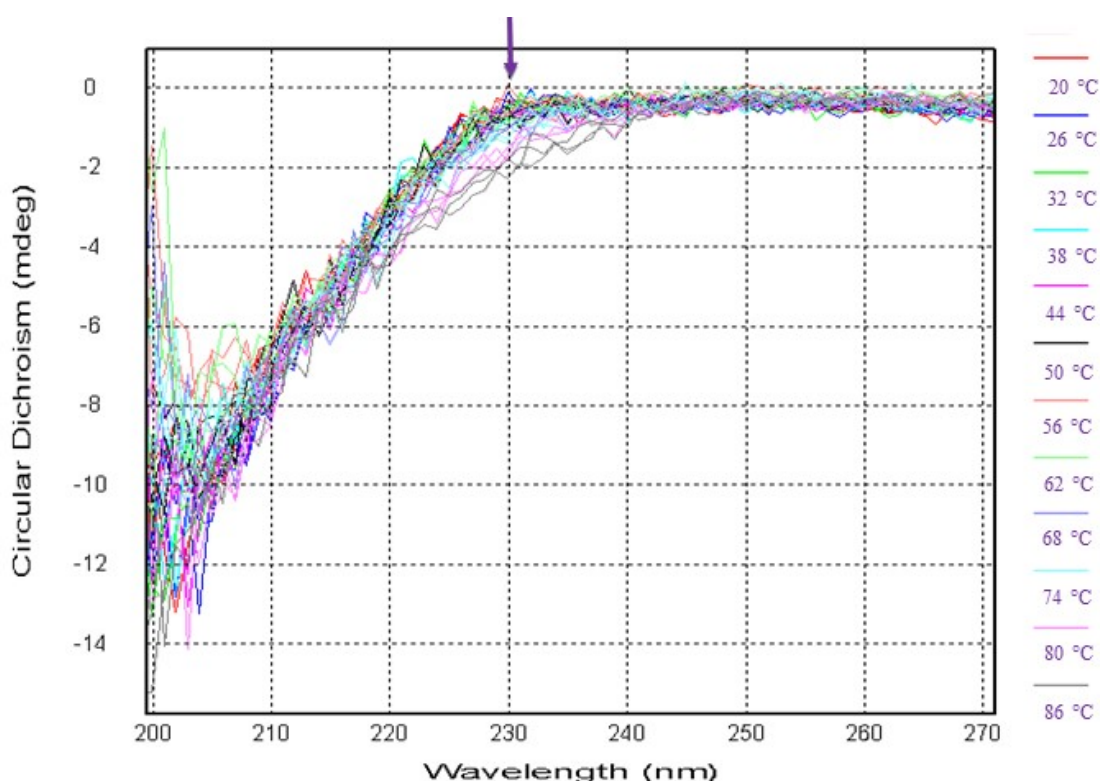
Figure 3-24: Thermo-unfolding of AcL1 measured by CD in the absence of Ca^{2+}. Far UV CD spectra of AcL1 were collected at 0.334 mg/ml AcL1 buffered in 10 Mm TRIS pH 7.4 in the absence of 2mM Ca^{2+} and analysed in 1 mm cell path-length applied Photophysics Chirascan™. At 221 nm wavelength (arrowed), thermo-unfolding across 20 - 86 °C was further studied.
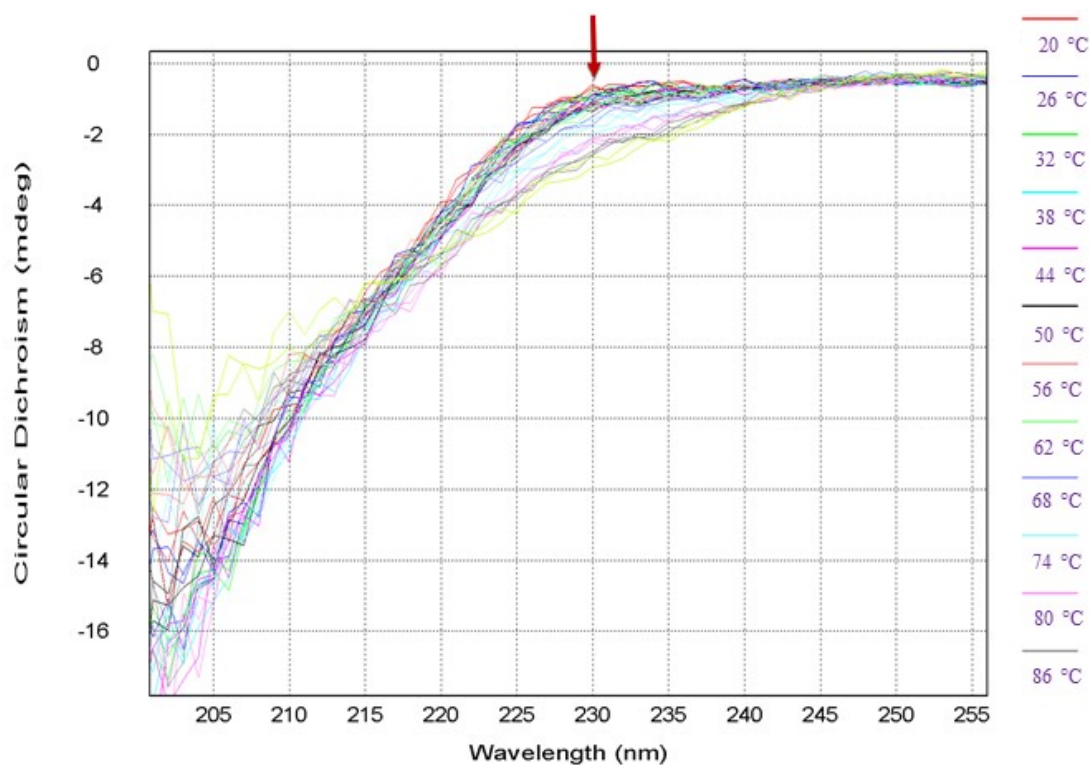
Figure 3-25: Thermo-unfolding of AcL1 measured by CD in the presence of Ca²⁺.
Far UV CD spectra of AcL1 were collected at 0.4 mg/ml AcL1 buffered in 10 Mm TRIS pH 7.4 in the presence of 2mM Ca^{2+} and analysed in 1 mm cell path-length applied Photophysics Chirascan™. At 221 nm wavelength (arrowed), thermo-unfolding across 20 - 86 °C was further studied.
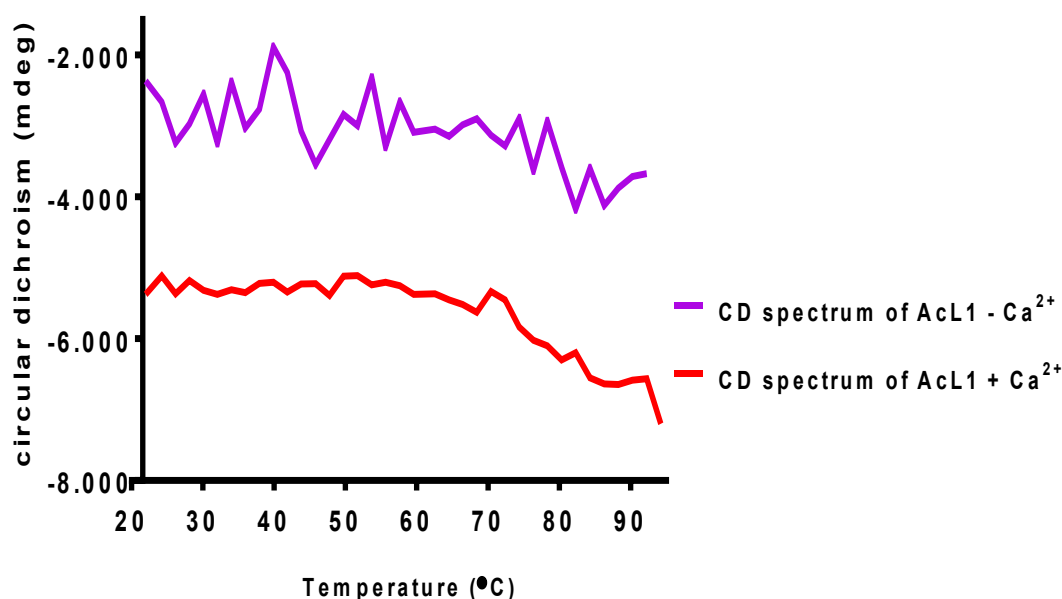
Figure 3-26: Unfolding of AcL1 measured by CD in the presence and absence of Ca^{2+}. Far UV CD spectra of AcL1 (0.4 mg/ml and 0.334 mg/ml in the presence and absence of 2mM Ca^{2+} respectively) from data at a wavelength of 230 nM (Figures 3.24 and 3.25 above) were plotted against temperature. The presence of Ca^{2+} show structural stability of AcL1 between temperature ranges of 20 – 65 °C in CD spectrum (-5500 to -5000 mdeg. AcL1 was thermo-unstable and characterised by high signal/noise ratio in the absence of Ca^{2+} at CD spectrum (-3000 to -2000) between temperature range of 20 – 72 °C. The high signal/noise ratio are correctable by either increasing intensity of incident polarised monochromatic light; increased quantum efficiency of the detector; collection of more data for average value.

Although the data were relatively noisy, plotting the CD value at 230 nm against temperature revealed a clear thermal transition at >70 °C both in the presence and absence of Ca^{2+} (Fig 3.26). It was not possible to determine the denaturation temperature because the signal did not plateau at high temperature. Nevertheless, denaturation occur at high temperature >70 °C and there was no obvious difference in the presence and absence of Ca^{2+}, indicating that Ca^{2+} did not stabilise folding of AcL1 overall, but rather the difference observed in the resistance to proteolysis was a more local effect.

AcL1 is likely to be a multidomain protein and different domains could fold and unfold independently. It is unclear which region/domain of the protein is responsible for the unfolding transition observed for AcL1.

3.4.10 Ligand binding by AcL1

The data described here show that AcL1 binds to mannose-Sepharose. Previous data (Garate et al., 2005) indicate that it does not bind to N-acetyl glucosamine or galactose, however, little is known about binding to larger oligosaccharides or glycoproteins. A dot-blot assay was therefore established in which biotinylated AcL1 was incubated with serial dilution of different glycoproteins including thyroglobulin, mannan, conalbumin, ferritin, ovalbumin, invertase, IgG, IgM. Rabbit muscle aldolase and BSA, which are not glycosylated were used as controls. IgM, thyroglobulin, yeast invertase and mannan all contain high-mannose oligosaccharides. As expected, biotinylated AcL1 did not bind to BSA but binding was detected to rabbit muscle aldolase, an intracellular enzyme of glycolysis. Binding was also detected towards thyroglobulin, conalbumin, ferritin, ovalbumin, IgG and IgM. Surprisingly, AcL1 did not bind to mannan and bound only weakly to yeast invertase, both of which contain high-mannose oligosaccharides. To further explore binding and ELISA was developed in which glycoproteins were immobilised and incubated with increasing concentrations of biotinylated AcL1. As shown in Figure 3.27, binding was detected to different ligands and the order of binding was similar to that observed in the dot-blot experiment. Binding was detected in either the presence or absence of Ca^{2+} (Figures 3.27, 3.28, 3.29 & 3.30).

Binding was detected to several glycoproteins and was not dependent on Ca^{2+}. One possible explanation for these data is that there may be additional binding sites on AcL1 for carbohydrates that not dependent on Ca^{2+}. The results of the binding experiment must be interpreted with care, however, because binding was detected to aldolase, which is not glycosylated. Thus, further analysis is required to be able to make firm conclusions on the binding properties of AcL1.
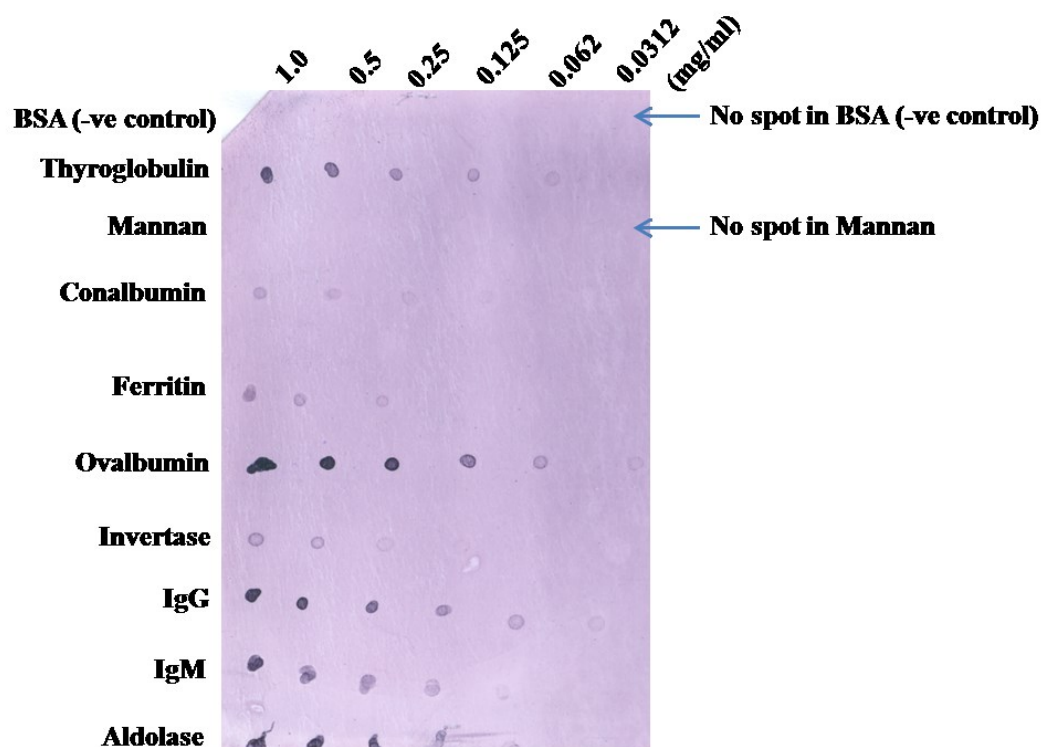
Figure 3-27: Dot-blot analysis of biotinylated AcL1 binding to immobilised proteins. Two-fold serial dilutions of glycoprotein (0.5 μl at a starting concentration of 1 mg/ml) were spotted onto a nitrocellulose membrane and allowed to dry for 30 minutes at room temperature. The membrane was blocked with 5% milk powder in 25mM Tris-HCl, pH 7.5 containing 150mM NaCl for two hours, washed with buffer + 0.5% Tween-20 and incubated with biotinylated AcL1 (0.06mg/ml) at room temperature for one hour. Afterwards, the membrane was incubated with streptavidin-ALP conjugate (2μg/ml) and developed with BCIP-NBT substrate (Sigma) and absorbance was measured at 405nm. All experiment was repeated at least thrice.
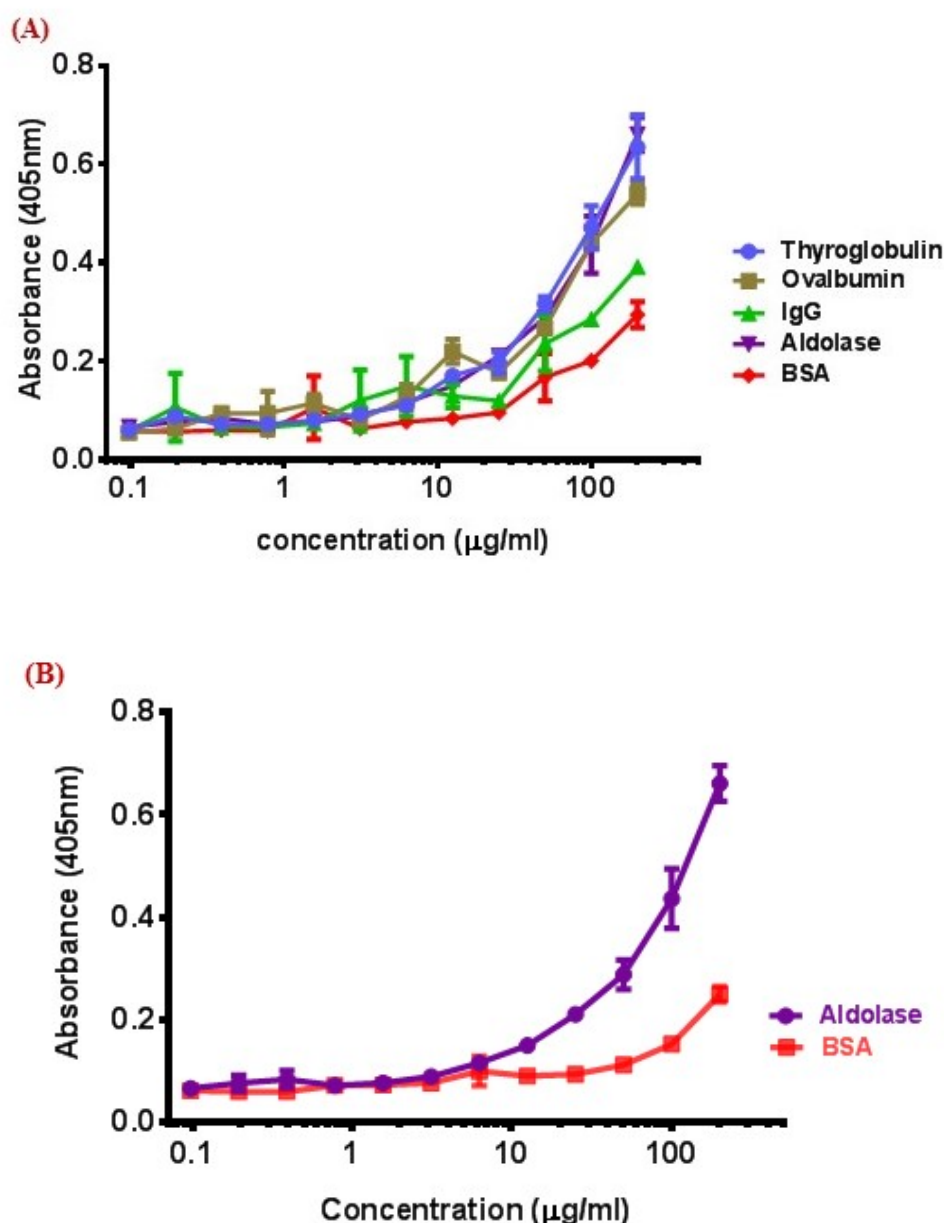
Figure 3-28: ELISA-binding assay of AcL1 with selected high mannose glycans: A 96 well ELISA plates was coated with 100 μl of 10μg/ml of Ovalbumin or BSA (control) in coating buffer (0·3 M NaHCO₃, 0·2 M Na₂CO₃ at pH 9·6) and incubated at 4°C overnight. Plates were washed three times using 200 μl PBS + 0.05 % tween 20. Afterwards, we blocked non-specific ligands with 200 μl/well of 1% BSA w/v in (PBS) and incubated at room temperature for one hr. Washed, then, I added 100 μl of biotinylated AcL1 (1.24mg/ml) in a 2-fold serial dilution, incubated at room temperature for 2-hour in-order to investigate increasing binding signal with the ligand. After repeated washing, binding of biotinylated AcL1 to ligand--ovalbumin was achieved and detection with 0.1μg/ml streptavidin was incubated for two hours. I repeated the wash step followed by the addition of 100 μl alkaline phosphatase substrate to each well and allowed to stand at room temperature for 15 min. The amount of biotinylated AcL1 bound

to Ovalbumin (or BSA) was confirmed by reading the absorbance at wavelength 405 nm.**(a)** Aldolase and thyroglobulin elicit pronounced binding effect on AcL1 (0.2mg/ml) from the selected high mannose glycans in the previous dot blot assay. **(b)** Aldolase was chosen for titration against BSA to determine the most appropriate glycan concentration required for subsequent ELISA-based binding assay and Competitive (inhibitory) ELISA assays thereafter.
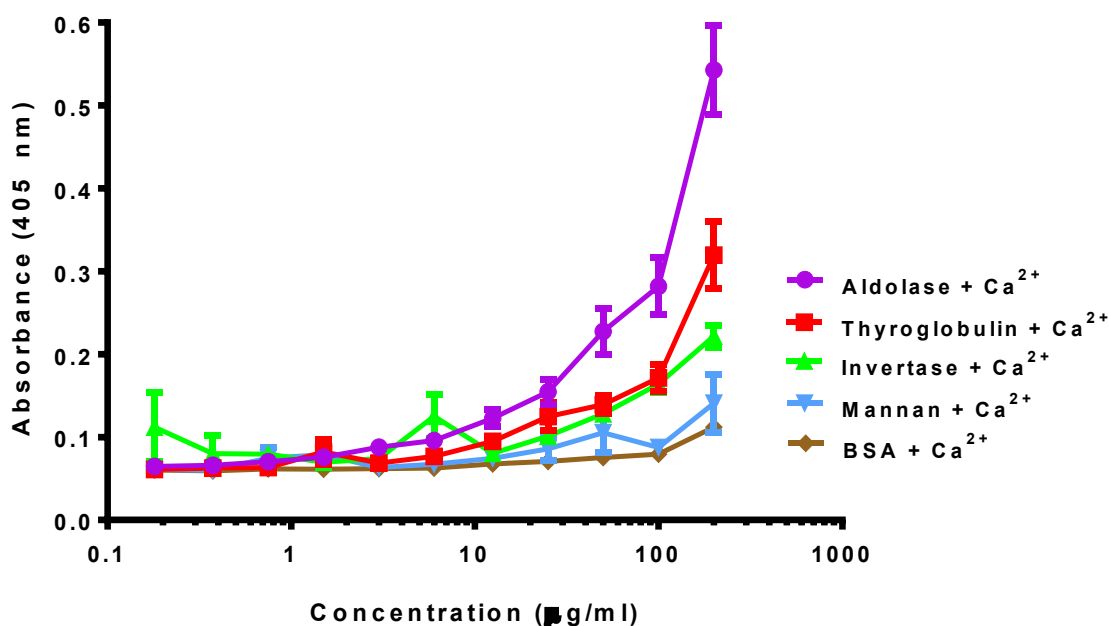
Figure 3-29: ELISA showing biotinylated AcL1 binding to different proteins in the presence of Ca^{2+}. Wells of a 96 well ELISA plate were coated with 100 μl of 10μg/ml of different proteins in coating buffer (0·3 M NaHCO$_3$, 0·2 M Na$_2$CO$_3$ at pH 9·6) and incubated at 4°C overnight. Plates were washed three times using 200 μl PBS + 0.05 % tween 20 and blocked with 200 μl/well of 1% w/v BSA in (PBS) and incubated at room temperature for one hr. Purified 100 μl of biotinylated AcL1 (1.24 mg/ml) in a 2-fold serial dilutions, were added and incubated at room temperature for 2-hour. After washing followed alkaline phosphatase substrate (100 μl) was added to each well and allowed to stand at room temperature for 15 min. The amount of biotinylated AcL1 bound was measured by reading the absorbance at 405 nm. The data was recorded in triplicate and the error is the SEM. Graph pad Prism 7 software was used to make the figures.
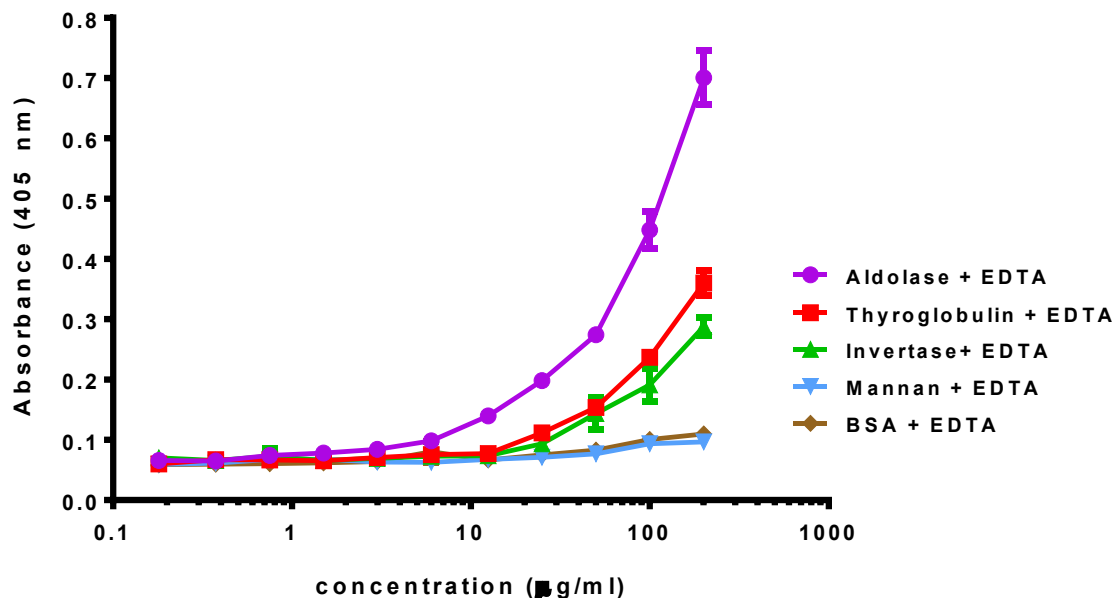
Figure 3-30: ELISA showing biotinylated AcL1 binding to different proteins in the presence of EDTA. A 96 well ELISA plates was coated with 100 μl of 10μg/ml of Aldolase or BSA (control BSA) in coating buffer (0·3 M NaHCO3, 0·2 M Na2CO3 at pH 9·6) and incubated at 4°C overnight. Plates were washed three times using 200 μl PBS + 0.05 % tween 20. Afterwards, we blocked non-specific ligands with 200 μl/well of 1% w/v BSA in (PBS) and incubated at room temperature for one hr. Then, we added 100 μl of biotinylated AcL1 (1.24 mg/ml) in a 2-fold serial dilution, incubated at room temperature for 2-hour in-order to investigate increasing binding signal with the ligand as previously described. AcL1 (0.2mg/ml) elicit a more pronounced binding effect on Aldolase more than thyroglobulin both in the absence of calcium (i.e presence of EDTA); and least is Mannan and BSA (Control). Absorbance was determined at 405 nm. The data was recorded in quadruplate and the error is the SEM. Graph pad Prism 7 software was used to make the figures.
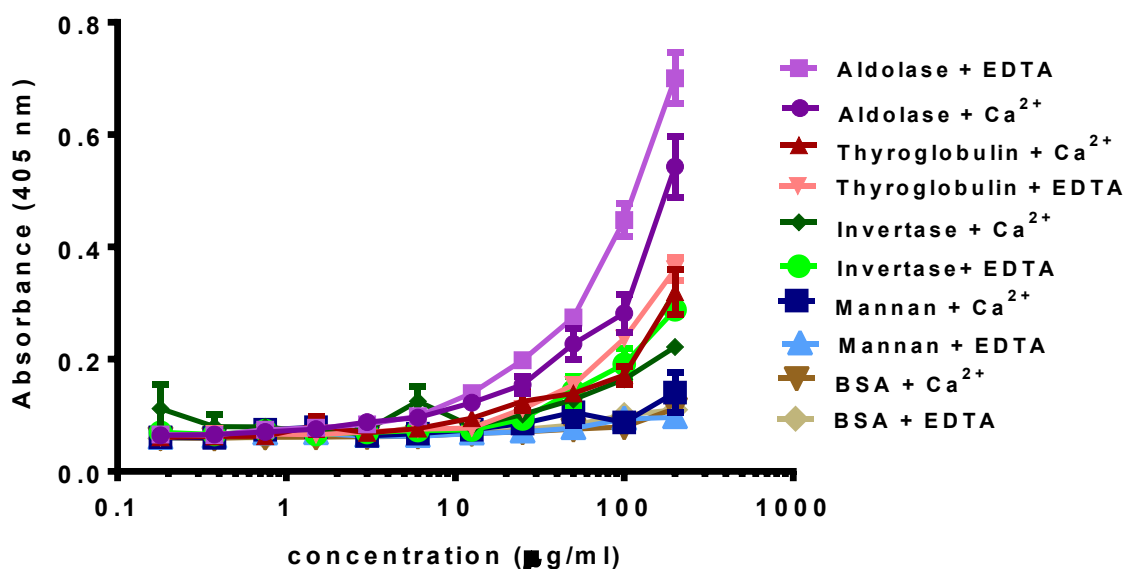
Figure 3-31: Comparison of binding of biotinylated AcL1 to proteins in the presence and absence of Ca^{2+}. A 96 well ELISA plates was coated with 100 μl of 10μg/ml of Aldolase or BSA (control BSA) in coating buffer (0·3 M NaHCO$_3$, 0·2 M Na$_2$CO$_3$ at pH 9·6) and incubated at 4°C overnight. Plates were washed three times using 200 μl PBS + 0.05 % tween 20. Afterwards, we blocked non-specific ligands with 200 μl/well of 1% w/v BSA in (PBS) and incubated at room temperature for one hr. Then, we added 100 μl of biotinylated AcL1 (1.24mg/ml) in a 2-fold serial dilution, incubated at room temperature for 2-hour in-order to investigate increasing binding signal with the ligand as previously described. AcL1 (0.2mg/ml) elicit a more pronounced binding effect on Aldolase more than thyroglobulin both in the absence of calcium (i.e presence of EDTA); and least is Mannan and BSA (Control). There was a comparatively mild binding effect in the absence of Ca^{2+} relative to the reduced binding effect in the presence of Ca^{2+}. Aldolase may possess both Ca^{2+}-dependent and other functional binding site(s)/affinity for AcL1 according to its highest binding signal over the period of exposure in the presence and absence of EDTA. Absorbance was determined at 405 nm. The data was recorded in quadruplate and the error is the SEM. Graph pad Prism 7 software was used to make the figures.

3.4.11 Crystallisation trials for AcL1

In order to try to crystallise AcL1 for structural analysis, purified protein was concentrated to ~7.55 mg/ml. Varieties of commercial screens were used including JSGC, PACT, Proplex, Morpheus and Midas (Molecular Dimensions). Using a sitting

drop method, the commercial crystallisation screens were set up by mixing 0.1 µl reservoir buffer with 0.1 µl of purified AcL1 on MRC crystallisation plates using a Mosquito NanoDrop crystallisation robot. Separate screens were tested at either room temperature or 4°C while screens were examined daily for possible crystals formation after at least one week of onset of the experiment. Unfortunately, no crystals grew under any of the conditions tested. I also set up screens using AcL1 previously deglycosylated using PNGaseF, but without success.

3.4.11.1 Crystallisation theory and X-ray diffraction

Crystallisation entails either natural or artificial methods of precipitating solid crystals from aqueous protein solution that is brought into supersaturation. To obtain protein crystals, there is the need (i) to identify the crystallisation conditions, which are dependent on the chemical, physical, and biochemical conditions; and (ii) optimise the crystal conditions by incremental modification of the initial conditions for high-quality crystals required for quality diffraction analysis (McPherson and Cudney, 2014). In addition, the protein must be concentrated and/or reduced its solubility to be considered 'supersaturated' while precipitants are used to cause the protein to nucleate and grow. Nucleation is a process whereby solute molecules are dispersed in the solvent to initiate the gathering of clusters. The growth of large well-organized crystals is essentially dependent on its ability to reach a 'metastable zone', whereby the best possible conditions are established. Nonetheless, crystallisation and precipitation are two competing processes that may decrease the protein concentration in the supersaturated state (Figure 3.32).

With increasing concentrations of either protein or precipitants, the protein moves to the supersaturation and precipitation zones. At optimal conditions, a single nucleation centre will form around which crystals will grow as more protein attaches onto the surface. Even, more growth will be observed at concentrations above the lower precipitation limit. However, neither nucleation nor protein crystals will form at concentrations below the nucleation curve (Russo Krauss et al., 2013). Upon successful protein crystallisation, the 3D structural characteristics of the protein are usually determined by X-ray diffraction (Elias et al., 2007).
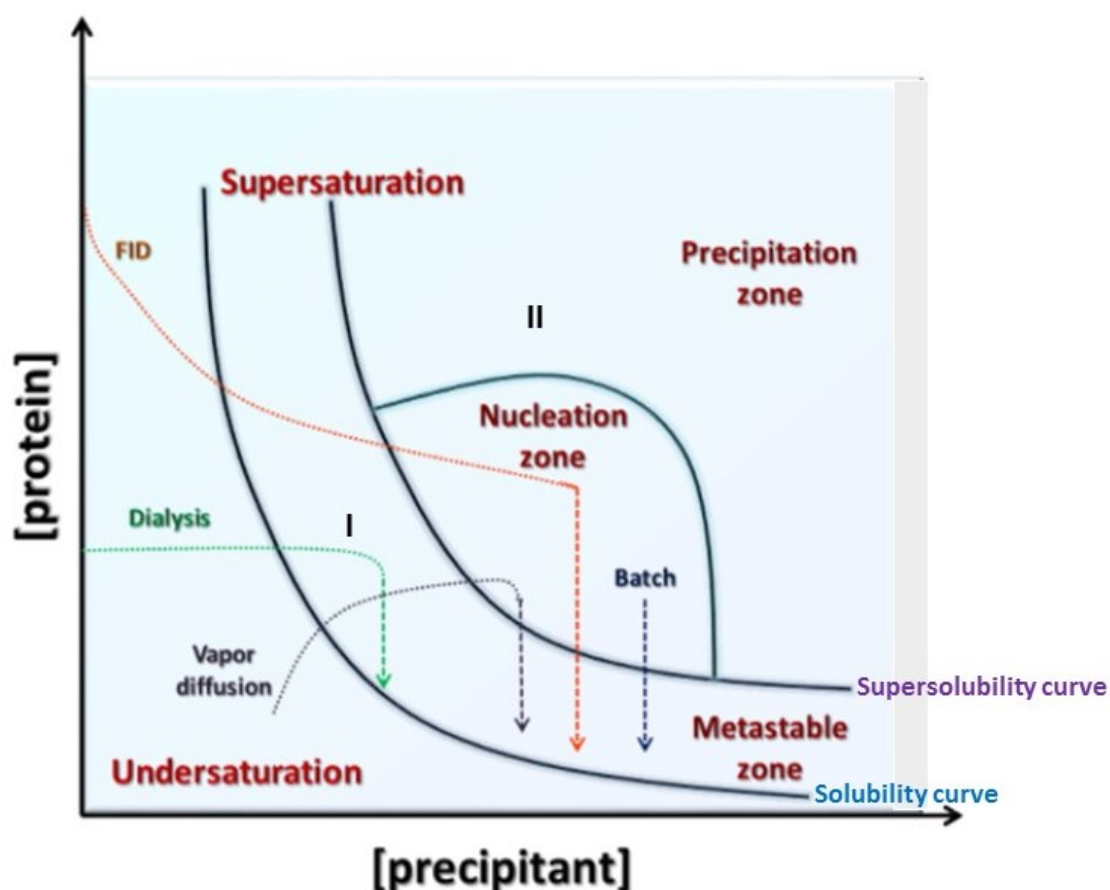
Figure 3-32: A schematic diagram of protein crystallisation phase. Crystals grow from 'supersaturated' aqueous protein solution. Crystallisation proceeds in two stages namely nucleation and growth. After nucleation, it grows into large well-ordered crystals under the best conditions characteristics of the 'metastable zone'. The adjustable parameters may include additive concentration or precipitant, pH and temperature. Four different zones including precipitation, nucleation, metastable and understability conditions are produced according to the different degree of supersaturaytion conditions. Two competing processes namely: (I) crystallisation, (II) precipitation may decrease the protein concentration in the supersaturated state. Adapted from Krauss (Russo Krauss et al., 2013).

3.5 Conclusions

I purified crystallisation-grade AcL1 protein by using AKTA (GE Healthcare) with multiple chromatographic methods including affinity and size-exclusion chromatography; and checked the protein purity by SDS-PAGE. The overaching purpose of the spectroscopic techniques (mass spectrometry, circular dichroism, dynamic light scattering) and other complimentary methods adapted in this chapter were to obtain

comprehensive clues about the purity, stability and structure of extracellular AcL1. The work described in this Chapter confirm that AcMBP is a mannose-binding protein and show for the first time that mannose binding is Ca^{2+} dependent. Ca^{2+} is likely to stabilise the lectin domain and may interact with the mannose directly, as is observed in C-type lectins.

The extracellular region of AcMBP is asymmetrical and likely consists of an elongated neck region comprising the cysteine-rich domain with the lectin domains outermost from the membrane. The protein is heavily glycosylated with sugars both in the neck region and in the additional domains. The cysteine-rich domain is unlikely to have a α-helical or β-sheet structure given its unusual sequence. The rest of the protein is probably predominantly β-sheet with little α-helical secondary structure. As expected for an extracellular protein, the AcMBP is relatively thermostable, only losing secondary structure at temperatures >70 ºC.

In addition to binding mannose, AcMBP might bind other carbohydrates. However, additional studies are needed to exclude the possibility of non-specific binding.

4. Truncated fragments of extracellular *Acanthamoeba* MBP

4.1 Introduction and Objectives

In the previous chapter of this thesis, the structure and lectin activity of full length (wild type) extracellular AcMBP (known as AcL1) were investigated. Very little is known about the domain structure of AcMBP. The repeating sequence and localisation of cysteine-rich domain, proximal to the membrane suggest a stem-like structure, with a globular lectin domain(s) more distal to the membrane. The cysteine rich domain is likely to be stabilised by multiple disulphide bonds via the repeating CXCXC motifs. In this chapter, I have sought to determine the molecular characteristics of different functional domains of AcMBP to localise the lectin domain.

4.2 Materials and Methods

4.2.1 Materials

All the DNA restriction and modifying enzymes used for the cloning, expression and purification of AcMBP were procured from New England Biolabs. Minimum Essential Medium (MEM) & serum free medium (SFM); and protein molecular markers for SDS-polyacrylamide gel electrophoresis were from Life Technologies, U.K. Methotrexate was from Sigma, U.K. Plasmid pED4 was kindly provided by Professor Russell Wallis; pLEICS-01 vector provided by PNACL, University of Leicester.

4.2.2 Methods

4.2.2.1 Bacterial strain (*E. coli*), Plasmids and Growth conditions

The plasmids used for expression of bacterial clones for this study is shown in figure 4.6. All growth media was sterilised by autoclaving (at 121 °C for 15 mins) while antibiotics (ampicillin) were filter sterilised (syringe filter steriliser 0.22 μm, Merck Millipore) prior to use.

4.2.2.2 Expression of truncated Fragments of AcMBP in CHO cells

4.2.2.3 Production of globular domains (AcE5 & AcF5) of AcMBP

Two different fragments, called AcF5 (encoding 22 – 280) and AcE5 (residues 22 - 270), encompassing the region N-terminal to the cysteine-rich domain were expressed in CHO cells.
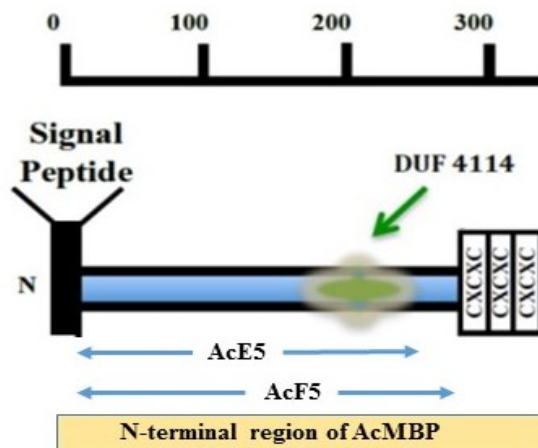
Figure 4-1: *Acanthamoeba* **gene highlighting at least three functional domains.** The N-terminal region showing of truncated globular AcE5, AcF5 (blue arrows), DUF 4114 (green arrow) and fragment of the C×C×C domain from the existing full length extracellular AcMBP. The arrows and schematic illustration of DUF 4114 are not shown to scale. AcF5 is 12 amino acid residues longer than AcE5 and contains an additional cysteine residue. AcE5 contains 9 cysteine residues and AcF5, 10 cysteines. The DUF4114 domain contains only one cysteine Fragments of AcE5 and AcF5 were produced in CHO cells and DUF 4114 were produced in *E. coli*.

The synthetic cDNA synthesised by Gene Art, (Life Technologies) and codon optimised for expression in Chinese hamster ovary cells (CHO) was used as a template. Constructs were synthesised with C-terminal hexahistadine tags to enable purification by affinity chromatography. AcF5 was slightly longer than AcE5 with an extra 12 amino acid residues because the position of the domain boundaries was not known.

4.2.2.3.1 Polymerase chain reactions (PCR) amplifications of AcE5 and AcF5

The cDNA fragments were amplified using PCR. Oligonucleotides and PCR conditions are shown in Tables 4.1 – 4.4. The PCR products were purified using the ECNA gel extraction kit, and cloned into the Sal1 restriction sites of the mammalian expression vector pED4 expression vector by homologous recombinantion as earlier described for AcL1 in Chapter 3.

Table 4-1: Sequence of oligonucleotides used for site-directed mutagenesis and cloning of globular truncated fragments AcE5 and AcF5

AcMBP	Oligonucleotides (5' → 3')	Primer codes
AcE5 (wild-type)	aggtccaactgcagg**gccacc**<u>atg</u> (24) **(FP)**	MBPF
	tccccgggtc<u>**tag**</u>agttcagtggtgatgatggtggtgggtggtcacggtagcgcagggcagc (62) **(RP)**	TMBPmidiR1
AcF5 (wild-type)	aggtccaactgcagg**gccacc**<u>atg</u> (24) **(FP)**	MBPF
	tccccgggtc<u>**tag**</u>agttcagtggtgatgatggtggtgcttggaggagtcgaaggtctgcttg (62) **(RP)**	TMBPmidiR2
Start and stop codons are represented in green and underlined; Kosak sequences (orange) were included prior to the start codon to enhance the initiation of translation. FP—forward primer and RP—reverse primer.		

The PCR amplification of either AcE5 or AcF5 DNA was performed in a 24-well PCR thermocycler. The PCR mixtures were prepared with ~50 ng of AcMBP DNA with 5 µl 10x reaction buffers, 1.5 µl of $MgSO_4$ (1 mM), 2 µl of dNTPs (0.3 mM), 1 µl of each forward and reverse primer (0.3 mM). Other components of the PCR mix included 5 µl of Enhancer, and 0.5 µl of polymerase (Platinum Pfx DNA (1 U)). The mixture was made up to a total volume of 50 µl with nH_2O. Thermal cycling conditions were varied according to the oligonucleotides used. A typical cycle comprised of an initial DNA denaturing phase at 94 °C for 60 seconds, primer annealing at 65 °C for 45 seconds, followed by extension at 72 °C for 1.5 min. The extension time was dependent on the size of the product (Sambrook et al., 1989). After 30 cycles, there was a final extension phase at 72 °C for 10 minutes. The reaction was maintained at a soak temperature held at 4 °C.

Table 4-2: PCR mix and conditions

	µl
DNA (10 nmol)	0.5
MgSO$_4$ (1 mM)	1.5
Buffer (1.5 x)	5.0
Enhancer (10 x)	5.0
dNTPs (0.3 mM)	2.0
Primers (F) (0.3 mM)	1.0
Primers (R) (0.3 mM)	1.0
Polymerase (Platinum Pfx DNA) (1 U)	0.5
H$_2$O	33.5
Total volume	**50.0**
The above volume are for a single reaction. Note: 1x = final concentrations of PCR mix relative to the concentration (1 U) of the Pfx DNA polymerase.	

Table 4-3: Typical Polymerase Chain reaction (PCR) conditions

PCR conditions	Temperature (°C)	Time (mins/secs)
Pre-denature	94	5 mins
Denature	94	1 min
Annealing	65	45 secs
Extension	72	1 min 30 secs
Final extension/delay	72	5 mins
Soak temperature	4	∞
No of cycles (Denature, Annealing & Extension) = 30 cycles		

4.2.2.3.2 DNA analysis by Agarose gel Electrophoresis

DNA fragments were isolated by agarose gel electrophoresis. A 1 % agarose-gel was prepared by dissolving 1.2 g of low-melting point agarose in 120 ml of 1× TBE buffer by heating the mixture in a microwave for about 5 mins. Next, 12 µl of DNA safe stain dye was added to the gel mix, and the mixture was cooled to 45°C and poured into a gel cassette with a comb. Then, 10 µl of 6 x blue DNA loading dye (Thermo-Fisher

Scientific) was added to each 50μl PCR DNA sample. Samples were loaded alongside a DNA marker, and the DNA was separated using 90 V and 400 mA for 1 hour. The gel was visualised using a UV trans-illuminator (305 - 327 nm) and the DNA bands were excised with a sharp scalpel blade. Slices of gel containing the DNA fragments were transferred into labelled Eppendorf tube for purification.

4.2.2.3.3 DNA purification from agarose gels

Extracted DNA was purified using the E.Z.N.A. gel extraction kit using the protocol provided. I measured the DNA concentration by using a Nanodrop spectrophotometer at 260 nm. The A_{260}/A_{280} ratio was used to gauge the purity of the DNA, a ratio of ~1.8 reflecting pure DNA.

4.2.2.3.4 Restriction enzyme digestion of vectors & Ligation of DNA into cloning vectors

Bulk restriction digestion of plasmid DNA (e.g. pED4) was carried out in a 0.5 ml Eppendorf by mixing ~30 μl of pED4 DNA, 13 μl of Smart Cut Buffer (NEB), 2.5 μl *Sal*I high fidelity and H_2O to a final volume of 200 μl. The mixture was incubated at 37 °C for 3 hours. Thereafter, samples were separated by gel electrophoresis. PCR products were introduced into SalI restriction site within the polylinker of pED4 by homologous recombination using the GeneArt® Seamless Cloning Kit.

4.2.2.3.5 Production of competent *E. coli* cells

Competent *E. coli* cells were prepared using the protocol developed by Promega, (U.K) using rubidium chloride for the production of cells with a transformation efficiency of > 1.5×10^7 cfu/μg of plasmid DNA. The detailed method as earlier described for AcL1 is in chapter 3 of this thesis.

4.2.2.3.6 Transformation of competent *E. coli* cells

The DNA samples of either AcE5 or AcF5 were mixed separately with 200 μl aliquots of competent cells. These were left on ice for 30 minutes, with occasional gentle mixing. Cells were then heat shocked at 42 °C for 45 seconds and transferred to ice for 2 minutes. 200 μl of LB was added and cells were left to recover in a 250 rpm shaking incubator at 37 °C for 1 hour. A 200 μl of the transformation mix was spread on LB agar plates containing 100 μg/ml of ampicillin. All plates were incubated overnight at 37 °C. Next day, single distinct colonies were picked and then grown in Luria broth that was already

supplemented with ampicillin (100 μg/ml); in a LB culture in a 200-rpm shaking incubator at 37 °C.

4.2.2.3.7 Plasmid preparations

Plasmids were purified using Qiagen® plasmid mini or midi-prep kits (QIAGEN Ltd) based on the alkaline-lysis technique using the protocol provided as described earlier for AcL1. The AcE5 or AcF5 plasmids were resuspended in H_2O and quantified using a Nanodrop spectrometer as described above.

4.2.2.3.8 Sequencing and analysis of sequence

All new clones were sequenced by the Protein Nuclear Acid Chemistry Laboratory (PNACL, University of Leicester, U.K.). The sequence data were viewed using Chromas software (http://en.bio-soft.net/dna/chromas.html).

4.2.2.3.9 Generation of stable mammalian (CHO) cell lines for transfection

DXB11 CHO cells were transfected with pED4 clones to produce AcE5 and AcF5 as described in Chapter 3. Expression was optimised by including increasing concentration of methotrexate into the growth media up to 0.5 μM.

4.2.2.3.10 Production and purification of AcE5 or AcF5

AcE5 or AcF5 were produced according to the methods described in Chapter 3 of this thesis. For large scale purification, cells were grown 500 cm^2 tissue culture flasks with 75 ml of MEM α⁻ supplemented with 10 % (v/v) DHFCS, with penicillin/streptomycin and 0.5 μM methotrexate. When the cells reached confluence, the spent media was replaced with 100 ml of CHO serum-free II medium supplemented with 50 mM HEPES buffer, pH 7.55 with penicillin/streptomycin and 0.5 μM methotrexate. Media was harvested and replaced every other day for 5 harvests, centrifuged at 3000 × g for 5 minutes, to remove any available cell debris; and stored at -20 ºC for purification.

AcE5 or AcF5 proteins were purified by affinity chromatography on a nickel-Sepharose column as described for AcL1. Aliquots of protein fractions were run on a 15% SDS-PAGE gel and were stained with Coomassie blue.

4.2.2.3.11 Gel filtration chromatography

AcE5 and AcF5 were further purified by gel filtration chromatography on AKTA Superdex 75 HiLoad column (10mm × 300 mm, GE Healthcare) equilibrated in 25mM

Tris-HCl, pH 7.5, containing 150mM NaCl and 1mM EDTA at a flow rate of 0.5 ml/min at room temperature. Superdex is made from dextran covalently linked to agarose. Fractions were collected across the elution profile. Samples were checked by gel electrophoresis on 15% (w/v) SDS-PAGE followed by Coomassie blue staining and gel scanning to confirm the purity of the purified protein. Protein was stored at -80 °C until use.

4.2.2.4 Production of the Ac-DUF 4114 domain of AcMBP

The Ac-DUF 4114 domain comprises 73 amino acids (residues 178 - 250). I attempted to express this domain in *E. coli* to characterise its functional and structural properties (Table 4.4).

Table 4-4: Sequence of oligonucleotides used for site-directed mutagenesis and cloning of AcDUF

AcMBP	Oligonucleotides	Primer codes
AcDUF	TACTTCCAATCCATGggccctttcagctctacccaggccg (FP)	TMBPF
	TATCCACCTTTACTGTCAgttgctggtcacgctgaacacgttg (RP)	TMBPRev

The start codon is in red. FP—forward primer and RP—reverse primer.

The fragment encoding AcDUF was amplified by PCR as described above and cloned into the bacterial expression plasmid pLEICS-01 (Figure 4.2).
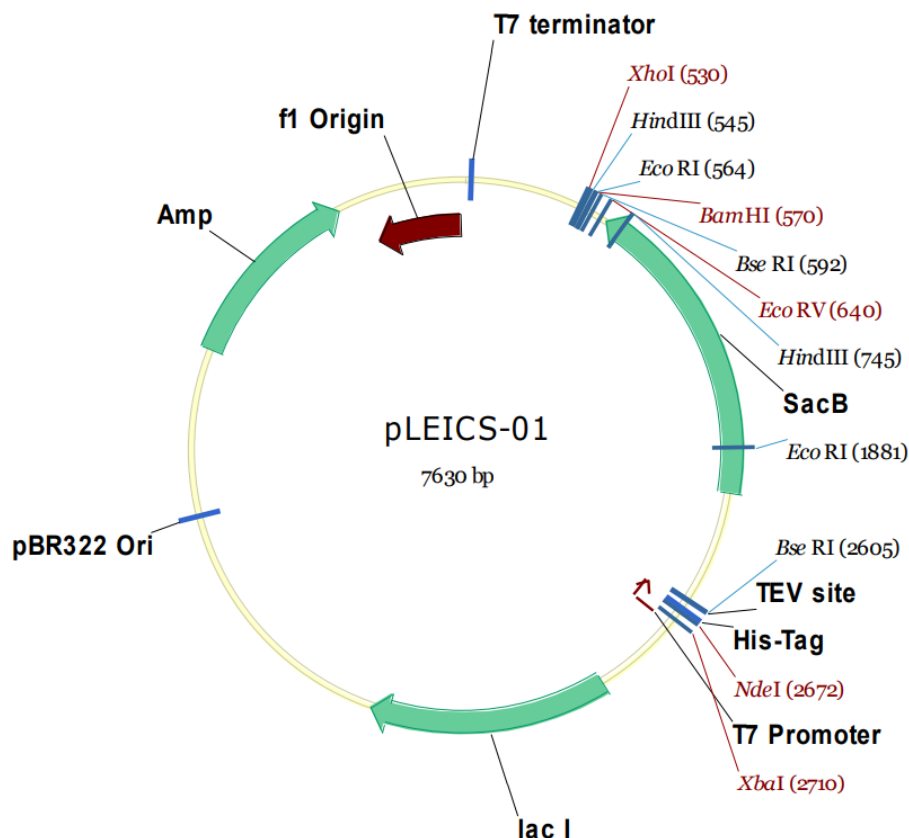
Figure 4-2: Circular map of *E. coli* plasmid vector named pLEICS-01. A 7630 bp vector that express T7 RNA polymerase, contains the ampicillin-resistance gene and encodes an N-terminal affinity tag followed by a TEV cleavage site: N-HIS$_6$-SSGVDLGT-TEV site 1.

The pLEICS-01 contains a cloning site for the DNA insert, a T7 promoter, an origin of replication for replication of the plasmid within the host cell; and selectable antibiotic resistant gene marker (Amp^r) for identification of positive clones. Cloning was carried out by homologous recombination (incorporation of foreign coding sequence into the plasmid vector) by Protein Expression Laboratory (PROTEX), at University of Leicester. Positive clones were sequenced to ensure that no additional mutations were introduced.

4.2.2.4.1 Small scale expression of Ac-DUF 4114 domain of AcMBP

The recombinant DNA encoding the Ac-DUF 4114 domain of AcMBP (herein referred as either AcDUF or AcDUFCS) was transformed into BL21 (DE3) competent cells. I inoculated a single colony of transformed cells into 10 ml of LB containing 100 mg/ml

of ampicillin and incubated at 37 °C until an OD_{550} of 0.6 – 0.8 was attained. Then, the culture was induced with IPTG (1 mM final concentration). After 3 hours of incubation, the cells were centrifuged and washed with PBS. The pellets were resuspended in 100 µl Bugbuster and later incubated at room temperature for 15 minutes. The sample was further centrifuged while supernatant was collected for analysis. Next, the pellet was mixed with 100 µl PBS. Finally, the supernatant and the sample pellet were vanalysed on a 15% w/v SDS-PAGE to establish protein expression and purity.

4.2.2.4.2 Large scale expression of Ac-DUF 4114 domain of AcMBP

For production, the expression plasmid was transformed into *E. coli* BL21 (DE3), under T7 promoter. Cells were grown in 500 ml LB media containing 100 mg/ml ampicillin with shaking at 37ºC in LB medium. Protein expression was induced at OD_{550} of 0.6 – 0.8 with 1 mM IPTG. The cells were grown overnight and harvested by centrifugation at 5000 × g for 15 min. Cells were lysed and inclusion bodies were prepared using BugBuster by following the recommended protocol from BugBuster Protein Extraction Reagent kit.

4.2.2.4.3 Inclusion body preparation

The choice of BugBuster for preparing the inclusion body was based on its proprietary formulation, which utilizes a mixture of non-ionic detergents that are capable of cell wall perforation without denaturing the soluble protein. BugBuster is an enzymatic lysozyme treatment for a gentle distruption of the *E. coli* cell wall to release the expressed target insoluble protein for further purification and functional studies. The inclusion bodies were re-suspended in 1:10 diluted bug-buster at 10 ml/gm of original paste and mixed before centrifugation at 5000 × g for 15 minutes at 4°C to remove supernatant.

Approximately 10 ml aliquot of solubilising buffer at 5ml/gm original wet pellet sample into eppendorf tubes and micro-centrifuged at 14000 rpm for 10 minutes at 37°C, discarding supernatant. Suspended pellets samples were snap-frozen in liquid nitrogen and stored at -80°C. Aliquot samples were analysed by electrophoresis and 15% SDS-PAGE.

4.2.2.4.4 Inclusion body solubilisation and refolding of AcDUF

Inclusion bodies were solublised in 25mM TRIS at pH 7.5 containing 8 M Urea and 5mM Dithiothreitol (DDT) using freshly prepared DTT. To establish the best conditions for

refolding AcDUF, I screened each of the 15 different buffer components in QuickFold™ Protein Screening Kit by following the protocol provided. Briefly, solublised protein is diluted into 15 different refolding buffers (to give a final concentration of 0.1 mg/ml). Best conditions are identified by spinning the sample to remove any aggregated protein and running the samples on an SDS-PAGE gel. Buffer 9 [50mM TRIS, 9.6mM NaCl, 0.4mM KCl, 1mM EDTA, 0.5M arginine, 0.75M Guanidine HCL, 0.05% polyethylene glycol 3550, 1mM EDTA, 1mM DTT (prepared fresh) at pH 8.5] was found to give the most soluble protein.

For large-scale preparation, protein was refolded by drop dilution in refolding buffer 9 overnight at 4 ºC. Protein was then dialysed into 25mM TRIS at pH 7.4 containing 150mM NaCl, to remove residual EDTA and DTT. AcDUF was then purified by affinity chromatography on a 1 ml Nickel-Sepharose column followed by gel filtration on a Superdex 75 16/60 column in 50mM TRIS, 150mM NaCl and 2mM EDTA at pH 7.5.

4.2.2.5 Production of a mutant form of the extracellular regions of AcMBP called AcL1DD

Site directed mutagenesis was used to introduce two mutations into the extracellular region of AcMBP to disrupt the putative mannose-binding site: Asp-238 and Asp-241. Mutations were introduced using overlapping PCR using mutagenic primers shown in Table 4.5. In this process, the cDNA was synthesised in two overlapping fragments to introduce the mutation. These products were then combined and the complete cDNA containing the mutations was synthesised using the forward and reverse primers. The mutant cDNA was introduced into pED4 by homologous recombinantion and transfected into CHO DXB11 cells by Ca^{2+}-phosphate method.

Table 4-5: Sequence of oligonucleotides used for site-directed mutagenesis AcMBPmut (AcL1 DD) - the positions of the mutations are highlighted in blue.

AcMBP	Oligonucleotides	Primer codes
AcL1DD Full length (mutant)	5'—gaggactcccctgccggctccaactccgactacaacga—3' (FP)	AcMBPDADNF
	5'—tcgttgtagtcggagttggagccggcaggggagtcctc—3' (RP)	AcMBPDADNRev

4.3 Results

4.3.1 Production of truncated forms of AcMBP

The extracellular region of AcMBP consists of an N-terminal portion containing the DUF4114 domain followed by a cystein-rich domain containing multiple C×C×C motifs. The cystein-rich domain is closest to the cell membrane and probably forms a stem/stalk with the lectin domain or domains furthest from the cell.

To determine the properties of the N-terminal region, two fragments were produced in CHO cells called AcE5 and AcF5 (Figure 4.1). AcMBP contains multiple cysteine residues and the precise location of the domain boundaries is unclear (Fig 4.3). The two fragments (alignments) produced respresent different start positions of the cysteine-rich domain.

```
         CRNSKQTFDSSK
CTCSCPNPVTCTAPQVYSTDL
CACTCPNATQTCTAPLTWNSAT
CQCDCPSTKPSGVTCSNLQQWSNVVAT
CGCKCPDPATYTCSDNRFVLRTSD
CTCNCPSTGSCSGNLKWNSANSV
CGCQCPSTPPTPCSGNLKWNSTASK
CACECPATAALAGVTCKDKEVWDTAS
CSCKCPATASAADTTCPNVNYQWNYNGK
CDCVCPATSAEAGINCTALGLGNTVWDTTA
CNCACPPTGTCPGNKVWNPSNDPAK
CGCSCPASAPAGKECKGNFYWNTSDDV
CDCYCPLEAPADDPCIGYTTWNRTE
CDCYCPLEPPFEGGCPGVQVWDRDQ
CQCVCPDDDPC


CRNSKQTFDSSKCTCSCPNPVT
CTAPQVYSTDLCACTCPNATQT
CTAPLTWNSATCQCDCPSTKPSGVT
CSNLQQWSNVVATCGCKCPDPATYT
CSDNRFVLRTSDCTCNCPSTGS
CSGNLKWNSANSVCGCQCPSTPPTP
CSGNLKWNSTASKCACECPATAALAGVT
CKDKEVWDTASCSCKCPATASAADTT
CPNVNYQWNYNGKCDCVCPATSAEAGIN
CTALGLGNTVWDTTACNCACPPTGT
CPGNKVWNPSNDPAKCGCSCPASAPAGKE
CKGNFYWNTSDDVCDCYCPLEAPADDP
CIGYTTWNRTECDCYCPLEPPFEGG
CPGVQVWDRDQCQCVCPDDDP
CAAQSTA
```

Figure 4-3: The sequence of the cysteine-rich domain (residues 282-701) of AcMBP.
Constructs were designed based on the two different start positions of aligments of the cysteine-rich domain. The yellow highlights show a total of 57 cysteine residues comprising of 15 single cysteines and 14 CxCxC residues each next to proline residues (blue), amino acid known to form structural kinks. Other residues include aromatic amino acid such as tryptophan (green) and phenyl alanine (grey).

AcF5 is 12 amino acid residues longer than AcE5 and contains an additional cysteine residue. AcE5 contains 9 cysteine residues and AcF5, 10 cysteines. The DUF4114 domain contains only one cysteine.

```
        10         20         30         40         50         60
MYRMQLLSCI ALSLALVTNS GTCNLSGAIK QPGLDCSSTS CSITSGTFPF PLPQGETYDS

        70         80         90        100        110        120
FYSWILGVIG TDGATVNAQY VDYTKADPNI YFTAGQTNCM VNLTFVYEVA FYRNSMGYFT

       130        140        150        160        170        180
FTRDSKPTSV GSVTLKPVFS ETTVDCSRTS SQPLPGTSCL APGSTISLGP FSSTQAVGFY

       190        200        210        220        230        240
LKQDSICSGT TTFYSVDALN KVTSRWKPIP AAHGRMIAVL RDPNTLRAYL GFEDSPDGSD

       250                         260                         270
SDYNDNVFSV TSNCEIDTSL LPCATVTTHH HHHH
```

Figure 4-4: The amino acid sequence of AcE5. The signal peptide is in blue, the DUF4114 domain in yellow and the 6-Histag is in green. Cysteine residues are shaded in grey. The other residues in white (no colour) represent the remaining part of the N-terminal region of the truncated AcE5 protein (Theoretical pI/Mw: 4.56 / 26534.56).

```
        10         20         30         40         50         60
MYRMQLLSCI ALSLALVTNS GTCNLSGAIK QPGLDCSSTS CSITSGTFPF PLPQGETYDS

        70         80         90        100        110        120
FYSWILGVIG TDGATVNAQY VDYTKADPNI YFTAGQTNCM VNLTFVYEVA FYRNSMGYFT

       130        140        150        160        170        180
FTRDSKPTSV GSVTLKPVFS ETTVDCSRTS SQPLPGTSCL APGSTISLGP FSSTQAVGFY

       190        200        210        220        230        240
LKQDSICSGT TTFYSVDALN KVTSRWKPIP AAHGRMIAVL RDPNTLRAYL GFEDSPDGSD

       250                  260                  270                  280
SDYNDNVFSV TSNCEIDTSL LPCATVTTCR NSKQTFDSSK HHHHHH
```

Figure 4-5: The amino acid sequence of AcF5. The signal peptide is in blue, the DUF4114 domain in yellow and the 6-Histag is in green. Cysteine residues are shaded in grey. The other residues in white (no colour) represent the remaining part of the N-terminal region of the truncated AcF5 protein (Theoretical pI/Mw: 4.81 / 27917.08).

4.3.2 Cloning of the truncated N-terminal fragments of AcMBP

Fragments encoding AcE5 and AcF5, were amplified by PCR and were separated on a 1% agarose gel (Figure 4.6). The products was excised, purified, and then cloned into the *Sal*I restriction site of the mammalian expression vector pED4 by homologous recombination as previously described for the AcL1 above. The natural signal sequence was replaced by the signal sequence for interleukin 2 and a Kozak sequence (GCCACC) was introduced immediately 5' of the start codon. A C-terminal hexahistidine tag was added for purification as earlier described for the AcL1 (Figures 4.4 & 4.5).

Minipreps were prepared and clones containing the insert were identified by PCR (Figure 4.7). All the eight clones tested gave products of the expected size for the AcE5 and AcF5 cDNA (~ 800 bp). Two of these clones each from AcE5 and AcF5 were sequenced by PNACL (University of Leicester) to confirm that no mutations were induced by the PCR (Figure 4.8).
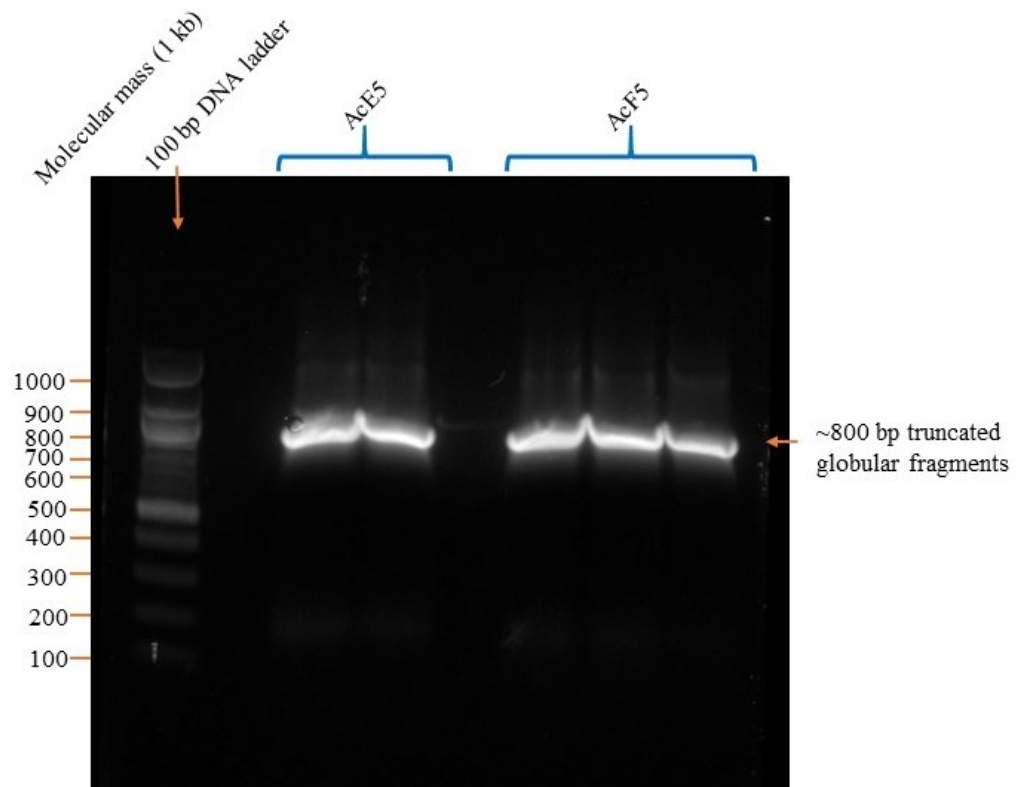
Figure 4-6: A 1% agarose gel showing PCR amplification of the cDNA fragments encoding AcE5 and AcF5. The first lane is 100 bp DNA ladder; lanes 3-4 are AcE5 and lanes 6-8 are AcF5. The amplified product was ~800 bp as expected.
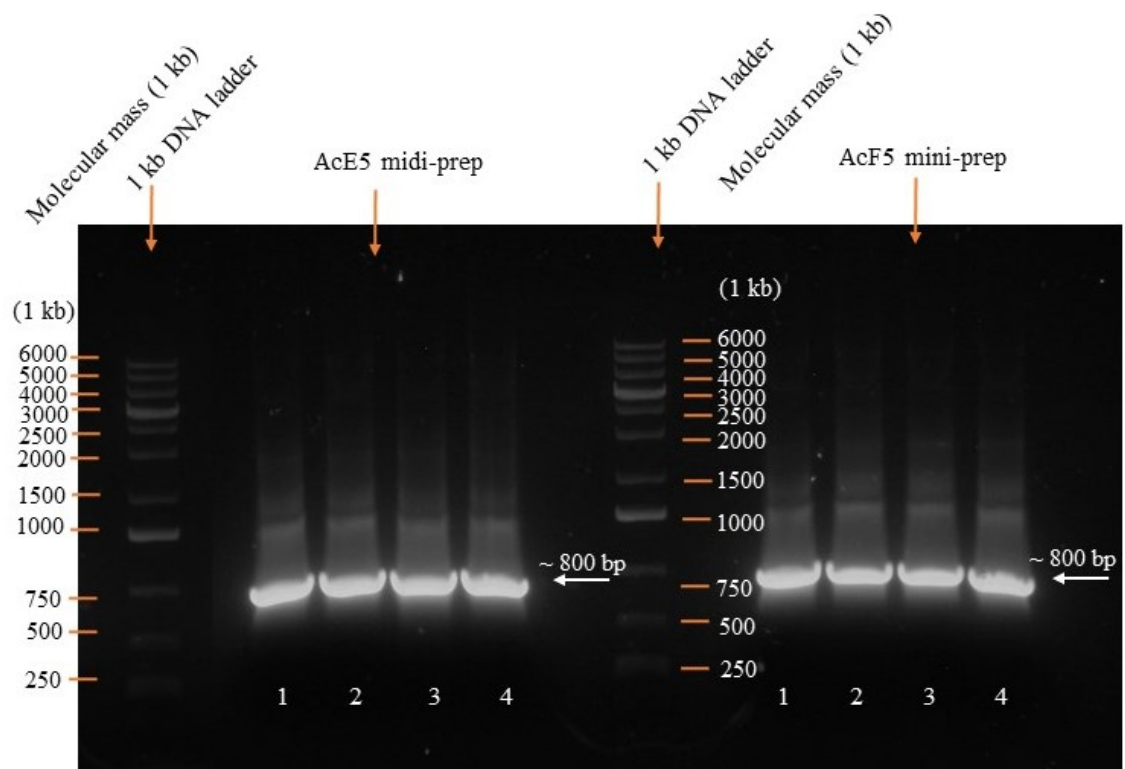
Figure 4-7: Test PCR of eight pED4 clones following recombination. A 1% agarose gel showing a pair of four mini-prep tested for the presence of the AcE5 and AcF5 cDNA by PCR respectively. The products of the expected size were detected in the eight clones.
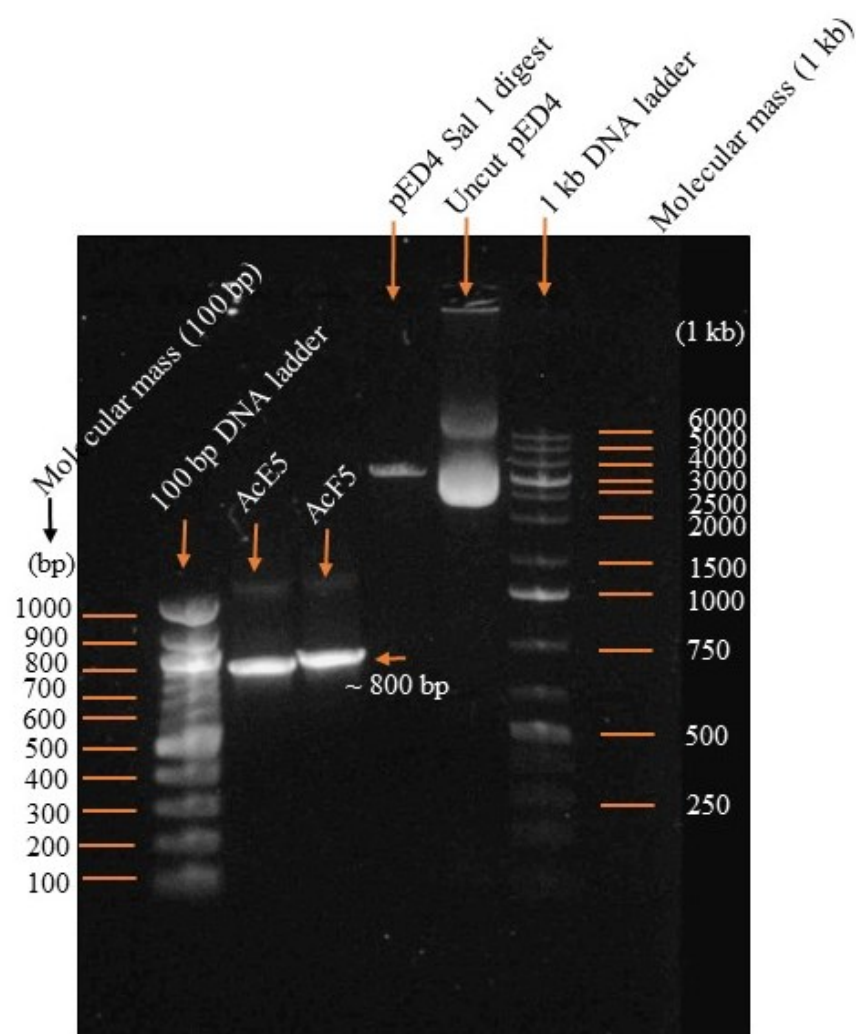
Figure 4-8: AcE5 and AcF5 PCR products. A 1% agarose showing AcE5, AcF5, plasmid pED4 Sal 1 digest and uncut pED4 PCR products. The first lane is 100 bp DNA ladder. AcE5 (lane 2) is slightly smaller than AcF5 (lane 3) due to the difference of 12 amino acid residues. Both amplified products of AcE5 and AcF5 were ~800 bp as expected. The plasmid DNA pED4 (30 µl) was bulk-digested with smart cut buffer (13 µl), Sal 1 (2.5 µl, high fidelity) and ddH2O (to a final volume of 200 µl) at 37 °C for 3 hrs to produce the pED4 Sal 1 digest (lane 4).The uncut pED4 vector (control, lane 5) was ~ 5.4 kb in size as expected. After digestion of recombinant AcE5 or AcF5, the right size of band was cut from the gel and purified. These were cloned into the digested pED4 vector. Ratio of vector to insert was approximately 3:1 to ensure that a small amount of vector will self-ligate. The last lane (lane 6) is the 1 kb DNA ladder for the confirmation of the molecular mass of the pED4 vector. Digests were loaded and run on 1 % agarose gel to check for the presence of insert and no self-ligated plasmid. Sequencing was the final verification step to establish that gene of interest was cloned. Gel was visualised using UV trans-illuminator (305-327 nm) instead of < 270 nm that damages DNA and compromises subsequent downstream experiments.

4.3.3 Protein purification and analysis of recombinant AcMBP

pED4 clones containing the two AcMBP fragments were transfected into CHO cells by the calcium phosphate method. Cells containing the plasmid were selected on media lacking nucleosides and production was increased over several months by passaging cells into increasing concentrations of methotrexate (an inhibitor of dihydrofolate reductase) up to a concentration of 0.5 µM. Protein was isolated from CHO cells in serum-free medium as described (Wallis and Drickamer, 1999). Media was harvested every other day for five (5) harvests.

Recombinant AcE5 and AcF5 was purified by affinity chromatography on nickel-Sepharose (Figure 4.9) followed by gel filtration chromatography on a Superdex 75 10/300 column (GE Healthcare). Yields of protein were very low with ~ 0.25 mg of pure AcF5 per L of culture medium and even lower yields for AcE5. For this reason, subsequent experiments were conducted with AcF5 (Figures 4.10 & 4.11).
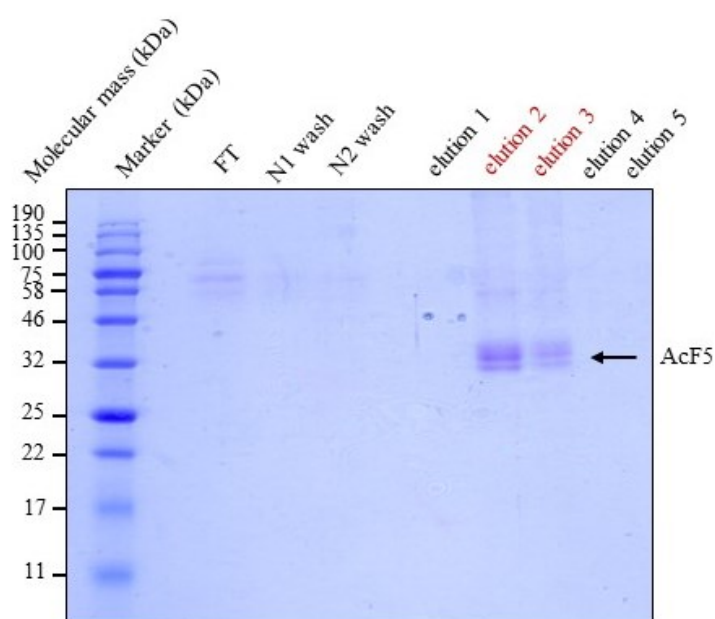
Figure 4-9: SDS-PAGE of AcF5 purified by affinity chromatography on a nickel-Sepharose column. Serum-free medium from AcF5-producing CHO cells was loaded onto the Nickel-Sepharose column. After 2 wash steps proteins were eluted using buffer containing 500 mM imidazole. The band corresponding to AcF5 is marked with an arrow. These triplet protein bands were sequenced by MALDI-TOF mass spectroscopy and confirmed expected protein identity with possible post translational modification. A 15% SDS gel stained with Coomassie blue. FT is the flow through. The apparent molecular mass was ~32 kDa.

(A)
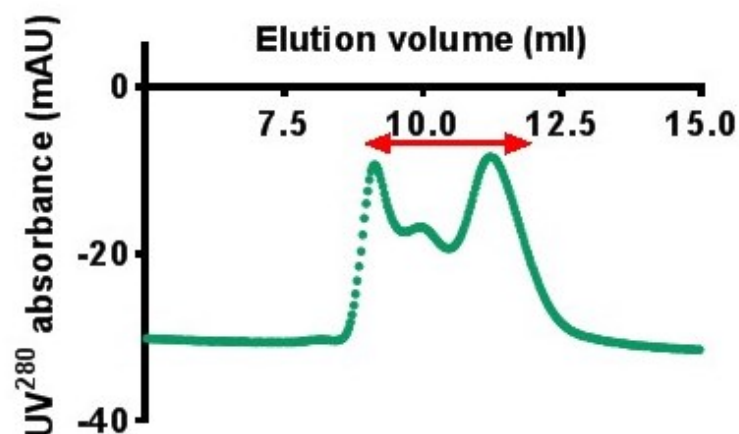
(B)
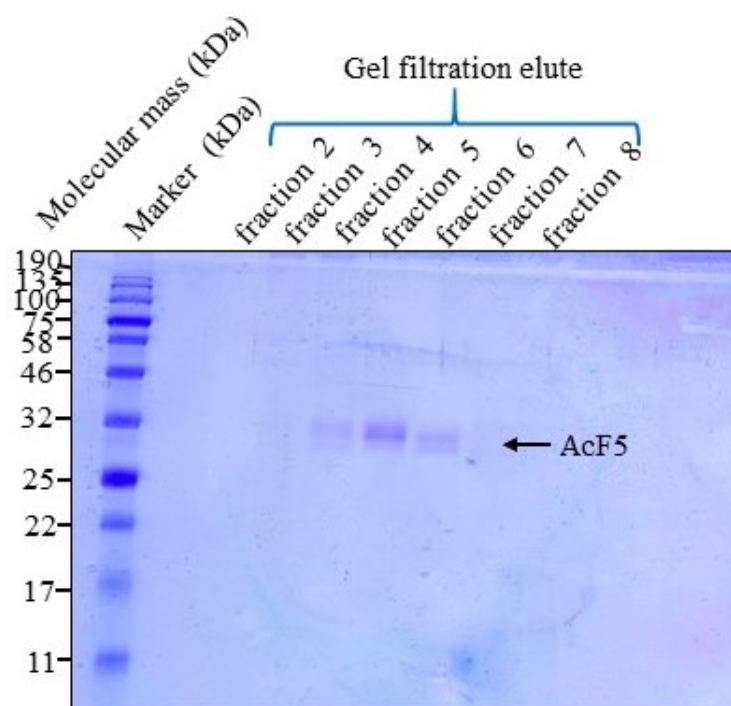
Figure 4-10: Purification of AcF5 by gel filtration chromatography. (A) Gel-filtration of AcF5 on a superdex 75 10/300 at a flow rate of 0.5 ml/min. Graph pad Prism 7 software was used to make the figure. **(B)** A 15% SDS-PAGE gel showing fractions collected across the gel filtration peak. The last peak to elute from the column was AcF5. The three protein bands in lanes 5 were sent for analysis using MALDI-TOF mass spectrometry. Ladder (L) = molecular weight standard, blue-prestained protein standard broad-range 11-190 kDa. Protein was stained with Coomassie blue. Ladder (L) = molecular weight standard, blue-pre-stained protein standard broad-range 11-190 kDa.

AcF5 migrated as triple bands with an apparent molecular mass of ~32 kDa on SDS-PAGE under both reducing and non-reducing conditions. The expected molecular mass was ~29 kDa, indicating that the protein is likely to be post-translationally modified. Recombinant AcF5 eluted from the gel filtration column with an apparent molecular mass of ~30 kDa indicating that it is monomeric under native conditions.
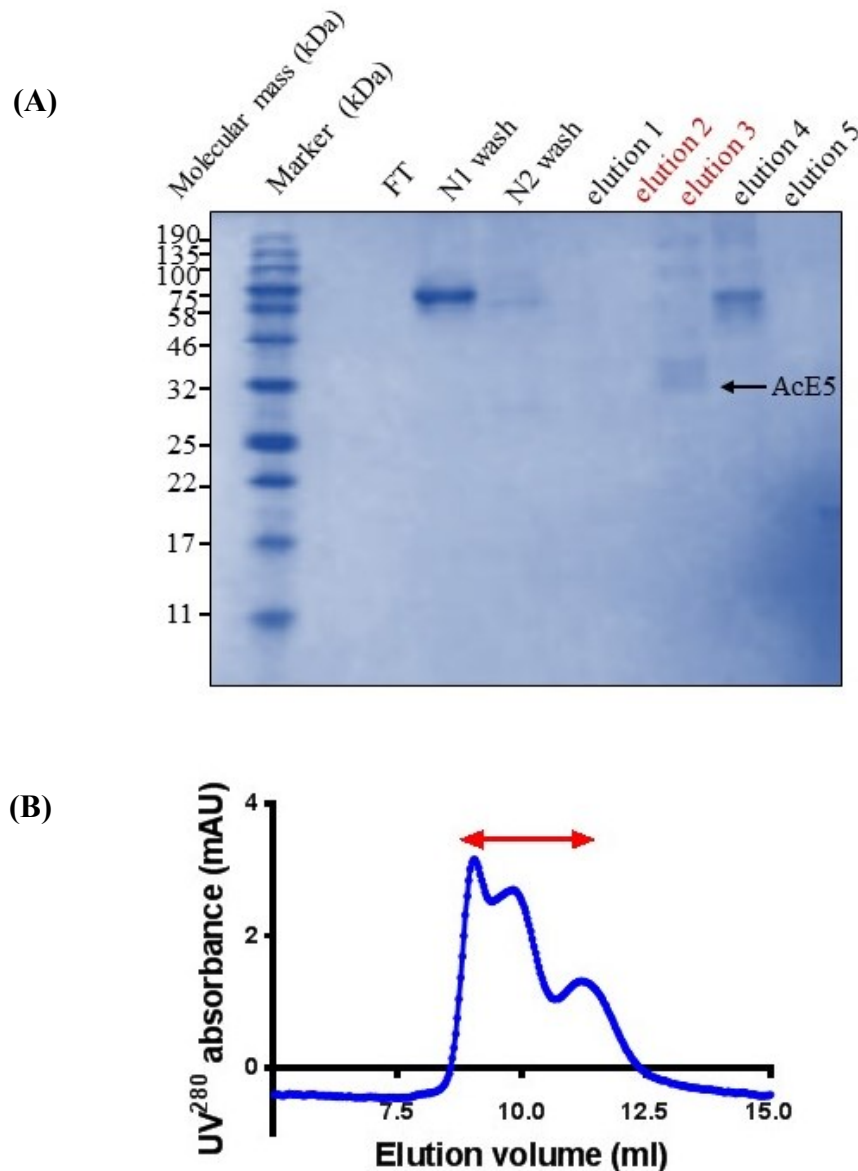
Figure 4-11: SDS-PAGE of AcE5 purified by affinity chromatography on a nickel-Sepharose column. (A): A 15% SDS gel stained with Coomassie blue. Medium from AcE5-producing CHO cells containing 10% foetal calf serum was loaded onto a Nickel-Sepharose column. After 2 wash steps proteins were eluted using buffer containing 500 mM imidazole. The band in elution fraction 3 corresponding to AcE5 (apparent molecular mass ~28 kDa) was marked with an arrow. The larger protein in elution 4 is likely to be

a contaminant. FT is the flow through. **(B):** Gel-filtration of AcE5 on a superdex 75 10/300 at a flow rate of 0.5 ml/min. Graph pad Prism 7 software was used to make the figures. (This experiment was carried out at least thrice).

4.3.3.1 Mass spectrometry of AcF5

To confirm the identity of AcF5, samples was excised from the SDS-PAGE gel, digested with trypsin and analysed by mass spectrometry (Figure 4.12). Peptides identified are shown in red.

(A)

```
  1 MYRMQLLSCI ALSLALVTNS GTCNLSGAIK QPGLDCSSTS CSITSGTFPF

 51 PLPQGETYDS FYSWILGVIG TDGATVNAQY VDYTKADPNI YFTAGQTNCM

101 VNLTFVYEVA FYRNSMGYFT FTRDSKPTSV GSVTLKPVFS ETTVDCSRTS

151 SQPLPGTSCL APGSTISLGP FSSTQAVGFY LKQDSICSGT TTFYSVDALN

201 KVTSRWKPIP AAHGRMIAVL RDPNTLRAYL GFEDSPDGSD SDYNDNVFSV

251 TSNCEIDTSL LPCATVTTCR NSKQTFDSSK HHHHHH
```

(B)
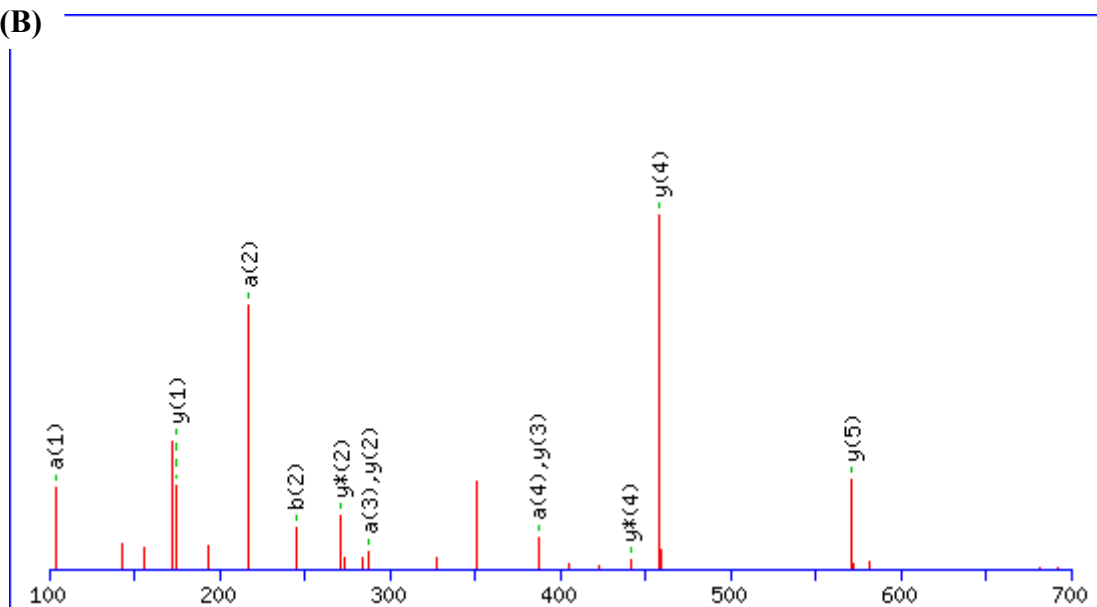
Figure 4-12: MALDI-TOF mass spectrometry of AcF5 following trypsin digestion. **(A)** the MALDI-TOF mass spectroscopy of AcF5 after trypsin digestion **(B)** Sequence of AcF5. Peptides identified by MS are shown in **Bold Red.** Sequence Coverage= **25%.** **(**Analysis type= Trypsin digestion; LC-MS/MS; Mass spectrometer = LTQ-Orbitrap-Velos-ETD - SN03106B; Database search algorithm Mascot v2.2.04; MS/MS Ion Sear.

As shown in Figure 4.12, several peptides were identified throughout the entire sequence of AcF5 (including the hexahistadine tag) confirming that the purified protein was AcF5. All three bands tested were confirmed as AcF5.

4.3.3.2 AcF5 binding to mannose-Sepharose

To test to see if the recombinant protein bound to mannose, purified AcF5 was loaded onto a mannose-Sepharose column in Ca^{2+} containing buffer. After two wash steps, five elution fractions were collected using buffer containing EDTA followed by additional elution steps using buffer containing mannose. As shown in Figure 4.13, all protein eluted in the flow-through, so did not bind to the column. Thus, unlike the full-length extracellular fragment AcL1, the N-terminal fragment, AcF5, alone does not bind to mannose, implying either that the mannose-binding domain is located in the cysteine-rich region or that the cysteine-rich region is necessary for the structural/functional integrity of the lectin domain. Given the unusual repeating sequence of the cysteine-like domain, the latter explanation seems most likely.
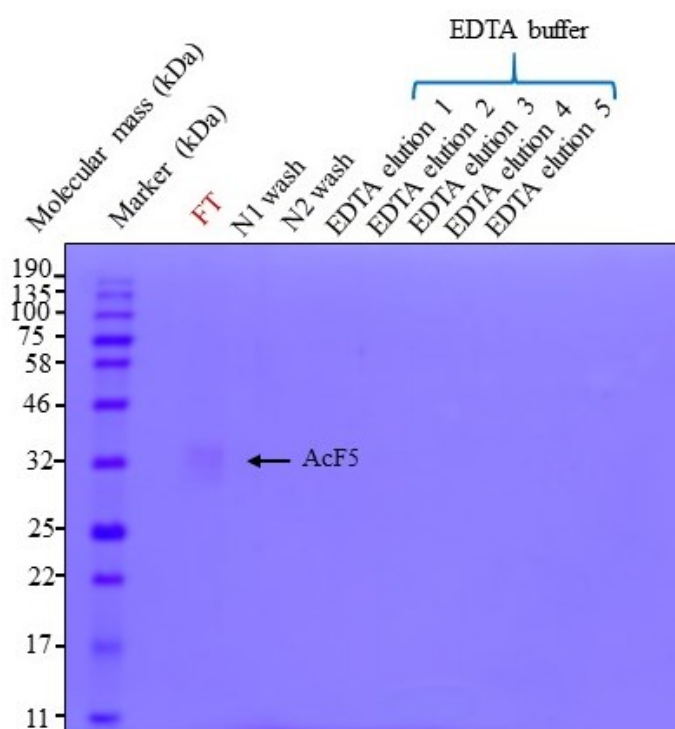
Figure 4-13: SDS-PAGE AcF5 on a mannose-Sepharose column. AcF5 did not bind to the mannose-Sepharose column in buffer containing Ca^{2+} but eluted in the flow through (FT). The experiment was carried out thrice.

4.3.4 Bioinformatics analysis of the DUF4114 domain

The DUF4114 domain is classified as a domain of unknown function found in many different types of protein. There are highly conserved glutamate and aspartate residues suggesting that this domain might carry enzymic activity. Careful sequence analysis against all proteins in the protein data base revealed low level sequence identity to two proteins: Blc2A and Blc2C from *Burkholderia cenocepacia* (Lameignere et al., 2008) (Figure 4.14). Intriguingly, both are Ca^{2+}-dependent lectins and Blc2A was crystallised bound to mannose.
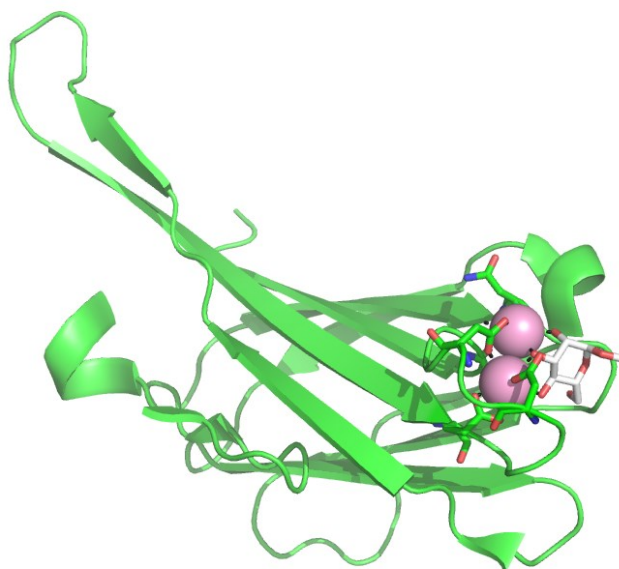
Figure 4-14: Structure of *Burkholderia cenocepacia* (Blc2A), a Ca^{2+}-binding lectin. Mannose binds to residues coordinating two Ca^{2+} and forms coordination bonds to the Ca^{2+} (Lameignere et al., 2008).

Sequence comparison shows that although the overall identity is only ~20%, four out of the five Ca^{2+} binding residues as well as an aspartate residue that interacts with the mannose are conserved in AcMBP, indicating that AcMBP is homologous to BlcA and that DUF4114 domains are likely to have lectin activity (Figure 4.15).

(A)

Mannose

Ca²⁺

Ca²⁺ Asp

Asp

Asp Asp

Glu

(B)

```
AcMBP    SSTQAVGFYLKQDSICSGTTTFY------SVDALNKVTSRWKPIPAAHGRMIAV-----
         +..|.+-.|+.++..-   +.||-      ....||--+.+-.-.-.+.||--..
BclA     AEQQHIKLFIGDSQEP--AAYHKLTTRDGPREATLNSGNGKIRFEVSVNGKPSATDARLA


AcMBP    LRDPNTL----RAYLGFEDSPDGSDSDYNDNV
         --.-+++     ..|.|.--|+||+|.||||-|
BclA     PINGKKSDGSEFTVNFGIVVSEDGHDSDYNDGI
```

Yellow: identical residues

Green: Ca²⁺-binding residues

Red: Mannose-binding residues
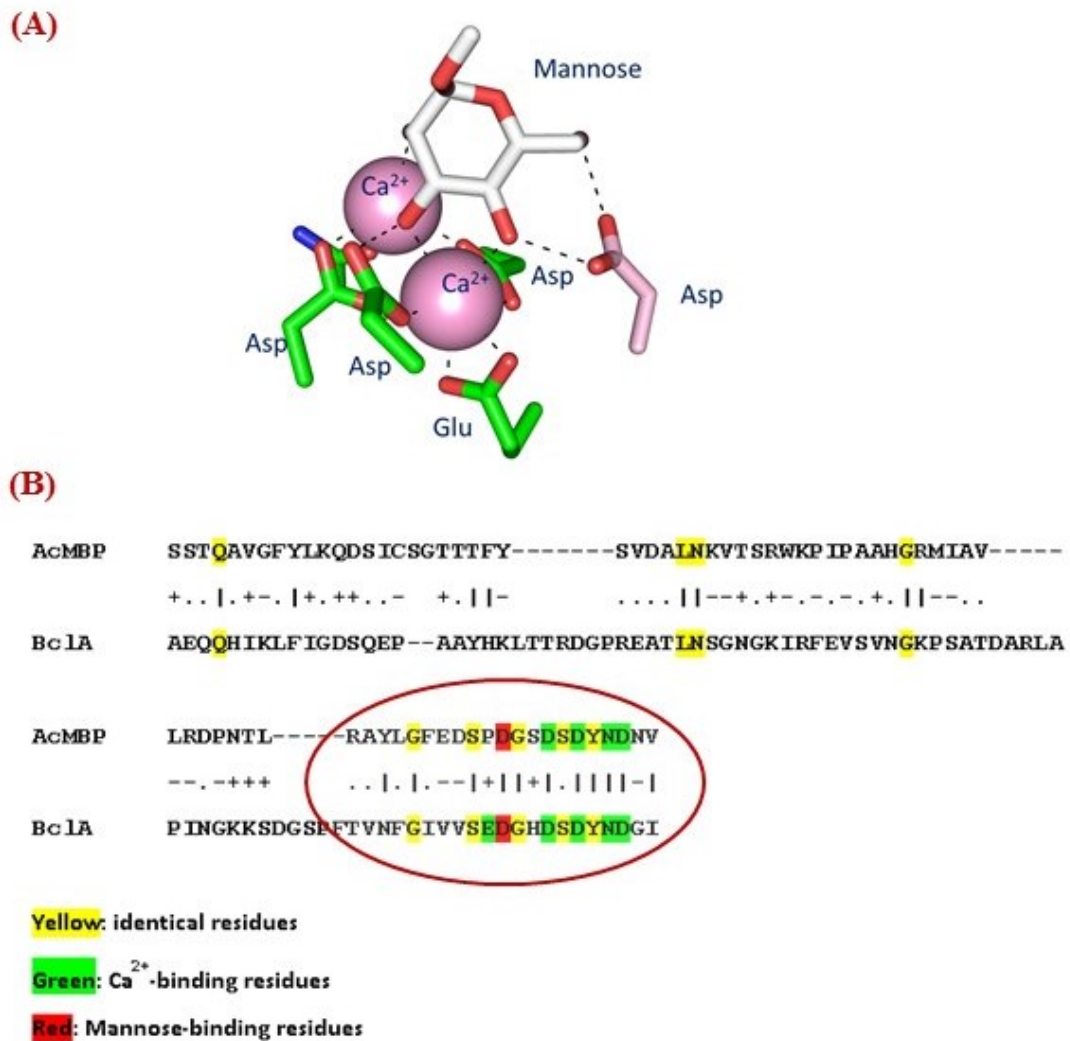
Figure 4-15: Sequence alignment of AcMBP versus BclA: (A) the Ca²⁺-binding site of BclA. The mannose is in white **(B)** Alignment of the DUF 4114 domain with BclA from *Burkhoderia cenocepacia*. The red eclipse identifies region of conserved sequence homology between AcMBP and BclA represented by the 3D structure in figure 4.15a.

4.3.5 Cloning, expression and production of recombinant AcDUF in *E. coli*

Given the homology with BclA, I attempted to express the DUF domain in *E. coli*. Two constructs were synthesised, the DUF domain alone (AcDUF) and the DUF domain containing a single mutation to convert the single cysteine residues to a serine: (AcDUFCS). The cDNA fragments were amplified by PCR and cloned into the bacterial expression plasmid pLEICS-01 (Figures 4.16 & 4.17).
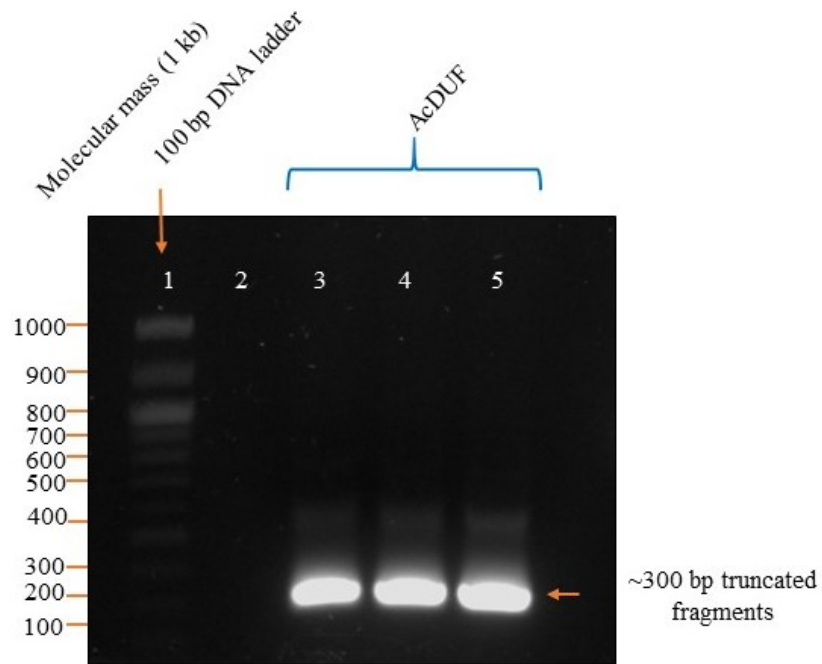
Figure 4-16: Agarose gel showing the PCR product encoding AcDUF. Lane 1 is 100 bp DNA ladder, lane 2 is blank space, and lane 3 – 5 is AcDUF (~ 300 bp). The cDNA amplicon was cloned into pLEICS-01 vector by the Leicester cloning service.
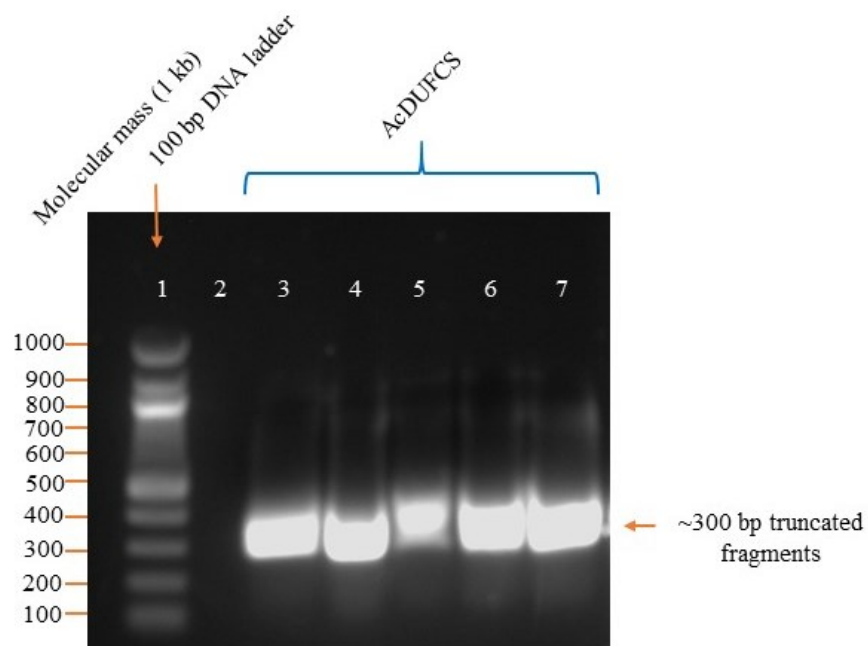
Figure 4-17: Agarose gel showing the PCR product encoding AcDUFCS. Lane 1 is 100 bp DNA ladder, lane 2 is blank space, and lane 3 – 7 is AcDUFCS (~ 300 bp). The fragment was purified from the gel and cloned into pLEICS-01 expression vector by the Leicester cloning service.

Plasmids were introduced into BL 21 (DE3) *E. coli* by transformation. Expression was induced using IPTG to induce production of the T7 RNA polymerase by the robust promoter system upstream of the coding sequence. Preliminary experiments showed that recombinant proteins were in the insoluble fractions of the *E. coli* cells (Figure 4.18). For this reason, cell pellets were isolated after overnight growth and proteins were purified as inclusion bodies (Figure 4.19).
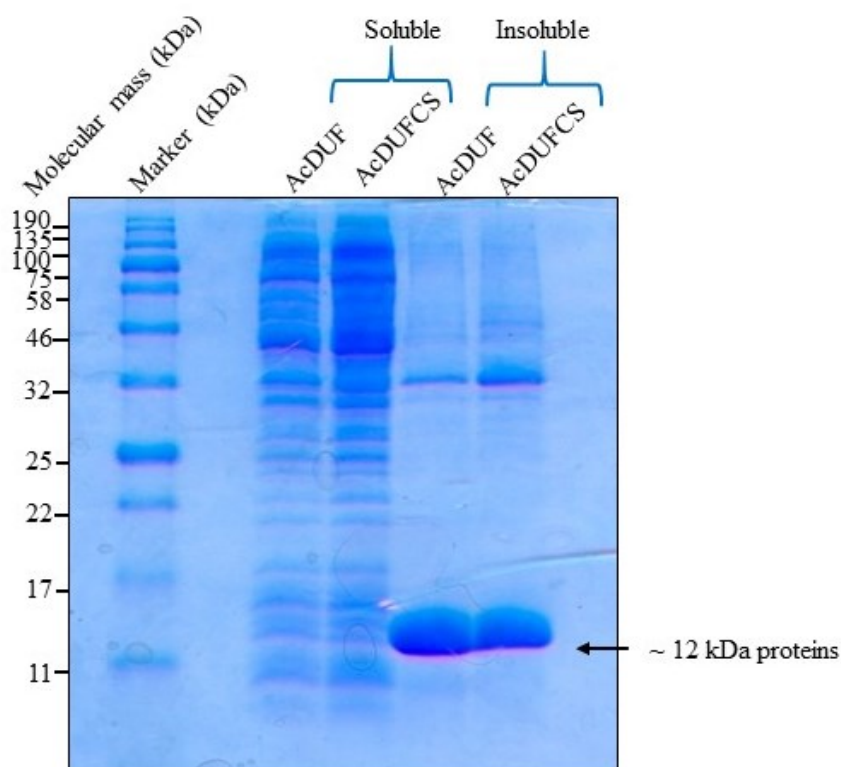
Figure 4-18: AcDUF and AcDUFCS are expressed as insoluble inclusion bodies. SDS-PAGE analysis of small-scale protein preparations. Preliminary tes**t** of bacterial culture grow-ups and analysis of AcDUF and AcDUFCS soluble and insoluble fractions show that AcDUF and AcDUFCS expressed in insoluble inclusion bodies following induction with IPTG. They were purified to remove protein, lipid and nucleic acid contaminants prior to solubilisation in 8 M urea. The protein sample was run on a 15% SDS-PAGE gel under reducing condition with β-mercaptoethanol and stained with Coomassie blue. The purified AcDUFCS migrates at the expected molecular mass of ~12 kDa. Experiment was repeated at least four times.
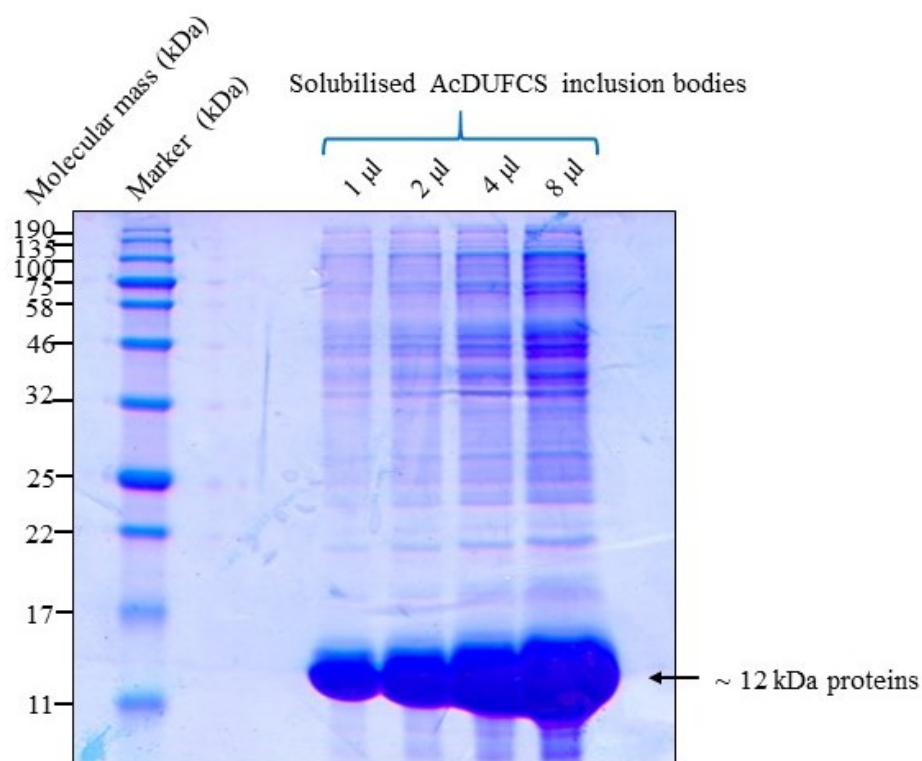
Figure 4-19: Inclusion body preparation of AcDUFCS showing increasing loading amounts on a 15% SDS-PAGE gel and stained with Coomassie blue. Expressed AcDUFCS inclusion bodies was isolated and purified from *E. coli* cells by using Bugbuster. Aliquots of increasing amount (1, 2, 4, 8 μl) of purified AcDUFCS were loaded from left to right as shown above. The purified AcDUFCS migrates at the expected molecular mass of ~12 kDa. Experiment was carried out at least four times.

To determine the best conditions for refolding, inclusion body preparations were solublised in urea and diluted 1:10 into 15 different buffers (to a final concentration of 0.1 mg/ml) using the QuickFold refolding kit. Samples were incubated overnight and centrifuged to pellet any aggregated material and then run on SDS-PAGE gel. The basis of this approach is that misfolding will lead to aggregation, so only soluble (hence refolded protein) will be detected on the gel. Sample gels are shown in Figure 4.20.
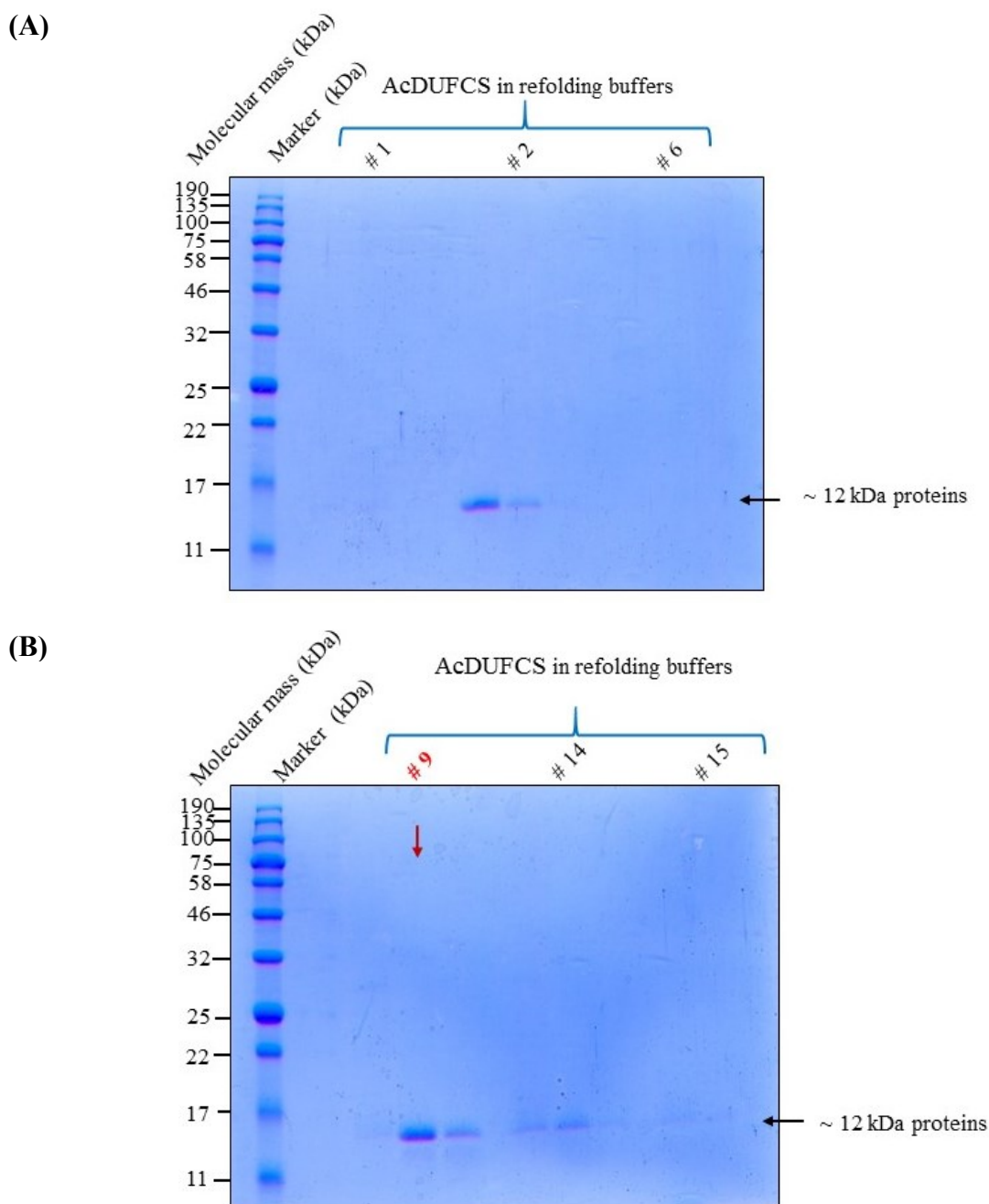
Figure 4-20: QuickFold protein refolding analysed by SDS-PAGE. Of the 16 different refolding buffer (RB) conditions, refolding buffers 1, 2, 6, 9, 14 and 15 gave clear bands. The best buffers were #1 and #9. Buffer #9 comprises of 50 mM Tris-Cl pH 8.5 containing 9.6 mM NaCl, 0.4 mM KCl, 1 mM EDTA, 0.5 M arginine, 0.75 M guanidine HCl, 0.05 % propylene glycol 3,350 and 1 mM DTT. Refolding trials were carried out twice.

Following the refolding trials a large scale refold was attempted. After refolding, the sample was dialysed into 25 mM Tris with 500 mM NaCl and loaded onto a 1 ml nickle-

Sepharose column. As shown in Figure 4.21, protein of the correct size (~12 kDa) was detected in elution fractions from the column. However the yields were low and significant amounts of contaminating proteins were still present. Samples were then loaded onto a Superdex-75 gel filtration column and fractions were collected across the elution peaks. When applied to a large column (16/60) no protein of the correct size was obtained, suggesting that the AcDUF binds to the column matrix. However, some protein did elute when applied to a 10/30 column (Figure 4.22).
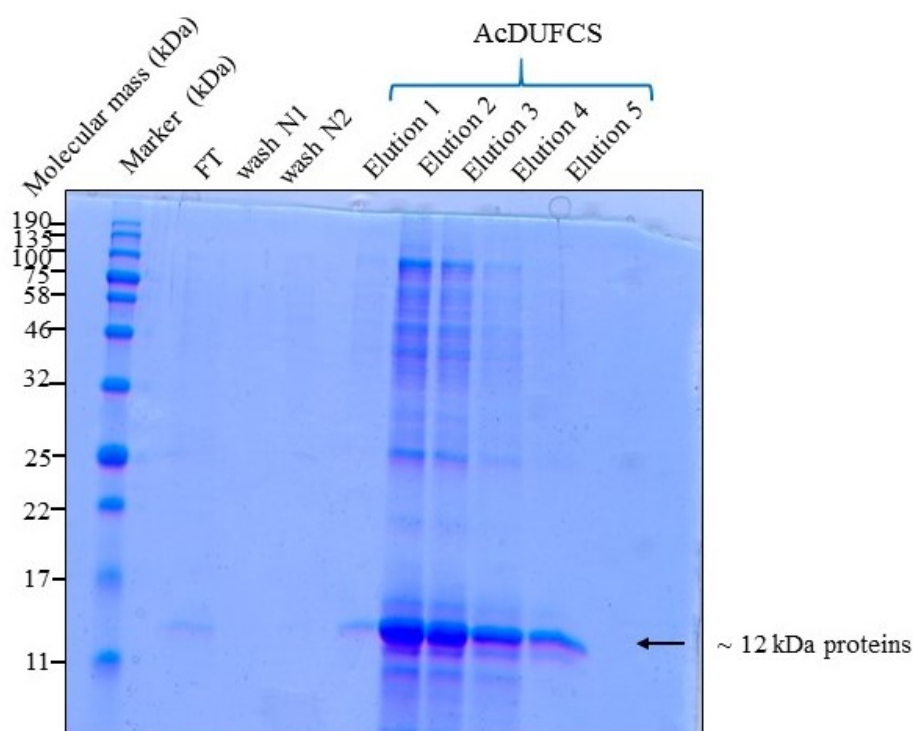
Figure 4-21: AcDUFCS Nickel analysis. A 15% SDS-PAGE analysis of the AcDUFCS elution fractions following nickel-affinity chromatography. AcDUFCS elutes from a nickel column by the addition of buffer containing 500 mM imidazole (Elution fractions 2 - 5). The purified AcDUFCS migrates at the expected molecular mass of ~12 kDa. Other bands in elution fractions 2 – 4 were possibly due to the traces of *E. coli* protein, lipid and nucleic acid contaminants. Experiment was repeated at least thrice.
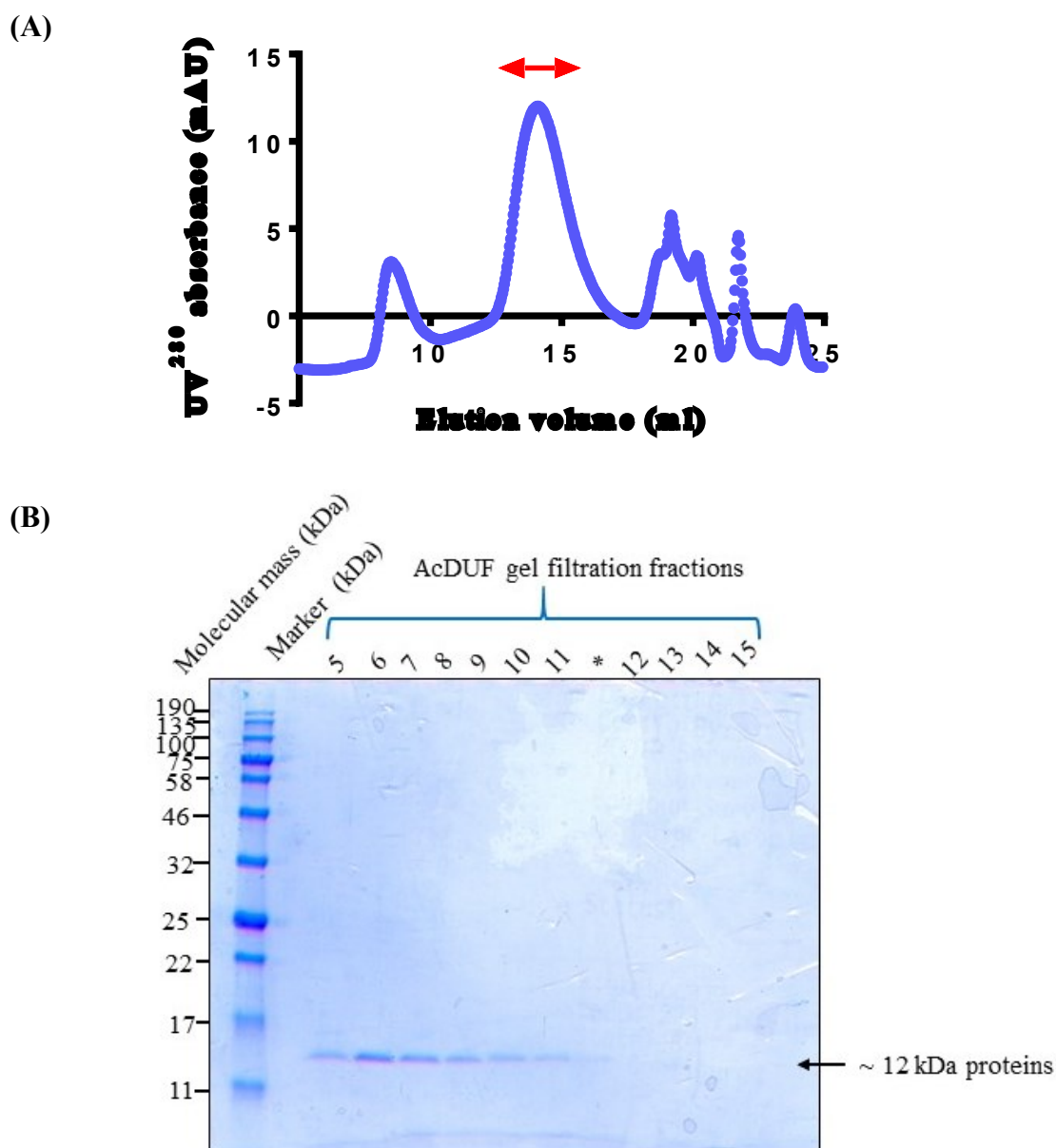
Figure 4-22: Gel filtration of AcDUF on a Superdex-75 column. (A) The elution profile of AcDUF on superdex 75 10 300 gel filtration column. Approximately 450µl of sample was loaded using a flow rate of 0.5 ml/min. The first peak is aggregate. **(B)** Fractions of AcDUF across the main peak (indicated by red arrow in figure 4.22a above) were collected and run on a 15% SDS-PAGE gel under reducing condition with β-mercaptoethanol and stained with Coomassie blue. The purified AcDUFCS migrates at the expected molecular mass of ~15 kDa. Experiment was repeated at least thrice.

The apparent molecular mass of AcDUF was ~15 kDa based on elution from the gel filtration column, suggesting that it is monomeric and folded. Unfolded proteins typical elute much earlier than expected (due to their larger size). Fractions containing protein

were pooled and concentrated. However, during concentration, a significant amount of the protein precipitated. Futhermore when analysed by SDS-PAGE, additional bands were detected suggesting that protein was rapidly degraded, presumably through proteolysis (Figure 4.23).
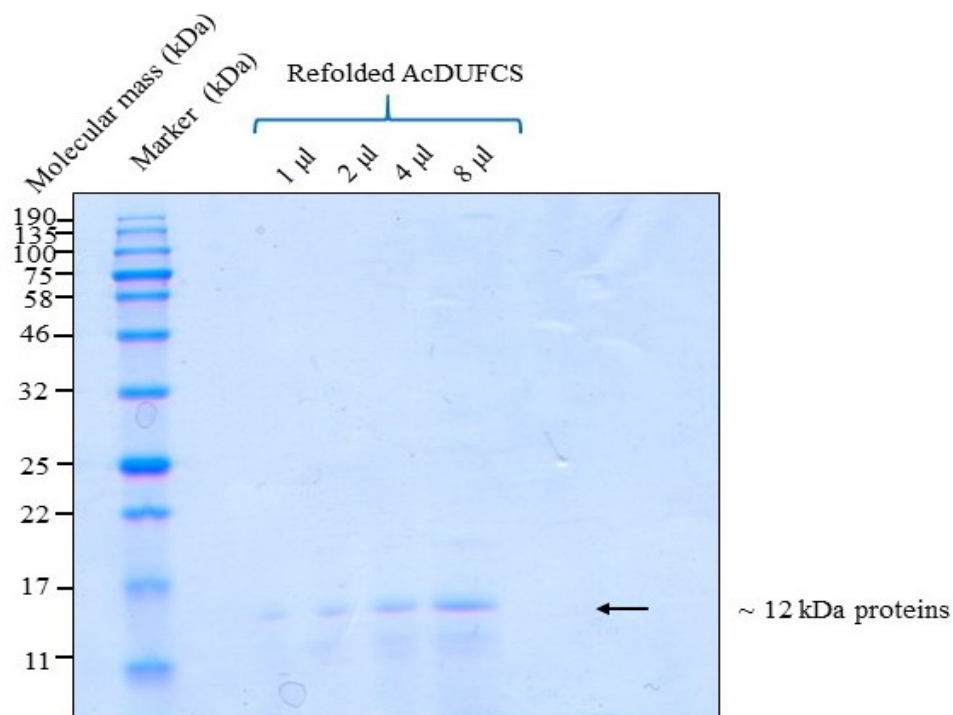
Figure 4-23: Concentrated refolded AcDUFCS samples were analysed by 15% SDS-PAGE. The purified AcDUFCS migrates at the expected molecular mass of ~12 kDa. Yields were low and additional bands were detected suggesting autocleavage of AcDUFCS possibly degraded by proteases.

4.3.6 Binding to mannose-Sepharose

Purified AcDUF was tested for mannose-binding by applying purified protein to a mannose-Sepharose column in buffer containing Ca^{2+}. As with AcE5 and AcF5, AcDUF eluted from the column in the flow through indicating that it did not bind to mannose (Figure 4.24).
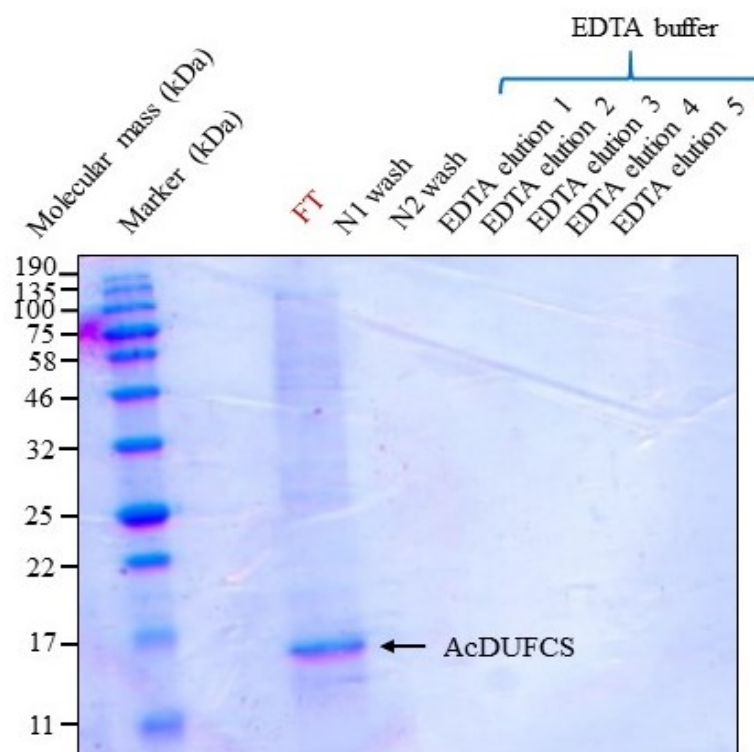
Figure 4-24: SDS-PAGE analysis of AcDUFCS showing purification by affinity chromatography on a mannose-sepharose column. AcDUFCS does not bind to column in buffer containing Ca^{2+} and was eluted from column as a flow through (FT). The protein sample was run on a 15% SDS-PAGE gel under reducing condition with β-mercaptoethanol and stained with Coomassie blue. The purified AcDUFCS migrates at the expected molecular mass of ~15 kDa. Experiment was repeated at least thrice.

4.3.7 Monomeric characteristics of extracellular AcMBP

Figure 4.25 shows that extracellular AcMBP are monomer either under reducing or non-reducing conditions.
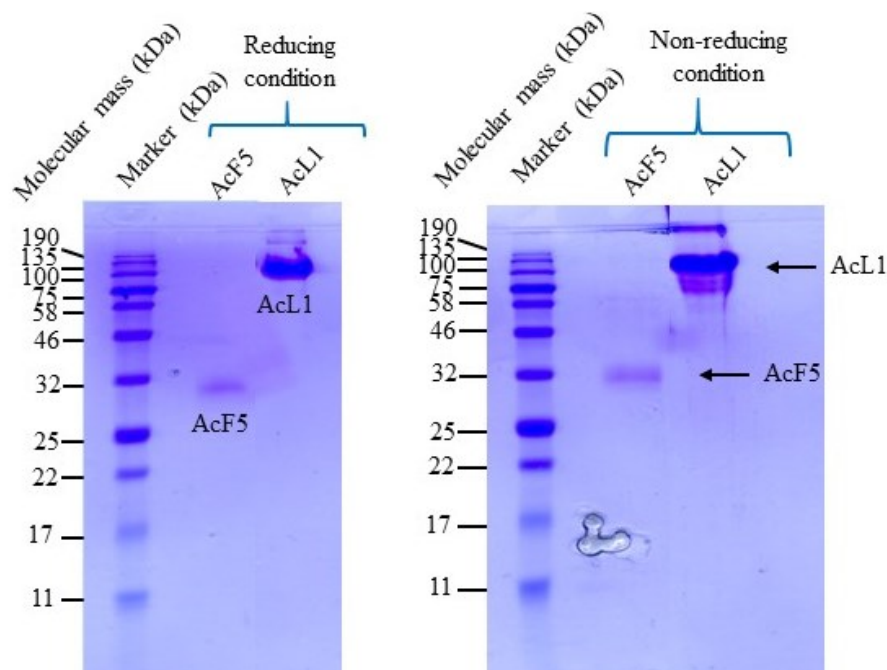
Figure 4-25: SDS-PAGE analysis of extracellular AcMBP showing either AcF5 or AcL1 as monomeric proteins under both reducing and non-reducing conditions after purification by affinity chromatography on a nickel column. The protein samples were run on a 15% SDS-PAGE gel under reducing and non-reducing conditions with or without β-mercaptoethanol respectively and subsequently stained with Coomassie blue. The purified AcF5 and AcL1 migrate at the expected molecular mass of ~32 and ~120 kDa respectively. Experiment was repeated at least twice.

4.3.8 Cloning, expression and production of recombinant AcL1DD

As an alternative strategy to investigate the lectin activity of AcMBP, mutations were introduced into the the DUF4114 domain of AcMBP, with the aim of knocking out lectin activity. Two mutations were introduced into the DUF4114 domain: $Asp^{217} \rightarrow Ala$ and $Asp^{220} \rightarrow Asn$. Both residues interact with the mannose in BclA and Asp-220 also interacts with the Ca^{2+}. The mutations were designed to prevent mannose-binding but retain Ca^{2+} binding (Figure 4.26). Whereas the $Asp^{217} \rightarrow Ala$ mutation removes the acidic site chain completely, the $Asp^{220} \rightarrow Asn$ retains the ability to coordinate the Ca^{2+} via its carbonyl group but cannot form a hydrogen bond to the mannose:

$-CH_2COO^-$ to $-CH_2CONH_2$
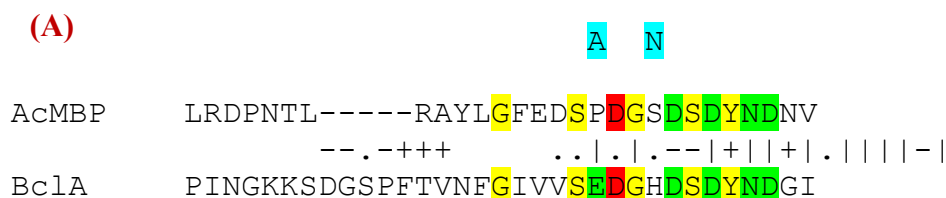
(A)

```
                                    A   N
AcMBP    LRDPNTL-----RAYLGFEDSPDGSDSDYNDNV
                --.-+++       ..|.|.--|+||+|.||||-|
BclA     PINGKKSDGSPFTVNFGIVVSEDGHDSDYNDGI
```

Yellow: identical residues

Green: Ca^{2+}-binding residues

Red: Mannose-binding residues

(B)

Asp217
→Ala
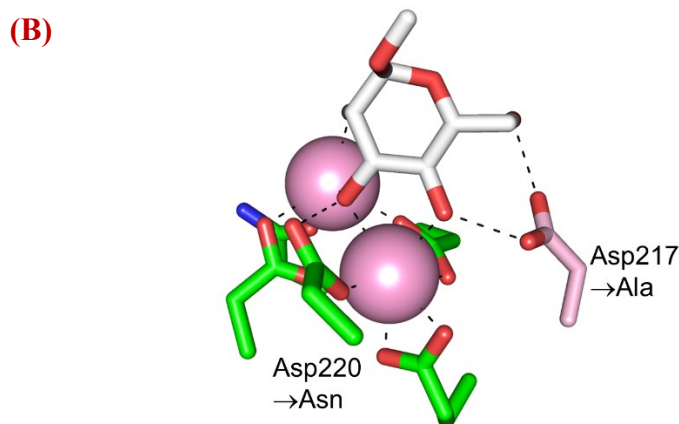
Asp220
→Asn

Figure 4-26: Mutations introduced into AcL1. (A) Mutation was introduced at Asp^{217}Ala and Asp^{220}Asn to produce the full length (mutant) AcL1DD that is designed to knock out the mannose-binding protein but retain the Ca^{2+}-binding region of AcMBP. **(B)** 3D structural **feature showing sites of point mutation of** Asp^{217}Ala and Asp^{220}Asn in BclA, as conserved in AcMBP, to illustrate the full length (mutant) AcL1DD.

The clone was created and introduced into pED4 as before but due to time constraints, the protein has not yet been produced.

4.4 Discussion

One of the main objectives of this chapter was to produce purified recombinant truncated fragments of AcMBP in order to define the structure and binding-sites of AcMBP. To achieve this aim, I attempted to produce functional domains encompassing the DUF 4114 region of AcMBP. Three different fragments were produced: two fragments of varying sizes comprised of the N-terminal region up until the cysteine-rich domain and the third fragment was the DUF4114 domain alone. None of the fragments bound to mannose-

Sepharose. Whilst this could mean that the lectin activity is located in the cysteine-rich domain, it is much more likely that the domain boundaries of the truncated constructs were incorrect resulting in loss of activity. Consistent with this possibility, yields of all three fragments were very low. Furthermore, the DUF4114 domain degraded rapidly suggesting that it is not a stable domain. Notably, the DUF4114 contains only four out of the five Ca^{2+} coordination ligands. The addition ligand could come from a different part of the protein (Figure 4.26).

To overcome these problems I have produced an additional full-length extracellular fragment containing mutations that are designed to knock out the mannose-binding activity but retain the ability to bind Ca^{2+}. The advantage of this approach is that AcL1 produces well in CHO cells, so loss of activity due to protein instability (through incorrect choice of domain boundaries can be avoided. Unfortunately, I ran out of time before this protein could be produced but this approach is likely to yield interesting results. Subject to the outcome of this experiment, I may further establish the biological function of AcMBP in life *Acanthamoeba castellanii* cells by knocking out the either the extracellular region or the complete AcMBP using the technique of interference RNA (RNAi) according to the methods of Tuschl and coworkers (Elbashir et al., 2001). Beyond doubt, if I could further establish the role of AcMBP in the cytopathology of *Acanthamoeba* corneal infection, then, I would design polyclonal antibodies (anti-MBP) and study its effects on laboratory animals like rabbit in order to re-establish the potential of AcMBP as a likely therapeutic target against AK.

5. General Discussions

This chapter summarises the work in this thesis aimed at understanding the role of *Acanthamoeba* mannose-binding protein (AcMBP). The sporadic outbreaks of *Acanthamoeba* keratitis (AK) infections, due to *Acanthamoeba,* often lead to blindness and this in turn is associated with traumatised cornea often caused by contact lens use (Tomlinson et al., 2000, Zimmerman et al., 2016). Numerous studies have suggested the involvement of *Acanthamoeba* mannose-binding protein (AcMBP) as a critical virulence factor that initiates the parasitic adhesion and subsequently induces cytopathic effect (CPE) (Panjwani, 2010). Consequently, there was no suggestion of alternative surface protein of *Acanthamoeba spp.* that is pertinent to the host invasion and/or infction of caused by this free-living amoeba (Sanchez et al., 2016).

AcMBP triggers *Acanthamoeba* adhesion, a key step in AK pathogenesis leading to 'a near-irreversible' corneal tissue destruction that is predominant among the currently estimated 140 millions contact lens users worldwide (Lim et al., 2016). Yet, there has been little molecular characterisation of AcMBP.

Therapeutic unresponsiveness of AK cases is often attributed to the similarities in the biological processes that *Acanthamoeba* shares with its human subjects (Roberts and Henriquez, 2010) and its ability to form cysts that are resistant to drugs. During infection, immune cells (neutrophils and macrophages) migrate to the cornea to affect the killing of *Acanthamoeba* (van Klink et al., 1996, Hurt et al., 2001, Clarke and Niederkorn, 2006a). However, neutrophils have been documented to exacerbate the severity of AK lesions through the release of proteases that damage host tissue (Marciano-Cabral and Cabral, 2003). Late diagnosis and/or therapeutic failure are considered to be further impaired by the persistent resistance of the mature cysts to biocides, inappropriate drugs with non-target-mechanism of action and/or potential toxicity of chemical compounds to corneal tissue (Carrijo-Carvalho et al., 2017).

Often, the migration of immune cells and consequent destructions of the corneal architecture may impair the corneal transparency by impeding optimal transmission of light and consequently causing vision impairment (Giménez et al., 2013, Pearlman et al., 2013). The absence of resident antigen-presenting cells (APC) in the cornea or the masked *Acanthamoeba* antigens from cellular immune response (Mathers et al., 1987) may further explain its inability to induce cell-mediated or humoral responses; likewise

the failure to stimulate delayed-type hypersensitivity reaction of serum IgG against *Acanthamoeba* antigen (van Klink et al., 1996). *In-vitro* studies have established that *Acanthamoeba* often activate the alternative complement pathway independent of antibody activation (Marciano-Cabral and Cabral, 2003); however this is insufficient to stop the infection. Currently there is no vaccine for *Acanthamoeba* infections (Jiang et al., 2015).

5.1 *Acanthamoeba* differentiates and inter-switches between three different life forms

In Chapter 2, I established *in-vitro* conditions to promote differentiation to the two well-characterised life forms of *Acanthamoeba,* namely the actively motile trophozoites; and the double-layered, immotile, dormant mature-cysts (Schuster, 2002, Khan, 2006a, Siddiqui and Khan, 2012a). In addition, I was able to determine conditions for differentiation into the third life form of *Acanthamoeba* - fragile protocysts, in the presence of propylene glycol (a major preservative constituent of commercial contact lens solutions). Of particular interest was the novel discovery that while both protocysts and mature cysts can convert to trophozoites, they cannot interconvert directly. This is potentially important with respect to treatment, because, the fragile protocysts are likely to be more susceptible to anti-parasitic drugs because they lack the double cell wall of mature cysts. Thus, combining drugs with propylene glycol (in contact lens solutions and or in eye drops during treatment of AK) to maintain *Acanthamoeba* as protocysts may be beneficial.

As with previous studies, mannose reduced *Acanthamoeba* adhesion to human corneal epithelial (HCEC) cells but in contrast to other work, this did not inhibit cytopathology. Notably, the data described here showed that *Acanthamoeba* were able to bind to many surfaces even in the presence of mannose so AcMBP is not the only adhesion molecule required to initiate *Acanthamoeba* binding to surfaces.

5.2 Structural and functional characteristics of AcMBP

The work of Garate and colleagues has highlighted the importance of AcMBP in *Acanthamoeba* adhesion onto corneal tissues and the resulting cytopathic effect (Garate et al., 2004, Garate et al., 2005, Garate et al., 2006). My findings, in chapters 3 and 4, have shown that mannose binding is Ca^{2+} dependent and is almost certainly located in

the DUF 4114 domain. (~10 kDa) (Figures 3.2, 4.4 & 4.5). Alignment of other DUF 4114 domains shows that four of the five Ca^{2+} ligands are completely conserved in most members of the family, suggesting that they also bind Ca^{2+}. The Asp residue that interacts with the mannose in BclA (in red in Fig 5.1) is not conserved. Nevertheless, other proteins containing DUF 4114 domains are likely to be lectins. This is because the sequence from AcMBP DUF 4114 aligns with the DUF 4114 consensus sequences of different bacterial organisms such *Hypothetical protein* (*Bacteroides spp.*), *Simiduia agarnorans* depicting similar structural and functional characteristics (Marchler-Bauer et al., 2017).

```
consensus    IGFFLVANGIGNGKGPYFSTSSLN-------PDDGLNTHQVA-LKDGKGGKVIFGFEDLP  52
             +GF+L  + I +G   ++S  +LN         P     +A L+D    +   GFED P
AcMBP        VGFYLKQDSICSGTTTFYSVDALNKVTSRWKPIPAAHGRMIAVLRDPNTLRAYLGFEDSP  68


consensus        RPGGDRDFNDVIF 65
                  G D D+ND +F
AcMBP        D-GSDSDYNDNVF  80
gi 81445284      ANRSFCDLLFY  403
gi 511755920     GENDFNDAVFS  239
gi 501490475     GENDFNDCIFY  383
gi 495787752     CENDFNDIVFY  394
gi 503397774     SENDFNDLVFf  378
gi 504843553     CENDFNDAIFY  375
gi 503969692     GEYDFNDCIFY  391
gi 380883278     SENDFNDAILA  258
gi 505293298     CENDFNDAIFY  229
gi 503784705     CEHDFNDVMFY  372
```

Figure 5-1: Alignment of DUF 4114 consensus sequence with the sequence from AcMBP. Residues that form the binding site for mannose in BclA are highlighted in green. The C-terminal regions of 10 DUF 4114 domains are shown (with accession numbers) Source: (Marchler-Bauer et al., 2017).

To test the putative sugar binding site in AcMBP, a strategic approach was adopted to construct a mutant (AcL1DD) by site–directed mutagenesis using the strategy previously employed for C-type lectins (Drickamer, 1993) in which Ca^{2+}-binding is retained but mannose-binding residue is abolished. Unfortunately, although the construct encoding this mutant was generated, I did not have enough time to produce or characterise this protein. This approach seems to be the most likely to succeed for confirming the location of the sugar binding site in AcMBP because none of the truncated proteins bound to mannose.

5.3 Directions for Future work

A useful direction for future studies is to further investigate the carbohydrate-binding properties of AcMBP. Preliminary data suggested that AcMBP might have additional lectin activities because it bound to a variety of glycoproteins including those that lacked high mannose sugars. One strategy is to use glycan arrays and I have sent a sample of AcL1 for analysis at the Glycosciences Laboratory at Imperial College (run by Professor Ten Feizi). In this process protein is added to a series of sequence define carbohydrates. Binding is identified by immunodetection e.g. using an anti-His tag antibody associated with each glycan. The results may reveal the relative target specificity of AcMBP towards the defined carbohydrate structure.

The work described here questions the importance of AcMBP in adhesion and cytopathic effect because *Acanthamoeba* were able to bind to a variety of cells and surfaces in the presence of mannose. For this reason, it would be of interest to delete the gene encoding AcMBP in *Acanthamoeba* and test the resulting deficient strain with respect to its binding and cytopathic effect. Despite the limiting factor of time constrain in the course of this research, my future plan is to use mutagenesis to determine the role of AcMBP. Here, I hope to adopt the technique of interference RNA (RNAi) according to the methods of Elbashir and colleagues (Elbashir et al., 2001) to knock down or down regulate the expression of the adhesion protein (AcMBP) level in life *Acanthamoeba*. It is essential to determine the sufficient amount of small interference RNA (siRNA) enough to achieve the protein breakdown thus finding the observable phenotypic and/or functional roles in *Acanthamoeba*, which may ultimately provide novel insight into nthe AcMBP function with respect to the cytopathology of AK. Although, RNAi rarely achieve 100% loss of protein from most cells, it results in degradation of target mRNA which is easily determined by reverse transcription polymerase chain reaction (RT-PCR). Hence, the loss of functional AcMBP from *Acanthamoeba* may reveal a knockdown phenotype. Then, I will use RT-PCR to assess the mRNA knockdown while western blotting or immunofluorescence may help assess the AcMBP knocked down from *Acanthamoeba*.

According to Zhang and colleagues (Zhang et al., 1994), the gene knockout or gene targeting by homologous recombination technology are invaluable methods that provides highest level of control over mutation in an endogenous gene. In addition, it allows for

the understanding of the functional role of AcMBP in *Acanthamoeba* adhesion, cytopathology and as potential therapeutic agent for *Acanthamoeba* keratitis.

While both western blotting and immunofluorescence uses specific antibodies to detect AcMBP, unlike western blotting, individual cells are visualised by immunofluorescence techniques with the added advantage of allowing assessment of the knockdown protein at the specific subcellular localisation. Hence, it gives the possibility of correlating the knockdown level and phenotype of the AcMBP. Control experiment could be carried out using mock transfection containing no siRNA or transfection of siRNA in an unrelated protein to ensure that the phenotype is a result of the loss of protein of interest. Further to the above, and upon the determination of functional roles of AcMBP, I will proceed to design polyclonal antibodies (anti-MBP) as the most possible therapeutic target against AK.

Structural analysis of AcMBP would be extremely useful in defining the structural/functional domains of the protein and determining how it binds to mannose. So far, no crystallisation conditions have been found but studies are still ongoing (Jeudy et al., 2005) The generation of a stable folded fragment encompassing the mannose-binding domain would be extremely useful, but the studies described here indicate that is likely to be difficult.

AcMBP contains 80 cysteine residues that probably mostly form disulphide bonds. Thus, finding the precise domain boundaries is likely to be critical for producing a stable fragment. It is also possible that the domains in AcMBP are non-contiguous, so generation of a stable fragment might not be possible. Full-length AcMBP is too large for nuclear magnetic resonance (NMR) but electron microscopy represents a possible approach for structural analysis. The full-length protein is ~100 kDa, so is on the lower edge of what has been done by cryo-electron microscopy (cryoEM). Low resolution approaches e.g. small-angle X-ray scattering (SAXS) might also yield useful information about the overall shape of the molecule. The SAXS determines the nanoscale density differences in sample (size/shape, pore-size) by examining the elastic scattering behaviour of X-ray when travelling through the protein sample. The relative advantage of SAXS over the 3D crystallography is that no crystalline protein sample is required for the structural analysis.

Further still, other strategies that I might employ may involve the evaluation of the immunodiagnostic potential of recombinant AcMBP antigen-based ELISA with sera obtained from experimentally infected rabbits that have developed *Acanthamoeba* keratitis. In addition, I may set up chemotactic assay for the direct observation and analysis of chemotactic behaviour of axenically grown *Acanthamoeba castellanii* under study by using a visual assay slide chamber in conjuction with time-lapse videomicroscopy according to the methods of Schuster and Levandowsky (Schuster and Levandowsky, 1996). *Acanthamoeba* membrane are thought to have sensitive receptors to bacterial and chemotactic peptide--- formyl-methionyl-leucyl-phenylalanine (fMLP), lipopolysaccharides, cyclic AMP, lipoteichoic acid,and N-acetyl glucosamine by moving actively toward the attractant, which are different from the chemotactic peptide antagonists which include mannose, mannosylated bovine serum albumin and N-acetyl muramic acid (Schuster and Levandowsky, 1996).

Further functional assays on *Acanthamoeba castellanii* are required to enable the understanding of the roles of AcMBP; trophozoites would be treated with methyl-alpha-D-mannopyranoside (mannose) prior to the analysis of adhesion and cytotoxicity of *Acanthamoeba.* This cytotoxicity assay determines the ability of *Acanthamoeba* to trigger host cell death as earlier described in chapter two of this thesis. In addition, according to the methods of Yoo and Jung (Kim et al., 2012a, Yoo and Jung, 2012), phagocytotic assay is essential to understand the correlation between the AcMBP in *Acanthamoeba* phagocytosis using non-pathogenic (non-invasive) bacteria such as *Escheriscia coli* K12.

Finally, the use of antibodies against the AcMBP domains are further strategies of establishing the therapeutic potential of AcMBP.

APPENDICES

APPENDIX I - *Acanthamoeba* **strains classified according to genotypes and species**

Seq.type	Species classification	Strain name	GeneBank Account #	Reference
T1	*A. castellanii*	CDC:0981:V006	U07400	(Gast et al., 1996b)
T2	*A. palestinensis*	Reich (ATCC 30870)	U07411	(Gast et al., 1996b)
T2	*A. pustulosa*	GE3a (ATCC 50252)	AF019050	(Stothard et al., 1998b)
T2	*A. polyphaga*	OX-1; CCAP:1501/3c	AF019051	(Stothard et al., 1998b)
T3	*A. pearcei*	ATCC 50435	AF019053	(Stothard et al., 1998b)
T3	*A. griffini*	S-7 (ATCC 30731)	*U07412	(Gast et al., 1994, Gast et al., 1996b)
T3	*A. polyphaga*	Panola Mountain (ATCC 30487)	AF019052	(Stothard et al., 1998b)
T3	*A. griffini*	TIO:H37	*S81337	(Stothard et al., 1998b)
T4	*A. species*	Jin-E5 (ATCC 50710)	AF019054	(Stothard et al., 1998b)
T4	*A. species*	Liu-E1 (ATCC 50709)	AF019055	(Stothard et al., 1998b)
T4	*A. polyphaga*	HC-2	AF019056	(Stothard et al., 1998b)
T4	*A. culbertsoni*	Diamond	AF019057	(Stothard et al., 1998b)
T4	*A. species*	Vazaldua (CEI:M95:5:27)	AF019058	(Stothard et al., 1998b)
T4	*A. species*	CEI:M95:7:45 (ATCC 50711)	AF019059	(Stothard et al., 1998b)
T4	*A. hatchetti*	2AX1 (ATCC 30731)	AF019060	(Stothard et al., 1998b)
T4	*A. polyphaga*	Page-23 (ATCC 30871)	AF019061	(Stothard et al., 1998b)
T4	*A. polyphaga*	Nagington (ATCC 30873)	AF019062	(Stothard et al., 1998b)
T4	*A. castellanii*	CDC:0184:V014 (ATCC 50492)	U07401	(Gast et al., 1996b)
T4	*A. polyphaga*	CDC:0884:V029	U07402	(Gast et al., 1996b)
T4	*A. castellanii*	CDC:0786:V042 (ATCC 50493)	U07403	(Gast et al., 1996b)
T4	*A. species*	CDC:0688:V125 (ATCC 50498)	U07404	(Gast et al., 1996b)
T4	*A. castellanii*	CDC:0180:1	U07405	(Gast et al., 1996b)
T4	*A. rhysodes*	BCM:0685:116 (ATCC 50368)	U07406	(Gast et al., 1996b)

T4	*A. polyphaga*	BCM:0173:16 (ATCC 50371)	U07407	(Gast et al., 1996b)
T4	*A.* species	BCM:1282:324 (ATCC 50496)	U07408	(Gast et al., 1996b)
T4	*A.* species	BCM:0288:27 (ATCC 50369)	U07409	(Gast et al., 1996b)
T4	*A.* species	BCM:0288:37 (ATCC 50497)	U07410	(Gast et al., 1996b)
T4	*A. castellanii*	Castellani (ATCC 50374)	U07413	(Gast et al., 1996b)
T4	*A. castellanii*	Ma (ATCC 50370)	U07414	(Gast et al., 1996b)
T4	*A. polyphaga*	JAC/S2 (ATCC 50372)	U07415	(Gast et al., 1996b)
T4	*A. castellanii*	Neff (ATCC 50373)	U07416	(Gast et al., 1996b)
T4	*A. royreba*	Oak Ridge (ATCC 30884)	U07417	(Gast et al., 1996b)
T5	*A. lenticulata*	45 (ATCC50703)	U94730	(Schroeder-Diedrich et al., 1998, Stothard et al., 1998b)
T5	*A. lenticulata*	7327 (ATCC50705)	U94731	(Schroeder-Diedrich et al., 1998, Stothard et al., 1998b)
T5	*A. lenticulata*	72/2 (ATCC50704)	U94732	(Schroeder-Diedrich et al., 1998, Stothard et al., 1998b)
T5	*A. lenticulata*	68-2 (ATCC50427)	U94733	(Schroeder-Diedrich et al., 1998, Stothard et al., 1998b)
T5	*A. lenticulata*	407-3a (ATCC50692)	*U94734	(Schroeder-Diedrich et al., 1998, Stothard et al., 1998b)
T5	*A. lenticulata*	E18-2 (ATCC50690)	*U94735	(Schroeder-Diedrich et al., 1998, Stothard et al., 1998b)
T5	*A. lenticulata*	118 (ATCC50706)	*U94736	(Schroeder-Diedrich et al., 1998, Stothard et al., 1998b)
T5	*A. lenticulata*	53-2 (ATCC50641)	*U94737	(Schroeder-Diedrich et al., 1998, Stothard et al., 1998b)
T5	*A. lenticulata*	NJSP-3-2 (ATCC50429)	*U94738	(Schroeder-Diedrich et al., 1998, Stothard et al., 1998b)
T5	*A. lenticulata*	Jc-1 (ATCC50428)	*U94739	(Schroeder-Diedrich et al., 1998, Stothard et al., 1998b)

T5	*A. lenticulata*	25/1 (ATCC50707)	*U94740	(Schroeder-Diedrich et al., 1998, Stothard et al., 1998b)
T5	*A. lenticulata*	PD2S (ATCC30841)	*U94741	(Schroeder-Diedrich et al., 1998, Stothard et al., 1998b)
T6	*A. palestinensis*	2802 (ATCC 50708)	AF019063	(Stothard et al., 1998b)
T7	*A. astronyxis*	Ray & Hayes (ATCC 30137)	AF019064	(Stothard et al., 1998b)
T8	*A. tubiashi*	OC-15C (ATCC 30867)	AF019065	(Stothard et al., 1998b)
T9	*A. comandoni*	Comandon & de Fonbrune (ATCC 30135)	AF019066	(Stothard et al., 1998b)
T10	*A. culbertsoni*	Lilly A-1 (ATCC 30171)	AF019067	(Stothard et al., 1998b)
T11	*A. hatchetti*	BH-2	AF019068	(Stothard et al., 1998b)
T11	*A. stevensoni*	RB:F:1 (ATCC 50388)	AF019069	(Stothard et al., 1998b)
T12	*A. healyi*	CDC 1283:V013	AF019070	(Stothard et al., 1998b)
T13	*A.* species	UWC9	AF132134	(Horn et al., 1999)
T13	*A.* species	UWET39	AF132136	(Horn et al., 1999)
T14	*A.* species	PN15	AF333607	(Gast, 2001)
T15	*A. jacobsi*	ATCC 30732	AY262360	(Hewett et al., 2003)
T15	*A. jacobsi*	AC080	AY262361	(Hewett et al., 2003)
T15	*A. jacobsi*	AC194	AY262362	(Hewett et al., 2003)
T15	*A. jacobsi*	AC227	AY262363	(Hewett et al., 2003)
T15	*A. jacobsi*	AC304	AY262364	(Hewett et al., 2003)
T15	*A. jacobsi*	AC305	AY262365	(Hewett et al., 2003)
T16	*A.* species	cvX	GQ380408	(Corsaro and Venditti, 2010)
T16	*A.* species	U/H-C1	AY026245	(Corsaro and Venditti, 2010)
T17	*A.* species	Ac_E9b	GU808302	(Nuprasert et al., 2010)
T18	*A. byersi*	CDC:V621	KC822461	(Qvarnstrom et al., 2013b)

(Adapted from Magnet et al., (2014)).

APPENDIX II – Selected DNA Sequences/ Amino acids residues

(i) Amino acids residues of membrane-spanning AcMBP – cDNA (complete)

```
        10          20          30          40          50          60
MRSLPVFVVL  MVALFAAVAS  AGTCNLSGAI  KQPGLDCSST  SCSITSGTFP  FPLPQGETYD

        70          80          90         100         110         120
SFYSWILGVI  GTDGATVNAQ  YVDYTKADPN  IYFTAGQTNC  MVNLTFVYEV  AFYRNSMGYF

       130         140         150         160         170         180
TFTRDSKPTS  VGSVTLKPVF  SETTVDCSRT  SSQPLPGTSC  LAPGSTISLG  PFSSTQAVGF

       190         200         210         220         230         240
YLKQDSICSG  TTTFYSVDAL  NKVTSRWKPI  PAAHGRMIAV  LRDPNTLRAY  LGFEDSPDGS

       250         260         270         280         290         300
DSDYNDNVFS  VTSNCEIDTS  LLPCATVTTC  RNSKQTFDSS  KCTCSCPNPV  TCTAPQVYST

       310         320         330         340         350         360
DLCACTCPNA  TQTCTAPLTW  NSATCQCDCP  STKPSGVTCS  NLQQWSNVVA  TCGCKCPDPA

       370         380         390         400         410         420
TYTCSDNRFV  LRTSDCTCNC  PSTGSCSGNL  KWNSANSVCG  CQCPSTPPTP  CSGNLKWNST

       430         440         450         460         470         480
ASKCACECPA  TAALAGVTCK  DKEVWDTASC  SCKCPATASA  ADTTCPNVNY  QWNYNGKCDC

       490         500         510         520         530         540
VCPATSAEAG  INCTALGLGN  TVWDTTACNC  ACPPTGTCPG  NKVWNPSNDP  AKCGCSCPAS

       550         560         570         580         590         600
APAGKECKGN  FYWNTSDDVC  DCYCPLEAPA  DDPCIGYTTW  NRTECDCYCP  LEPPFEGGCP

       610         620         630         640         650         660
GVQVWDRDQC  QCVCPDDDPC  AAQSTACKQF  YCSSSTGECA  LVYEDTCASQ  KLQFNTTGCL

       670         680         690         700         710         720
SWQCDPDLGC  VRKANGSCCD  DYKDCPTCAK  YDGCDWIGTK  CADSGQVLTS  PIDQADHPDC

       730         740         750         760         770         780
FPSTGLSAGE  TAGITVGIVA  GVTVGVGGAA  GLFGAGYILY  RMLNKPPPPE  QLPTIENLDT

       790         800         810         820         830
EAGTDDNPLF  HKNEIEMTNP  MFSAAGAGGG  GDAGAMFAQG  GGASAVPADL  HTL
```

N.B: Signal peptide = 1 – 21 in GREY

AcMBP chain = 22 – 833 in GREEN, BLUE & YELLOW

Extracellular region of AcMBP in PURPLE, BLUE, YELLOW

DUF4114 = 176 – 254 in BLUE

Cysteine-rich domain = 282 – 701 in YELLOW

168

Transmembrane region of AcMBP in DARK GREEN

Intracellular regions of AcMBP in BRIGHT GREEN

Complete length of AcMBP: 833 a.a

Theoretical pI/Mw of entire AcMBP: 4.41 / 87415.75

(ii) Amino acids residues of full-length (wild type) cDNA extracellular portion C-terminal His Tag codon optimised AcL1.

```
        10         20         30         40         50         60
MYRMQLLSCI ALSLALVTNS GTCNLSGAIK QPGLDCSSTS CSITSGTFPF PLPQGETYDS

        70         80         90        100        110        120
FYSWILGVIG TDGATVNAQY VDYTKADPNI YFTAGQTNCM VNLTFVYEVA FYRNSMGYFT

       130        140        150        160        170        180
FTRDSKPTSV GSVTLKPVFS ETTVDCSRTS SQPLPGTSCL APGSTISLGP FSSTQAVGFY

       190        200        210        220        230        240
LKQDSICSGT TTFYSVDALN KVTSRWKPIP AAHGRMIAVL RDPNTLRAYL GFEDSPDGSD

       250        260        270        280        290        300
SDYNDNVFSV TSNCEIDTSL LPCATVTTCR NSKQTFDSSK CTCSCPNPVT CTAPQVYSTD

       310        320        330        340        350        360
LCACTCPNAT QTCTAPLTWN SATCQCDCPS TKPSGVTCSN LQQWSNVVAT CGCKCPDPAT

       370        380        390        400        410        420
YTCSDNRFVL RTSDCTCNCP STGSCSGNLK WNSANSVCGC QCPSTPPTPC SGNLKWNSTA

       430        440        450        460        470        480
SKCACECPAT AALAGVTCKD KEVWDTASCS CKCPATASAA DTTCPNVNYQ WNYNGKCDCV

       490        500        510        520        530        540
CPATSAEAGI NCTALGLGNT VWDTTACNCA CPPTGTCPGN KVWNPSNDPA KCGCSCPASA

       550        560        570        580        590        600
PAGKECKGNF YWNTSDDVCD CYCPLEAPAD DPCIGYTTWN RTECDCYCPL EPPFEGGCPG

       610        620        630        640        650        660
VQVWDRDQCQ CVCPDDDPCA AQSTACKQFY CSSSTGECAL VYEDTCASQK LQFNTTGCLS

       670        680        690        700        710        720
WQCDPDLGCV RKANGSCCDD YKDCPTCAKY DGCDWIGTKC ADSGQVLTSP IDQADHPDCF

       730
PSTGLSAGET AGHHHHHH
```

Theoretical pI/Mw: 4.59 / 76142.68. Full length (wild type) extracellular AcMBP (known as AcL1) retains the Asp-217 and Asp-220 (red highlights) residues (in the absence of the signal sequence (light blue)). This is designed to preserve both the mannose-binding and Ca^{2+}-binding region of AcMBP.

(iii) Amino acid sequence of mutant full-length (mutant) cDNA extracellular portion C-terminal His Tag codon optimised AcL1DD.

```
        10          20          30          40          50          60
MYRMQLLSCI  ALSLALVTNS  GTCNLSGAIK  QPGLDCSSTS  CSITSGTFPF  PLPQGETYDS

        70          80          90         100         110         120
FYSWILGVIG  TDGATVNAQY  VDYTKADPNI  YFTAGQTNCM  VNLTFVYEVA  FYRNSMGYFT

       130         140         150         160         170         180
FTRDSKPTSV  GSVTLKPVFS  ETTVDCSRTS  SQPLPGTSCL  APGSTISLGP  FSSTQAVGFY

       190         200         210         220         230         240
LKQDSICSGT  TTFYSVDALN  KVTSRWKPIP  AAHGRMIAVL  RDPNTLRAYL  GFEDSPAGSN

       250         260         270         280         290         300
SDYNDNVFSV  TSNCEIDTSL  LPCATVTTCR  NSKQTFDSSK  CTCSCPNPVT  CTAPQVYSTD

       310         320         330         340         350         360
LCACTCPNAT  QTCTAPLTWN  SATCQCDCPS  TKPSGVTCSN  LQQWSNVVAT  CGCKCPDPAT

       370         380         390         400         410         420
YTCSDNRFVL  RTSDCTCNCP  STGSCSGNLK  WNSANSVCGC  QCPSTPPTPC  SGNLKWNSTA

       430         440         450         460         470         480
SKCACECPAT  AALAGVTCKD  KEVWDTASCS  CKCPATASAA  DTTCPNVNYQ  WNYNGKCDCV

       490         500         510         520         530         540
CPATSAEAGI  NCTALGLGNT  VWDTTACNCA  CPPTGTCPGN  KVWNPSNDPA  KCGCSCPASA

       550         560         570         580         590         600
PAGKECKGNF  YWNTSDDVCD  CYCPLEAPAD  DPCIGYTTWN  RTECDCYCPL  EPPFEGGCPG

       610         620         630         640         650         660
VQVWDRDQCQ  CVCPDDDPCA  AQSTACKQFY  CSSSTGECAL  VYEDTCASQK  LQFNTTGCLS

       670         680         690         700         710         720
WQCDPDLGCV  RKANGSCCDD  YKDCPTCAKY  DGCDWIGTKC  ADSGQVLTSP  IDQADHPDCF

       730
PSTGLSAGET  AGHHHHHH
```

Theoretical pI/Mw: 4.64 / 76097.69 (Mutation introduced into full length (wild type) AcMBP (AcL1) at Asp^{217}Ala andAsp^{220}Asn (dark green) (in the absence of the signal sequence (light blue)). This is to produce the full length (mutant) AcL1DD designed to knock out the mannose-binding protein but retain the Ca^{2+}-binding region of AcMBP.

Graphic Summary

Distribution of 1 Blast Hits on the Query Sequence
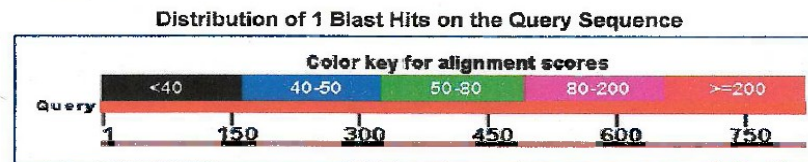
Alignments

Sequence ID: lcl|Query_37607 Length: 823 Number of Matches: 1

Range 1: 1 to 823

Score	Expect	Identities	Gaps	Strand	Frame
1520 bits(823)	0.0()	823/823(100%)	0/823(0%)	Plus/Plus	

Features:

```
Query  1    TGCACCGCCCCTCAGGTGTACTCTACCGACCTGTGCGCCTGCACCTGTCCCAACGCCACC   60
            ||||||||||||||||||||||||||||||||||||||||||||||||||||||||||||
Sbjct  1    TGCACCGCCCCTCAGGTGTACTCTACCGACCTGTGCGCCTGCACCTGTCCCAACGCCACC   60

Query  61   CAGACCTGTACAGCCCCCTGACCTGGAACTCCGCTACCTGCCAGTGCGACTGCCCTTCC   120
            |||||||||||||||||||||||||||||||||||||||||||||||||||||||||||||
Sbjct  61   CAGACCTGTACAGCCCCCTGACCTGGAACTCCGCTACCTGCCAGTGCGACTGCCCTTCC   120

Query  121  ACCAAGCCCTCCGGCGTGACATGCTCCAACCTGCAGCAGTGGTCCAACGTGGTGGCCACC   180
            ||||||||||||||||||||||||||||||||||||||||||||||||||||||||||||
Sbjct  121  ACCAAGCCCTCCGGCGTGACATGCTCCAACCTGCAGCAGTGGTCCAACGTGGTGGCCACC   180

Query  181  TGTGGCTGCAAGTGCCCCGACCCAGCCACCTACACCTGTTCCGACAACAGATTCGTGCTG   240
            ||||||||||||||||||||||||||||||||||||||||||||||||||||||||||||
Sbjct  181  TGTGGCTGCAAGTGCCCCGACCCAGCCACCTACACCTGTTCCGACAACAGATTCGTGCTG   240

Query  241  AGAACCTCCGACTGCACATGCAACTGCCCCTCTACCGGCAGCTGCAGCGGCAACCTGAAG   300
            ||||||||||||||||||||||||||||||||||||||||||||||||||||||||||||
Sbjct  241  AGAACCTCCGACTGCACATGCAACTGCCCCTCTACCGGCAGCTGCAGCGGCAACCTGAAG   300

Query  301  TGGAACAGCGCCAACAGCGTGTGCGGCTGTCAGTGCCCCAGCACCCCTCCTACCCCTTGC   360
            ||||||||||||||||||||||||||||||||||||||||||||||||||||||||||||
Sbjct  301  TGGAACAGCGCCAACAGCGTGTGCGGCTGTCAGTGCCCCAGCACCCCTCCTACCCCTTGC   360

Query  361  TCCGGAAATCTGAAATGGAATTCCACCGCCAGCAAGTGCGCTTGCGAGTGTCCTGCCACC   420
            ||||||||||||||||||||||||||||||||||||||||||||||||||||||||||||
Sbjct  361  TCCGGAAATCTGAAATGGAATTCCACCGCCAGCAAGTGCGCTTGCGAGTGTCCTGCCACC   420

Query  421  GCCGCTCTGGCTGGCGTCACATGTAAAGACAAAGAAGTGTGGGACACCGCCTCTTGCTCT   480
            ||||||||||||||||||||||||||||||||||||||||||||||||||||||||||||
Sbjct  421  GCCGCTCTGGCTGGCGTCACATGTAAAGACAAAGAAGTGTGGGACACCGCCTCTTGCTCT   480

Query  481  TGCAAATGCCCTGCTACCGCCTCCGCCGCTGACACCACATGCCCCAACGTGAACTACCAG   540
            ||||||||||||||||||||||||||||||||||||||||||||||||||||||||||||
Sbjct  481  TGCAAATGCCCTGCTACCGCCTCCGCCGCTGACACCACATGCCCCAACGTGAACTACCAG   540

Query  541  TGGAACTACAATGGCAAGTGTGACTGCGTGTGCCCAGCCACCTCTGCCGAGGCCGGCATC   600
            ||||||||||||||||||||||||||||||||||||||||||||||||||||||||||||
Sbjct  541  TGGAACTACAATGGCAAGTGTGACTGCGTGTGCCCAGCCACCTCTGCCGAGGCCGGCATC   600

Query  601  AATTGCACAGCTCTGGGCCTGGGCAACACCGTGTGGGATACCACCGCCTGTAACTGCGCC   660
            ||||||||||||||||||||||||||||||||||||||||||||||||||||||||||||
Sbjct  601  AATTGCACAGCTCTGGGCCTGGGCAACACCGTGTGGGATACCACCGCCTGTAACTGCGCC   660

Query  661  TGTCCTCCAACCGGAACCTGCCCCGGCAACAAAGTCTGGAACCCCTCCAACGATCCCGCC   720
            ||||||||||||||||||||||||||||||||||||||||||||||||||||||||||||
Sbjct  661  TGTCCTCCAACCGGAACCTGCCCCGGCAACAAAGTCTGGAACCCCTCCAACGATCCCGCC   720

Query  721  AAGTGTGGCTGTTCTTGCCCCGCTTCCGCCCCTGCCGGCAAAGAGTGCAAGGGCAACTTC   780
            ||||||||||||||||||||||||||||||||||||||||||||||||||||||||||||
Sbjct  721  AAGTGTGGCTGTTCTTGCCCCGCTTCCGCCCCTGCCGGCAAAGAGTGCAAGGGCAACTTC   780

Query  781  TACTGGAATACCAGCGACGACGTGTGCGATTGCTACTGCCCCC   823
            ||||||||||||||||||||||||||||||||||||||||||||
Sbjct  781  TACTGGAATACCAGCGACGACGTGTGCGATTGCTACTGCCCCC   823
```

APPENDIX IV - Media, Buffers and Reagents recipes

A. Bovine serum albumin

Bovine serum albumin powder (Europa)..1 g

Deionised water ....10 ml

Dissolve by layering powder onto the surface of liquid-capped tube; rock gently until dissolved. Store at -20 °C.

B. Neff's encystment medium

i.   Prepare 100 ml stock solutions of the underlisted

$CaCl_2.2H_2O$ (Sigma C3306)..0.5 M

$MgSO_4.6H_2O$ (Sigma M2393) ....1 M

$NaHCO_3$ (BDH 10247 4V)..1 M

TRIS (Sigma T1503)...1 M

Phenol red (Sodium salt, Sigma P5530)...1.5 % (w/v)

Autoclave at 121 °C for 15 min

ii.   Add the following into a clean sterile 1000 ml Duran bottle

KCl_2 (Sigma P9541) ....7.46 g (0.1 M)

$MgSO_4$ (1M) ....8 ml (0.008 M)

$NaHCO_3$ (1M) ....1 ml (0.001 M)

TRIS (1M)..20ml (0.02 M)

$CaCl_2$ (0.5 M)..0.4 ml (0.004M)

Phenol red (1.5 % w/v)...25µl

Deionised water...to make up 1000ml

Allow to dissolve and adjust pH 8.8 – 9.0 at 25 °C then filter sterile with a disposable unit (0.22 µm pore size). Store at room temperature for use within 2 months.

C. *Acanthamoeba* axenic growth medium (Ac#6)

i.   Basal medium:

Biosate (BBL: BD 211862)...20.0 g

D-glucose (Sigma, G7021)..5.0 g

KH_2PO_4 (anhydrous: Fluka, 60219)...0.3 g

Vitamin B_{12} (10µg/ml: Sigma, B4051)....................................100 µl

L-Methionine (5 mg/ml: Fluka, 64319)...3 ml

Deionised water...make up to 1000 ml

Aliquot in 250 ml volumes into, sterile labelled Duran bottles and autoclave at 121 °C for 15 min. Store at room temperature for use within 4 weeks

ii.   **N.B:** For use, add to 225 ml of basal medium:

Penicillin + Streptomycin (10,000 U/ml: Sigma, P4333)................................1 ml

Store complete medium at 4 °C and use within 4 weeks

D. Luria Bertani (LB) Broth in 1 Litre

Tryptone...10 g

Yeast Extract..5 g

NaCl...10 g

Deionised water...1 L

Autoclave at 121 °C for 15 min

E. Luria Bertani (LA) Agar in 1 Litre

Tryptone...10 g

Yeast Extract..5 g

NaCl...10 g

Agar No 1...15 g

Deionised water...1 L

Autoclave at 121 °C for 15 min, allow cooling to approximately 50 °C and dispensing unto sterile petri plates. Store at 4 °C.

F. Buffer N1

Tris ....25 mM

NaCl...1 M

pH 7.5

G. Buffer N2

Tris ....25 mM

NaCl...1 M

Imidazole... 20 mM

pH 7.5

H. Buffer N3

Tris ....25 mM

NaCl...1 M

Imidazole... 500 mM

pH 7.5

I. Refolding buffer # 9

Tris-HCl...50 mM

NaCl...9.6 mM

EDTA..1 mM

KCl...0.4 mM

Arginine..0.5 M

Polyethylene glycol (3550)...0.05 %

DTT..1 mM

Allow dissolving and adjusting pH 8.5 at 25 °C then filter sterile with a disposable unit (0.22 μm pore size). Store at 4 °C

APPENDIX V - Suppliers

The Amoebae Laboratory	Department of Infection, Immunity and Inflammation, Maurice Shock Medical Sciences Building, University Road, Leicester, LE1 7RH
ATCC	American Type Culture Collection (ATCC), LGC Standards, Queens Road, Teddington,Middlesex, TW11 0LY, United Kingdom
Bausch & Lomb	Bausch & Lomb U.K. Ltd, 106LondonRoad, Kingston upon Thames, Surrey, KT2 6TN, U.K
BD Biosciences	BD Biosciences, Edmund Halley Road, Oxford Science Park, Oxford, OX4 4DQ, U.K
Eurofins Genomics	Eurofins Genomics, Anzingerstraße 7a, D-85560 Ebersberg
Fisher Scientific UK (NUNC & Nalgene)	Fisher Scientific UK, Bishop Meadow Road, Loughborough, Leicestershire, LE11 5RJ, U.K
Invitrogen	Invitrogen Ltd, 3 Fountain Drive, Inchinnan Business Park, Paisley, PA4 9RF, U.K
Johnson & Johnson	Johnson & Johnson, 1 Johnson & Johnson Plaza, New Brunswick, New Jersey, 08933, USA
Life Technologies	Life Technologies Ltd, 3 Fountain Drive, Inchinnan Business Park, Paisley, PA4 9RF, U.K
Millipore	Millipore, Units 3 & 5, The Courtyards, Hatters Lane, Watford, WD18 8YH, U.K
PNACL	PNACL, The University of Leicester, University Road, Leicester, LE1 7RH, U.K
Promega	Promega UK, Delta House, Chilworth Science Park, Southampton, SO16 7NS, U.K
Qiagen Ltd	Qiagen Ltd, QIAGEN House, Flemming Way, Crawley, W. Sussex, RH10 9NQ, U.K
Sigma-Aldrich	Sigma-Aldrich Company Ltd, The Old Brick Yard, New Road, Gillingham, Dorset, SP8 4XT, U.K

VWR
VWR International Ltd, Hunter Boulevard, Magna Park,
Lutterworth, LE17 4NX, U.K

BIBLIOGRAPHY

ADAM, K. M. G. 1964. The Amino Acid Requirements of Acanthamoeba sp. Neff. *The Journal of Protozoology,* 11**,** 98-100.

ADAMSKA, M. 2016. Molecular Characterization of Acanthamoeba spp. Occurring in Water Bodies and Patients in Poland and Redefinition of Polish T16 Genotype. *Journal of Eukaryotic Microbiology,* 63**,** 262-270.

AHMED KHAN, N. 2003. Pathogenesis of Acanthamoeba infections. *Microbial Pathogenesis,* 34**,** 277-285.

AICHELBURG, A. C., WALOCHNIK, J., ASSADIAN, O., PROSCH, H., STEUER, A., PERNECZKY, G., VISVESVARA, G. S., ASPÖCK, H. & VETTER, N. 2008. Successful Treatment of Disseminated Acanthamoeba sp. Infection with Miltefosine. *Emerging Infectious Diseases,* 14**,** 1743-1746.

AKSOZEK, A., MCCLELLAN, K., HOWARD, K., NIEDERKORN, J. Y. & ALIZADEH, H. 2002a. Resistance of Acanthamoeba castellanii cysts to physical, chemical, and radiological conditions. *J Parasitol,* 88**,** 621-623.

ALLEN, P. G. & DAWIDOWICZ, E. A. 1990. Phagocytosis in Acanthamoeba: I. A mannose receptor is responsible for the binding and phagocytosis of yeast. *Journal of Cellular Physiology,* 145**,** 508-513.

ALSWIED, A. & PAREKH, A. B. 2015. Ca(2+) Influx through Store-operated Calcium Channels Replenishes the Functional Phosphatidylinositol 4,5-Bisphosphate Pool Used by Cysteinyl Leukotriene Type I Receptors. *The Journal of Biological Chemistry,* 290**,** 29555-29566.

AMMERMAN, N. C., BEIER-SEXTON, M. & AZAD, A. F. 2008. Growth and Maintenance of Vero Cell Lines. *Current Protocols in Microbiology,* 11**,** A.4E.1-A.4E.7.

ANDERSON, I. J., WATKINS, R. F., SAMUELSON, J., SPENCER, D. F., MAJOROS, W. H., GRAY, M. W. & LOFTUS, B. J. 2005. Gene discovery in the Acanthamoeba castellanii genome. *Protist,* 156**,** 203-214.

AQEEL, Y., SIDDIQUI, R., MANAN, Z. & KHAN, N. A. 2015. The role of G protein coupled receptor-mediated signaling in the biological properties of Acanthamoeba castellanii of the T4 genotype. *Microbial Pathogenesis,* 81**,** 22-27.

AURAN, J. D., STARR, M. B. & JAKOBIEC, F. A. 1987. Acanthamoeba keratitis. A review of the literature. *Cornea,* 6**,** 2-26.

BACON, A. S., DART, J. K. G., FICKER, L. A., MATHESON, M. M. & WRIGHT, P. 1993b. Acanthamoeba Keratitis: The Value of Early Diagnosis. *Ophthalmology,* 100**,** 1238-1243.

BAND, R. N. & MOHRLOK, S. 1973. The Cell Cycle and Induced Amitosis in Acanthamoeba*. *The Journal of Protozoology,* 20**,** 654-657.

BARBEAU, J. & BUHLER, T. 2001. Biofilms augment the number of free-living amoebae in dental unit waterlines. *Research in Microbiology,* 152**,** 753-760.

BARKER, J. & BROWN, M. R. 1994. Trojan horses of the microbial world: protozoa and the survival of bacterial pathogens in the environment. *Microbiology,* 140 (Pt 6)**,** 1253-1259.

BARKER, J., BROWN, M. R., COLLIER, P. J., FARRELL, I. & GILBERT, P. 1992. Relationship between Legionella pneumophila and Acanthamoeba polyphaga: physiological status and susceptibility to chemical inactivation. *Appl Environ Microbiol,* 58**,** 2420-2425.

BEATTIE, T. K., SEAL, D. V., TOMLINSON, A., MCFADYEN, A. K. & GRIMASON, A. M. 2003. Determination of amoebicidal activities of multipurpose contact lens solutions by using a most probable number enumeration technique. *J Clin Microbiol,* 41**,** 2992-3000.

BÍNOVÁ, E., BÍNA, D., ASHFORD, D. A., THOMAS-OATES, J. & NOHÝNKOVÁ, E. 2017. Trehalose During Two Stress Responses in Acanthamoeba: Differentiation Between Encystation and Pseudocyst Formation. *Protist,* 168**,** 649-662.

BLACKMAN, H. J., RAO, N. A., LEMP, M. A. & VISVESVARA, G. S. 1984. Acanthamoeba keratitis successfully treated with penetrating keratoplasty: suggested immunogenic mechanisms of action. *Cornea,* 3**,** 125-130.

BLANTON, W. E. & VILLEMEZ, C. L. 1978. Molecular Size and Chain Length Distribution in Acanthamoeba Cellulose*. *The Journal of Protozoology,* 25**,** 264-267.

BONILLA-LEMUS, P., CABALLERO VILLEGAS, A. S., CARMONA JIMÉNEZ, J. & LUGO VÁZQUEZ, A. 2014a. Occurrence of free-living amoebae in streams of the Mexico Basin. *Experimental Parasitology,* 145**,** S28-S33.

BONILLA-LEMUS, P., RAMÍREZ-BAUTISTA, G. A., ZAMORA-MUÑOZ, C., IBARRA-MONTES, M. D. R., RAMÍREZ-FLORES, E. & HERNÁNDEZ-MARTÍNEZ, M. D. 2010. Acanthamoeba spp. in domestic tap water in houses of contact lens wearers in the metropolitan area of Mexico City. *Experimental Parasitology,* 126**,** 54-58.

BOOTON, G. C., VISVESVARA, G. S., BYERS, T. J., KELLY, D. J. & FUERST, P. A. 2005. Identification and distribution of Acanthamoeba species genotypes associated with nonkeratitis infections. *J Clin Microb,* 43(4), 1689 - 1693.

BOWERS, B. & KORN, E. D. 1969. The fine structure of Acanthamoeba castellanii (Neff strain). II. Encystment. *J Cell Biol,* 41**,** 786-805.

BREWITT, H. 1997. [Contact lenses. Infections and hygiene]. *Ophthalmologe,* 94**,** 311-316.

BROWN, A. C., ROSS, J., JONES, D. B., COLLIER, S. A., AYERS, T. L., HOEKSTRA, R. M., BACKENSEN, B., ROY, S. L., BEACH, M. J. & YODER,

J. S. 2017. Risk Factors for Acanthamoeba Keratitis-A Multistate Case-Control Study, 2008-2011. *Eye Contact Lens*. .0000000000000365. [Epub ahead of print]

BURGER, G., PLANTE, I., LONERGAN, K. M. & GRAY, M. W. 1995. The mitochondrial DNA of the amoeboid protozoon, Acanthamoeba castellanii: complete sequence, gene content and genome organization. *J Mol Biol,* 245(5):522-537.

BYERS, T. J., KIM, B. G., KING, L. E. & HUGO, E. R. 1991. Molecular Aspects of the Cell Cycle and Encystment of Acanthamoeba. *Reviews of Infectious Diseases,* 13**,** S373-S384.

CAO, Z., JEFFERSON, D. M. & PANJWANI, N. 1998. Role of carbohydrate-mediated adherence in cytopathogenic mechanisms of Acanthamoeba. *J Biol Chem,* 273**,** 15838-15845.

CARNT, N. & STAPLETON, F. 2016. Strategies for the prevention of contact lens-related Acanthamoeba keratitis: a review. *Ophthalmic Physiol Opt,* 36**,** 77-92.

CARRIJO-CARVALHO, L. C., SANT'ANA, V. P., FORONDA, A. S., DE FREITAS, D. & DE SOUZA CARVALHO, F. R. 2017. Therapeutic agents and biocides for ocular infections by free-living amoebae of Acanthamoeba genus. *Survey of Ophthalmology,* 62**,** 203-218.

CASERO, R., MONGI, F., LACONTE, L., RIVERO, F., SASTRE, D., TEHERÁN, A., HERRERA, G. & RAMÍREZ, J. D. 2017. *Molecular and morphological characterization of Acanthamoeba isolated from corneal scrapes and contact lens wearers in Argentina*. 54:170-175.

CENTRE FOR DISEASE CONTROL AND PREVENTION, 2016. Pathogens and Environment. U.S. Department of of Health & Human services.

CHÁVEZ-MUNGUÍA, B., OMAÑA-MOLINA, M., GONZÁLEZ-LÁZARO, M., GONZÁLEZ-ROBLES, A., BONILLA, P. & MARTÍNEZ-PALOMO, A. 2005. Ultrastructural Study of Encystation and Excystation in Acanthamoeba castellanii. *Journal of Eukaryotic Microbiology,* 52**,** 153-158.

CHÁVEZ-MUNGUÍA, B., SALAZAR-VILLATORO, L., LAGUNES-GUILLÉN, A., OMAÑA-MOLINA, M., ESPINOSA-CANTELLANO, M. & MARTÍNEZ-PALOMO, A. 2013. Acanthamoeba castellanii cysts: new ultrastructural findings. *Parasitology Research,* 112**,** 1125-1130.

CLARKE, B., SINHA, A., PARMAR, D. N. & SYKAKIS, E. 2012. Advances in the Diagnosis and Treatment of Acanthamoeba Keratitis. *Journal of Ophthalmology,* 2012**,** 6.

CLARKE, D. W., ALIZADEH, H. & NIEDERKORN, J. Y. 2006. Intracorneal instillation of latex beads induces macrophage-dependent protection against Acanthamoeba keratitis. *Investigative Ophthalmology & Visual Science,* 47**,** 4917-4925.

CLARKE, D. W. & NIEDERKORN, J. Y. 2006a. The immunobiology of Acanthamoeba keratitis. *Microbes Infect,* 8**,** 1400-1405.

CLARKE, D. W. & NIEDERKORN, J. Y. 2006b. The pathophysiology of Acanthamoeba keratitis. *Trends Parasitol,* 22**,** 175-180.

CLARKE, M., LOHAN, A. J., LIU, B., LAGKOUVARDOS, I., ROY, S., ZAFAR, N., BERTELLI, C., SCHILDE, C., KIANIANMOMENI, A., BURGLIN, T. R., FRECH, C., TURCOTTE, B., KOPEC, K. O., SYNNOTT, J. M., CHOO, C., PAPONOV, I., FINKLER, A., HENG TAN, C. S., HUTCHINS, A. P., WEINMEIER, T., RATTEI, T., CHU, J. S., GIMENEZ, G., IRIMIA, M., RIGDEN, D. J., FITZPATRICK, D. A., LORENZO-MORALES, J., BATEMAN, A., CHIU, C. H., TANG, P., HEGEMANN, P., FROMM, H., RAOULT, D., GREUB, G., MIRANDA-SAAVEDRA, D., CHEN, N., NASH, P., GINGER, M. L., HORN, M., SCHAAP, P., CALER, L. & LOFTUS, B. J. 2013. Genome of Acanthamoeba castellanii highlights extensive lateral gene transfer and early evolution of tyrosine kinase signaling. *Genome Biol,* 14**,** R11.

CONNELL, C., RUTTER, A., HILL, B., SULLER, M. & LLOYD, D. 2001. Encystation of Acanthamoeba castellanii: Dye uptake for assessment by flow cytometry and confocal laser scanning microscopy. *Journal of Applied Microbiology,* 90**,** 706-712.

CORSARO, D., PAGES, G. S., CATALAN, V., LORET, J.-F. & GREUB, G. 2010. Biodiversity of amoebae and amoeba-associated bacteria in water treatment plants. *International Journal of Hygiene and Environmental Health,* 213**,** 158-166.

CORSARO, D. & VENDITTI, D. 2010. Phylogenetic evidence for a new genotype of Acanthamoeba (Amoebozoa, Acanthamoebida). *Parasitol Res,* 107**,** 233-238.

CORSARO, D., WALOCHNIK, J., KÖHSLER, M. & ROTT, M. B. 2015. Acanthamoeba misidentification and multiple labels: redefining genotypes T16, T19, and T20 and proposal for Acanthamoeba micheli sp. nov. (genotype T19). *Parasitology Research,* 114**,** 2481-2490.

COSTA, A. O., FURST, C., ROCHA, L. O., CIRELLI, C., CARDOSO, C. N., NEIVA, F. S., POSSAMAI, C. O., DE ASSIS SANTOS, D. & THOMAZ-SOCCOL, V. 2017. Molecular diagnosis of Acanthamoeba keratitis: evaluation in rat model and application in suspected human cases. *Parasitol Res,* 116**,** 1339-1344.

COSTAS, M., EDWARDS, S. W., LLOYD, D., GRIFFITHS, A. J. & TURNER, G. 1983. Restriction enzyme analysis of mitochondrial DNA of members of the genus Acanthamoeba as an aid in taxonomy. *FEMS Microbiology Letters,* 17**,** 231-234.

DA ROCHA-AZEVEDO, B., TANOWITZ, H. B. & MARCIANO-CABRAL, F. 2009. Diagnosis of infections caused by pathogenic free-living amoebae. *Interdiscip Perspect Infect Dis,* 2009**,** 251406.

DART, J. K., SAW, V. P. & KILVINGTON, S. 2009. Acanthamoeba keratitis: diagnosis and treatment update 2009. *Am J Ophthalmol,* 148**,** 487-499 e2.

DE JONCKHEERE, J. F. 1980. Growth characteristics, cytopathic effect in cell culture, and virulence in mice of 36 type strains belonging to 19 different Acanthamoeba spp. *Appl Environ Microbiol,* 39**,** 681-685.

DE JONCKHEERE, J. F. 2002. A century of research on the Amoeboflagellate Genus Naegleria. *Acta Protozool,* 41, 309 - 342.

DE PASCALE, G., CUTULI, S. L., PENNISI, M. A. & ANTONELLI, M. 2013. The Role of Mannose-Binding Lectin in Severe Sepsis and Septic Shock. *Mediators of Inflammation,* 2013**,** 8.

DEARBORN, D. G. & KORN, E. D. 1974. Lipophophonoglycan of the plasma membrane of Acanthamoeba castellanii, fatty acid composition. *J Biol Chem,* 249.

DOBROWSKY, P. H., KHAN, S. & KHAN, W. 2017. Resistance of Legionella and Acanthamoeba mauritaniensis to heat treatment as determined by relative and quantitative polymerase chain reactions. *Environ Res,* 158**,** 82-93.

DRICKAMER, K. 1993. Evolution of Ca2+-dependent Animal Lectins11Abbreviations: CRD, carbohydrate-recognition domain; EGF, epidermal growth factor. *In:* COHN, W. E. & MOLDAVE, K. (eds.) *Progress in Nucleic Acid Research and Molecular Biology.* Academic Press. 9, 237-264

DUARTE, J. L., FURST, C., KLISIOWICZ, D. R., KLASSEN, G. & COSTA, A. O. 2013. Morphological, genotypic, and physiological characterization of Acanthamoeba isolates from keratitis patients and the domestic environment in Vitoria, Espírito Santo, Brazil. *Experimental Parasitology,* 135**,** 9-14.

DUDLEY, R., JARROLL, E. L. & KHAN, N. A. 2009. Carbohydrate analysis of Acanthamoeba castellanii. *Exp Parasitol,* 122 (4); 338 - 343.

EISEN, D. P., DEAN, M. M., THOMAS, P., MARSHALL, P., GERNS, N., HEATLEY, S., QUINN, J., MINCHINTON, R. M. & LIPMAN, J. 2006. Low mannose-binding lectin function is associated with sepsis in adult patients. *FEMS Immunology & Medical Microbiology,* 48**,** 274-282.

EKLÖV, S., NILSSON, S., LARSON, A., BJÖRK, P. & HARTLEY-ASP, B. 1992. Evidence for a non-estrogenic cytostatic effect of estramustine on human prostatic carcinoma cells in vivo. *The Prostate,* 20**,** 43-50.

EL-SAYED, N. M., YOUNIS, M. S., ELHAMSHARY, A. M., ABD-ELMABOUD, A. I. & KISHIK, S. M. 2014. Acanthamoeba DNA can be directly amplified from corneal scrapings. *Parasitology Research,* 113**,** 3267-3272.

ELBASHIR, S. M., HARBORTH, J., LENDECKEL, W., YALCIN, A., WEBER, K. & TUSCHL, T. 2001. Duplexes of 21-nucleotide RNAs mediate RNA interference in cultured mammalian cells. *Nature,* 411**,** 494.

ELBEIN, A. D., PAN, Y. T., PASTUSZAK, I. & CARROLL, D. 2003. New insights on trehalose: a multifunctional molecule. *Glycobiology,* 13**,** 17R-27R.

ELDER, M. J., KILVINGTON, S. & DART, J. K. 1994. A clinicopathologic study of in vitro sensitivity testing and Acanthamoeba keratitis. *Invest Ophthalmol Vis Sci,* 35**,** 1059-1064.

ELIAS, M., DUPUY, J., MERONE, L., LECOMTE, C., ROSSI, M., MASSON, P., MANCO, G. & CHABRIERE, E. 2007. Crystallization and preliminary X-ray diffraction analysis of the hyperthermophilic Sulfolobus solfataricus phosphotriesterase. *Acta Crystallographica Section F: Structural Biology and Crystallization Communications,* 63**,** 553-555.

EVANS, G. A. Molecular cloning: A laboratory manual. Second edition. Volumes 1, 2, and 3. Current protocols in molecular biology. Volumes 1 and 2. *Cell,* 61**,** 17-18.

FABRES LAURA, F., ROSA DOS SANTOS SAYONARA, P., BENITEZ LISIANNE, B. & ROTT MARILISE, B. 2016. Isolation and identification of Acanthamoeba spp. from thermal swimming pools and spas in Southern Brazil. *Acta Parasitologica.* https://doi.org/10.1515/ap-2016-0031.

FOUQUE, E., TROUILHÉ, M.-C., THOMAS, V., HARTEMANN, P., RODIER, M.-H. & HÉCHARD, Y. 2012. Cellular, Biochemical, and Molecular Changes during Encystment of Free-Living Amoebae. *Eukaryotic Cell,* 11**,** 382-387.

FUERST, P. A., BOOTON, G. C. & CRARY, M. 2015. Phylogenetic Analysis and the Evolution of the 18S rRNA Gene Typing System of Acanthamoeba. *Journal of Eukaryotic Microbiology,* 62**,** 69-84.

GARATE, M., CAO, Z., BATEMAN, E. & PANJWANI, N. 2004. Cloning and characterization of a novel mannose-binding protein of Acanthamoeba. *J Biol Chem,* 279, 29849-29856.

GARATE, M., CUBILLOS, I., MARCHANT, J. & PANJWANI, N. 2005. Biochemical characterization and functional studies of Acanthamoeba mannose-binding protein. *Infect Immun,* 73**,** 5775-5781.

GARATE, M., MARCHANT, J., CUBILLOS, I., CAO, Z., KHAN, N. A. & PANJWANI, N. 2006. In vitro pathogenicity of Acanthamoeba is associated with the expression of the mannose-binding protein. *Invest Ophthalmol Vis Sci,* 47**,** 1056-1062.

GARCÍA, A., GOÑI, P., CLAVEL, A., LOBEZ, S., FERNANDEZ, M. T. & ORMAD, M. P. 2011. Potentially pathogenic free-living amoebae (FLA) isolated in Spanish wastewater treatment plants. *Environmental Microbiology Reports,* 3**,** 622-626.

GAST, R. J. 2001. Development of an Acanthamoeba-specific reverse dot-blot and the discovery of a new ribotype. *J Eukaryot Microbiol,* 48**,** 609-615.

GAST, R. J., FUERST, P. A. & BYERS, T. J. 1994. Discovery of group I introns in the nuclear small subunit ribosomal RNA genes of Acanthamoeba. *Nucleic Acids Res,* 22**,** 592-596.

GAST, R. J., LEDEE, D. R., FUERST, P. A. & BYERS, T. J. 1996a. Subgenus Systematics of Acanthamoeba: Four Nuclear 18S rDNA Sequence Types. *Journal of Eukaryotic Microbiology,* 43**,** 498-504.

GELMAN, B. B., RAUF, S. J., NADER, R., POPOV, V., BORKOWSKI, J., CHALJUB, G., NAUTA, H. W. & VISVESVARA, G. S. 2001. Amoebic encephalitis due to Sappinia diploidea. *J Am Med Assoc,* 285 (19);2450 - 2451.

GIMÉNEZ, F., SURYAWANSHI, A. & ROUSE, B. T. 2013. Pathogenesis of herpes stromal keratitis – A focus on corneal neovascularization. *Progress in Retinal and Eye Research,* 33**,** 1-9.

GLASER, K. C., HETRICK, N. D. & MOLESTINA, R. E. 2011. Evidence for a previously unrecognized mycobacterial endosymbiont in Acanthamoeba castellanii strain Ma (ATCC (R) 50370). *J Eukaryot Microbiol,* 58**,** 75-76.

GOMES, T. D. S., MAGNET, A., IZQUIERDO, F., VACCARO, L., REDONDO, F., BUENO, S., SÁNCHEZ, M. L., ANGULO, S., FENOY, S., HURTADO, C. & DEL AGUILA, C. 2016. Acanthamoeba spp. in Contact Lenses from Healthy Individuals from Madrid, Spain. *PLOS ONE,* 11**,** e0154246.

GONZÁLEZ-ROBLES, A., SALAZAR-VILLATORO, L., OMAÑA-MOLINA, M., REYES-BATLLE, M., MARTÍN-NAVARRO, C. M. & LORENZO-MORALES, J. 2014. Morphological Features and In Vitro Cytopathic Effect of Acanthamoeba griffini Trophozoites Isolated from a Clinical Case. *Journal of Parasitology Research,* 2014**,** 256310.

GREENFIELD, D., MCEVOY, A. L., SHROFF, H., CROOKS, G. E., WINGREEN, N. S., BETZIG, E. & LIPHARDT, J. 2009. Self-Organization of the Escherichia coli Chemotaxis Network Imaged with Super-Resolution Light Microscopy. *PLOS Biology,* 7**,** e1000137.

GREUB, G. & RAOULT, D. 2004b. Microorganisms resistant to free-living amoebae. *Clin Microbiol Rev,* 17**,** 413-433.

GROUT, B., MORRIS, J. & MCLELLAN, M. Cryopreservation and the maintenance of cell lines. *Trends in Biotechnology,* 8**,** 293-297.

GUIMARAES, A. J., GOMES, K. X., CORTINES, J. R., PERALTA, J. M. & PERALTA, R. H. 2016. Acanthamoeba spp. as a universal host for pathogenic microorganisms: One bridge from environment to host virulence. *Microbiol Res,* 193**,** 30-38.

HALL, M. O., BURGESS, B. L., ARAKAWA, H. & FLIESLER, S. J. 1990. The effect of inhibitors of glycoprotein synthesis and processing on the phagocytosis of rod outer segments by cultured retinal pigment epithelial cells. *Glycobiology,* 1**,** 51-61.

HARB, O. S., GAO, L.-Y. & KWAIK, Y. A. 2000. From protozoa to mammalian cells: a new paradigm in the life cycle of intracellular bacterial pathogens. *Environmental Microbiology,* 2**,** 251-265.

HAU, S. C., DART, J. K. G., VESALUOMA, M., PARMAR, D. N., CLAERHOUT, I., BIBI, K. & LARKIN, D. F. P. 2010. Diagnostic accuracy of microbial keratitis with in vivo scanning laser confocal microscopy. *British Journal of Ophthalmology,* 94**,** 982-987.

HEASELGRAVE, W. & KILVINGTON, S. 2016. The Characterization of an Adrenergic Signalling System Involved in the Encystment of the Ocular Pathogen Acanthamoeba spp. *J Eukaryot Microbiol,* 63**,** 629-634.

HENRIQUEZ, F. L. 2009. Khan NA: Acanthamoeba: Biology and Pathogenesis. *Parasites & Vectors,* 2**,** 16.

HEWETT, M. K., ROBINSON, B. S., MONIS, P. T. & SAINT, C. P. 2003. Identification of a New *Acanthamoeba* 18S rRNA Gene Sequence Type, Corresponding to the Species *Acanthamoeba jacobsi* Sawyer, Nerad and Visvesvara, 1992 (Lobosea: Acanthamoebidae). *Acta Protozoologica,* 42**,** 325-329.

HIRUKAWA, Y., NAKATO, H., IZUMI, S., TSURUHARA, T. & TOMINO, S. 1998. Structure and expression of a cyst specific protein of Acanthamoeba castellanii. *Biochim Biophys Acta,* 1398**,** 47-56.

HORN, M., FRITSCHE, T. R., GAUTOM, R. K., SCHLEIFER, K. H. & WAGNER, M. 1999. Novel bacterial endosymbionts of Acanthamoeba spp. related to the Paramecium caudatum symbiont Caedibacter caryophilus. *Environ Microbiol,* 1**,** 357-367.

HUGHES, R., ANDREW, P. W. & KILVINGTON, S. 2003a. Enhanced Killing of Acanthamoeba Cysts with a Plant Peroxidase-Hydrogen Peroxide-Halide Antimicrobial System. *Applied and Environmental Microbiology,* 69**,** 2563-2567.

HUGHES, R., DART, J. & KILVINGTON, S. 2003b. Activity of the amidoamine myristamidopropyl dimethylamine against keratitis pathogens. *Journal of Antimicrobial Chemotherapy,* 51**,** 1415-1418.

HUGHES, R., HEASELGRAVE, W. & KILVINGTON, S. 2003c. Acanthamoeba polyphaga Strain Age and Method of Cyst Production Influence the Observed Efficacy of Therapeutic Agents and Contact Lens Disinfectants. *Antimicrobial Agents and Chemotherapy,* 47**,** 3080-3084.

HUGHES, R. & KILVINGTON, S. 2001. Comparison of hydrogen peroxide contact lens disinfection systems and solutions against Acanthamoeba polyphaga. *Antimicrob Agents Chemother,* 45**,** 2038-2043.

HURT, M., APTE, S., LEHER, H., HOWARD, K., NIEDERKORN, J. & ALIZADEH, H. 2001. Exacerbation of Acanthamoeba Keratitis in Animals Treated with Anti-Macrophage Inflammatory Protein 2 or Antineutrophil Antibodies. *Infection and Immunity,* 69**,** 2988-2995.

HURT, M., NEELAM, S., NIEDERKORN, J. & ALIZADEH, H. 2003. Pathogenic Acanthamoeba spp. Secrete a Mannose-Induced Cytolytic Protein That Correlates with the Ability To Cause Disease. *Infection and Immunity,* 71**,** 6243-6255.

HUTH, S., REVEREY, J. F., LEIPPE, M. & SELHUBER-UNKEL, C. 2017. Adhesion forces and mechanics in mannose-mediated acanthamoeba interactions. *PLoS One,* 12**,** e0176207.

ILLINGWORTH, C. D. & COOK, S. D. 1998. Acanthamoeba keratitis. *Surv Ophthalmol,* 42**,** 493-508.

IMAYASU, M., TCHEDRE, K. T. & CAVANAGH, H. D. 2013. Effects of multipurpose solutions on the viability and encystment of acanthamoeba determined by flow cytometry. *Eye Contact Lens,* 39**,** 228-233.

IMBERT-BOUYER, S., MERLAUD, A., IMBERT, C., DANIAULT, G. & RODIER, M.-H. 2004. A mannose binding protein is involved in the adherence of Acanthamoeba species to inert surfaces. *FEMS Microbiology Letters,* 238**,** 207-211.

IOVIENO, A., GORE, D. M., CARNT, N. & DART, J. K. 2014. Acanthamoeba sclerokeratitis: epidemiology, clinical features, and treatment outcomes. *Ophthalmology,* 121**,** 2340-2347.

JAGER, B. V. & STAMM, W. P. 1972. BRAIN ABSCESSES CAUSED BY FREE-LIVING AMŒBA PROBABLY OF THE GENUS HARTMANNELLA IN A PATIENT WITH HODGKIN'S DISEASE. *The Lancet,* 300**,** 1343-1345.

JAISON, P. L., CAO, Z. & PANJWANI, N. 2009. Binding ofAcanthamoebato 23 mannose-glycoproteins of corneal epithelium: effect of injury. *Current Eye Research,* 17**,** 770-776.

JEONG, H. J. & YU, H. S. 2005. The role of domestic tap water in Acanthamoeba contamination in contact lens storage cases in Korea. *Korean J Parasitol,* 43**,** 47-50.

JEUDY, S., COUTARD, B., LEBRUN, R. & ABERGEL, C. 2005. Acanthamoeba polyphaga mimivirus NDK: preliminary crystallographic analysis of the first viral nucleoside diphosphate kinase. *Acta Crystallographica Section F,* 61**,** 569-572.

JIANG, C., SUN, X., WANG, Z. & ZHANG, Y. 2015. Acanthamoeba keratitis: clinical characteristics and management. *Ocul Surf,* 13**,** 164-168.

JONES, D. B. 1979. Initial therapy of suspected microbial corneal ulcers: II. Specific antibiotic therapy based on corneal smears. *Survey of Ophthalmology,* 24**,** 97-116.

JOSLIN, C. E., TU, E. Y., MCMAHON, T. T., PASSARO, D. J., STAYNER, L. T. & SUGAR, J. 2006. Epidemiological characteristics of a Chicago-area Acanthamoeba keratitis outbreak. *Am J Ophthalmol,* 142**,** 212-217.

KAO, P.-M., HSU, B.-M., CHEN, N.-H., HUANG, K.-H., HUANG, C.-C., JI, D.-D., CHEN, J.-S., LIN, W.-C., HUANG, S.-W. & CHIU, Y.-C. 2012. Molecular detection and comparison of Acanthamoeba genotypes in different functions of watersheds in Taiwan. *Environmental Monitoring and Assessment,* 184**,** 4335-4344.

KARABENCHEVA, T. & CHRISTOV, C. 2010. Mechanisms of protein circular dichroism: insights from computational modeling. *Adv Protein Chem Struct Biol,* 80**,** 85-115.

KHAN, N. A. 2001. Pathogenicity, Morphology, and Differentiation of Acanthamoeba. *Current Microbiology,* 43**,** 391-395.

KHAN, N. A. 2006a. Acanthamoeba: Biology and increasing importance in human health. *FEMS Microbiology Reviews,* 30**,** 564-595.

KHAN, N. A., GREENMAN, J., TOPPING, K. P., HOUGH, V. C., TEMPLE, G. S. & PAGET, T. A. 2000. Isolation of Acanthamoeba-specific antibodies from a bacteriophage display library. *J Clin Microbiol,* 38**,** 2374-2377.

KHAN, N. A., JARROLL, E. L. & PAGET, T. A. 2001. Acanthamoeba can be differentiated by the polymerase chain reaction and simple plating assays. *Curr Microbiol,* 43**,** 204-208.

KHAN, N. A. & SIDDIQUI, R. 2009. Acanthamoeba affects the integrity of human brain microvascular endothelial cells and degrades the tight junction proteins. *Int J Parasitol,* 39(14); 1611 - 1616.

KHUNKITTI, HANN, LLOYD, FURR & RUSSELL 1998. Biguanide-induced changes in Acanthamoeba castellanii: an electron microscopic study. *Journal of Applied Microbiology,* 84**,** 53-62.

KILVINGTON, S. 1991. Moist-Heat Disinfection of Acanthamoeba Cysts. *Reviews of Infectious Diseases,* 13**,** S418-S418.

KILVINGTON, S. 1993. Acanthamoeba trophozoite and cyst adherence to four types of soft contact lens and removal by cleaning agents. *Eye,* 7**,** 535.

KILVINGTON, S. 2004. Acanthamoeba Keratitis: The Role of Domestic Tap Water Contamination in the United Kingdom. *Investigative Ophthalmology & Visual Science,* 45**,** 165-169.

KILVINGTON, S., HEASELGRAVE, W., LALLY, J. M., AMBRUS, K. & POWELL, H. 2008. Encystment of Acanthamoeba during incubation in multipurpose contact lens disinfectant solutions and experimental formulations. *Eye Contact Lens,* 34**,** 133-139.

KILVINGTON, S. & LAM, A. 2013. Development of standardized methods for assessing biocidal efficacy of contact lens care solutions against Acanthamoeba trophozoites and cysts. *Invest Ophthalmol Vis Sci,* 54**,** 4527-4537.

KILVINGTON, S. & PRICE, J. 1990. Survival of Legionella pneumophila within cysts of Acanthamoeba polyphaga following chlorine exposure. *Journal of Applied Bacteriology,* 68**,** 519-525.

KILVINGTON, S. & WHITE, D. G. 1994. Acanthamoeba: biology, ecology and human disease. *Reviews in Medical Microbiology,* 5**,** 12-26.

KIM, J.-H., MATIN, A., SHIN, H.-J., PARK, H., YOO, K.-T., YUAN, X.-Z., KIM, K. S. & JUNG, S.-Y. 2012a. Functional roles of mannose-binding protein in the adhesion, cytotoxicity and phagocytosis of Acanthamoeba castellanii. *Experimental Parasitology,* 132**,** 287-292.

KIM, J. H., MATIN, A., SHIN, H. J., PARK, H., YOO, K. T., YUAN, X. Z., KIM, K. S. & JUNG, S. Y. 2012b. Functional roles of mannose-binding protein in the adhesion, cytotoxicity and phagocytosis of Acanthamoeba castellanii. *Experimental Parasitology,* 132**,** 287-292.

KLIESCIKOVA, J., KULDA, J. & NOHYNKOVA, E. 2011. Stress-Induced Pseudocyst Formation - A Newly Identified Mechanism of Protection against Organic Solvents in Acanthamoebae of the T4 Genotype. *Protist,* 162**,** 58-69.

KORN, E. D., DEARBORN, D. G. & WRIGHT, P. L. 1974. Lipophosphonoglycan of the Plasma Membrane of Acanthamoeba castellanii : ISOLATION FROM WHOLE AMOEBAE AND IDENTIFICATION OF THE WATER-SOLUBLE PRODUCTS OF ACID HYDROLYSIS. *Journal of Biological Chemistry,* 249**,** 3335-3341.

KRISHNA MURTI, C. R. & SHUKLA, O. P. 1984. Differentiation of pathogenic amoebae: encystation and excystation ofAcanthamoeba culbertsoni — A model. *Journal of Biosciences,* 6**,** 475-489.

KU, J. Y., CHAN, F. M. & BECKINGSALE, P. 2009. Acanthamoeba keratitis cluster: an increase in Acanthamoeba keratitis in Australia. *Clin Exp Ophthalmol,* 37, 181 - 190.

LAKHUNDI, S., SIDDIQUI, R. & KHAN, N. A. 2015. Cellulose degradation: a therapeutic strategy in the improved treatment of Acanthamoeba infections. *Parasit Vectors,* 8**,** 23.

LAMEIGNERE, E., MALINOVSKÁ, L., SLÁVIKOVÁ, M., DUCHAUD, E., MITCHELL, EDWARD P., VARROT, A., ŠEDO, O., IMBERTY, A. & WIMMEROVÁ, M. 2008. Structural basis for mannose recognition by a lectin from opportunistic bacteria Burkholderia cenocepacia. *Biochemical Journal,* 411**,** 307-318.

LANDELL, M. F., SALTON, J., CAUMO, K., BROETTO, L. & ROTT, M. B. 2013. Isolation and genotyping of free-living environmental isolates of Acanthamoeba spp. from bromeliads in Southern Brazil. *Experimental Parasitology,* 134**,** 290-294.

LARKIN, D. F., KILVINGTON, S. & EASTY, D. L. 1990. Contamination of contact lens storage cases by Acanthamoeba and bacteria. *Br J Ophthalmol,* 74**,** 133-135.

LASS, A., GUERRERO, M., LI, X., KARANIS, G., MA, L. & KARANIS, P. 2017. Detection of Acanthamoeba spp. in water samples collected from natural water reservoirs, sewages, and pharmaceutical factory drains using LAMP and PCR in China. *Sci Total Environ,* 584-585**,** 489-494.

LAU, Y. L., CHAN, S. Y., TURNER, M. W., FONG, J. & KARLBERG, J. 1995. Mannose-binding protein in preterm infants: developmental profile and clinical significance. *Clinical & Experimental Immunology,* 102**,** 649-654.

LEHER, H. F., ALIZADEH, H., TAYLOR, W. M., SHEA, A. S., SILVANY, R. S., VAN KLINK, F., JAGER, M. J. & NIEDERKORN, J. Y. 1998. Role of mucosal IgA in the resistance to Acanthamoeba keratitis. *Investigative Ophthalmology & Visual Science,* 39**,** 2666-2673.

LEHMANN, O. J., GREEN, S. M., MORLET, N., KILVINGTON, S., KEYS, M. F., MATHESON, M. M., DART, J. K., MCGILL, J. I. & WATT, P. J. 1998. Polymerase chain reaction analysis of corneal epithelial and tear samples in the diagnosis of Acanthamoeba keratitis. *Invest Ophthalmol Vis Sci,* 39**,** 1261-1265.

LIM, C. H., CARNT, N. A., FAROOK, M., LAM, J., TAN, D. T., MEHTA, J. S. & STAPLETON, F. 2016. Risk factors for contact lens-related microbial keratitis in Singapore. *Eye (Lond),* 30**,** 447-455.

LORENZO-MORALES, J., KHAN, N. A. & WALOCHNIK, J. 2015. An update on Acanthamoeba keratitis: Diagnosis, pathogenesis and treatment. *Parasite,* 22.

LORENZO-MORALES, J., KLIESCIKOVA, J., MARTINEZ-CARRETERO, E., DE PABLOS, L. M., PROFOTOVA, B., NOHYNKOVA, E., OSUNA, A. & VALLADARES, B. 2008. Glycogen Phosphorylase in Acanthamoeba spp.: Determining the Role of the Enzyme during the Encystment Process Using RNA Interference. *Eukaryotic Cell,* 7**,** 509-517.

LORENZO-MORALES, J., MARTIN-NAVARRO, C. M., LOPEZ-ARENCIBIA, A., ARNALICH-MONTIEL, F., PINERO, J. E. & VALLADARES, B. 2013. Acanthamoeba keratitis: an emerging disease gathering importance worldwide? *Trends Parasitol,* 29**,** 181-187.

LORENZO-MORALES, J., MARTÍN-NAVARRO, C. M., LÓPEZ-ARENCIBIA, A., SANTANA-MORALES, M. A., AFONSO-LEHMANN, R. N., MACIVER, S. K., VALLADARES, B. & MARTÍNEZ-CARRETERO, E. 2010. Therapeutic potential of a combination of two gene-specific small interfering RNAs against clinical strains of Acanthamoeba. *Antimicrob Agents Chemother,* 54(12); 5151 - 5155.

LY, T. M. & MULLER, H. E. 1990. Ingested Listeria monocytogenes survive and multiply in protozoa. *J Med Microbiol,* 33**,** 51-54.

MA, P., VISVESVARA, G. S., MARTINEZ, A. J., THEODORE, F. H., DAGGETT, P.-M. & SAWYER, T. K. 1990a. Naegleria and Acanthamoeba Infections: Review. *Reviews of Infectious Diseases,* 12**,** 490-513.

MA, P., VISVESVARA, G. S., MARTINEZ, A. J., THEODORE, F. H., DAGGETT, P. M. & SAWYER, T. K. 1990b. Naegleria and Acanthamoeba infections: review. *Rev Infect Dis,* 12**,** 490-513.

MAGNET, A., HENRIQUES-GIL, N., GALVÁN-DIAZ, A. L., IZQUIEDO, F., FENOY, S. & DEL AGUILA, C. 2014. Novel Acanthamoeba 18S rRNA gene sequence type from an environmental isolate. *Parasitology Research,* 113**,** 2845-2850.

MARCHENKO, N. R. & KASPAROVA, E. A. 2016. [Treatment of Acanthamoeba keratitis]. *Vestnik oftalmologii,* 132**,** 110-116.

MARCHLER-BAUER, A., BO, Y., HAN, L., HE, J., LANCZYCKI, C. J., LU, S., CHITSAZ, F., DERBYSHIRE, M. K., GEER, R. C., GONZALES, N. R., GWADZ, M., HURWITZ, D. I., LU, F., MARCHLER, G. H., SONG, J. S., THANKI, N., WANG, Z., YAMASHITA, R. A., ZHANG, D., ZHENG, C., GEER, L. Y. & BRYANT, S. H. 2017. CDD/SPARCLE: functional classification of proteins via subfamily domain architectures. *Nucleic Acids Res,* 45**,** D200-D203.

MARCIANO-CABRAL, F. & CABRAL, G. 2003. Acanthamoeba spp. as Agents of Disease in Humans. *Clinical Microbiology Reviews,* 16**,** 273-307.

MARCIANO-CABRAL, F., LUDWICK, C., PUFFENBARGER, R. A. & CABRAL, G. A. 2004. Differential Stimulation of Microglial Pro-Inflammatory Cytokines by Acanthamoeba culbertsoni versus Acanthamoeba castellanii. *Journal of Eukaryotic Microbiology,* 51**,** 472-479.

MARINES, H. M., OSATO, M. S. & FONT, R. L. 1987. The Value of Calcofluor White in the Diagnosis of Mycotic and Acanthamoeba Infections of the Eye and Ocular Adnexa. *Ophthalmology,* 94**,** 23-26.

MARTÍN-NAVARRO, C. M., LÓPEZ-ARENCIBIA, A., SIFAOUI, I., REYES-BATTLE, M., FOUQUE, E., OSUNA, A., VALLADARES, B., PIÑERO, J. E., HÉCHARD, Y., MACIVER, S. K. & LORENZO-MORALES, J. 2017. Amoebicidal activity of caffeine and maslinic acid by the induction of Programmed Cell Death in Acanthamoeba. *Antimicrobial Agents and Chemotherapy*, 61(6); e026600 - 026616.

MARTÍN-NAVARRO, C. M., LORENZO-MORALES, J., CABRERA-SERRA, M. G., RANCEL, F., CORONADO-ÁLVAREZ, N. M., PIÑERO, J. E. & VALLADARES, B. 2008. The potential pathogenicity of chlorhexidine-sensitive Acanthamoeba strains isolated from contact lens cases from asymptomatic individuals in Tenerife, Canary Islands, Spain. *Journal of Medical Microbiology,* 57**,** 1399-1404.

MARTÍNEZ-MAQUEDA, D., MIRALLES, B. & RECIO, I. 2015. HT29 Cell Line. *In:* VERHOECKX, K., COTTER, P., LÓPEZ-EXPÓSITO, I., KLEIVELAND, C., LEA, T., MACKIE, A., REQUENA, T., SWIATECKA, D. & WICHERS, H. (eds.) *The Impact of Food Bioactives on Health: in vitro and ex vivo models.* Cham: Springer International Publishing, DOI 10.1007/978-3-319-16104-4_11, pp 113-124.

MARTINEZ, A. J. & JANITSCHKE, K. 1985. Acanthamoeba, an opportunistic microorganism: a review. *Infection,* 13**,** 251-256.

MARTÍNEZ, A. J. & VISVESVARA, G. S. 2002. Pathogenic and Opportunistic Free-living Amebas: Naegleria fowleri, Acanthamoeba spp. and Balamuthia mandrillaris. *Principles and Practise of Clinical Parasitology.* John Wiley & Sons, Ltd.

MATHERS, W., STEVENS, G., JR., RODRIGUES, M., CHAN, C. C., GOLD, J., VISVESVARA, G. S., LEMP, M. A. & ZIMMERMAN, L. E. 1987. Immunopathology and electron microscopy of Acanthamoeba keratitis. *Am J Ophthalmol,* 103**,** 626-35.

MATHERS, W. D., GOLDBERG, M. A., SUTPHIN, J. E., DITKOFF, J. W. & FOLBERG, R. 1997. Coexistent acanthamoeba keratitis and herpetic keratitis. *Archives of Ophthalmology,* 115**,** 714-718.

MAYCOCK, N. & JAYASWAL, R. 2016. *Update on Acanthamoeba Keratitis: Diagnosis, Treatment, and Outcomes.* 35 (5), 713–720.

MCCLELLAN, K., HOWARD, K., MAYHEW, E., NIEDERKORN, J. Y. & ALIZADEH, H. 2002. Adaptive Immune Responses to Acanthamoeba Cysts. *Experimental Eye Research,* 75**,** 285-293.

MCPHERSON, A. & CUDNEY, B. 2014. Optimization of crystallization conditions for biological macromolecules. *Acta Crystallographica. Section F, Structural Biology Communications,* 70**,** 1445-1467.

MEHDI, H. & GARG, N. K. 1987. Changes in the lipid composition and activities of isocitrate dehydrogenase and isocitrate lyase during encystation of Acanthamoeba culbertsoni strain A-1. *Transactions of The Royal Society of Tropical Medicine and Hygiene,* 81**,** 633-636.

MEWARA, A., KHURANA, S., YOONUS, S., MEGHA, K., TANWAR, P., GUPTA, A. & SEHGAL, R. 2017. Evaluation of loop-mediated isothermal amplification assay for rapid diagnosis of Acanthamoeba keratitis. *Indian Journal of Medical Microbiology,* 35**,** 90-94.

MOON, E.-K., HONG, Y., CHUNG, D.-I., GOO, Y.-K. & KONG, H.-H. 2014. Down-Regulation of Cellulose Synthase Inhibits the Formation of Endocysts in Acanthamoeba. *The Korean Journal of Parasitology,* 52**,** 131-135.

MOON, E.-K., HONG, Y., LEE, H.-A., QUAN, F.-S. & KONG, H.-H. 2017. DNA Methylation of Gene Expression in Acanthamoeba castellanii Encystation. *The Korean Journal of Parasitology,* 55**,** 115-120.

MOON, E.-K. & KONG, H.-H. 2012. Short-Cut Pathway to Synthesize Cellulose of Encysting Acanthamoeba. *The Korean Journal of Parasitology,* 50**,** 361-364.

MOORE, M. B., MCCULLEY, J. P., NEWTON, C., COBO, L. M., FOULKS, G. N., O'DAY, D. M., JOHNS, K. J., DRIEBE, W. T., WILSON, L. A., EPSTEIN, R. J. & DOUGHMAN, D. J. 1987a. Acanthamoeba Keratitis: A Growing Problem in Soft and Hard Contact Lens Wearers. *Ophthalmology,* 94**,** 1654-1661.

MOORE, M. B., MCCULLEY, J. P., NEWTON, C., COBO, L. M., FOULKS, G. N., O'DAY, D. M., JOHNS, K. J., DRIEBE, W. T., WILSON, L. A., EPSTEIN, R. J. & ET AL. 1987b. Acanthamoeba keratitis. A growing problem in soft and hard contact lens wearers. *Ophthalmology,* 94**,** 1654-1661.

MUCHESA, P., LEIFELS, M., JURZIK, L., HOORZOOK, K. B., BARNARD, T. G. & BARTIE, C. 2017. Coexistence of free-living amoebae and bacteria in selected South African hospital water distribution systems. *Parasitol Res,* 116**,** 155-165.

NA, B.-K., KIM, J.-C. & SONG, C.-Y. 2001. Characterization and pathogenetic role of proteinase from Acanthamoeba castellanii. *Microbial Pathogenesis,* 30**,** 39-48.

NAGINGTON, J., WATSON, P. G., PLAYFAIR, T. J., MCGILL, J., JONES, B. & STEELE, A. D. M. 1974. AMŒBIC INFECTION OF THE EYE. *The Lancet,* 304**,** 1537-1540.

NAGYOVÁ, V., NAGY, A., JANEČEK, Š. & TIMKO, J. 2010. Morphological, physiological, molecular and phylogenetic characterization of new environmental isolates of Acanthamoeba spp. from the region of Bratislava, Slovakia. *Biologia,* 65**,** 81-91.

NEFF, R. J. & NEFF, R. H. 1969. The biochemistry of amoebic encystment. *Symp Soc Exp Biol,* 23, 51 - 81.

NEWELL, S. Y., SHERR, B. F., SHERR, E. B. & FALLON, R. D. 1983. Bacterial response to presence of eukaryote inhibitors in water from a coastal marine environment. *Marine Environmental Research,* 10**,** 147-157.

NUPRASERT, W., PUTAPORNTIP, C., PARIYAKANOK, L. & JONGWUTIWES, S. 2010. Identification of a novel t17 genotype of acanthamoeba from environmental isolates and t10 genotype causing keratitis in Thailand. *J Clin Microbiol,* 48**,** 4636-4640.

O'BRIEN, M. C. & BOLTON, W. E. 1995. Comparison of cell viability probes compatible with fixation and permeabilization for combined surface and intracellular staining in flow cytometry. *Cytometry,* 19**,** 243-255.

OLDENBURG, C. E., ACHARYA, N. R., TU, E. Y., ZEGANS, M. E., MANNIS, M. J., GAYNOR, B. D., WHITCHER, J. P., LIETMAN, T. M. & KEENAN, J. D. 2011. Practice patterns and opinions in the treatment of acanthamoeba keratitis. *Cornea,* 30**,** 1363-1368.

OMAÑA-MOLINA, M., GONZÁLEZ-ROBLES, A., SALAZAR-VILLATORO, L. I., CRISTÓBAL-RAMOS, A. R., GONZÁLEZ-LÁZARO, M., SALINAS-MORENO, E., MÉNDEZ-CRUZ, R., SÁNCHEZ-CORNEJO, M., DE LA TORRE-GONZÁLEZ, E. & MARTÍNEZ-PALOMO, A. 2010. Acanthamoeba castellanii: Morphological analysis of the interaction with human cornea. *Experimental Parasitology,* 126**,** 73-78.

P. STRATFORD, M. & GRIFFITHS, A. J. 1978. *Variations in the Properties and Morphology of Cysts of Acanthamoeba castellanii. Microbiology*, 108, 33-37.

PAGE, F. C. 1967. Re-Definition of the Genus Acanthamoeba with Descriptions of Three Species. *The Journal of Protozoology,* 14**,** 709-724.

PAGE, M. A. & MATHERS, W. D. 2013. Acanthamoeba Keratitis: A 12-Year Experience Covering a Wide Spectrum of Presentations, Diagnoses, and Outcomes. *Journal of Ophthalmology,* 2013**,** 670242.

PANJWANI, N. 2010. Pathogenesis of Acanthamoeba keratitis. *Ocul Surf,* 8(2), 70 -79.

PATEL, D. V. & MCGHEE, C. N. 2009. Acanthamoeba keratitis: a comprehensive photographic reference of common and uncommon signs. *Clin Exp Ophthalmol,* 37**,** 232-238.

PEARLMAN, E., SUN, Y., ROY, S., KARMAKAR, M., HISE, A. G., SZCZOTKA-FLYNN, L., GHANNOUM, M., CHINNERY, H. R., MCMENAMIN, P. G. & RIETSCH, A. 2013. Host Defense at the Ocular Surface. *International Reviews of Immunology,* 32**,** 4-18.

PEREIRA-NEVES, A. & BENCHIMOL, M. 2007. Phagocytosis by Trichomonas vaginalis: new insights. *Biology of the Cell,* 99**,** 87-101.

PEREIRA-NEVES, A., RIBEIRO, K. C. & BENCHIMOL, M. 2003. Pseudocysts in Trichomonads – New Insights. *Protist,* 154**,** 313-329.

PÉREZ-IREZÁBAL, J., MARTÍNEZ, I., ISASA, P. & BARRÓN, J. 2006. Keratitis due to Acanthamoeba. *Enfermedades Infecciosas y Microbiologia Clinica,* 24**,** 46-52.

PICKUP, Z. L., PICKUP, R. & PARRY, J. D. 2007. A comparison of the growth and starvation responses of Acanthamoeba castellanii and Hartmannella vermiformis in the presence of suspended and attached Escherichia coli K12. *FEMS Microbiology Ecology,* 59**,** 556-563.

POLLARD, T. D. & COOPER, J. A. 2009. Actin, a central player in cell shape and movement. *Science,* 326**,** 1208-1212.

POR, Y. M., MEHTA, J. S., CHUA, J. L. L., KOH, T.-H., KHOR, W. B., FONG, A. C. Y., LIM, J. W. K., HENG, W. J., LOH, R. S. K., LIM, L. & TAN, D. T. H. 2009. Acanthamoeba Keratitis Associated with Contact Lens Wear in Singapore. *American Journal of Ophthalmology,* 148**,** 7-12.e2.

POTTER, J. L. & WEISMAN, R. A. 1971. Differentiation in acanthamoeba: β-glucan synthesis during encystment. *Biochimica et Biophysica Acta (BBA) - General Subjects,* 237**,** 65-74.

PRESTON, T. M., RICHARDS, H. & WOTTON, R. S. 2001. Locomotion and feeding of Acanthamoeba at the water–air interface of ponds. *FEMS Microbiology Letters,* 194**,** 143-147.

QVARNSTROM, Y., NERAD, T. A. & VISVESVARA, G. S. 2013a. Characterization of a new pathogenic Acanthamoeba Species, A. byersi n. sp., isolated from a human with fatal amoebic encephalitis. *J Eukaryot Microbiol,* 60**,** 626-633.

RADFORD, C. F., LEHMANN, O. J. & DART, J. K. 1998. Acanthamoeba keratitis: multicentre survey in England 1992-6. National Acanthamoeba Keratitis Study Group. *Br J Ophthalmol,* 82**,** 1387-1392.

RADFORD, C. F., MINASSIAN, D. C. & DART, J. K. G. 2002. Acanthamoeba keratitis in England and Wales: incidence, outcome, and risk factors. *The British Journal of Ophthalmology,* 86**,** 536-542.

ROBAEI, D., CARNT, N., MINASSIAN, D. C. & DART, J. K. 2014. The impact of topical corticosteroid use before diagnosis on the outcome of Acanthamoeba keratitis. *Ophthalmology,* 121**,** 1383-1388.

ROBERTS, C. W. & HENRIQUEZ, F. L. 2010. Drug target identification, validation, characterisation and exploitation for treatment of Acanthamoeba (species) infections. *Exp Parasitol,* 126**,** 91-96.

RODRIGUEZ-ZARAGOZA, S. 1994. Ecology of free-living amoebae. *Crit Rev Microbiol,* 20**,** 225-241.

RUBIN, R. W. & MAHER, M. 1976. Actin turnover during encystation in Acanthamoeba. *Experimental Cell Research,* 103**,** 159-168.

RUSSO KRAUSS, I., MERLINO, A., VERGARA, A. & SICA, F. 2013. *An Overview of Biological Macromolecule Crystallization*.

SANCHEZ, A. G., VIRGINIO, V. G., MASCHIO, V. J., FERREIRA, H. B. & ROTT, M. B. 2016. Evaluation of the immunodiagnostic potential of a recombinant surface protein domain from Acanthamoeba castellanii. *Parasitology,* 143**,** 1656-1664.

SCHAUMBERG, D. A., SNOW, K. K. & DANA, M. R. 1998. The epidemic of Acanthamoeba keratitis: where do we stand? *Cornea,* 17**,** 3-10.

SCHEID, P. 2014. Relevance of free-living amoebae as hosts for phylogenetically diverse microorganisms. *Parasitology Research,* 113**,** 2407-2414.

SCHROEDER-DIEDRICH, J. M., FUERST, P. A. & BYERS, T. J. 1998. Group-I introns with unusual sequences occur at three sites in nuclear 18S rRNA genes of Acanthamoeba lenticulata. *Curr Genet,* 34**,** 71-78.

SCHUSTER, F. L. 2002. Cultivation of pathogenic and opportunistic free-living amebas. *Clin Microbiol Rev,* 15**,** 342-354.

SCHUSTER, F. L. & LEVANDOWSKY, M. 1996. Chemosensory responses of Acanthamoeba castellanii: visual analysis of random movement and responses to chemical signals. *J Eukaryot Microbiol,* 43**,** 150-158.

SCHUSTER, F. L. & VISVESVARA, G. S. 1998. Efficacy of Novel Antimicrobials Against Clinical Isolates of Opportunistic Amebas. *Journal of Eukaryotic Microbiology,* 45**,** 612-618.

SCHUSTER, F. L. & VISVESVARA, G. S. 2004. Free-living amoebae as opportunistic and non-opportunistic pathogens of humans and animals. *Int J Parasitol,* 34**,** 1001-1027.

SEAL, D., STAPLETON, F. & DART, J. 1992. Possible environmental sources of Acanthamoeba spp in contact lens wearers. *The British Journal of Ophthalmology,* 76**,** 424-427.

SHARMA, S., RAMACHANDRAN, L. & RAO, G. N. 1995. Adherence of Cysts and Trophozoites of Acanthamoeba to Unworn Rigid Gas Permeable and Soft Contact Lenses. *Eye & Contact Lens,* 21**,** 247-251.

SHOKRI, A., SARVI, S., DARYANI, A. & SHARIF, M. 2016. Isolation and Genotyping of Acanthamoeba spp. as Neglected Parasites in North of Iran. *The Korean Journal of Parasitology,* 54**,** 447-453.

SIDDIQUI, R., AQEEL, Y. & KHAN, N. A. 2016. The development of drugs against Acanthamoeba infections. *Antimicrobial Agents and Chemotherapy*, 60(11); 6441 - 6450.

SIDDIQUI, R. & KHAN, N. A. 2012a. Biology and pathogenesis of Acanthamoeba. *Parasites & Vectors,* 5**,** 6.

SIDDIQUI, R. & KHAN, N. A. 2012c. War of the microbial worlds: who is the beneficiary in Acanthamoeba-bacterial interactions? *Exp Parasitol,* 130**,** 311-313.

STEWART, J. R. & WEISMAN, R. A. 1972. EXOCYTOSIS OF LATEX BEADS DURING THE ENCYSTMENT OF ACANTHAMOEBA. *The Journal of Cell Biology,* 52**,** 117-130.

STICCA, M. P., CARRIJO-CARVALHO, L. C., SILVA, I. M. B., VIEIRA, L. A., SOUZA, L. B., JUNIOR, R. B., CARVALHO, F. R. S. & FREITAS, D. 2017. Acanthamoeba keratitis in patients wearing scleral contact lenses. *Contact Lens and Anterior Eye*.In press. http://doi.org/10.1016/j.clae.2017.12.004).

STOTHARD, D. R., HAY, J., SCHROEDER-DIEDRICH, J. M., SEAL, D. V. & BYERS, T. J. 1999. Fluorescent Oligonucleotide Probes for Clinical and Environmental Detection of Acanthamoeba and the T4 18S rRNA Gene Sequence Type. *Journal of Clinical Microbiology,* 37**,** 2687-2693.

STOTHARD, D. R., SCHROEDER-DIEDRICH, J. M., AWWAD, M. H., GAST, R. J., LEDEE, D. R., RODRIGUEZ-ZARAGOZA, S., DEAN, C. L., FUERST, P. A. & BYERS, T. J. 1998a. The evolutionary history of the genus Acanthamoeba and the identification of eight new 18S rRNA gene sequence types. *J Eukaryot Microbiol,* 45**,** 45-54.

SUN, X., ZHANG, Y., LI, R., WANG, Z., LUO, S., GAO, M., DENG, S., CHEN, W. & JIN, X. 2006. Acanthamoeba keratitis: clinical characteristics and management. *Ophthalmology,* 113**,** 412-416.

TABIN, G., TAYLOR, H., SNIBSON, G., MURCHISON, A., GUSHCHIN, A. & ROGERS, S. 2001. Atypical presentation of Acanthamoeba keratitis. *Cornea,* 20**,** 757-759.

TAYLOR, P. W. 1977. Isolation and Experimental Infection of Free-Living Amebae in Freshwater Fishes. *The Journal of Parasitology,* 63**,** 232-237.

THEBPATIPHAT, N., HAMMERSMITH, K. M., ROCHA, F. N., RAPUANO, C. J., AYRES, B. D., LAIBSON, P. R., EAGLE, R. C. & COHEN, E. J. 2007. Acanthamoeba keratitis: a parasite on the rise. *Cornea,* 26(6), 701-706.

THOMAS, V., MCDONNELL, G., DENYER, S. P. & MAILLARD, J. Y. 2010. Free-living amoebae and their intracellular pathogenic microorganisms: risks for water quality. *FEMS Microbiol Rev,* 34**,** 231-259.

TOMLINSON, A., SIMMONS, P. A., SEAL, D. V. & MCFADYEN, A. K. 2000. Salicylate inhibition of acanthamoeba attachment to contact lenses11The authors have a patent pending on the application described in this study.: A model to reduce risk of infection. *Ophthalmology,* 107**,** 112-117.

TOMLINSON, G. & JONES, E. A. 1962. Isolation of cellulose from the cyst wall of a soil amoeba. *Biochim Biophys Acta,* 63(1), 194 - 200.

TOMLINSON, G. U. S. 1967. The Glyoxylate Pathway in Acanthamoeba Sp.*. *The Journal of Protozoology,* 14**,** 114-116.

TOUTAIN, C. M., CAIZZA, N. C., ZEGANS, M. E. & O'TOOLE, G. A. 2007. Roles for flagellar stators in biofilm formation by Pseudomonas aeruginosa. *Research in Microbiology,* 158**,** 471-477.

TU, E. Y., JOSLIN, C. E., SUGAR, J., SHOFF, M. E. & BOOTON, G. C. 2008. Prognostic factors affecting visual outcome in Acanthamoeba keratitis. *Ophthalmology,* 115**,** 1998-2003.

TURNER, N. A., RUSSELL, A. D., FURR, J. R. & LLOYD, D. 2000. Emergence of resistance to biocides during differentiation of Acanthamoeba castellanii. *J Antimicrob Chemother,* 46**,** 27-34.

ULSAMER, A. G., SMITH, F. R. & KORN, E. D. 1969. LIPIDS OF ACANTHAMOEBA CASTELLANII : Composition and Effects of Phagocytosis on Incorporation of Radioactive Precursors. *The Journal of Cell Biology,* 43**,** 105-114.

VAN KLINK, F., ALIZADEH, H., HE, Y., MELLON, J. A., SILVANY, R. E., MCCULLEY, J. P. & NIEDERKORN, J. Y. 1993. The role of contact lenses, trauma, and Langerhans cells in a Chinese hamster model of Acanthamoeba keratitis. *Investigative Ophthalmology & Visual Science,* 34**,** 1937-1944.

VAN KLINK, F., TAYLOR, W. M., ALIZADEH, H., JAGER, M. J., VAN ROOIJEN, N. & NIEDERKORN, J. Y. 1996. The role of macrophages in Acanthamoeba keratitis. *Investigative Ophthalmology & Visual Science,* 37**,** 1271-1281.

VENKATRAMAN GIRIJA, U., FURZE, C. M., GINGRAS, A. R., YOSHIZAKI, T., OHTANI, K., MARSHALL, J. E., WALLIS, A. K., SCHWAEBLE, W. J., EL-MEZGUELDI, M., MITCHELL, D. A., MOODY, P. C., WAKAMIYA, N. & WALLIS, R. 2015. Molecular basis of sugar recognition by collectin-K1 and the effects of mutations associated with 3MC syndrome. *BMC Biology,* 13**,** 27.

VERANI, J. R., LORICK, S. A., YODER, J. S., BEACH, M. J., BRADEN, C. R., ROBERTS, J. M., CONOVER, C. S., CHEN, S., MCCONNELL, K. A., CHANG, D. C., PARK, B. J., JONES, D. B., VISVESVARA, G. S., ROY, S. L. & FOR THE ACANTHAMOEBA KERATITIS INVESTIGATION, T. 2009. National Outbreak of Acanthamoeba Keratitis Associated with Use of a Contact Lens Solution, United States. *Emerging Infectious Diseases,* 15**,** 1236-1242.

VISVESVARA, G. S. 1991. Classification of Acanthamoeba. *Rev Infect Dis,* 13 Suppl 5**,** S369-72.

VISVESVARA, G. S., JONES, D. B. & ROBINSON, N. M. 1975. Isolation, Identification, and Biological Characterization of Acanthamoeba Polyphaga from a Human Eye. *The American Journal of Tropical Medicine and Hygiene,* 24**,** 784-790.

VISVESVARA, G. S., MOURA, H. & SCHUSTER, F. L. 2007a. Pathogenic and opportunistic free-living amoebae: Acanthamoeba spp., Balamuthia mandrillaris, Naegleria fowleri, and Sappinia diploidea. *FEMS Immunol Med Microbiol,* 50, 1-26.

VISVESVARA, G. S., ROY, S. L. & MAGUIRE, J. H. 2011. Pathogenic and Opportunistic Free-Living Amebae. 707-713.

VISVESVARA, G. S., SCHUSTER, F. L. & MARTINEZ, A. J. 1993. Balamuthia mandrillaris, N. G., N. Sp., agent of amebic meningoencephalitis in humans and other animals. *J Euk Microbiol,* 40.DOI:10.1111/j.1550 - 7408.1993.tb04943.x

WALLIS, R. & DRICKAMER, K. 1999. Molecular determinants of oligomer formation and complement fixation in mannose-binding proteins. *J Biol Chem,* 274**,** 3580-3589.

WANG, L., ASEM, E. K. & MCLAUGHLIN, G. L. 1994. Calcium enhances Acanthamoeba polyphaga binding to extracellular matrix proteins. *Investigative Ophthalmology & Visual Science,* 35**,** 2421-2426.

WEEKERS, P. H. H., BODELIER, P. L. E., WIJEN, J. P. H. & VOGELS, G. D. 1993. Effects of Grazing by the Free-Living Soil Amoebae Acanthamoeba castellanii, Acanthamoeba polyphaga, and Hartmannella vermiformis on Various Bacteria. *Applied and Environmental Microbiology,* 59**,** 2317-2319.

WEISMAN, R. A. 1976. Differentiation in Acanthamoeba castellanii. *Ann Rev Microbiol,* 30, 189 - 218.

WEISMAN, R. A., SPIEGEL, R. S. & MCCAULEY, J. G. 1970. Differentiation in acanthamoeba: Glycogen levels and glycogen synthetase activity during

encystment. *Biochimica et Biophysica Acta (BBA) - General Subjects,* 201**,** 45-53.

YAGITA, K. & ENDO, T. 1990. Restriction enzyme analysis of mitochondrial DNA of Acanthamoeba strains in Japan. *Journal of Protozoology,* 37**,** 570-575.

YANG, Y. F., MATHESON, M., DART, J. K. & CREE, I. A. 2001. Persistence of acanthamoeba antigen following acanthamoeba keratitis. *Br J Ophthalmol,* 85**,** 277-280.

YANG, Z., CAO, Z. & PANJWANI, N. 1997. Pathogenesis of Acanthamoeba keratitis: carbohydrate-mediated host-parasite interactions. *Infection and Immunity,* 65**,** 439-445.

YOO, K.-T. & JUNG, S.-Y. 2012. Effects of Mannose on Pathogenesis of Acanthamoeba castellanii. *The Korean Journal of Parasitology,* 50**,** 365-369.

ZEGANS, M. E., BECKER, H. I., BUDZIK, J. & O'TOOLE, G. 2002. The Role of Bacterial Biofilms in Ocular Infections. *DNA and Cell Biology,* 21**,** 415-420.

ZHANG, H., HASTY, P. & BRADLEY, A. 1994. Targeting frequency for deletion vectors in embryonic stem cells. *Molecular and Cellular Biology,* 14**,** 2404-2410.

ZIMMERMAN, A., NIXON, A. & RUEFF, E. 2016. *Contact lens associated microbial keratitis: Practical considerations for the optometrist*, 2016 (8), 1 -12.